Cracow University of Technology
ul. Warszawska 24, 31-155 Cracow, POLAND

Development of Advanced Methods for Theoretical Prediction of Shakedown Stress States and Physically Based Enhancement of Experimental Data

(Grant DTFR53-95-G-00055)

Volume III

Phase VIII

Report to the

US Department of Transportation,
Federal Railroad Administration,
Washington, DC

Cracow, June 2003

Contents

Brief summaries of the reports.

Volume I

Volume II

Volume III

Summaries

Normal and tangent contact pressure distributions in railroad rails and wheels, new concepts

J.Krok

This work introduces new idea of normal and tangent forces (transverse and longitudinal traction) definition for smooth as well as for rough wheel/rail surfaces. The main features of proposed idea are: stochastic approach, and neural network analysis used to determine load parameters.

Error controlled 3D stress analysis in railroad rails under contact loadings by the adaptive FEM/MFDM and Fourier series. Progress report

J.Krok

Elastic solutions for a railroad wheel subject to various types of loadings simulating the true wheel/rail rolling contact forces may be obtained by new FEM/MFDM approximation presented here. Specially developed Generalized Finite Fourier Method, FEM and variational version of the Meshless Finite Difference Method (MFDM) are applied in the wheel cross section and Fourier series approach in the circumferential direction. The Fourier analysis is also used to reconstruct loads of biparabolic shape. Radial, transversal and tangent loads (friction) may be considered.

New, reproducibility conditions based, meshless FDM approximation and mixed FEM/MFDM approximation are given. A'posteriori error estimation technique, based on mixed FEM/MFDM approximation, is introduced.

h-adaptive FEM analysis of shakedown problems modeled by Zarka's approach

W.Cecot

The paper addresses development of numerical implementation of the Zarka shakedown model. The resulting boundary value problem is discretized by the h-adaptive finite element method. The paper presents also validation tests of the Zarka approach and its application to the analysis of selected engineering problems with special attention paid to reliability of the modeling as well as of the numerical analysis. The tests confirm possibility of a proper, for engineering purposes, estimation of residual stresses by the Zarka shakedown approach.

Extension of the constrained minimization shakedown model to the case of material exhibiting kinematic hardening. Sample engineering applications

M.Pazdanowski

An extension of the mechanical/numerical constrained minimization shakedown mechanical model to include the plastic strain incompressibility has been proposed and included in the algoritm. The developed numerical application has been tested and verified. Subsequently it has been applied to compute plastic strains and residual stresses in two problems interesting from the engineering point of view, i.e. "wheel wandering" phenomenon and sensitivity of residual stresses to changes in material constants (yield limit and hardening ratio).

Error controlled 3D stress analysis in railroad wheels under contact loadings by the adaptive FEM/MFDM and Fourier series.

J.Krok

Elastic solutions for a railroad wheel subject to various types of loadings simulating the true wheel/rail rolling contact forces are presented here. Specially developed Generalized Finite Fourier Method, FEM and variational version of the Meshless Finite Difference Method (MFDM) are applied in the wheel cross section and Fourier series approach in the circumferential direction. The Fourier analysis is also used to reconstruct loads of biparabolic shape. Radial, transversal and tangent loads (friction) may be considered.

Results of elastic stress analysis in test problems, as well as in wheels for normal contact pressure were given. New aposteriori error estimation technique, which removed main drawback of so called Zienkiewicz-Zhu error estimator, has been introduced and successfully tested.

On improving the estimation of residual stresses in bodies made of material exhibiting kinematic hardening

M.Pazdanowski

A new approach to approximation of the solution in the area of changing mesh density has been proposed as the remedy to the more pronounced sensitivity of the Meshless Finite Difference Method over the Hybrid Finite Element Method to the changes in mesh density. Such changes are necessary, if a large body with a localized loading of high intensity is to be analyzed with high accuracy. This approach, together with the accompanying changes in the underlying computer code has been tested and validated. An application of the code to determine residual stresses and plastic strains in a vehicle wheel is presented.

Incremental analysis of residual states by the elastic-plastic constitutive models. Part I. New element families in incremental plasticity - further research

J.Krok

The work addresses development of theory and techniques to obtain the solution of three dimensional elasto-plastic and elasto-viscoplastic (Perzyna's model) problems with a'posteriori error estimation, based on Zienkiewicz-Zhu stress recovery estimators. The 3D model has been considered.

A new family of brick elements of arbitrary order has been introduced and successfully tested on up to 7^{th} order.

Incremental analysis of residual states by the elastic-plastic constitutive models. Part II. Testing of the new element families in incremental plasticity

J.Krok

The work addresses development of theory and techniques to obtain the solution of two dimensional elasto-plastic and elasto-viscoplastic (Perzyna's model) problems with a'posteriori error estimation, based on Zienkiewicz-Zhu stress recovery estimators. The 2D models (2D stress, 2D strain and axially symmetric case) have been considered.

The most important advantages of the above mentioned models when compared with shakedown approach, lie in capability to describe various kinds of non-elastic material behavior like: creep, relaxation, strain softening, continuum damage and termomechanical fatigue. The models require yielding conditions and loading unloading criteria.

Numerical solutions of various boundary value problems illustrate effectiveness of the MFDM in a'posteriori error estimation of inelastic problems for various element types like simple and higher order triangular and quadrilateral ones.

2D Incremental analysis of residual stresses in railroad rails with plastic strain hardening taken into account

J.Krok

The objective of the work is to evaluate elastic and residual stresses in railroad rails, due to normal contact loads of different amplitudes on the rail/wheel interface, with hardening taken into account. Elasto-plastic analysis is performed to evaluate residual state in the railroad rails, under the assumption of plane stress state. Comparison of magnitudes and izolines of the axial stresses for different load levels, for incremental plasticity models, has been made.

h-adaptive FEM analysis of residual states in railroad rails by the Bodner-Partom constitutive model

W.Cecot

The paper addresses development of numerical implementation of the Bodner-Partom rate model. The resulting boundary value problem is discretized by the h-adaptive Finite Element Method.

These constitutive equations were used to model such phenomena as continuum damage and thermomechanical fatigue. The incremental results were compared with the shakedown Zarka's modeling.

Adaptive mesh generation and visualization for MFDM and FEM analysis of railroad rails and vehicle wheels

I.Jaworska, J.Orkisz, P.Przybylski

The report presents the research on the original mesh generation method, based on mesh density control. The method is designed for adaptive analysis of 2D and 3D objects, including railroad rails and vehicle wheels. It is capable of various mesh modifications especially focused on highly efficient multigrid solution approach, carried out by means of meshless FD and FE methods.

An unified approach to the adaptive meshless FDM and FEM

J.Krok, J.Orkisz

The work addresses the general topic of a Combined Adaptive Finite Element Method (AFEM) and Adaptive Meshless Finite Difference Method (AMFDM). Enhancement of numerical solution in both methods and, first of all, in a combined AFEM/AMFDM technique is considered. Several ways of possible formal unification and combination of the FE and MFD methods are examined.

Several benchmarks were analyzed as well as engineering type of stress analysis in railroad rails.

On development of Moving Weighted Least Squares approximation and a'posteriori error estimation in Meshless FDM

J.Krok

The work addresses the general topic of an Adaptive Meshless Finite Difference Method (AMFDM). Enhancement of numerical solution in meshless methods is considered. Several different MFDM approaches are examined. All MFDM approaches are oriented on determining a basic approximation matrix of the same type, and the full vector of derivatives based on a linear combination of nodal unknowns. In the MFDM, for a given fixed point of the domain, such approximation matrix presents full set of the finite difference formulas for all derivatives up to required order. Several benchmarks are analyzed as well as engineering examples of stress analysis in railroad rails.

Wear and grinding modeling by the Zarka shakedown model
W.Cecot

The paper addresses application of the Zarka shakedown approach to simplified analysis of grinding and cumulative wear. Also continuum damage is accounted for. The model was subject to further verification on the cylinder benchmark problem, then it was used for the preliminary analysis of the wear and grinding in railroad rails. The previous conclusions were confirmed.

Modern wear and grinding theories were briefly reviewed.

Further investigation of the rail wear and grinding process - stability tests
M.Pazdanowski

A model of grinding and cumulative wear was subject to further tests on the rail residual stress problem. The wheel wandering effect and elastic-perfectly plastic material model have been chosen as the testbed. Several grinding passes of various depths have been simulated. Cumulative effects of grinding passes (number of passes and thickness of single pass) are analyzed. Residual stress distributions obtained are presented as contour plots and in the tabular form.

Incremental analysis of an elastic-plastic bending beam rail model
G.Midura, W.Cecot, J.Orkisz

Development of a generalized beam model for elastic-plastic analysis of railroad rails is the main objective of this research. It is a part of an engineering approach to estimate residual stresses resulting from the roller straightening process. Proposed algorithm based on FDM will be used to analyze statically indeterminate, elastic-plastic beams.

During the last year an incremental approach taking into account residual deformation indispensable in simulation of rail motion has been proposed. Algorithm based on this technique has been developed, tested and successfully verified in comparison with both theory and ADINA commercial code.

Application of Zarka's model to railroad rail roller straightening analysis
W.Cecot

The paper presents verification of the algorithm of a simplified roller straightening analysis. The methodology was applied to evaluate residual states developed during the production. The initial deformation due to quenching was taken into account.

An approach using GL approximation to plan the optimal locations of experimental measurements
W.Karmowski

The analytical and numerical analysis in mechanics requires experimental verification. This work answers the question how to locate measurements to obtain the best result at the lowest cost of the experiments and taking into consideration experiment credibility and cost. This was The task has been accomplished using the global – local approximation technique. The results of this work will be applied to plan the railway rails and vehicle wheels experiments executed to determine residual stresses.

Testing of the global-local method version taking into account gradient and curvature to estimate a'posteriori error and its application to residual stress analysis in railroad rails

W.Karmowski, J.Orkisz

The version of global-local method taking into account gradient and curvature of the sought field has been tested on coarse FEM/MFDM data. This technique allows to smoothen obtained solution and estimate a`posteriori error. It may be used to plan the new mesh in adaptive FEM/FDM methods. The method takes into account given nodal values and equilibrium equations simultaneously. The method has been used to smoothen the residual stress field in the railroad rail obtained by the MFD method.

Further development of the global approach to the physically based approximation technique in experimental analysis of residual stresses

J.Magiera

The report presents results of the current research effort aimed at further development of the global method (GM) approach to the physically based approximation technique in experimental analysis of residual stresses. In the report presented are new studies of optional criteria for selecting weighting factors/gate widths for experimental data (two new criteria, four algorithms proposed), another formulation for the break-off criteria (Stage II optimization loop, in GM formulation proposed), further tests of the global method as a tool for experiment planning and a posteriori estimation of experimental error (a new error indicator proposed).

On using the radial basis function neural network and backpropagation neural network in analysis of residual stresses in railroad rails

J. Kogut, J. Orkisz

A neural network approach to theoretical prediction of required residual stresses is considered here. Artificial neural networks trained well and long enough on residual stresses induced by various contact loads may provide very fast response. Results of numerical meshless finite difference analyses were preprocessed and introduced into the neural networks as input and output parameters. The study was performed for two different types of neural networks: a backpropagation neural network (BPNN) and a newly examined radial basis function neural network (RBF).

Reconstruction of the full 3D rail residual stress field by the physically based global method fit to neutron diffraction data and transverse/oblique slicing data reduction algorithm

J.Magiera

The report presents the current work regarding reconstruction of the full 3D rail residual stress field by the physically based global method fit to neutron diffraction data and transverse/oblique slicing data reduction algorithm. The work concentrated currently on analysis of the neutron diffraction data (rail samples #1-5) for improved quality FE/FDM grids generated recently (sample #1 analyzed as an example), certain improvements in 2D solution strategy (a'posteriori analysis of experimental error), 3D analysis for the case of several independent data series for a sample, and introduction to a three slice procedure.

An extended adaptive procedure of experimental data collection and evaluation by a'posteriori error estimation

J.Krok

The work addresses extended formulation of a new approach proposed to measurements planning and carrying out by means of error control of experimental data.

It includes: development of postprocessing techniques to approximate data given in a discrete form, a'posteriori error estimation (evaluation) of measured data, estimation of new required experimental points location and density, definition of reliability index of experimental data.

Theoretical consideration and numerical analysis are based on the Adaptive Finite Element analysis (AFEM) and the Meshless Finite Difference (MFDM) approach. Differences in numerical and experimental data analysis are underlying.

Reconstruction of residual stresses in railroad vehicle wheels based on enhanced saw cut measurements

J.Orkisz, A.Skrzat

The results obtained for all investigated wheels on coarse finite element mesh are presented. The results for the wheel #3, obtained for the first time on the dense mesh are presented as well. Additionally benchmark tests which prove the efficiency and precision of the approach in numerical calculations of influence coefficients (20-node elements, element pressures as loading) are included.

Further investigation and testing of the proposed solution approach to analysis of life prediction of railroad rails

W.Karmowski, J.Orkisz

Further analysis of the influence the residual stresses exert on fatigue service life of railroad rails is the objective of this research. The crack nucleation problem is considered basing on the classic stress-life (S-N) approaches. Experiments and theoretical predictions indicate that residual stresses in railroad rails can be large and therefore the role of these stresses is investigated. A single point wheel/rail contact at several rail locations is taken into account. The needed computer programs have been developed and numerical analyses have been carried out. The shortest life to fatigue crack nucleation was predicted for a neighborhood of the rail running surface (top of the rail head). The fatigue life is mostly affected by contact loading, while influence of residual stresses is negligible.

Topic 2.3

Development and application of artificial neural networks and genetic algorithms to analysis of residual stresses in railroad rails and vehicle wheels

Development and application of artificial neural networks and genetic algorithms to analysis of residual stresses in railroad rails and vehicle wheels.

A neural network approach to theoretical prediction of residual stresses is considered. Artificial neural networks trained well and long enough for residual stresses induced by various contact loads may provide very fast response. Results of numerical meshless finite difference analyses were pre-processed and introduced into the neural networks as input and output parameters. The study was performed for two different types of neural networks: a backpropagation neural network (BPNN) and a newly examined radial basis function neural network (RBF).

In the last year this research, carried out within the topic 2.3 on application of artificial neural networks to residual stress analysis in railroad rails, was temporarily suspended, due to temporary absence of Dr. J. Kogut. However, within the scope of the last three years, the following two reports.

1. *On using the radial basis function neural network and backpropagation neural network in analysis of residual stresses in railroad rails.*
2. *Further improvement of the version of the global-local method including information on gradient and curvature of a searched field.*

presented earlier describe the current state of the art of our research performed within this topic.

As preliminary results of this research proved to be encouraging – especially from the point of view of practical applications – further research is planned with particular attention paid to increasing the NN learning process efficiency.

Cracow University of Technology
ul. Warszawska 24, 31-155 Cracow, POLAND

On using the radial basis function neural network and backpropagation neural network in analysis of residual stresses in railroad rails.

Janusz Kogut, Janusz Orkisz

Report to the

US Department of Transportation,
Federal Railroad Administration,
Washington, DC

Cracow, June 2003

Contents

1. Introduction

1.1. Theoretical and experimental background of residual stress states in rails and wheels

Investigation of the problem of residual stresses in railroad rails is required as permanent increases in traffic and axle loads take place. In engineering practice improved procedures are adopted, for instance, replacement of jointed rail with continuous welded rail (CWR). As a consequence of these developments more rails now stay in service long enough to develop fatigue cracks. These cracks are caused mostly by the repeated action of rolling wheel contact loads, and can be classified as either surface or subsurface cracks. The cracking phenomena cause eventual deterioration of the running surface and reduction of a rail service life. Crack nucleation and propagation are driven by stress concentrations in a body, and may be predicted if the stresses are known. These stresses are the total stresses i.e. sum of the live and residual stresses (which remain in the body when loading is removed). In railroad rails they are generated both in manufacturing and service (e.g. by the rail/wheel rolling contacts).

Most rails manufactured today contain an initial residual stress field, which is distributed over the entire rail cross section. These stresses result from many sources, such as cooling process following rail forming, and roller straightening operations employed by the mills to meet the stringent limits imposed on the curvature of rails intended for CWR construction. The service-induced residual stresses (concentrated in the rail head) are superimposed over these stresses. The objective of this report is to present the progress of a new approach to the residual stress analysis in rails, principally known as an artificial intelligent system or neurocomputing.

1.2. Actual "state of the art"

Residual stresses and strains arising in both railroad rails and vehicle wheels due to manufacturing and service are under permanent investigation. These stresses are generated and modified throughout the whole rail life. Typical rail life includes the following stages [1]: *manufacturing* (rolling process, cooling, roller-straightening), *track installation and maintenance* (welding, geometry adjustment, rail replacement, destressing, grinding, and lubrication), *service*

conditions (particularly repetitive wandering rail/wheel contacts and rail bending on foundation, and temperature changes, wear), and material degradation.

1.3. Scope

The analyzed problem concerns repetitive wandering rail/wheel contacts and rail bending on its foundation. Residual stresses are generated mostly due to plastic effects resulting from rail/wheel contact loading. Rail bending on its foundation (including possible rail/foundation motion) also contributes here as one of the vital factors influencing residual stresses. A theoretical approach, providing means for residual stress analysis, was proposed in [2], followed by the development of complex but effective computational solution methods. Numerical solution to such a problem by discrete (Finite Element - FE, Boundary Element - BE, Meshless Finite Difference - MFD) methods is possible, though troublesome and much computer time consuming. However, in engineering applications, it is often important to get almost immediate answers to a given input data. Therefore, a neural network approach to theoretical prediction of required residual stresses is considered here. It takes advantage of the fact, that artificial neural networks, when trained well and long enough on residual stresses induced by various contact loads locations may provide very fast response to a wide class of input data. A set of MFDM solutions was used here. Results of numerical analyses were pre-processed and introduced into the neural networks as input and output parameters. The study was extended to two different types of neural networks: a backpropagation neural network (BPNN) and a newly examined radial basis function neural network (RBF).

2. Outline of artificial neural networks

2.1. Single artificial neuron

Biological neural system able to carry information and control processes runs every organism living on Earth. It could be considered as a highly complex, nonlinear and parallel information processing system. Such a system consists of single basic elementary cells called neurons. In reality such neurons receive electrical signals and produce responses. In such a way they store and transmit information in a body.

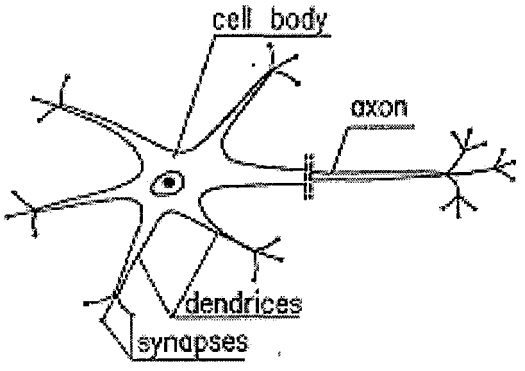

Figure 2.1 Real biological neuron.

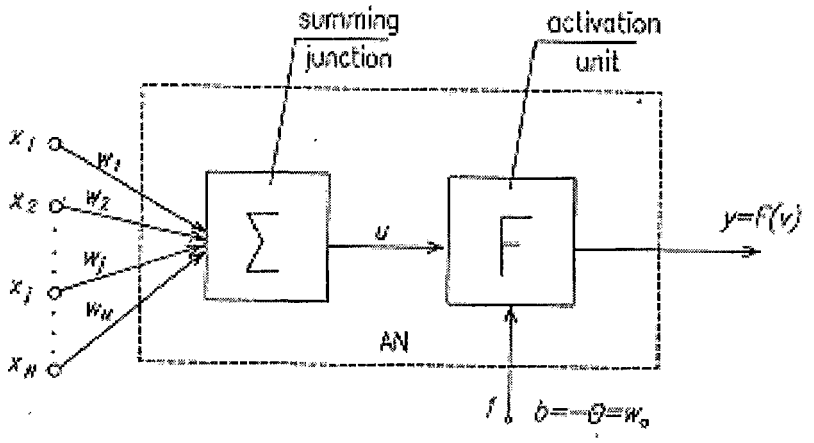

Figure 2.2 Artificial neuron.

Figure 2.1 presents a model of the real neuron. Such a neuron consists of *synapses* and *dendrites*, which receive signals and transmit them into *the cell body*. If the accumulated signal is strong enough it causes the neuron to produce an action potential as an output signal in the *axon*. Combining pointed elements and mapping them one may arrive at the simplest artificial neuron (Figure 2.2). Furthermore, such neurons are joined into neural networks. One of the most important elements of artificial neuron is an activation function (unit) - F. The following may be distinguished among activation functions:

unipolar (Figure 2.3):

$$F(u) = \begin{cases} 1 & if \quad u \geq u_0 \\ 0 & if \quad u < u_0 \end{cases} \tag{2.1}$$

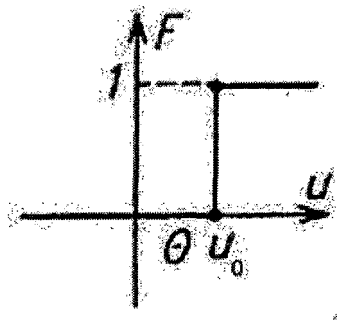

Figure 2.3 Unipolar activation function.

- bipolar (signum) – Figure 2.4:

$$F(u) = \begin{cases} 1 & if \quad u \geq 0 \\ -1 & if \quad u < 0 \end{cases} \tag{2.2}$$

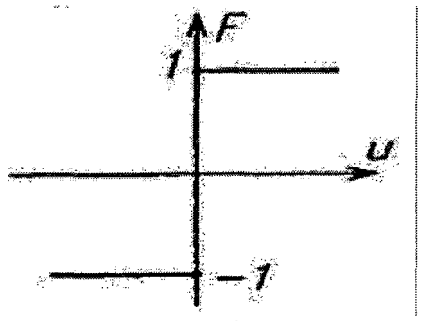

Figure 2.4 Bipolar activation function

- sigmoidal activation function – Figure 2.5:

$$F(u) = \frac{1}{1 + \exp(-\beta_1 u)} \tag{2.3}$$

where: β_1 - parameter;

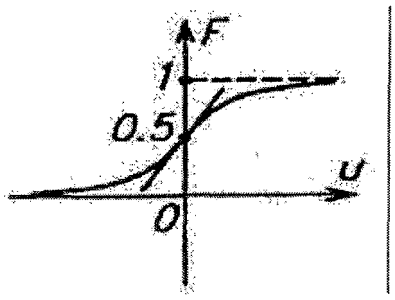

Figure 2.5 Sigmoidal activation function.

- sigmoidal bipolar activation function – Figure 2.6:

$$F(u) = \frac{1 - \exp(-\beta_1 u)}{1 + \exp(-\beta_1 u)} \tag{2.4}$$

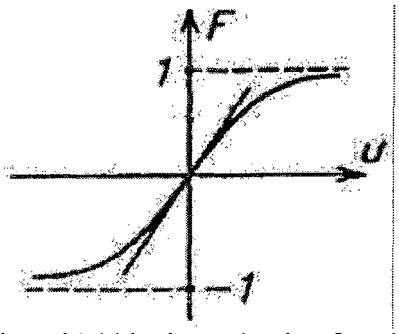

Figure 2.6 Sigmoidal bipolar activation function.

- linear:

$F(u) = bu$ if $b > 0$ (2.5)

- radial (Figure 2.7):

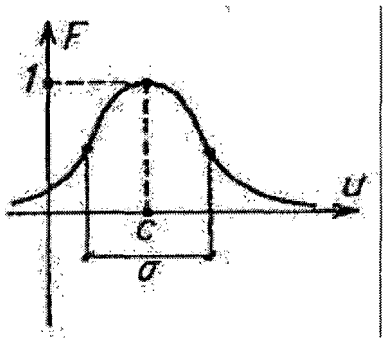

Figure 2.7 Gaussian radial basis function.

$$F(u) = \exp\left(-\frac{(u-c)^2}{2\sigma^2}\right) \tag{2.6}$$

where

c – the center

σ - the spread (support) of radial basis function.

2.2. Basic feedforward neural network

Arranged in layers, artificial neurons can be a primitive model of a biological nervous system and simulate in certain ways the real brain's behaviors. The arrangement in layers method is the best known. In this method neurons from the preceding layer are connected only to the neurons in the following layer (Figure 2.8). Such a network architecture is called a *feedforward neural network*. The first layer is called the *input layer*, the last one is the *output layer*. Between them *hidden layers* are placed. In this kind of network signals are transmitted only in one direction i.e. from inputs to outputs. The process of transmission is known as training of the network.

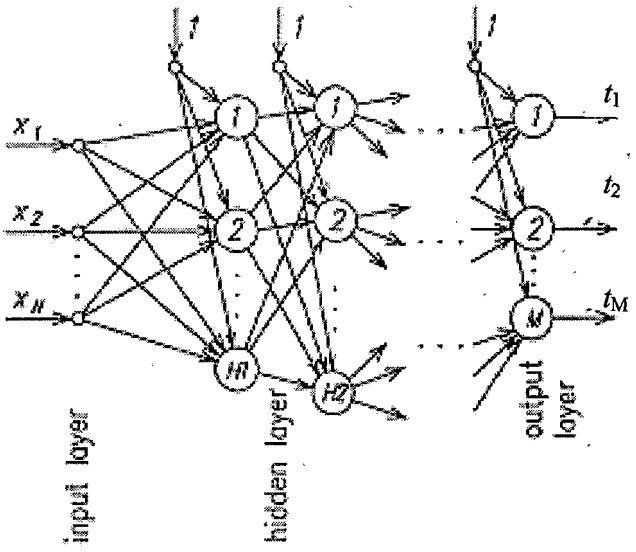

Figure 2.8 Artificial neural network.

The use of neural networks is described as *neurocomputation*. It has many features. One of them is natural massively parallel processing of information, the other is distributed processing and storing of information. These imply relatively low sensitivity of the neural network either to

its partial destruction or to errors caused by noisy information. A neural network (NN) when properly trained (teached) is able to generalize. This means, that the network is capable of efficient processing of data other than that used in the training procedure. The NN is also proficient in adapting to new information delivered to it.

2.3. Backpropagation neural network learning algorithm

As mentioned earlier the NN must be trained properly, to be flexible in later use. This means that it needs to be trained in a specific way i.e. by the *backpropagation* (BP) weights updating. The learning rule corresponding to the gradient method of the steepest descent is used very often (here as well). It helps in updating the *multilayer* NN. The least mean squared error of the network for a single pattern is computed as follows:

$$E_{LMS} = \frac{1}{2}\sum_{i=1}^{M}\left(t_i - O_i \right)^2 \tag{2.7}$$

where: t_i, O_i - target and computed values of i-th output

M - number of outputs.

Usually target values are normalized to accelerate convergence and improve the effectiveness of the training process. The least mean squared error of the network for all patterns is formulated as follows:

$$E = \frac{1}{2}\sum_{p=1}^{K}\sum_{i=1}^{M}\left(t_i^{(p)} - O_i^{(p)} \right)^2 \tag{2.8}$$

where: K – number of patterns

p – single pattern.

The average error is computed as follows:

$$E_{AV} = \frac{1}{K}\frac{1}{M}\ 2E \tag{2.9}$$

The weight of every neuron is adjusted according to the gradient formula in which the *learning rate* is included:

$$\Delta w_{ij} = -\eta \frac{\partial E_{AV}}{\partial w_{ij}} \tag{2.10}$$

where: η – learning rate.

w_{ij} – i-th weight of j-th layer (compare Figure 2.2)

Moreover, a *momentum term* which helps to increase the speed of learning and often to avoid the local minimum has been applied and formula (4) is changed as follows:

$$\Delta w_{ij}(s) = -\eta \frac{\partial E_{AV}(s)}{\partial w_{ij}} + \alpha \Delta w_{ij}(s-1) \tag{2.11}$$

where s – iteration step number
α – momentum term.

2.4. Regularization theory

An alternative method of neural network learning comes from the theory of regularization. It involves adding an extra term to the error function, designed to penalize mappings, which are not smooth [3]. In case of one single output (2.2) may have been changed into:

$$E = \frac{1}{2}\sum_{p=1}^{K}\left(t_i^{(p)} - O_i^{(p)} \right)^2 + \frac{\nu}{2}\int \left| P_y \right|^2 dx \tag{2.12}$$

where P is a differential operator, and ν is called *a regularization parameter.*

Considering the fact that each input vector is mapped onto an output vector O_i and the goal function is

$$h(t^{(p)}) = O^{(p)} \tag{2.13}$$

it is possible to introduce a set of basis functions for each data point, which take the form $\phi\left(\left\| x - x^p \right\|\right)$ where $\phi(\cdot)$ is a nonlinear function. p-th function depends then on the Euclidean distance $\left\| x - x^p \right\|$. The output of the mapping is the a linear combination of the basis functions

$$h(x) = \sum_p w_p \phi\left(\left\| x - x^p \right\|\right) \tag{2.14}$$

One can solve the *regularized least squares* problem of (2.12) setting the functional derivative with respect to y(x) to zero as

$$\sum_p \left[t(x^{(p)}) - O^{(p)} \right] \cdot \delta(x - x^{(p)}) + \nu \cdot \hat{P} \cdot P_y(x) = 0 \tag{2.15}$$

where $\hat{P}$ is adjoint differential operator to P and δ is the Dirac delta function. The equations (2.15) are the Euler-Lagrange equation corresponding to (2.12). A formal solution to these equations can be written down in terms of the Green's functions of the operator $\hat{P} \cdot P$, which are the function $G(x, x')$, satisfying

$$\hat{P} \cdot P \cdot G(x, x') = \delta(x - x') \tag{2.16}$$

If the operator P is translationally and rotationally invariant, the Green's functions depend only on the distance $\|x - x'\|$, and hence they are *radial functions* (2.6). The formal solution to (2.15) can then be written as

$$t(x) = \sum_p w_p G\left(\left\|x - x^p\right\|\right) \tag{2.17}$$

which has the form of a linear expansion into radial basis functions. Substituting (2.17) into (2.15) and using (2.16) one can obtain

$$\sum_p \left[t(x^{(p)}) - O^{(p)}\right] \cdot \delta(x - x^{(p)}) + \nu \cdot \sum_p w_p \delta\left(\left\|x - x^{(p)}\right\|\right) = 0 \tag{2.18}$$

Integration over a small region around $x^{(p)}$ shows that the coefficients w_n satisfy

$$y(x^{(p)}) - O^{(p)} + \nu \cdot w_{(p)} = 0 \tag{2.19}$$

Afterwards, the values of w_n can be obtained as the solution of the linear equation

$$(G + \nu \cdot I)w = O \tag{2.20}$$

where

$(G)_{pp'} = G\left(\left\|x^{p'} - x^p\right\|\right)$, $(w)_p = w_p$, $(O)_p = O^p$ and $\boldsymbol{I}$ denotes the unit matrix.

3. Shakedown problem definition

3.1. Shakedown MFDM formulation for the residual stress solution

The theoretical as well as hybrid experimental analysis of residual stresses in railroad rails present complex tasks formulated in terms of non-linear constrained optimization problems. The shake-down mechanical model for evaluation of residual stresses in elastic-perfectly plastic material proposed in [2], was extended for linearly strain hardening material [4]. It is formulated in two steps as follows:

(i) calculate the correlation matrix A_{ijkl}

$$\sigma_{ij}^{r} = A_{ijkl} \cdot \varepsilon_{ij}^{p} \tag{3.1}$$

solving nonlinear constrained optimization problem for self equilibrated stress σ_{ij}^{r} as a function of plastic distortions ε_{ij}^{p}.$\min_{\sigma_{ij}^{r}} \Theta(\sigma_{ij}^{r})$, $\Theta(\sigma_{ij}^{r}) = \int_{V} \sigma_{ij}^{r} \cdot C_{ijkl} \cdot \varepsilon_{ij}^{p} \cdot dV - \int_{V} \varepsilon_{ij}^{p} \cdot \sigma_{ij}^{r} \cdot dV$

(3.2)

satisfying the conditions

$\sigma_{ij,j}^{r} = 0$ in V - internal equilibrium conditions

$\sigma_{ij,j}^{r} \cdot n_j = 0$ on ∂V - static boundary conditions

(ii) Find ε_{ij}^{p},

which minimize the total complementary energy functional $\Psi(\varepsilon_{ij}^{p})$:

$$\min_{\varepsilon_{ij}^{p}} \Psi(\varepsilon_{ij}^{p}), \quad \Psi(\varepsilon_{ij}^{p}) = \int_{V} \varepsilon_{gh}^{p} \cdot A_{ghij}^{T} \cdot C_{ijkl} \cdot A_{klmn} \cdot \varepsilon_{mn}^{p} \cdot dV \quad \text{in } V \tag{3.3}$$

satisfying the conditions

$$\Psi((A_{ghij} - I_{ghij} \cdot c) \cdot \varepsilon_{gh}^{p} + \sigma_{ij}^{E}) - 1 \le 0 \qquad \text{in yield condition} \tag{3.4}$$

where $c = \dfrac{E \cdot H}{E - H}$ hardening parameter, and

σ_{ij}^{r} - estimated residual stresses in a body under consideration due to actual applied loads,

ε_{ij}^{p} - plastic strains,

$\overset{E}{\sigma}_{kl}$ - elastic stresses computed as if the object behavior was purely elastic during the loading process,

C_{ijkl} - elastic compliance matrix,

I_{ghij} - unit matrix,

E - Young modulus,

H - strain hardening modulus.

3.2. MFDM theoretical-numerical solution for the US 132 RE railroad rail

Residual stresses σ^r_{ij} due to the contact rail/wheel load were calculated by the Meshless Finite Different Method MFDM [5]. The following parameters were assumed

Young modulus	$E = 30\,000$ kpsi
Poisson ratio	$\nu^* = 0.3$
Yield limit	$\sigma_0 = 70$ kpsi
	Po = 33 000 lbf.

Figure 3.1 presents the mesh and the contact loads applied to the US 132 RE rail cross-section.

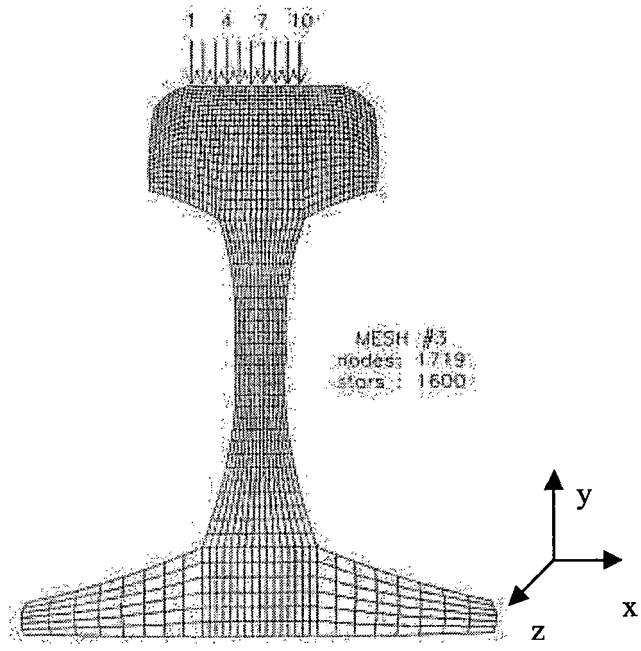

Figure 3.1 Locations of the contact loading (distributed on a patch) used in analyses, and the mesh applied in the rail cross-section.

The results were obtained for a certain number of different locations of the rail/wheel contact zone. For the different contact load locations on the railhead, theoretical-numerical solutions in 1600 mesh-points were applied. The file of residual stresses contained four independent stress components located in every mesh-point. There were ten load locations altogether. One of the

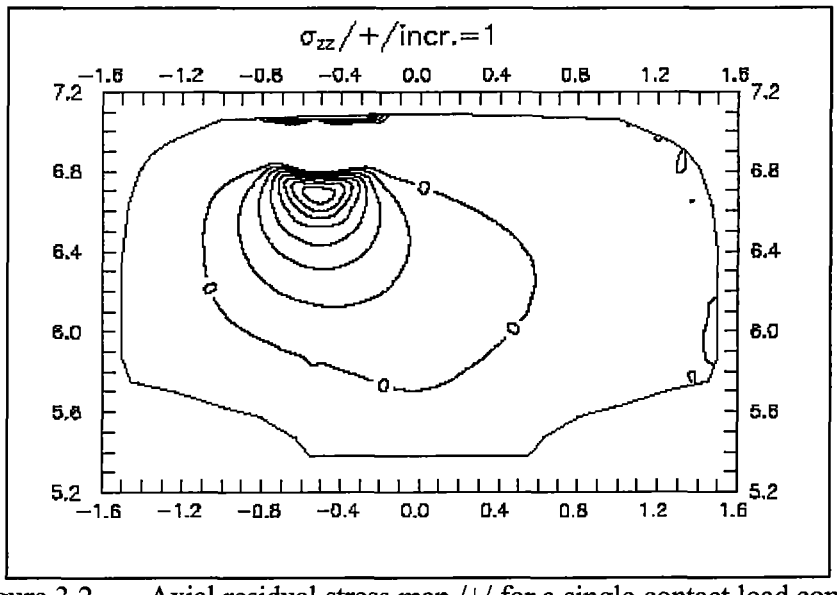

Figure 3.2 Axial residual stress map /+/ for a single contact load computed by MFDM. Increment = 1 kpsi.

solutions for the axial residual stresses is presented in Figure 3.2.

3.3. Neural networks definition based on the MFDM formulation

As mentioned earlier the NN as a kind of nonlinear simulator has strong abilities to generalize results which were input into it, and then is capable of efficient processing of data other than those used in the procedure of training. Two different types of NN were examined here BPNN and RBF. BPNN oughts to have a well-organized structure, and its learning process may consume a considerable amount of time. Regarding the structure, the basic formula for the number of neurons in hidden layers was suggested in [6], and it included two elements: the first is dependent on the number of inputs and outputs, the other depends on the number of patterns.

The formula was proposed as follows:

$$n_H = 0.5 \cdot (I + M) + \sqrt{K} \tag{3.5}$$

where:

I - number of inputs

M - number of outputs

K – number of training patterns.

For various purposes the number of neurons in hidden layers may be flexible [7], [8] and without loss of accuracy might be changed by up to 10%. In the considered problem of rail/wheel contact, one has to emphasize those parameters, which have considerable amount of influence on the level of residual stresses in the rail cross-section. For this purpose it is important to know especially [9], load magnitude and its location on the railhead, the position of every point in rail cross-section, and several of the characteristics uniquely describing the state. In the problem depicted above, input values include the load location on the surface, the mesh-point coordinates in the cross-section, and the linear values at those points. As an output parameter the residual stress σ^r_{zz} computed in the mesh-points has been used. The network outputs were compared with the MFDM values. A file of 16,000 patterns has been generated. Hence BPNN structure consists of four inputs, two hidden layers of 61 neurons each, and one neuron in the output layer.

The strategy of producing training and testing files from the pattern file is important for the BPNN. Therefore the pattern file was divided into two parts: the training file and the testing one. Usually the training file contains 80 to 90% of the patterns, while the testing one from 10 to 20% of them. The training file applied here consisted of approximately 80% and the testing file of 20% of the patterns. The training file contained eight complete solutions for different locations of wandering load. The testing file included two other solutions of the rail/wheel contact problem.

RBF neural network consists of the input layer, one hidden layer and the output layer. Hidden layer contains neurons, which have radial basis activation functions (2.6). The output layer neurons have linear activation function (2.5). RBF neural networks learning is based on finding the distance in a space between the target and the output value. It is possible to train such a network in different ways: supervised – with use of a typical backpropagation algorithm (2.8) and unsupervised – finding the solution of equation (2.20) in regularization process. The second method is achievable in two ways: first, when the number of patterns is exactly the same as the number of neurons in the hidden layer, second, when the number of neurons is increased one by

one after every iteration from certain starting point to the minimal number of neurons which satisfies the error goal or maximum number of neurons is reached. In this way one may reach the so called clustering of the solution. It depends also on the spread of the activation function (2.6). In both situations the number of hidden neurons is large. This implies that the RBF neural networks are related to local approximations around the centers in the space of input variables and often applied to the classification problems.

3.4. Comparison of the results of backpropagation and radial basis function neural networks.

Figure 3.2 and 3.3 present the example of the axial residual stress maps computed by MFDM and reconstructed by the single residual stress BPNN output.

On the other hand Figure 3.4 presents axial residual stress map for a single contact load,

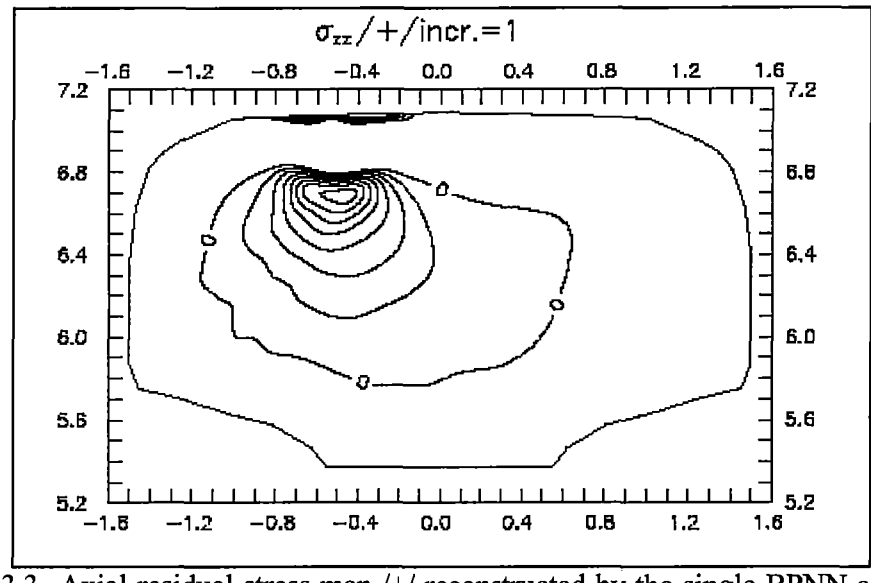

Figure 3.3 Axial residual stress map /+/ reconstructed by the single BPNN after 100 thousand epochs of training [10]. Increment = 1 kpsi

reconstructed by the RBF network for the same loading as original MFDM solution presented in Figure 3.2. The RBF type of network is characterized by rather fast learning time in comparison to BPNN and larger number of neurons in the hidden layer (here 12,000).

For the axial residual stress component relevant error norms have been calculated, namely the maximum norm:

$$\varepsilon_{MAX} = \max_j \left| \sigma^r_{kl\,j} - \sigma^{NN}_{kl\,j} \right| \tag{3.6}$$

and the average (L2) norm:

$$\varepsilon_{AVG} = \sqrt{\frac{1}{q} \sum_{i=1}^{q} \left(\sigma^r_{kl\,i} - \sigma^{NN}_{kl\,i} \right)^2} \tag{3.7}$$

where:

s^r_{kl} - residual stress – input data provided by the MFDM solution,

s^{NN}_{kl} - residual stress – result of NN analysis,

q – number of iteration points.

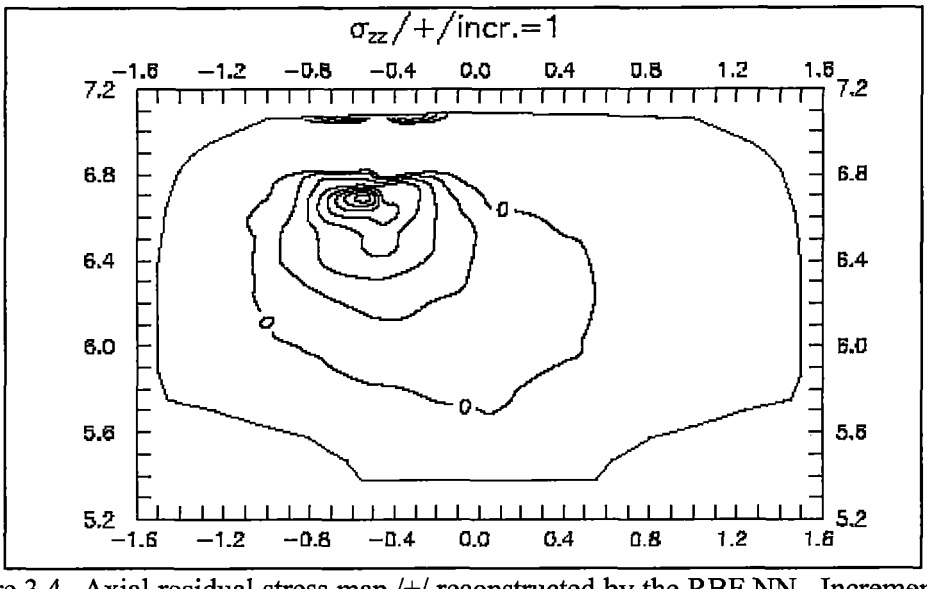

Figure 3.4 Axial residual stress map /+/ reconstructed by the RBF NN. Increment = 1 kpsi

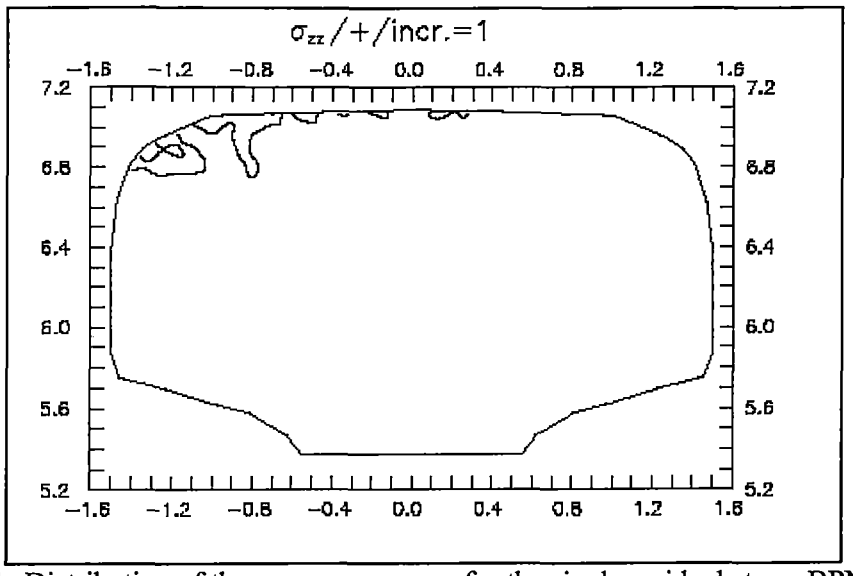

Figure 3.4 Distribution of the s_{zz} average error for the single residual stress BPNN after 100 thousand epochs. Increment = 1 kpsi.

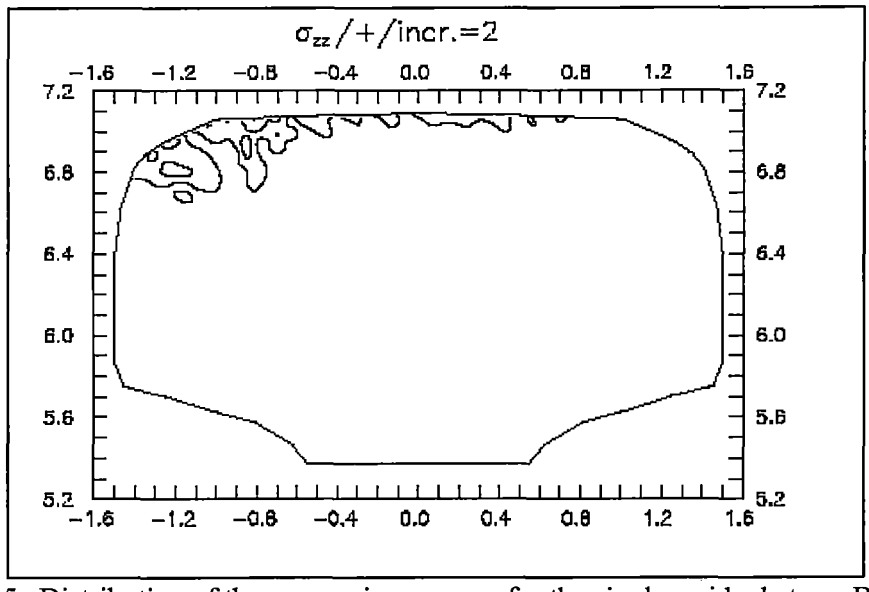

Figure 3.5 Distribution of the s_{zz} maximum error for the single residual stress BPNN after 100 thousand epochs. Increment = 2 kpsi.

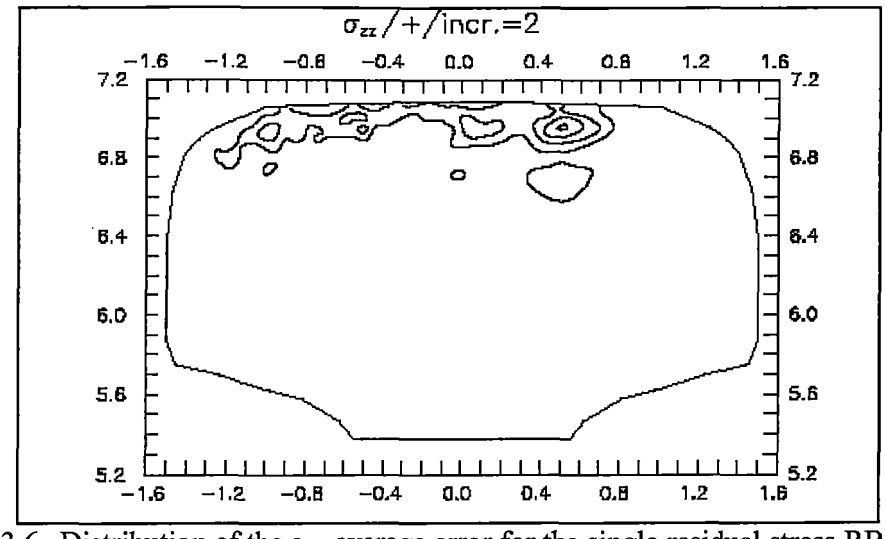

Figure 3.6 Distribution of the s_{zz} average error for the single residual stress RBF NN. Increment = 2 kpsi.

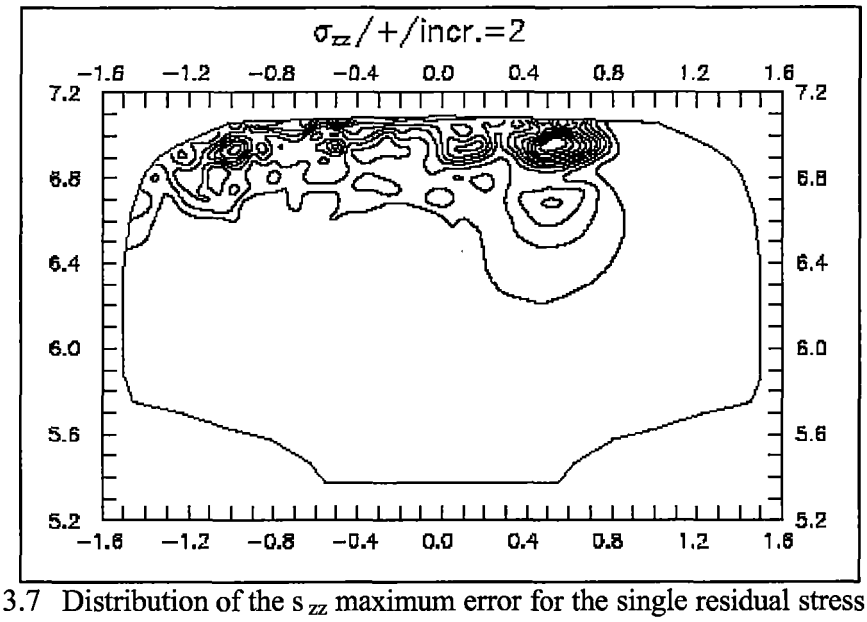

Figure 3.7 Distribution of the s_{zz} maximum error for the single residual stress RBF NN. Increment = 2 kpsi.

4 Final remarks

This report presents the progress of the application of neurocomputational mechanics to the analysis of residual stresses in railroad rails, preceded by[11],[12], and outlines the background for the future analysis of residual stress states in vehicle wheels as well. It is worth mentioning that neural networks are a new investigation tool, which was successfully applied here and might be used in the nearest future in the analysis and enhancement of both theoretical and experimental data.

The first part of the report describes the background of artificial neural networks. It emphasizes not only the feedforward neural network and its backpropagation algorithm of learning but also radial basis function neural networks and the regularization theory of their learning.

Subsequently the next chapter is dedicated to the formulation of the residual stress task in the neural network environment. Results of training and testing using elastic-perfectly plastic solutions based on MFD Method were presented. Single component analyses of axial residual stress were illustrated. The results were obtained and compared for different neural network types. These are followed by the analysis of several types of error.

The study confirmed the usefullness of this new method in the analysis ofresidual stresses in railroad rails and led us to take the closer look on the RBF neural networks. The future plans are aimed at developing the hybrid meshless methods and RBF based neural network with constraints based on experimental analysis of the residual stresses, dedicated to railroad rails and wheels.

References

[1] Orkisz J; Residual stress/strain analysis in railroad rails and vehicle wheels. US DOT Report VNTSC Cambridge, MA, 2000.

[2] Orkisz J; Prediction of actual stresses by constrained minimization of energy, in Orkisz J, Orringer O, Swiderski Z (eds.); "Residual Stress in Rails", Kluwer Academic Publishers, Dortrecht 1992, Vol. II, pp. 101-124.

[3] Bishop Ch.M; Neural Networks for Pattern Recognition. Clarendon Press Oxford 1998.

[4] Cecot W, Orkisz J; Prediction of actual residual stresses resulting from cyclic loading in kinematic hardening material. Proc. Int. Conf. COMPLAS V, pp. 1879-1891, Barcelona 1997.

[5] Pazdanowski M; Evaluation of the residual stresses induced in a rail by a single point contact load. US DOT Washington Report – Grant DTFR53-95-G-00055.

[6] Neuroshell 2, Release 4.0 Users Manual, Ward Systems Group, Inc. Frederick, MD 2000.

[7] Beale M, Demuth H; Neural Network Toolbox. For Use with Matlab. User's Guide v. 3. The Math Works, Inc. 1998.

[8] Haykin S; Neural Networks – A Comprehensive Foundations, Macmillan College Publ. Co., Englewood Cliffs, NJ 1994.

[9] Kogut J; Neural networks in analysis of residual stresses, XIV Polish Conference on Computer Methods in Mechanics, Rzeszow 1999, pp. 159-160.

[10] Kogut J, Orkisz J; Neural network analysis of residual stresses in railroad rails, ECCM, Cracow 2001.

[11] Kogut J, Orkisz J; Development and application of artificial neural networks and genetic algorithms to analysis of residual stresses in railroad rails and vehicle wheels. US DOT Washington – Grant DTFR53-95-G-00055. Final Report, Cracow 2000.

[12] Kogut J, Orkisz J; Investigation of the Use of Neural Network Methods in Residual Stress Analysis of Railroad Rails and Wheels. US DOT VNTSC – DTRS57-00-P-80419 Report, Cambridge MA, 2000.

Topic 2.4

Reconstruction of the full 3D rail residual stress by physically based global method fit to neutron diffraction data and transverse/oblique slicing data reduction algorithm

RECONSTRUCTION OF THE FULL 3D RAIL RESIDUAL STRESS FIELD BY THE PHYSICALLY BASED GLOBAL METHOD FIT TO NEUTRON DIFFRACTION DATA AND TRANSVERSE/OBLIQUE SLICING DATA REDUCTION ALGORITHM

The research on the 3D technique in the current research year was split into work on mastering the algorithms/numerical techniques applied, analysis of optional sectioning scheme(-s) and practical analysis of the currently available ND data performed on new, enhanced grids.

In particular, the research program planned for the 2002/2003 research year included:

1. further development and mastering the 3D solution procedure;
2. 3D analysis of new rail residual stress data;
3. a study (on simulated data) of a three slice procedures: horizontal and vertical O/T/O with a special attention to the case of symmetrical O/T/O;
4. 3D analysis of residual stresses for the case of several independent data series for the same rail sample, as it takes place in the case of the Sample #3, for which three independent data series are available.

The report contains research material regarding the items 1, 2 (not performed substitute material enclosed – explanation follows in Introduction), 3 and 4 (fully covered).

Cracow University of Technology
ul. Warszawska 24, 31-155 Cracow, POLAND

Reconstruction of the full 3D rail residual stress field by the physically based global method fit to neutron diffraction data and transverse/ oblique slicing data reduction algorithm.

Jacek Magiera

Report to the

US Department of Transportation,
Federal Railroad Administration,
Washington, DC

Cracow, June 2003

CONTENTS

LIST OF FIGURES

RECONSTRUCTION OF THE FULL 3D RAIL RESIDUAL STRESS FIELD BY THE PHYSICALLY BASED GLOBAL METHOD FIT TO NEUTRON DIFFRACTION DATA AND TRANSVERSE/OBLIQUE SLICING DATA REDUCTION ALGORITHM

Jacek Magiera,

Cracow University of Technology

Summary

The report presents results of research devoted to reconstruction of the full 3D rail residual stress field by the physically based global method fit to neutron diffraction data and the transverse/oblique slicing data reduction algorithm. The work concentrated on analysis of the neutron diffraction data (rail samples #1-5) for improved FE/FDM grids (sample #1 analyzed as an example), certain improvements in 2D solution strategy (*a posteriori* analysis of experimental error), 3D analysis for the case of several independent data series for a sample, and analysis of a three slice procedure. An independent effort was aimed at development of a higher order 3D brick finite element family that will replace the currently used 8-node linear 3D elements.

1. INTRODUCTION

The research on the 3D technique in the current research year was split into work on mastering the algorithms/numerical techniques applied, analysis of optional sectioning scheme(-s) and practical analysis of the currently available ND data performed on new, enhanced grids and with *a posteriori* experimental data error analysis.

In particular, the research program planned for the 2002/2003 research year included:

1. further development and mastering of the 3D solution procedure;
2. 3D analysis of new rail residual stress data;
3. a study of a three slice procedure: horizontal and vertical O/T/O with a special attention to the case of symmetrical O/T/O;
4. 3D analysis of residual stresses for the case of several independent data series for the same rail sample, as it takes place in the case of the Sample #3, for which three independent data series are available.

Generally, all the research tasks listed above were addressed even though there were certain modifications to the task list required.

As far as the item 1 (further development and mastering of the 3D solution procedure) is concerned, the report contains description of improvements introduced on the 2D level[1], the new family of improved FEM/FDM grids generated for rail samples #1-5. Another task performed in this topic was analysis of influence the grid density has on results. Part of the work concerning item 1 research that focused on development of a new, non-linear 3D brick element family for enhanced analysis of elastic behavior of rail slice samples was performed by J. Krok, the author of the NAFDEM-PC FEM/FDM code used in the TOS-3DRS[2] system, and is reported elsewhere in the group report as the paper entitled: *Incremental analysis of residual states by the elastic-plastic constitutive models. New elements families in incremental plasticity* [1].

The research on the task listed as item 2 (3D analysis of new rail residual stress data) was impossible to be carried out due to lack of the new data[3]. This tasks will be performed when the new data is available. To compensate for the lack of

---

1 by the 2D level it is understood here the global method procedure for experimental data analysis and enhancement

2 an acronym for **T**ransverse-**O**blique **S**licing - **3D** **R**esidual **S**tress

3 supposed to be available by the end of 2003 year

this material, the author performed new improved 3D analysis of the old neutron diffraction (ND) data [9] that made use of the newest advancements on the both 2D and 3D levels. Exemplary results for ND sample #1 data are presented.

The material regarding item 3 (a study of a three slice procedure) contains introduction of the concept of three slice procedure, algorithms and exemplary results. Unfortunately, not all tests planned were performed due to numerical instabilities observed.

As far as item 4 (3D analysis of residual stresses for the case of several independent data series for the same rail sample) is concerned, the report contains results for combined analysis of data series #2 and #3 for ND rail sample #3.

2. FURTHER DEVELOPMENT AND MASTERING OF THE 3D SOLUTION PROCEDURE

Certain enhancements in the 3D rail residual stress reconstruction procedure proposed in the last report [4] like different techniques for pre-smoothing of the FEM solutions or tests for higher order approximation on the "between slices" level provided mixed results: the procedure worked but it was hard to conclude that certain variants are definitely better than others. Introduction of those modifications undoubtedly cut down the total number of iterations required for observing convergence on the assumed error norm level, but the quality of final results sometimes suffered from those modifications. The general conclusion was that the previously used version of the procedure seemed a sound and reasonable choice.

In the current work several different areas of possible improvements were considered and explored. They included:

- improvements on the 2D level (data smoothing);

- *a posteriori* error estimation for assessment of experimental data credibility
- generation of improved FE/FDM grids
- analysis of influence the grid density has on final results

As mentioned in Introduction, there was also an independent effort aimed at development of higher order 3D finite elements that should vastly improve the quality of FE rail slice modeling but it is not reported here.

2.1 Improvements on the 2D level

The 2D level, even though formally independent from the 3D level analysis and treated as separate research topic [2], is in fact an important ingredient of the Transverse/Oblique Slicing (T/O-S) approach and as such, it significantly contributes to the overall outcome of the 3D rail residual stress analysis. Thus work on mastering of the 3D procedure naturally encompasses 2D level procedures and benefits from improvements worked out there.

The main improvements on the 2D level worked out recently include:

- work on criteria for automatic selection of reasonable weighting factors ascribed to experimental data points (four methods proposed, each as iterative or non-iterative)
- a new formulation of the global method that make it possible to find the maximum gate width parameter used in the classical GM formulation for break-off criterion

A detailed report on these improvements is contained elsewhere in this volume as Topic 2.2 [2].

2.2 *A posteriori* error estimation for assessment of experimental data credibility

Practical applications of the T/O-S approach to 3D analysis of rail specimens would benefit greatly from the knowledge of data credibility that may serve for assessment of overall quality of results. Such estimation has been difficult so far with the classical, statistically based methods of data credibility assessment as the experimental techniques used were destructive and the prohibitive cost level prevented examinations of more than one rail sample of a kind [3]. Thus almost all that could be done, as in the case of the quoted J.J. Groom examinations [3] was to apply certain complementary approaches to provide redundant data for such estimations. In case of the recalled examinations it was e.g., applying scribe marks on peripheries of the rail slab prior to cutting of the examined section and to record the length change observed upon specimen removal. This data was then used for general verification of the data obtained from the Yasojima-Machii and Meier samples. Such techniques are perhaps suitable for general validation of the data but do not provide any quantitative measure of error. Needless to say, the outcome of J.J. Groom error assessment was the conclusion that the error was on average 10% (i.e., ca. 20-30MPa)[4], the newly developed techniques show its level as high as even more than 400 MPa at separate experimental points.

The methodology for *a posteriori* evaluation of experimental data error makes use of the high quality data fits the global method provides. Thanks to its built-in physical relations, the smoothing of the data produces not only visibly attractive results but also guarantee fulfillment of those relations and as such, the smoothened fields may serve as a reference solutions for evaluation of experimental error.

---

[4] max. it was found to be 44%

Several general error estimator were proposed, out of which two were tested and intensively used in analysis:

1. the stress based, component-by-component (SBCC) estimator
2. the relative local curvature (RLC) estimator

Use of both of them and the results they provide for exemplary experimental data derived from the J.J. Groom work [3] are shown in the quoted report [2].

2.3 Generation of improved FE/FDM grids

The problem with the currently used grid generator GRID [11] was that due to its internal organization (generation of structured grids in generalized quadrilateral sub-domains) it was unable to exactly follow the profile of the boundary line and the discrepancies were especially visible in the areas of intensive plastic flow where material formed cusp-like projections. This problem has been already discussed and to a degree addressed in [10] when new grids were generated for samples #1-5 with help of ADINA FE grid generator but it turned out that even though the quality of the boundary representation was improved the grids had very uneven distributions of nodes and it was difficult to control the total number of nodes. Another difficulty with ADINA's grid generator was that it was impossible to generate a family of "hierarchical", denser and denser, grids which would have the feature that a denser grid contains all the nodes of a coarser grid. This would be beneficial for validation of results of the planned for research problem of the minimum number of nodes required for analysis of neutron diffraction data.

The new grids were generated with the GRID generator as it lends itself well for generating "hierarchical" grids but a manual correction procedure at the peripheral layer of nodes was applied to rectify the boundary problems that affected the originally generated grids. This procedure was applied to all five rail

samples for grids of exactly the same density like the previously used 971 nodes (for comparative computations).

Results of this procedure for rail samples #1-5 are shown in Figs. 1 to 5. In each figure the original profile (a) (as provided by NIST), the old (b) (i.e., generated with GRID generator) and the corrected (c) grids are shown. As mentioned, the new grids are topologically equivalent to the old ones, but corrections were applied that make the new grids to conform to the original profiles. They are visible especially in the tread-parts of the profiles where the material subject to plastic flow formed local cusps or sharp points (see e.g., areas denoted as *A* and *A'* in Fig. 3) or in the areas where the GRID program generated nodes forming locally, at the cross-segments boundaries defining its profile approximation regions, concave boundary line where it should form either straight line or convex curve (see areas denoted *B* and *B'* in Fig. 5).

2.4 Influence of grid density on final results

One of the essential questions when performing numerical analysis with either the finite element method or finite difference method (and the TOS-3DRS system makes use of both) is the question about the required grid density and its sufficiency for the considered problem. In the area of theoretical computations the prevailing approach now is to use one of the range of adaptive methods which through *a posteriori* error estimates provide a tool for building mesh/grid density indicators. With help of this indicators and usually at the expense of iterative procedure, a correct (or sufficient) density might be evaluated.

In the case of enhanced numerical analysis of experimental data, which is a subject of the research activity reported here, the adaptive approaches are almost useless. The main reason is that what has the dominating influence on the error now is not like previously the order p of the approximation (or its derivatives) spanned, jumps of certain derivatives at the cross-elements boundaries j or element/star's characteristic dimension h – even thought those

factors are present in the FE/FDM analyses performed – but the quality of experimental data and error committed while it was collected. Thus the techniques for evaluation of the required grid density worked out in the field of theoretical analysis are not (at least easily) transformable to the field of experimental data reduction algorithms. Instead, in all analyses performed by the author and reported to the US DOT, FRA over the last several years a heuristic approach has been applied that bounds the grid density to the experimental data points density, keeping the FEM/FDM grids ca. 1.5-2 times denser than the experimental ones. For such a choice all the procedures worked and no problems with numerical instabilities were encountered, but the question whether it is a sound reasoning has remained open.

To investigate the problem, a new higher density grid was generated for NIST sample #1 profile. It is almost twice as dense as the old one, having 1835 nodes (vs. 971) and 1720 quadrilateral, 3440 triangular elements. This new grid was used in standard 2D NIST data smoothing procedure with use of the global method and the results were compared.

In Figs. 7 – 9 results for σ_{xx}, σ_{yy} and σ_{xy} for the old and new grid are juxtaposed, in Fig. 10 differences between them are plotted. As it may be seen, the new results do not visually differ significantly except for the area close to the peripheries of the rail where certain more significant differences manifest their presence. Their amplitude is on average equal to ca. 20-60 MPa (which is ca. 5-15% of the stress magnitudes at those areas), but such extreme values happen only at very localized points (e.g., on the right-hand side of the railhead for the vertical stress σ_{yy}, where very steep gradients are recorded). The differences in the shear stress modeling (Fig. 10c) are a little bit more penetrating into the inward part of the railhead but this is not surprising as this stress component was numerically restored and is naturally more sensitive to even slight fluctuations in numerical procedure parameters. Their magnitude, though, at majority of data points remain on a stable level of ca. 5-10 MPa (ca. 6-15%), at certain points

close to peripheries it reaches the level of ca. 30-40 MPa (ca. 40-50% of difference).

Generally, the test with the new twice as dense grid, showed a reasonably good agreement with the older grids family, used throughout the analysis of residual stress in the examined rail samples. The data reduced in the inner part of the railhead on both grids shows a very good to excellent agreement, with differences usually not exceeding the level of 10 MPa (which gives ca. 1-8% of error, depending on the region), at certain regions in the outer parts, it rises to 20-60 MPa.

The 3D procedure, which for both simulated experimental data [5,6] and ND actual data [7,8] was found to change the stress magnitudes recorded in the 2D specimens (rail slices) by a comparable in both cases level of ca. 15-35%, might be also expected to incur the grid related errors, estimated on the 2D level as the 1%-8% at majority of data points (and up to 40% at extremums) will be projected to the 3D space with the same factor of 15-35%, thus the resulting 3D error due to grid phenomena might be estimated at the 0.15% to 3% in the inner part of the railhead and might approach the amplitude of ca. 15% at separated peripheral nodes.

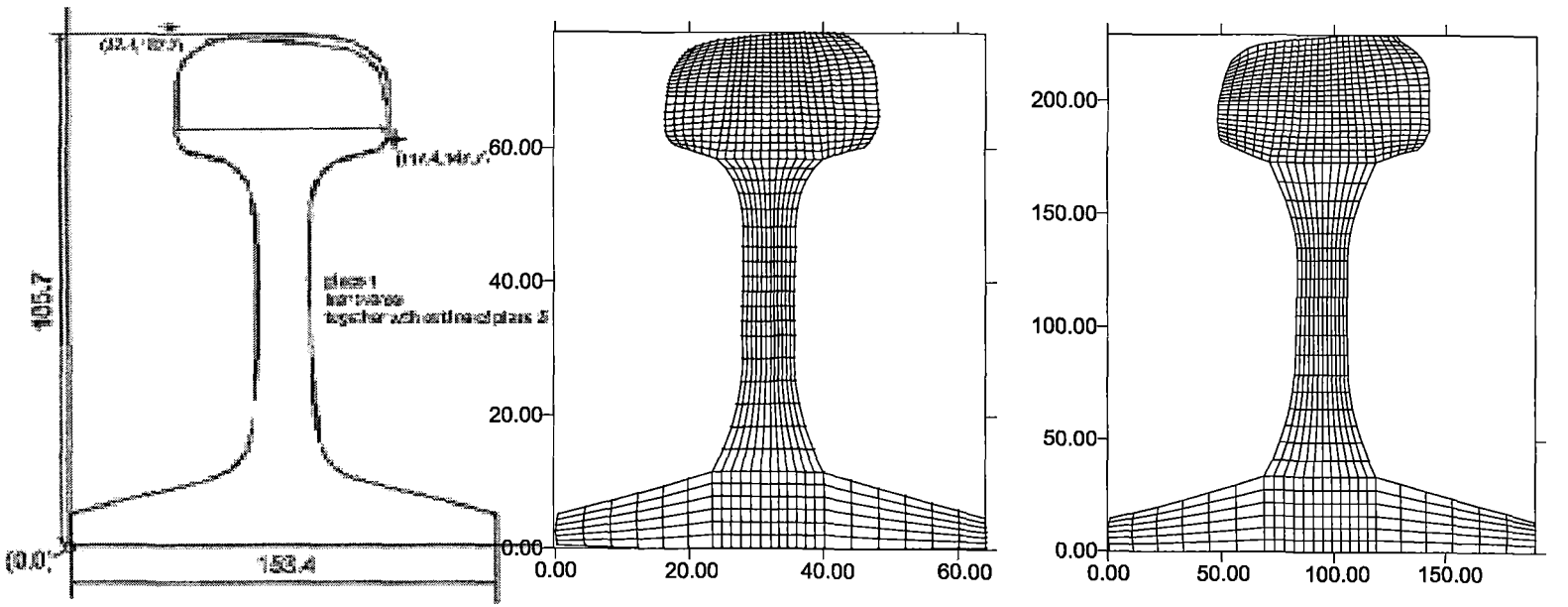

a) NIST delivered profile b) Old grid c) New corrected grid

Fig. 1

Old and new grids for NIST sample #1

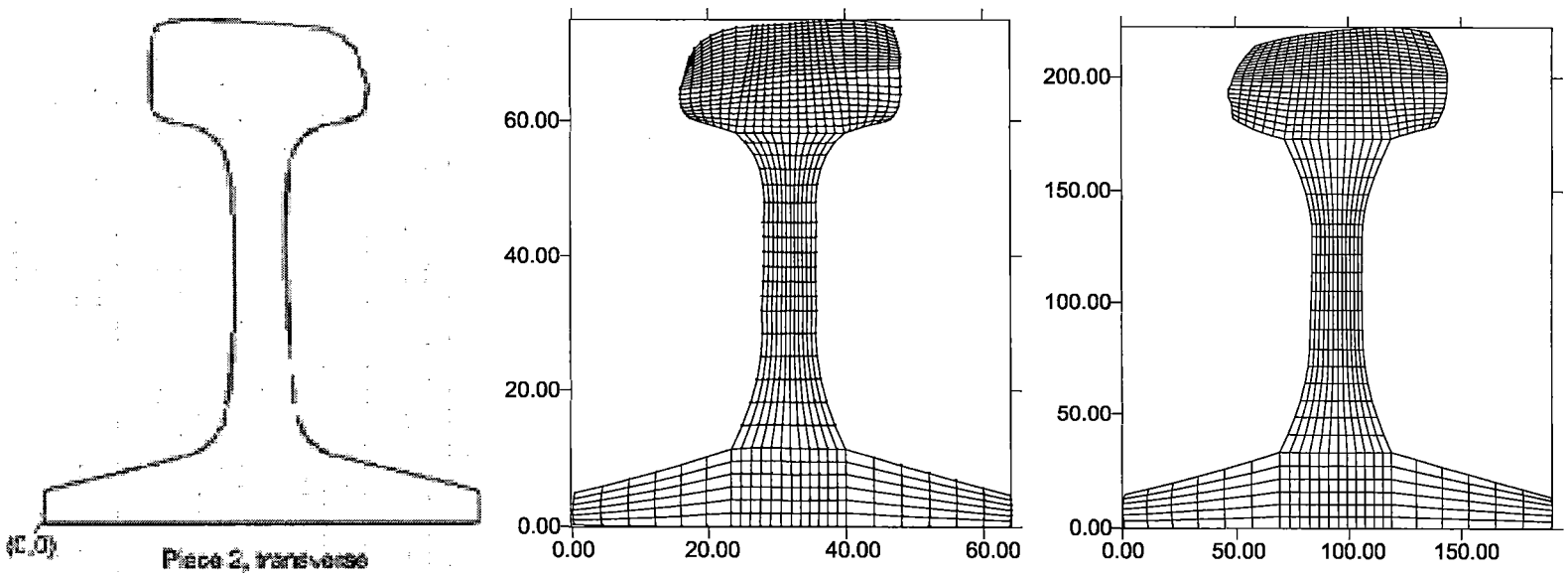

a) NIST delivered profile b) Old grid c) New corrected grid

Fig. 2

Old and new grids for NIST sample #2

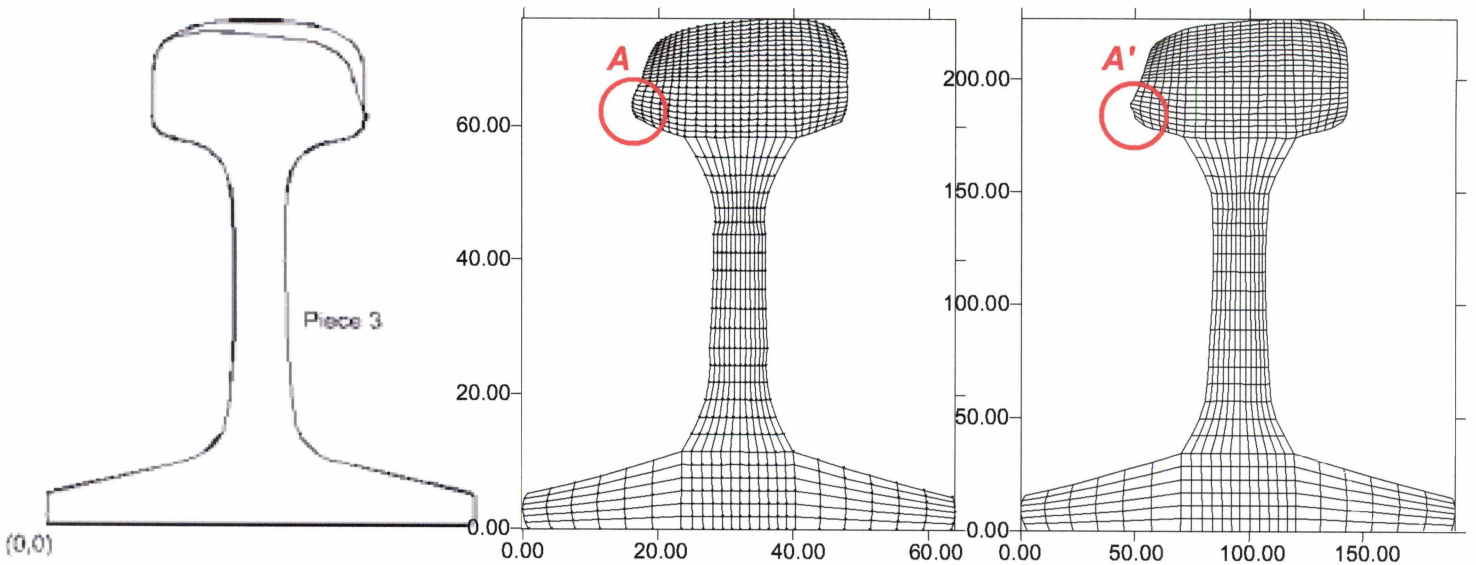

a) NIST delivered profile

b) Old grid

c) New corrected grid

Fig. 3

Old and new grids for NIST sample #3

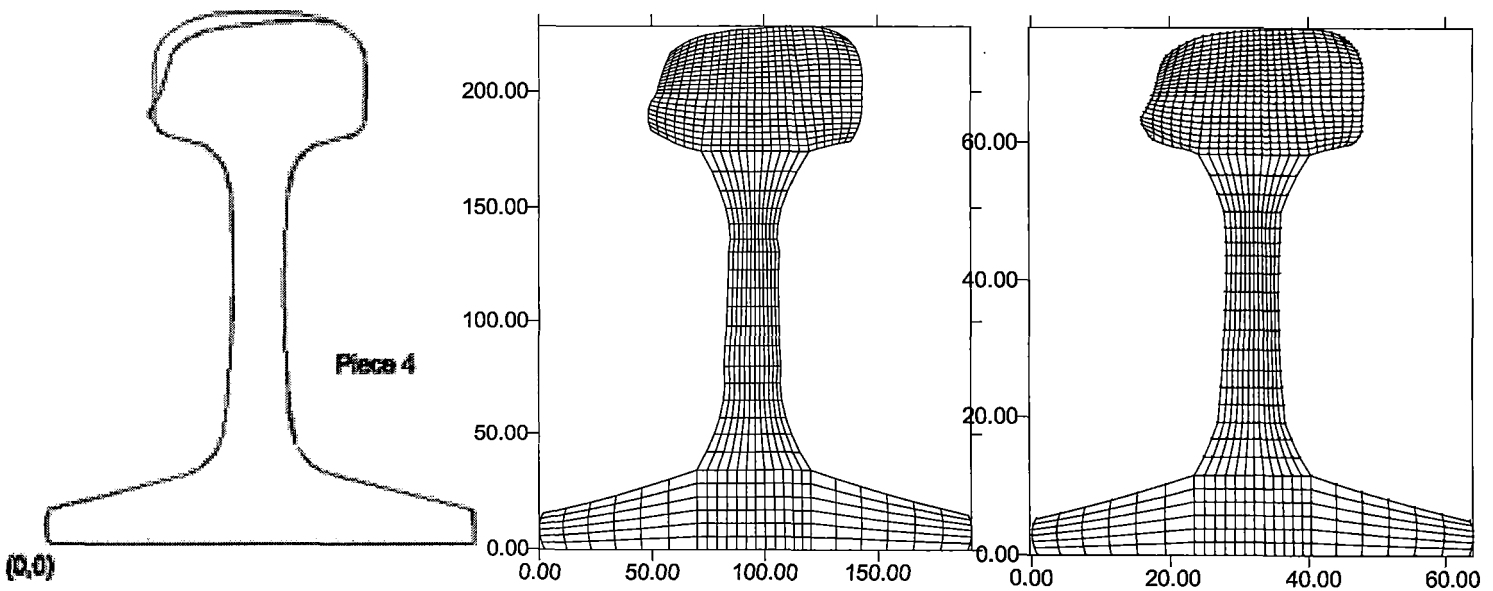

a) NIST delivered profile b) Old grid c) New corrected grid

Fig. 4

Old and new grids for NIST sample #4

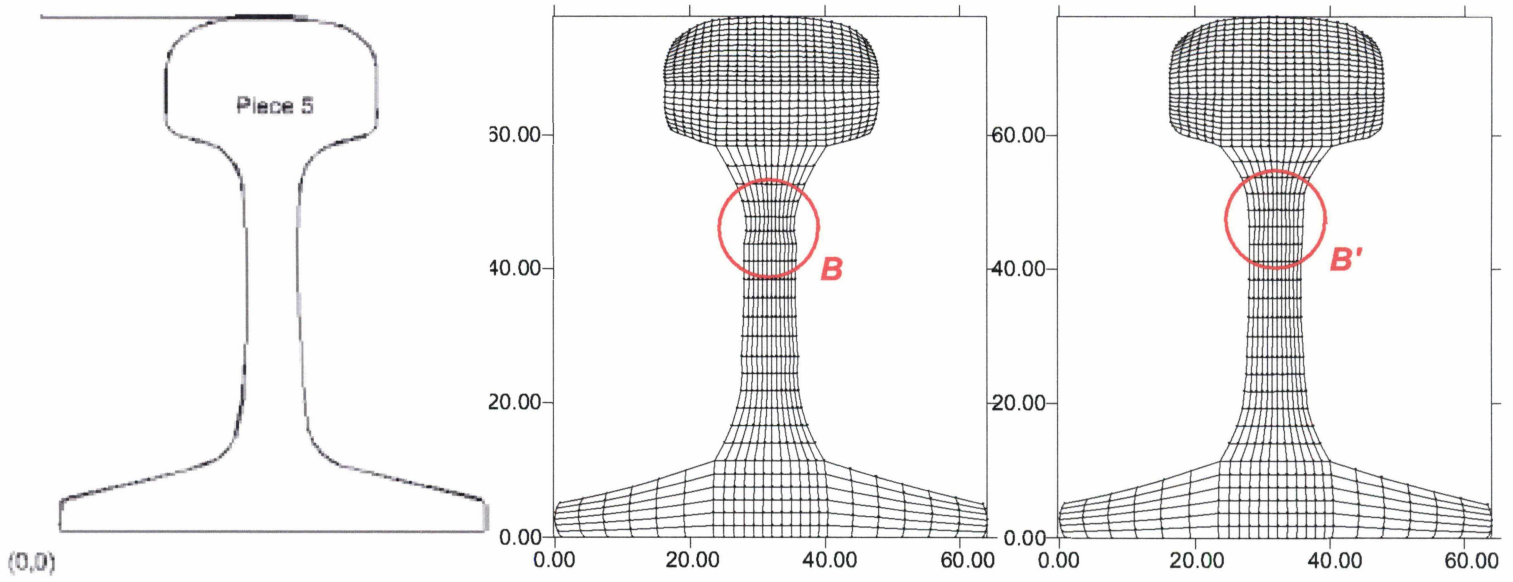

a) NIST delivered profile b) Old grid c) New corrected grid

Fig. 5

Old and new grids for NIST sample #5

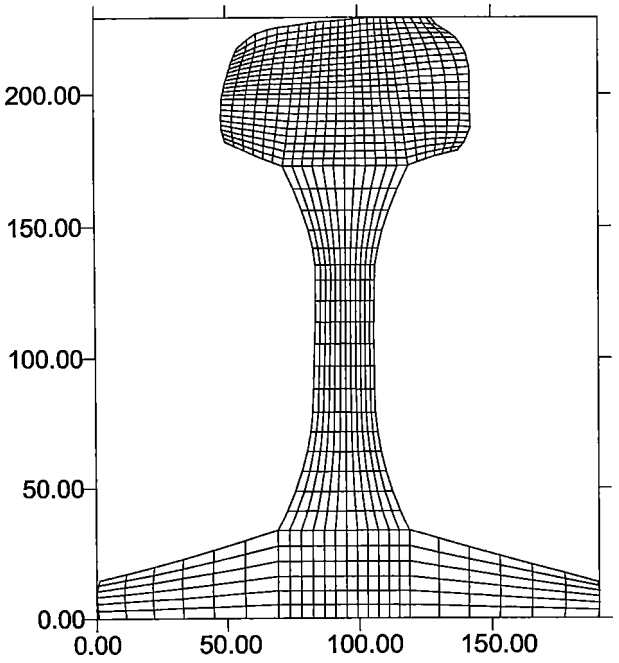

a) old grid, 971 nodes, 888 elements

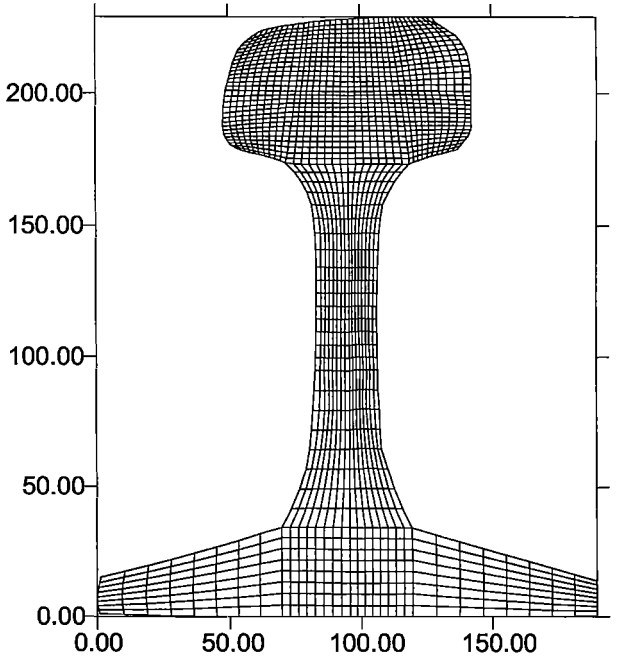

b) new grid, 1835 nodes, 1720 elements

Fig. 6

Old and new FEM/FDM grids for sample #1

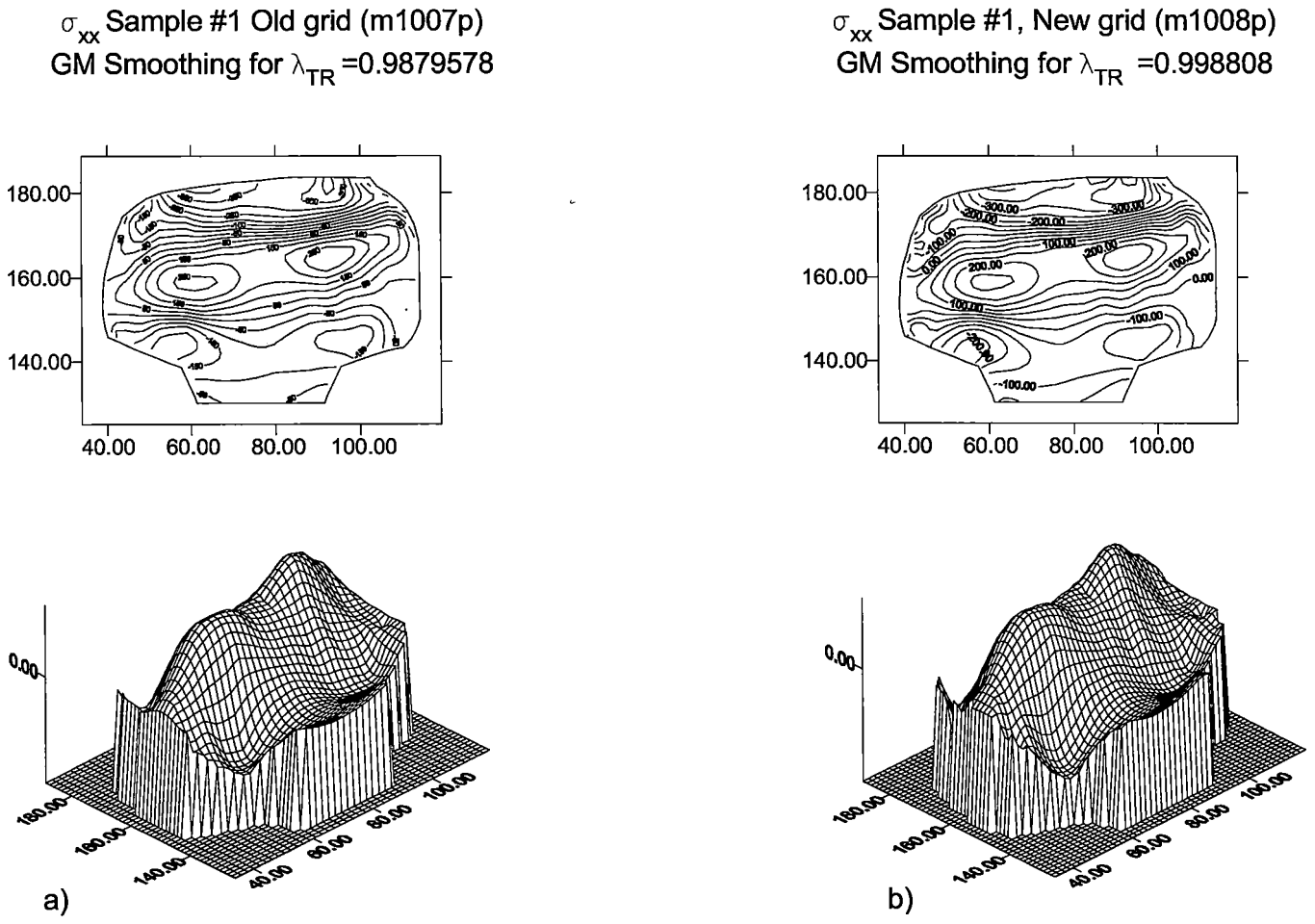

Fig. 7

Solutions for σ_{xx} for old and new grids compared

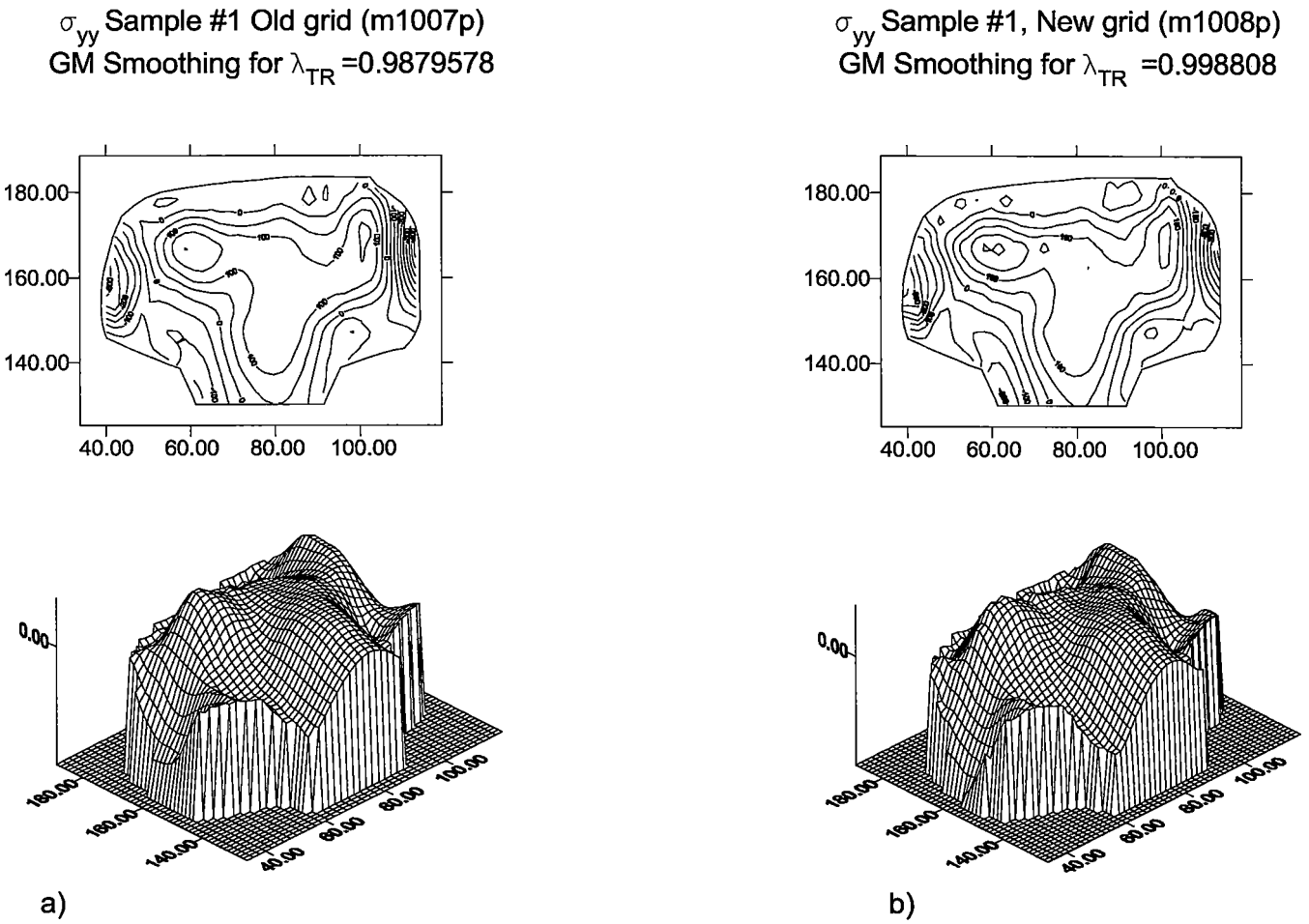

Fig. 8

Solutions for σ_{yy} for old and new grids compared

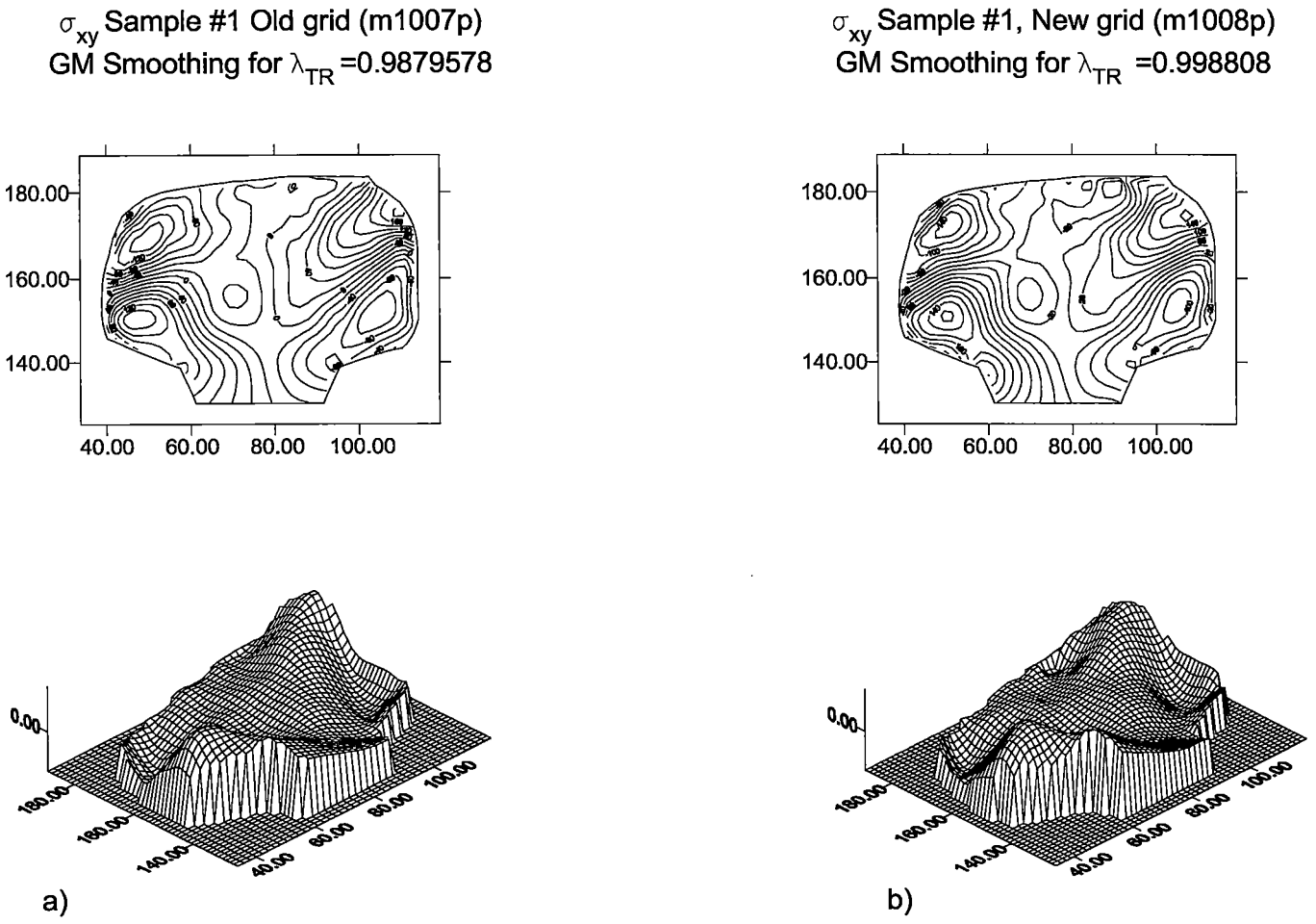

Fig. 9

Solutions for σ_{xy} for old and new grids compared

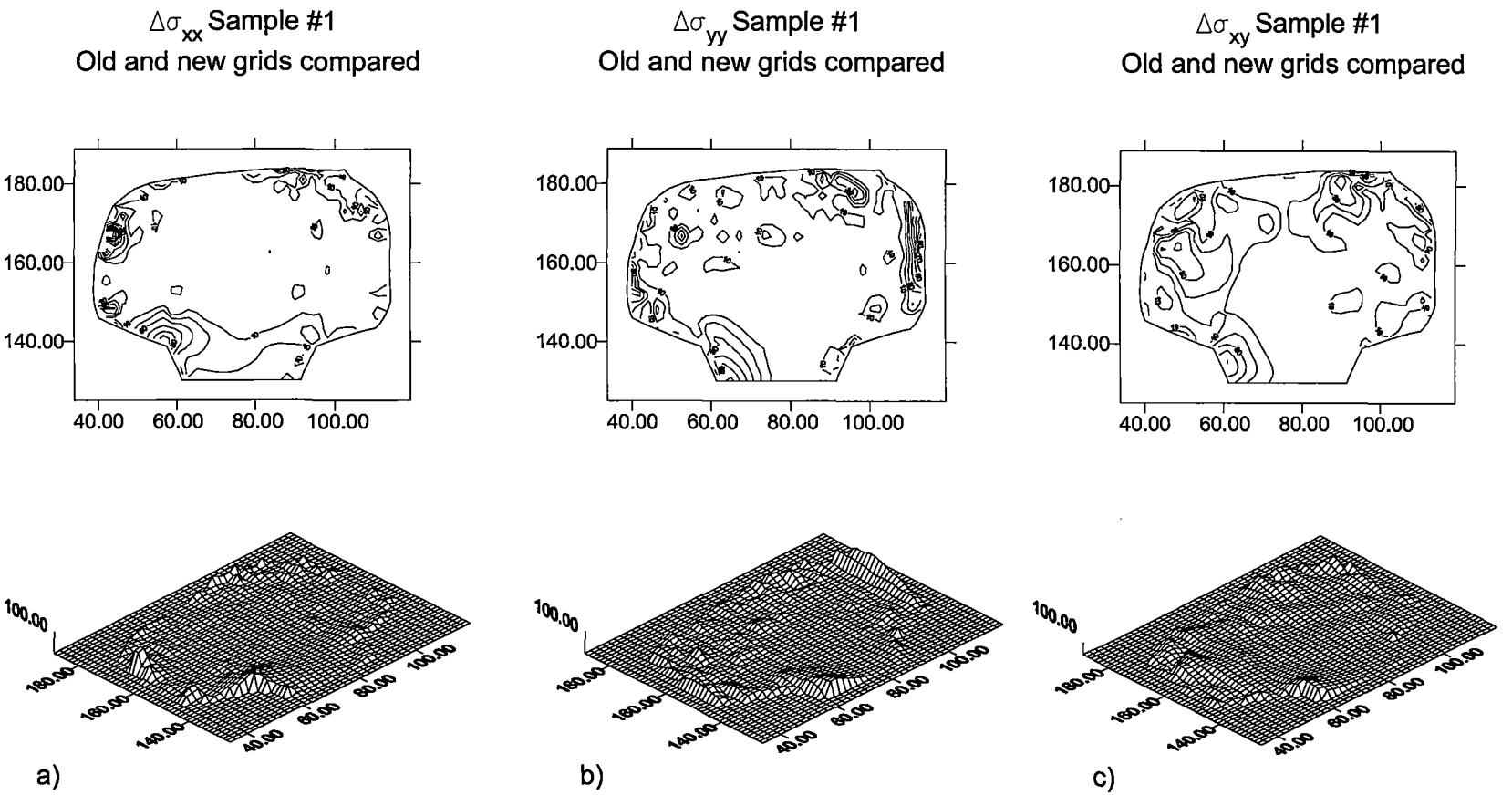

Fig. 10

Differences of stresses (absolute values) between the old and new grids

3. 3D ANALYSIS OF NEW RAIL RESIDUAL STRESS DATA

As mentioned, the research task listed as this item was impossible to be performed due to lack of the new data and will be performed, as planned, when the new data is available. To compensate for this lack, analysis of the old ND data was repeated for all rail samples #1-5 with all the improvements/ advancements on both 2D and 3D levels worked out lately (new grids, new strategies in GM smoothing, *a posteriori* experimental error estimates, etc.). A complete description of those results is provided in the final report [4], here exemplary results obtained for sample #1 will be shown.

In Fig. 1a original profile of sample #1 as delivered by NIST [9], in Fig. 1b the old and in Fig. 1c the new corrected grids are shown. The improvements are visible e.g., on the running surface of the rail or vertical parts of the head profile.
In Fig. 11-13 presented are 2D results obtained for the considered rail on the new grid (Fig. 11a, 12a, 13a) altogether with reference 2D solutions obtained for the old grid (Fig. 11b, 12b, 13b). In Fig. 11c, 12c and 13c contour/surface plots of differences in solutions for the new and old grids are shown.

The first impression when examining solutions in Fig. 11-13 might be that there are no essential differences between solutions for the new and old grids. However, when one sees the plots of differences[5] between those two families of solutions (Figs. 11c, 12c and 13c) it is clearly visible that the representation of the profile of rail sample does affect the solutions – especially in the peripheral areas of the head and that the differences might be at certain points as high as 100 MPa for σ_{xx} stress component, 240 MPa for σ_{yy} stress component and 140 MPa for σ_{xy} stress component. Shear stress component is different from the other two in-plane stresses in that it exhibits the biggest fluctuations in the middle of the head. This results confirms the aforementioned feature of the shear stress that,

---

5 absolute values of to be exact

being numerically reconstructed, is subject to the biggest sensitivity to the approximation parameters.

The outcome of this test proves the thesis that pretty minor differences in representation of the rail profile might lead to significant differences in the solutions so having as exact as possible representation of the rail profiles is crucial.

Results of analysis for reconstructed 3D solutions are presented in Figs. 14-17. Figs. 14a, 15a, 16a and 17a contain stress patterns obtained on the old grid, Figs. 14b, 15b, 16b and 17b stress patterns obtained on the new grid. Again, there are no bigger differences spotted in the solutions but there are certain differences between those two solution families thus the above listed conclusions for the 2D levels hold also for 3D level.

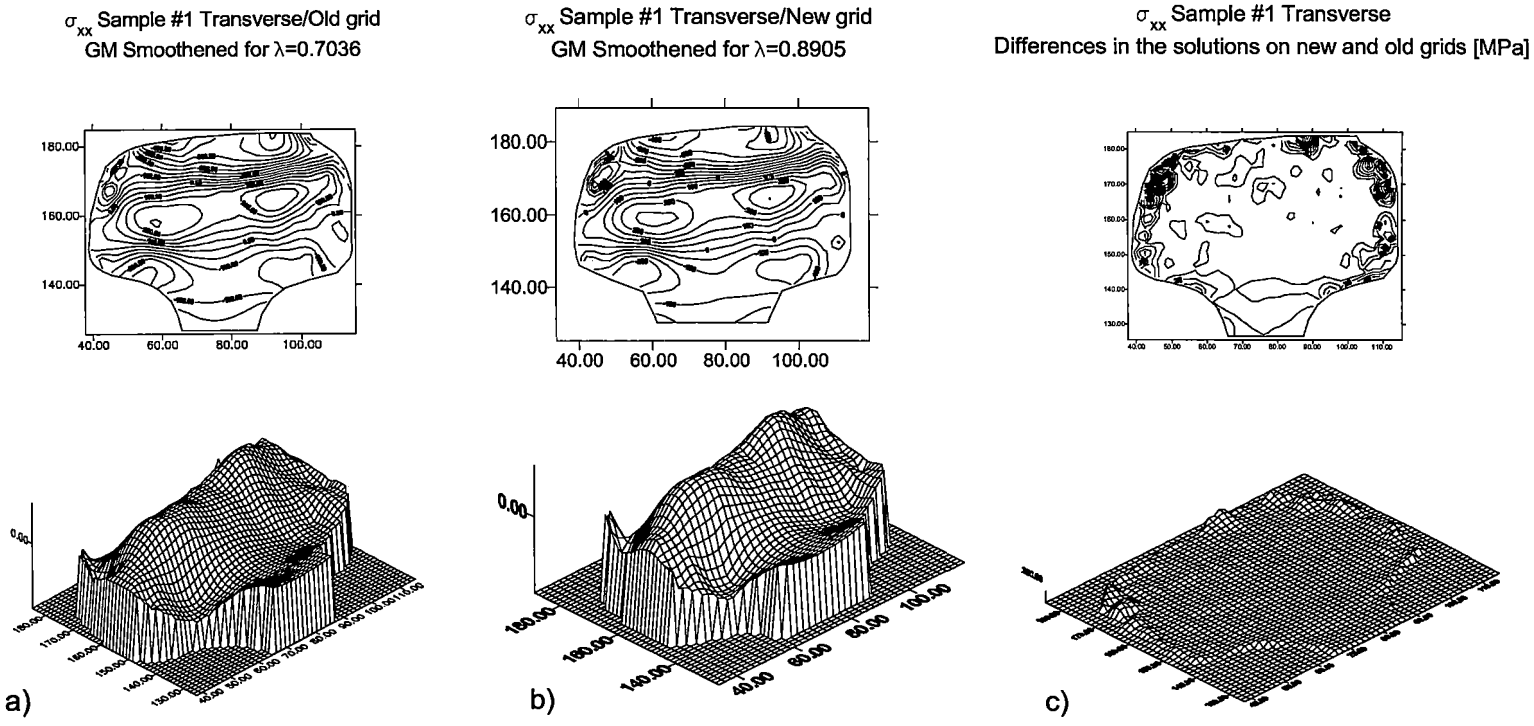

Fig. 11

Solutions for σ_{xx} for old and new grids compared

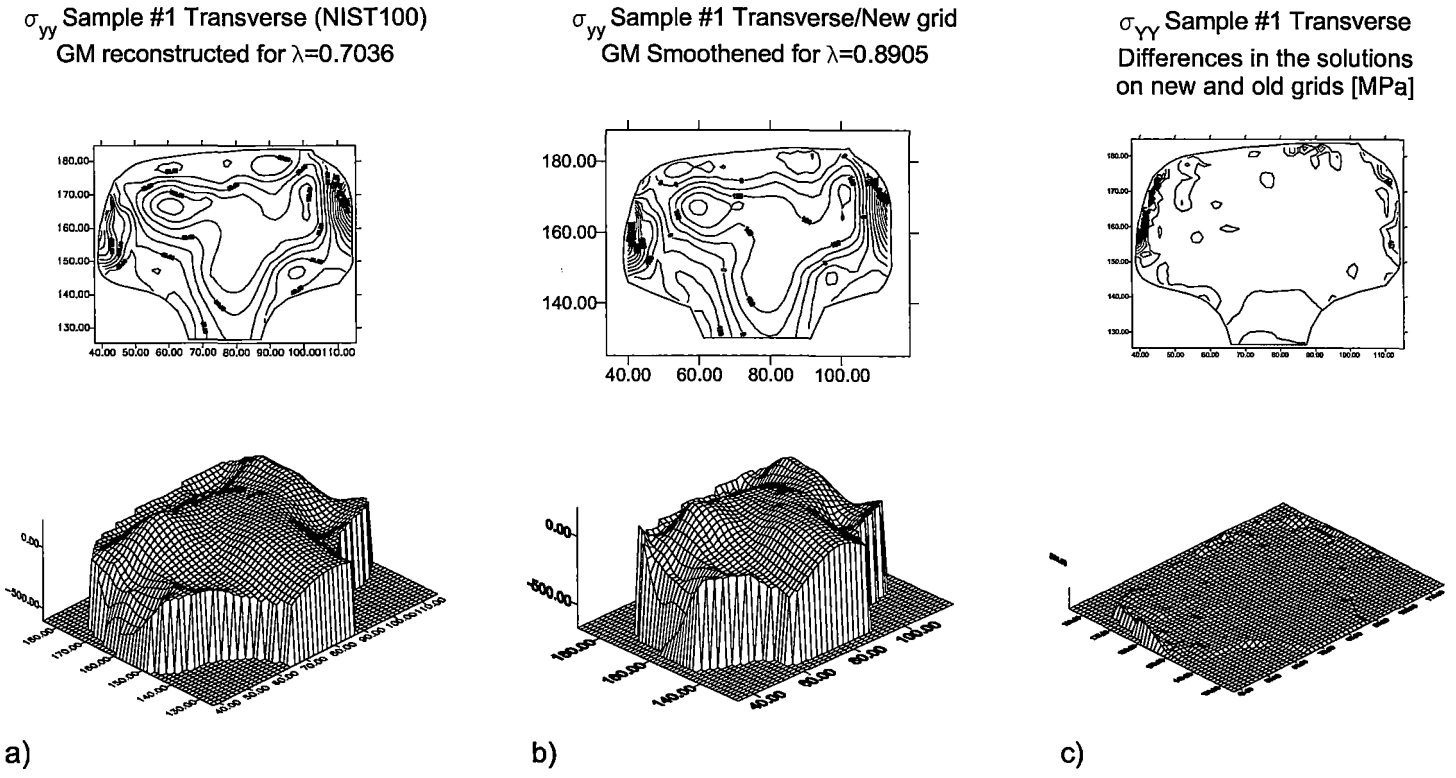

Fig. 12

Solutions for σ_{yy} for old and new grids compared

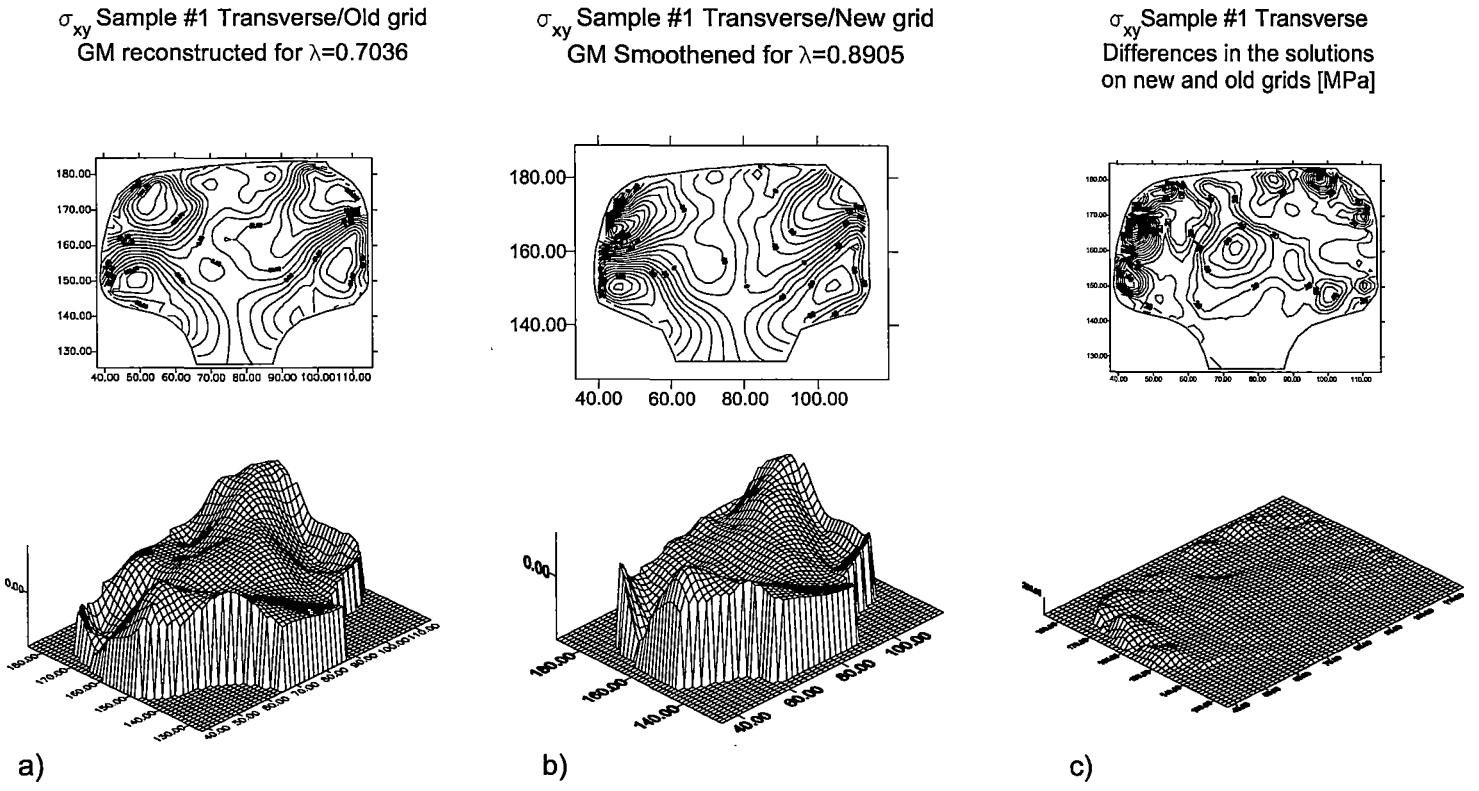

Fig. 13

Solutions for σ_{xy} for old and new grids compared

σ_{xx} Sample #1/Old grid,

3D State Restored by TOS-3DRS [MPa]

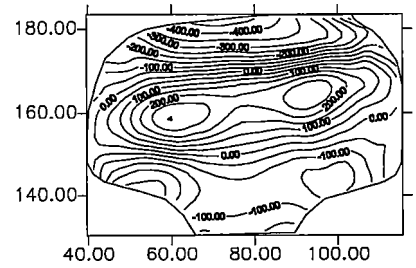

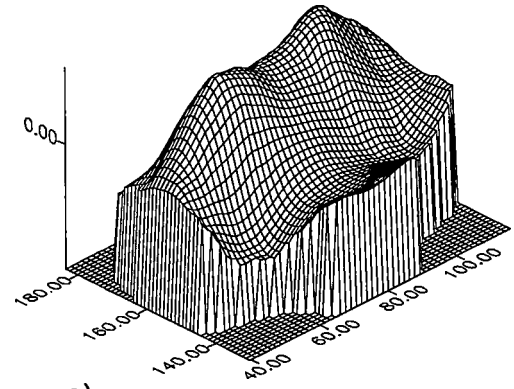

a)

Fig. 14

Comparison of 3D residual stress σ_{xx}

σ_{xx} Sample #1/New grid,
3D State Restored by TOS-3DRS [MPa]

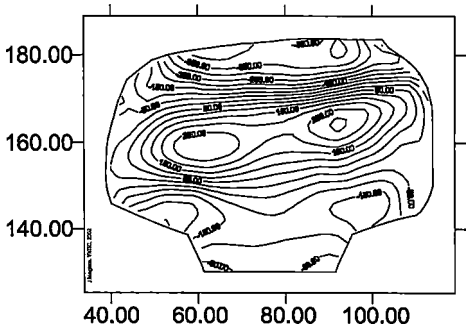

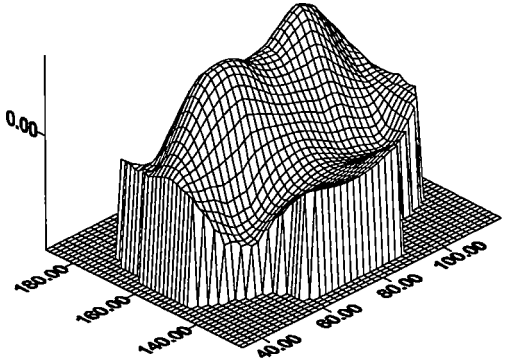

b)

on the old and new grids

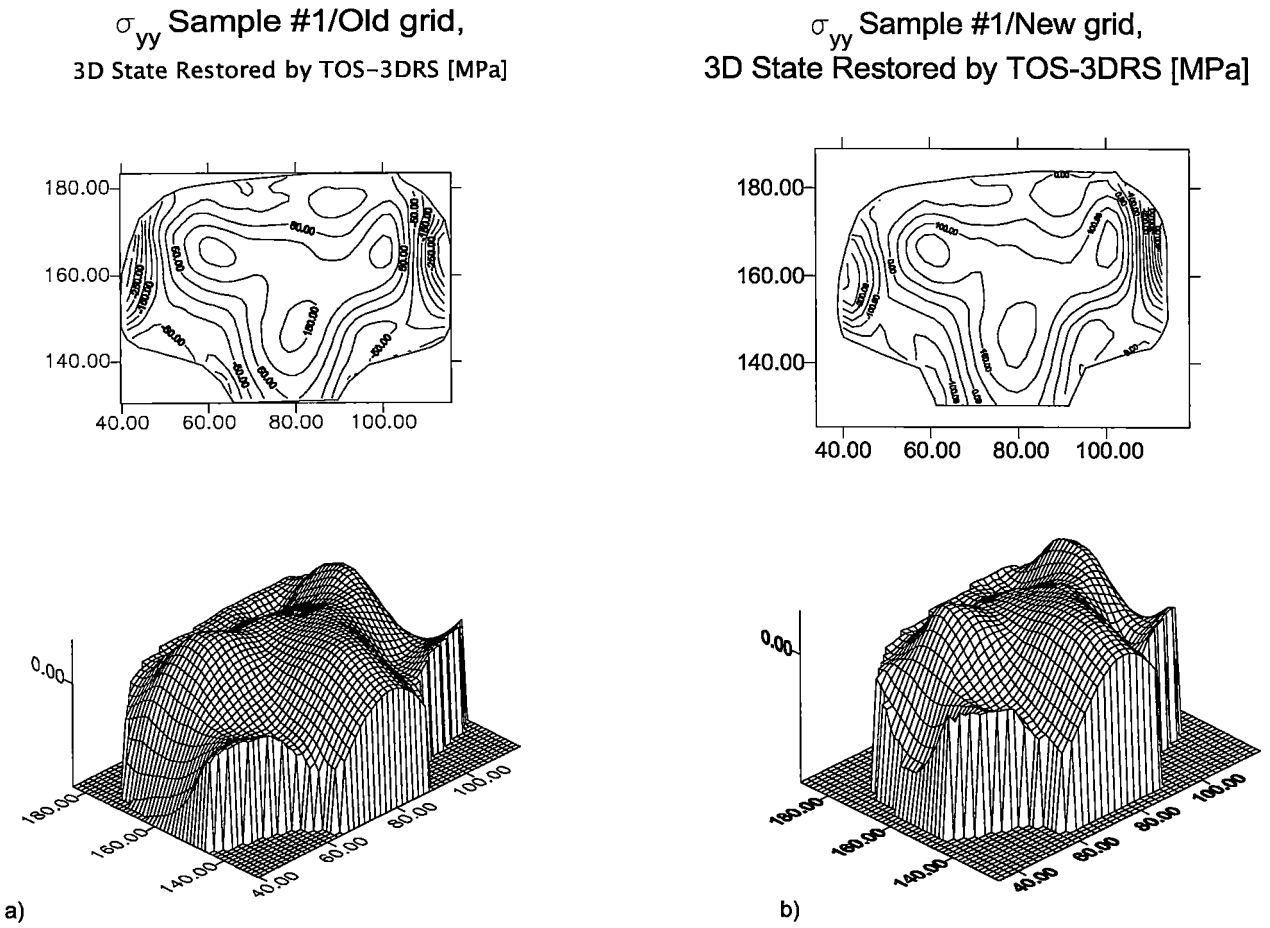

Fig. 15

Comparison of 3D residual stress σ_{yy} on the old and new grids

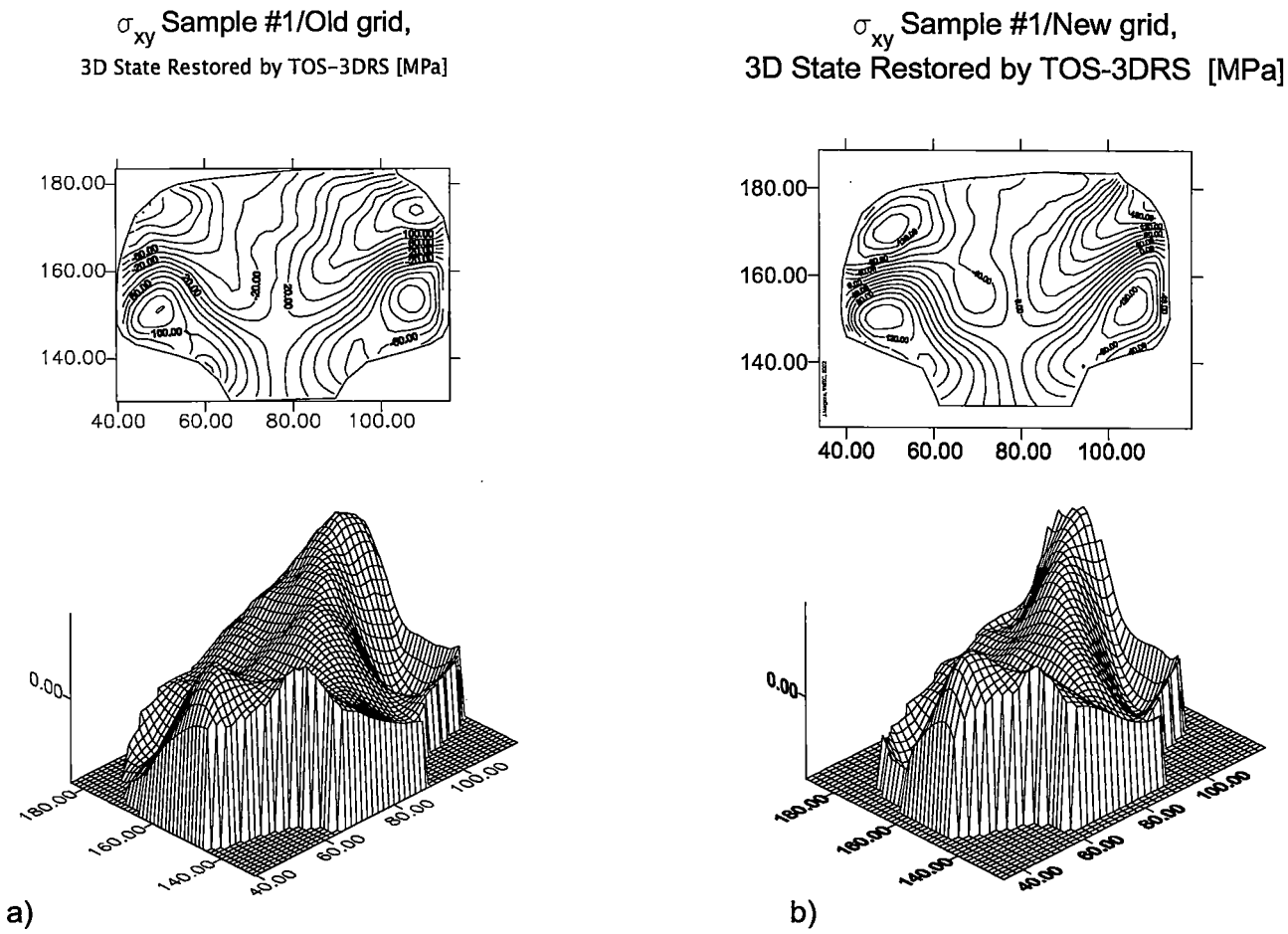

Fig. 16

Comparison of 3D residual stress σ_{xy} on the old and new grids

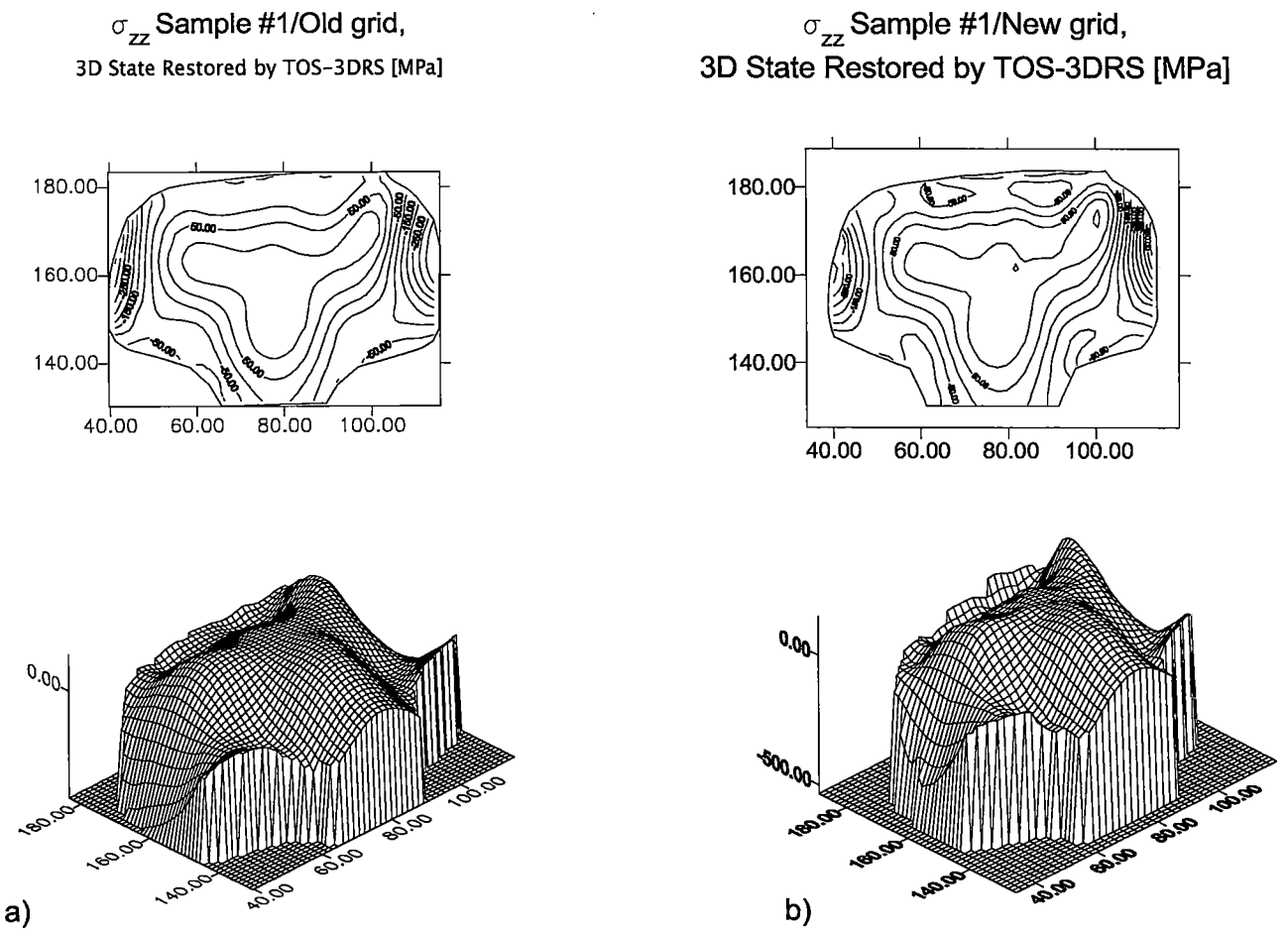

Fig. 17

Comparison of 3D residual stress σ_{zz} on the old and new grids

4. A STUDY OF THREE SLICE PROCEDURE

4.1 Introductory remarks

The transverse/oblique slicing (T/O-S) method, proposed at the end of the 80's, has been investigated so far as a two-slice procedure, in both possible versions of rotation of the oblique slice: firstly around the horizontal axis *X* [5,6], secondly around the *Z* axis [12][6]. Both setups were proved workable, the iterative procedures convergent and stable. Out of those two, the originally examined version [5,6] was indicated as better and in fact so far it has been the only one that found practical applications.

In this study another possible setups are considered, namely the proposed by Orkisz [13] three slice procedures T/O/O and O/T/O (Fig. 18b and 18c) and the T/O/T[7] setup adopted recently in the Agreement [14] (Fig. 18e).

The advantage a three slice procedure has over a two slice one is that the third slice might be used either for performing independent computation (thus provide a means for verification of assumptions or validation of the results) or it might be processed simultaneously with the two other slices for additional gain in quality of results or simplification of certain relations[8].

4.2 Three slice procedures – general formulation

The theoretical background for three slice procedures considered here will be now given. As far as the T/O/O and O/T/O setups are considered, the concept was worked out in 1990 by Orkisz [13], the T/O/T concept was proposed during

---

[6] of course, directions of the oblique slice around both of those axes simultaneously is also possible but was not considered due to complexity of transformation relations and no gain in accuracy; the two-slice scheme O/O shown in Fig. 18d was not considered, too

[7] also called "N" for resemblance of this setup to the capital N letter

[8] in that case it will not be used as a source of redundant information for improvements in data reduction results

the author's scientific visit to the Volpe Center in summer 2002.

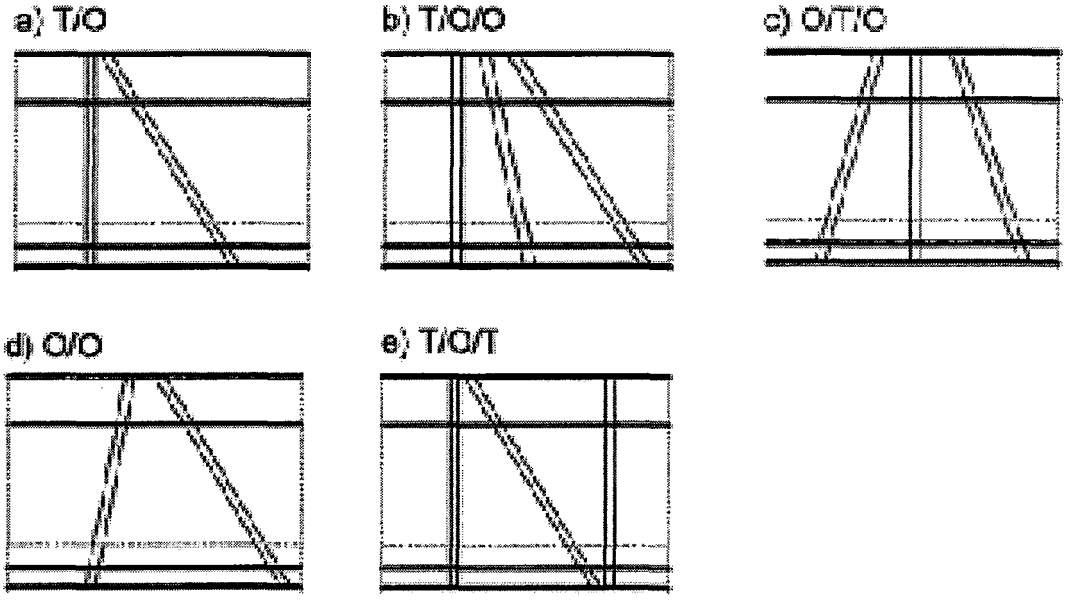

Fig. 18

Sectioning schemes, inclination to the vertical axis

Let us consider now a general three slice T/O/O procedure as schematically shown in Fig. 19. in this setup there are one transverse slice and two oblique slices, inclined under the angles α and β.

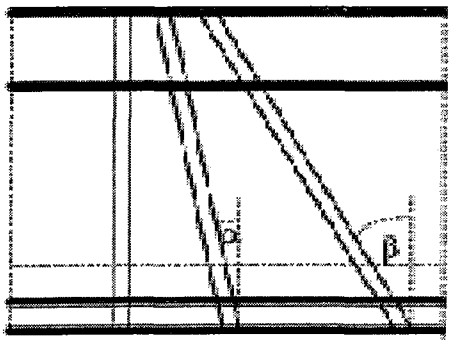

Fig. 19

A general, three slice procedure

In that case – and assuming the body is not sectioned yet – the stress states in the oblique slices might be expressed as tensor transformation of the stress state in the transverse slice as:

1. In the slice inclined by α:

$$\begin{aligned}
\sigma^{\alpha}{}_{ss} &= \sigma_{xx} \\
\sigma^{\alpha}{}_{st} &= \sigma_{xy}\cos\alpha + \sigma_{zx}\sin\alpha \\
\sigma^{\alpha}{}_{tt} &= \sigma_{yy}\cos^2\alpha + \sigma_{zz}\sin^2\alpha - \sigma_{zy}\sin 2\alpha \\
\sigma^{\alpha}{}_{nn} &= \sigma_{yy}\sin^2\alpha + \sigma_{zz}\cos^2\alpha + \sigma_{zy}\sin 2\alpha \qquad (1) \\
\sigma^{\alpha}{}_{ns} &= \sigma_{xy}\sin\alpha + \sigma_{zx}\cos\alpha \\
\sigma^{\alpha}{}_{nt} &= \frac{1}{2}\sigma_{yy}\sin 2\alpha - \frac{1}{2}\sigma_{zz}\sin 2\alpha + \sigma_{zy}\cos 2\alpha .
\end{aligned}$$

2. In the slice inclined by β:

$$\begin{aligned}
\sigma^{\beta}{}_{ss} &= \sigma_{xx} \\
\sigma^{\beta}{}_{st} &= \sigma_{xy}\cos\beta + \sigma_{zx}\sin\beta \\
\sigma^{\beta}{}_{tt} &= \sigma_{yy}\cos^2\beta + \sigma_{zz}\sin^2\beta - \sigma_{zy}\sin 2\beta \\
\sigma^{\beta}{}_{nn} &= \sigma_{yy}\sin^2\beta + \sigma_{zz}\cos^2\beta + \sigma_{zy}\sin 2\beta \qquad (2) \\
\sigma^{\beta}{}_{ns} &= \sigma_{xy}\sin\beta + \sigma_{zx}\cos\beta \\
\sigma^{\beta}{}_{nt} &= \frac{1}{2}\sigma_{yy}\sin 2\beta - \frac{1}{2}\sigma_{zz}\sin 2\beta + \sigma_{zy}\cos 2\beta .
\end{aligned}$$

Then, the perpendicular to the transverse slice face stress components σ_{zz}, σ_{xz} and σ_{zy} might be expressed as [13]:

$$\sigma_{zz} = \sigma_{yy}\frac{\cos\alpha\cos\beta}{\sin\alpha\sin\beta} + \frac{\sigma^{\alpha}{}_{tt}\sin 2\beta - \sigma^{\beta}{}_{tt}\sin 2\alpha}{2\sin\alpha\sin\beta\sin(\alpha-\beta)}$$

$$\sigma_{xz} = \sigma_{xy}\frac{\cos\alpha}{\sin\alpha} - \sigma^{\alpha}{}_{st}\frac{1}{\sin\alpha} = \sigma_{xy}\frac{\cos\beta}{\sin\beta} - \sigma^{\beta}{}_{st}\frac{1}{\sin\beta} \qquad (3)$$

$$\sigma_{zy} = \sigma_{yy}\frac{\sin(\alpha+\beta)}{2\sin\alpha\sin\beta} - \frac{\sigma^{\alpha}{}_{tt}\sin^2\beta - \sigma^{\beta}{}_{tt}\sin^2\alpha}{2\sin\alpha\sin\beta\sin(\alpha-\beta)}$$

The advantage of the three slice procedure is visible in relations (1), (2) and (3) by:

1. additional information about validity of assumption that the stress state is independent of the axial coordinate Z thanks to the fact that $\sigma_{xx} = \sigma^{\alpha}{}_{ss} = \sigma^{\beta}{}_{ss}$ for each point of the rail cross-section;
2. additional information for verification of the quality of experimental technique thanks to relation for σ_{xz} in 2nd of the Eqs. (3)
3. a direct relation for the σ_{zy} stress component (if required); in the T/O setup it had to be determined from a boundary value problem:

$$\Delta\sigma_{yz} = 0 \quad in \ V, \quad \sigma_{yz}\frac{dy}{dx} = \sigma_{xz} \quad on \ \partial V \qquad (4)$$

A particularly interesting cases of the three slice procedure are symmetrical O/T/O (as in Fig. 18c), where $\alpha = -\beta$ and the "N" ($\beta = 0$, T/O/T in Fig. 18e) setups. The symmetrical O/T/O and the "N" cases are analyzed in the next two sections.

4.3 Symmetrical O/T/O procedure

The case when $\alpha = -\beta$ is interesting by the fact that for this setup and the symmetric/anti-symmetric behavior of the sine and cosine functions, additional advantages might be achieved. Let us denote $\sigma^{+}{}_{ij} = \frac{1}{2}(\sigma^{\alpha}{}_{ij} + \sigma^{-\alpha}{}_{ij})$,

$\sigma^{-}_{ij} = \frac{1}{2}(\sigma^{\alpha}_{ij} - \sigma^{-\alpha}_{ij})$. Then the following relations hold for transformation of the stress state from the transverse slice to the σ^{+} and σ^{-} tensors:

$$\sigma^{+}_{ss} = \sigma_{xx},\ \sigma^{+}_{st} = \sigma_{xy}\cos\alpha,\ \sigma^{+}_{tt} = \sigma_{yy}\cos^2\alpha + \sigma_{zz}\sin^2\alpha,$$
$$\sigma^{+}_{nn} = \sigma_{yy}\sin^2\alpha + \sigma_{zz}\cos^2\alpha,\ \sigma^{+}_{ns} = \sigma_{zx}\cos\alpha,\ \sigma^{+}_{nt} = \sigma_{zy}\cos 2\alpha \quad (5)$$

$$\sigma^{-}_{ss} = 0,\ \sigma^{-}_{st} = \sigma_{zx}\sin\alpha,\ \sigma^{-}_{tt} = -\sigma_{zy}\sin 2\alpha,$$
$$\sigma^{-}_{nn} = \sigma_{zy}\sin 2\alpha,\ \sigma^{-}_{ns} = \sigma_{xy}\sin\alpha,\ \sigma^{-}_{nt} = \frac{1}{2}\sigma_{yy}\sin 2\alpha - \frac{1}{2}\sigma_{zz}\sin 2\alpha \quad (6)$$

In that case, the relations for the stresses totally lost during sectioning might be expressed as:

$$\sigma_{zz} = -\sigma_{yy}\frac{\cos^2\alpha}{\sin^2\alpha} + \frac{\sigma^{+}_{tt}}{\sin^2\alpha}$$
$$\sigma_{xz} = -\sigma^{-}_{st}\frac{1}{\sin\alpha} \quad (7)$$
$$\sigma_{zy} = -\sigma^{-}_{tt}\frac{1}{\sin 2\alpha}$$

Relations (5)-(7), thanks to the tensor transformation rule, are simplified now and the influence of the shear stresses might be controlled (it is strengthened in the case of subtraction and weakened in the case of addition of the stresses from the counterpart oblique slices. There is, too, an additional equation for controlling the quality of either the approximation or the experiment itself:

$\sigma_{xx} = \sigma^{+}_{ss}$ (as previously in the T/O procedure)
$\sigma^{+}_{st} = \sigma_{xy}\cos\alpha$ (additional relation) (8)

4.4 The "N" setup

The advantage of the "N" type setup, where there are two transverse slices and on oblique (Fig. 18e), is that this setup lends itself well to performing the vital check of fulfillment of the basic assumption about independence of the stress state of the longitudinal coordinate *Z*, and, in case such dependence is confirmed, to introduce corrections.

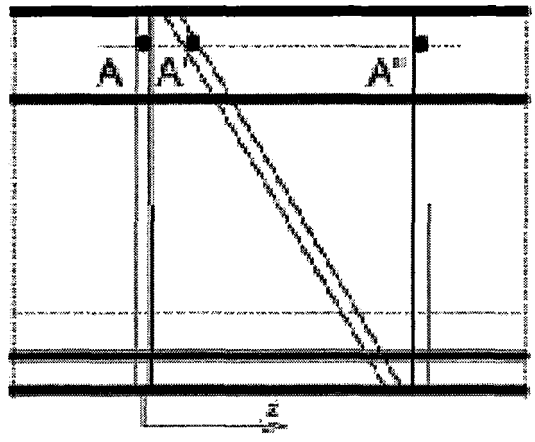

Fig. 20
Evaluating fulfillment of basic assumptions

The validation procedure might resort to the fact that due to the features of the transformation rule that nominally (if the *Z*-axis independence assumption holds) guaranties that horizontal stress is exactly the same in all three slices. If not, there are now three different but corresponding to each other points: A, A', A" (Fig. 20) thus for each such triplets of points, a second order approximation of the stress variation might be assumed:

$$\sigma_{ij}(x,y,z) = az^2 + bz + \sigma_{ij}(x,y,0) \qquad (9)$$

where the parameters a and b are found from the interpolation conditions:

$$\sigma_{xx}(x,y,z') = a(z')^2 + b(z') + \sigma_{ij}(x,y,0) = \sigma^{\alpha}{}_{ss} \qquad (10)$$

$$\sigma_{xx}(x,y,z'') = a(z'')^2 + b(z'') + \sigma_{ij}(x,y,0) = \sigma_{xx}(x,y,z'')$$

In such a way, by repetition of the procedure at locations of all data points, a spatial distribution of the $a = a(x,y)$ and $b = b(x,y)$ parameters might be determined and this might be used for enhanced analysis of experimental data, where with help of FEM (or equivalent) approach corrections to the data might be computed[9].

4.5 Tests for simulated data for symmetrical O/T/O

It was planned in the proposal to test the approach on the simulated experimental data obtained from the hybrid finite element method program by M. Hołowiński [15]. This program is dedicated to computing 3D residual stress states in railroad rails based on shake-down type analysis and the minimum complementary energy principle and its results were extensively used in simulation tests performed, either for the original T/O formulation [5,6] or its *X-T* plane version [12]. Thus it seemed to be natural choice to propose to test the three slice procedure(-s) also for this pseudo-data. But, unfortunately, due to internal restrictions of this program[10] and the fact that it arbitrarily limits the stress tensor to the σ_{xx}, σ_{xy}, σ_{yy} and σ_{zz} components, the aforementioned tests were not possible. The source of this problem lies in the fact that if the σ_{xz} and σ_{yz} stresses are identically equal to zero in the whole domain, then the tensor transformation rule gives:

$$\sigma^{\alpha}{}_{ss} = \sigma^{-\alpha}{}_{ss} = \sigma_{xx}$$

$$\sigma^{\alpha}{}_{st} = \sigma^{-\alpha}{}_{st} = \sigma_{xy}\cos\alpha$$

---

9 it is also conceivable to employ least square approach and obtain global values of parameters a and b

10 so called 10β linear approximation for the stresses spanned

$$\sigma^{\alpha}{}_{tt} = \sigma^{-\alpha}{}_{tt} = \sigma_{yy}\cos^2\alpha + \sigma_{zz}\sin^2\alpha$$

$$\sigma^{\alpha}{}_{nn} = \sigma^{-\alpha}{}_{nn} = \sigma_{yy}\sin^2\alpha + \sigma_{zz}\cos^2\alpha \qquad (11)$$

$$\sigma^{\alpha}{}_{ns} = -\sigma^{-\alpha}{}_{ns} = \sigma_{xy}\sin\alpha$$

$$\sigma^{\alpha}{}_{nt} = -\sigma^{-\alpha}{}_{nt} = \frac{1}{2}\sigma_{yy}\sin 2\alpha - \frac{1}{2}\sigma_{zz}\sin 2\alpha$$

due to anti-symmetric behavior of the sin(x) function and symmetric behavior of the cos(x) function. As it may be seen, out of the six stress components only σ_{ns} and σ_{nt} are different (anti-symmetric, in fact) in the two corresponding oblique slices, the rest is exactly the same. Therefore, the

$$\sigma^{+}{}_{ij} \equiv \sigma^{\pm\alpha}{}_{ij}, \quad \sigma^{-}{}_{ij} \equiv 0 \qquad (12)$$

for all components except for σ_{ns} and σ_{nt}, but those two component are neglected[11] to simplify the FEM modeling of rail samples. But this renders the three slice procedure equal to the classic two slice T/O procedure thus no benefits of three slice procedure might be seen in the results.

The tests for the three slice procedure will have to wait then for the new ND data where this concept is explored[12].

5. 3D ANALYSIS OF RESIDUAL STRESSES FOR THE CASE OF SEVERAL INDEPENDENT DATA SERIES

The analysis of 3D residual stress reported here was performed for the case when for a sample several independent data series were available. Happily, the neutron diffraction technique on the 2D level is non-destructive thus it was

---

11 it was proved [5, 6] that this might be done with error amplitude of ca. 0.5%

12 as is the "N" setup

possible to perform repeated scans of a sample (sample #3 data of [9]) and collect several data series. In the case of this particular sample there were three data series collected, one for a coarse 5x5 mm grid, the second for a fine 3x3 mm grid, and the third one for the coarse but spatially extended grid. In fact, the first and third data series are the same for majority of data points except for four rows[13] of data points beneath the limit for all other data series/samples line of y=147.7 mm (in Fig. 21 the gray squares mark data series #1, the white ones beneath them – data series #3).

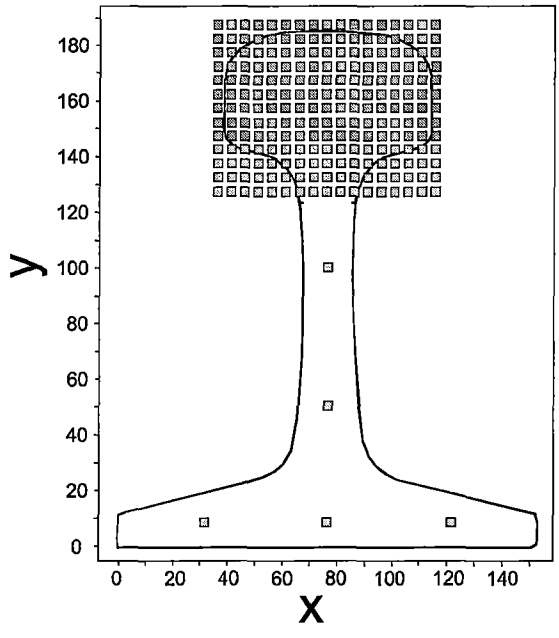

Fig. 21

Data series #1 and #3, NIST ND examinations (figure source [9])

The main aim of this analysis was to test whether a simultaneous processing of independent data sets will provide better results while not affecting convergence and stability of solutions.

[13] and several other in the web and foot of the rail

In the report [2] enclosed in this volume, the details of 2D analysis were discussed and the results obtained were shown. The outcome of the tests on the 2D level was that the 2D procedure was convergent and stable and that – due to apparently not equal numbers of the qualified data points in those two sets (275 vs. 105) – the final patterns bore a strong resemblance to the fine grid data smoothing results.

On the 3D level the procedure was also proved to be stable and convergent though – alike to the 2D level – the solutions are more noisy and showing small fluctuations in their stress patterns (Fig. 22a-d). Not surprising, the conclusion about similarity of the result to the fine data patterns is also confirmed on the 3D level.

A general conclusion of this test is that combined processing of independent data sets gave mixed results. From numerical point of view, it is more demanding as it e.g., requires finding proper weights between the data sets. However, despite those cons, it might be a valuable addition to the physically based approximation technique.

6. CONCLUSIONS

In the report presented were results of the newest research dedicated to 3D procedure. They regarded such issues like:

- improvements in algorithms (three slice procedure)
- improvements in data preparation (new FE/FDM grids)
- improvements in overall data reliability (*a posteriori* error estimates)
- study of influence of the distribution of nodes and/or boundary representation on the final results
- study of grid density influence on the final result

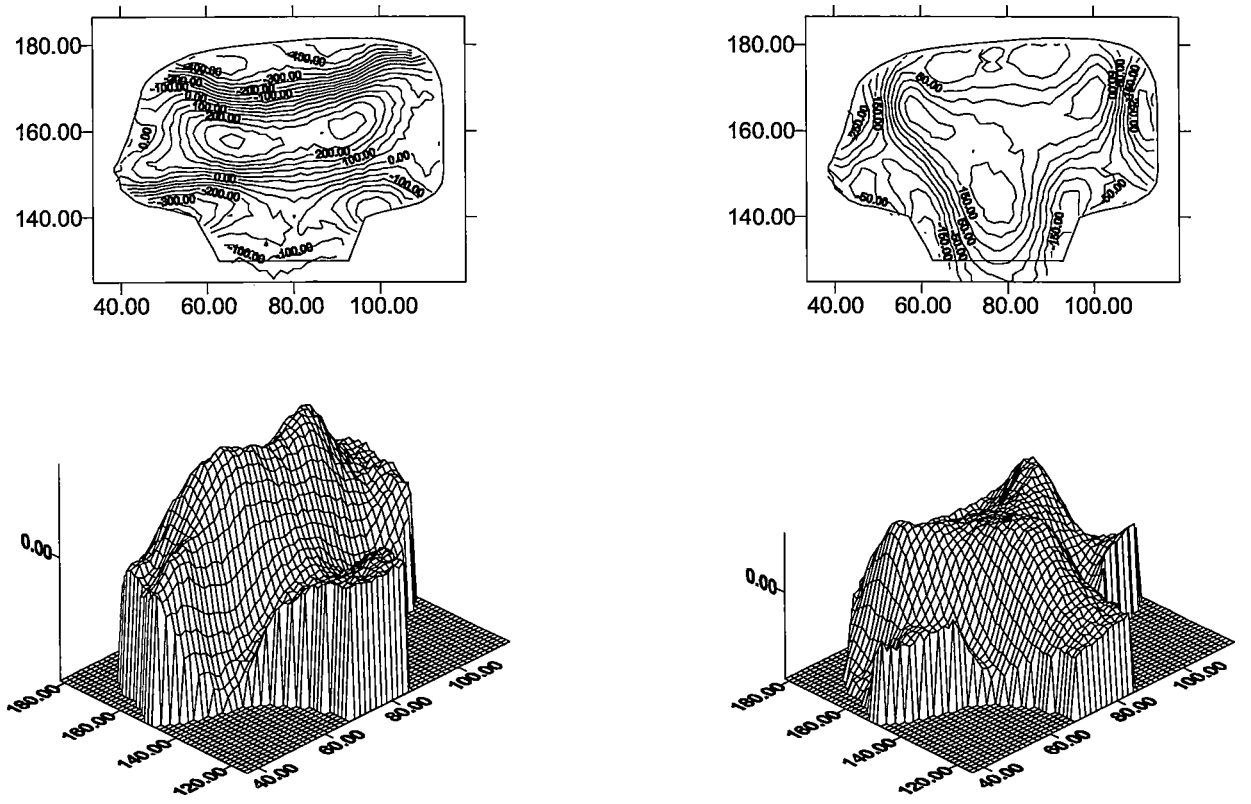

a) σ_{xx} Sample #3, Reconstructed 3D State
Combined data series #2 and #3

b) σ_{yy} Sample #3, Reconstructed 3D State
Combined data series #2 and #3

Fig. 22 (a-b)

Reconstructed 3D patterns for σ_{xx} and σ_{yy} for combined data sets

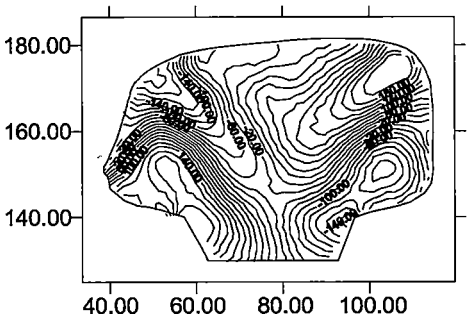

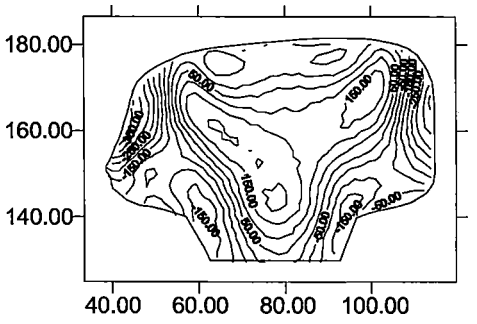

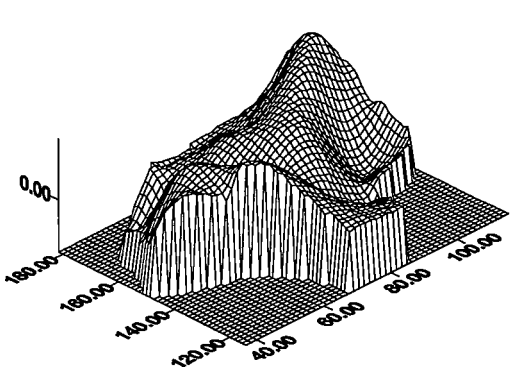

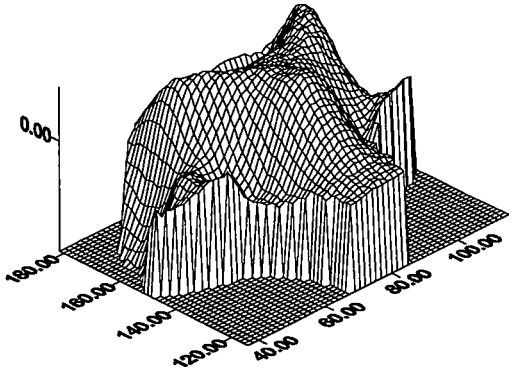

c) σ_{xy} Sample #3, Reconstructed 3D State
Combined data series #2 and #3

d) σ_{zz} Sample #3, Reconstructed 3D State
Combined data series #2 and #3

Fig. 22 (c-d)

Reconstructed 3D patterns for σ_{xy} and σ_{zz} for combined data sets

- practical analysis of ND data

The outcome of these tests/studies is that:

- the quality of the final results strongly depends on the quality of grids and their strict conformance to the true profiles of rail samples
- it also depends on the grid density and the possible errors manifest themselves at the sample's peripheries; the magnitude of this error is not high and it is further reduced on the 3D level
- the tests for the three slice procedures for currently available simulated data hardly could be done; they require either a new theoretical approach (incremental analysis) or actual experimental data for tests
- simultaneous processing of independent data sets is possible and the iterative procedure convergent though the results might be a little bit more noisy than in the case of a separated processing of the data.

REFERENCES

1. J. Krok, Incremental analysis of residual states by the elastic-plastic constitutive models. New elements families in incremental plasticity, Report to the US DOT, FRA under the DTFR53-95-G-00055 research project "Development of advanced methods for the prediction of shakedown stress states and physically based enhancement of experimental data" DTFR53-95-G-00055, Cracow, June, 2003
2. J. Magiera, Further development of the global approach to the physically based approximation technique in experimental analysis of residual stresses, Interim report to the US DOT, FRA under the DTFR53-95-G-00055 research project "Development of advanced methods for the prediction of shakedown stress states and physically based enhancement of experimental data" DTFR53-95-G-00055, Cracow, 2003 [in this volume as Topic 2.2 report]
3. J.J. Groom, Determination of Residual Stresses in Rails, Final Report to the US DOT No. DOT/FRA/ORD–83/05, May (1983)
4. J. Magiera, Reconstruction of the full 3D rail residual stress field by the physically based global method fit to neutron diffraction data and transverse/oblique slicing data reduction algorithm, Report to the US DOT, FRA under the DTFR53-95-G-00055 research project "Development of advanced methods for the prediction of shakedown stress states and

physically based enhancement of experimental data" DTFR53-95-G- 00055, Cracow, (June 2002)
5. J. Magiera, J. Orkisz, W. Karmowski, Reconstruction of residual stresses in railroad rails from measurements made on vertical and oblique slices, Wear Vol. 191, pp. 78-89, 1996
6. J. Magiera, W. Karmowski, J. Orkisz, Experimental-Numerical Analysis of 3D Residual Stress State in Railroad Rails by Means of Oblique Slicing Technique, Trans. SPIE Vol. 2342, 1995
7. J. Magiera, Analysis of 3D rail residual stress based on neutron diffraction data and transverse/oblique slicicng technique, Progress Report to US DOT, VNTSC, Cambridge, MA, September 1998; Revised Version: Cracow, May 1999
8. J. Magiera, Enhanced 3D analysis of residual stress in rails by physically based fit to neutron diffraction data, WEAR, Vol. 253/1-2, pp 229-241, 2002
9. T. Gnäupel-Herold, P.C. Brand, H.J. Prask, "Neutron Diffraction Investigation of Residual Stresses in Transverse/Oblique Rail Slices subjected to Different Grinding Strategies", Final Report to the US DOT, VNTSC, Gaithersburg, MD, December 1998
10. J. Magiera, Reconstruction of the full 3D rail residual stress field by the physically based global method fit to neutron diffraction data and transverse/oblique slicing data reduction algorithm, Report to the US DOT, FRA under the DTFR53-95-G-00055 research project "Development of advanced methods for the prediction of shakedown stress states and physically based enhancement of experimental data" DTFR53-95-G- 00055, Cracow, (June 2001)
11. Gordon J., "GGRID FEM mesh generator", Private communication, 1990
12. J. Magiera, Reconstruction of the full 3D rail residual stress field by the physically based global method fit to neutron diffraction data and transverse/oblique slicing data reduction algorithm. A study of optional sectioning schemes, Report to the US DOT, FRA under the DTFR53-95-G-00055 research project "Development of advanced methods for the prediction of shakedown stress states and physically based enhancement of experimental data" DTFR53-95-G- 00055, Cracow, (June 2002)
13. J. Orkisz, *Investigation of a Novel Approach to 3D Residual Stress Measurements Based on Angled Slicing*. Report to US DOT VNTSC, August, 1990 [manuscript]
14. REIMBURSABLE AGREEMENT between US DOT, RSPA, VNTSC and DOC, NIST, PR 76-3334, 2003
15. M. Hołowiński, J. Orkisz, Hybrid finite element method for estimation of actual residual stresses, [in:] "Residual Stresses in Rails: Effects on Rail Integrity and Railroad Economics", O. Orringer et al. (eds.), Kluwer Acad. Publ., Dordrecht, Boston, London, Vol. I, pp. 169-184, (1992).

Topic 2.5

Error control in approximation, smoothing and evaluation of physical data measured and calculated for railroad rails and vehicle wheels

Error control in approximation, smoothing and evaluation of physical data measured and calculated for railroad rails and vehicle wheels.

The report, entitled:

An extended adaptive procedure of experimental data collection and evaluation by a' posteriorir error estimation. Revised version.

deals with the problem under consideration, and pertains to all the topics (2.5.1 – 2.5.7). The work addresses extended and revised formulation of a new approach proposed to measurements planning and carrying out by means of error control of experimental data. It includes: development of postprocessing techniques for approximation of data given in a discrete form, a'posteriori error estimation (evaluation) of measured data, estimation of a new required experimental points location and density, definition of reliability index of experimental data. Theoretical consideration and numerical analysis are based on the Adaptive Finite element Analysis (AFEM) and the Meshless Finite Difference (MFDM) approach. Differences in numerical and experimental data analysis are underlying.

See also report entitled:

2D Incremental analysis of residual stresses in railroad rails with plastic hardening taken into account.

in topic 1.3.

Cracow University of Technology
ul. Warszawska 24, 31-155 Cracow, POLAND

An extended adaptive procedure of experimental data collection and evaluation by a'posteriori error estimation.

Józef Krok

Report to the

US Department of Transportation,
Federal Railroad Administration,
Washington, DC

Cracow, June 2003

AN EXTENDED ADAPTIVE PROCEDURE OF EXPERIMENTAL DATA COLLECTION AND EVALUATION BY A'POSTERIOR ERROR ESTIMATION

REVISED VERSION

Contents

1. Introduction

This work addresses validation of an approach proposed to control error in smoothing/ approximation of experimental/numerical data. On the base of aposteriori error analysis of data, adaptive procedure of experimental data collection and evaluation is presented.

One often has to transfer discrete data known at certain points to other points, for instance one may need e.g. a much clearer picture or require data smoothing. Sometimes one may also need additional data. How can this be done at the minimal loss of accuracy? Is it possible to measure the degree of information loss and if so, how? Is it possible to recover, as a by-product, additional information on the data (regularity, smoothness) and locations of data points (guaranteing the highest accuracy, when distributions of data points density and function gradients are similar). Positive answers to above-mentioned questions are crucial in proper interpretation of experimental/numerical data.

The present research is concentrated on further development of an approximation technique of physical/numerical data, based on the MWLS (Moving Weighted Least Squares) [7, 8, 9, 11] and finite difference formulae (FDM) and formulation of a new approach to experimental data measurements planning and carrying out. It includes:

- introducing and validation of postprocessing techniques for data approximation done in a discrete form,
- validation of an iterative approach to additional enhancement of data at new locations,
- formulation of *aposteriori* error technique to trace the loss of accuracy of original data by using different "error norms", *aposteriori* error estimation,
- evaluation of experimental points density in experimental data taking into account equal error distribution,
- formulation of the new *adaptive approach to experiment planning and carrying out*, taking into account aposteriori error estimation and distribution of experimental points with equidistributed error,
- analysis of the wheel saw cut data, especially for the wheel #2 (see [[3] ,11,8]), as a sample application of the proposed approach

Part of the theoretical considerations is based on the Adaptive Finite Element Analysis (AFEM). AFEM gives tools to solve the problem under consideration, even though the problem does not necessarily conform to the AFEM case, because several assumptions are violated (for example one does not know the rate of convergence and degree of smoothness, i.e. regularity of the physical data).

The theory of aposteriori error estimation in discrete methods like in the FEM or MFDM is already well established. As a result one obtains new mesh density to solve boundary value problems with highest possible accuracy i.e. with equidistributed errors. Now the same idea is proposed for experimental mechanics. Theory presented here allows to evaluate results obtained in experiment and to give very precise information on location and density of gauges or on size of moire interferometry grid (output of any experimental method may be evaluated). If it is not possible to improve measurement quality, one gets precise information on data measured with insufficient precision. Reliability indices defined in presented work

yield tools to assign very objective weights to measurements differing in quality. A'posteriori error estimation in FEM, which may be (however indirectly) used to introduce proposed idea, is presented here to explain our intent.

2. A posteriori error estimation of discrete data

2.1 Zienkiewicz-Zhu aposteriori error estimator – approach #1

For the *aposteriori* error estimators used in FEM and MFDM, based on the postprocessing of the stresses (or fluxes) - see Zienkiewicz, Zhu –ZZ [14-17] - one has

$$\|e\| = [\int_{\Omega} (\sigma - \sigma^h)^T D^{-1} (\sigma - \sigma^h) d\Omega]^{\frac{1}{2}} \qquad (2.1)$$

where σ^h are stresses obtained by the FEM, $\mathbf{D}$ is elasticity matrix.

The exact stresses σ are approximated by new stresses obtained using the stress recovery procedure (the Meshless Finite Difference Method - MFDM - is used here [9,15])

$$\sigma^* = N\overline{\sigma}^* \qquad (2.2)$$

where $\overline{\sigma}^*$ are nodal values obtained by the MFDM recovery procedure, and N is a shape functions matrix. The exact strain energy and an error of the energy norm are expressed as

$$\|U\| = [\int_{\Omega} (\sigma^h)^T D^{-1} (\sigma^h) d\Omega]^{\frac{1}{2}} + \|e\|^2, \quad \|e\| = [\int_{\Omega} (\sigma^* - \sigma^h)^T D^{-1} (\sigma^* - \sigma^h) d\Omega]^{\frac{1}{2}} \qquad (2.3)$$

Both $\|e\|$ and $\|U\|$ norms may be evaluated as a sum of their respective element contributions so that (n denotes the total number of elements in the mesh)

$$\|e\|^2 = \sum_{i=1}^{n} \|e\|_i^2, \quad \|U\|^2 = \sum_{i=1}^{n} \|U\|_i^2 \qquad (2.4)$$

Remark: An *aposteriori* error procedure can be split into two main stages:

- stage 1: calculation of stresses (or other primary values) at Gaussian points - the primary set of points,
- stage 2: approximation of the Gaussian-located stresses at nodal positions (secondary set of points), retrieval of the nodal values to Gauss points using (for example) standard shape functions or other kind of approximation.

Having two sets of values of different accuracy at the same points, one may calculate local $\|e\|_i, \|U\|_i$ and global $\|e\|, \|U\|$ norms.

2.2 Approximation and error analysis of physical (experimental) or numerical data – approach #2

New idea of a'posteriori error estimation of randomly distributed experimental data or numerical data coming from FEM or MFDM analysis is presented here.

Let us define the following problem:

- data, (not necessary stresses like in eq. (2.3)) coming from experiment, located at certain points - set #1 (see experimental points-set of primary points, fig 2.1) is given,
- the fictitious sets of points used later in calculation - set #2 (see fictitious points – set of secondary points - fig.2.1) is given.

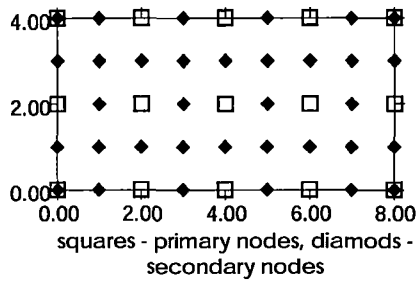

Figure 2.1. *Primary and secondary mesh for approximation of physical or numerical data*

The problem lies in data translation (approximation) from #1 points set to #2 points set. The problem is exactly the same as in error estimator (2.3), but now one has two different sets of points with, in fact, arbitrary (not elemental) locations and one has no information on regularity, smoothness and reliability of the data.

Differences between two surfaces defined by data #1 and #2 may be measured as

$$\|e\| = [\int_{\Omega} (u^* - u^h)^T (u^* - u^h) + (\nabla u^* - \nabla u^h)^T (\nabla u^* - \nabla u^h) + (\kappa u^* - \kappa u^h)^T (\kappa u^* - \kappa u^h) d\Omega]^{\frac{1}{2}} \qquad (2.6)$$

where u^h is the vector of experimental data (in experimental points) and u^* is the vector of fictitious sought data. Sometimes weighting factors may be used to equilibrate dimensions of terms. In the above formula one can omit (sometimes not) the gradients and curvature terms (κ - see generalized curvature [[5] ,[6]]). One can also use discrete form of this formula, summing up differences between values at experimental points.

To solve this problem, data from experimental points is approximated to fictitious ones (using FDM approximation - see next part of this work) and later on, taking values at fictitious points as original data, approximated back from fictitious points to experimental ones. In this two-stage approximation part of data is lost, but if differences between original data in the experimental points and fictitious data in the same points are small enough, one may expect that the approximation in first step does not introduce too large error. As it will be seen from numerical analysis this assumption holds true.

Additionally, in the zones where the gradients of approximated function are larger, the error magnitude is considerably higher as compared to the zones with smaller data gradients. Moreover, if irregularity in data is large the error increases. Those facts may be used, as by-product important information, to evaluate experimental data. Having a vector of differences between experimental and fictitious values at experimental points one can "smear" the error, approximating vector of differences from experimental to fictitious points. Adding correction to initial fictitious values one can obtain new enhanced fictitious values. This process can be repeated (iteration process gives possibility to avoid fluctuation, especially when data is very smooth, like MFDM solution). In this way, the very well known approach elaborated mainly in AFEM is unified, extended and generalized.

The total norm of the measured values may be expressed as (the discrete form of the below norms may be used):

$$\|U\|^2 = [\int_{\Omega} (u^h)^T u^h + (\nabla u^h)^T \nabla u^h + (\kappa u^h)^T \kappa u^h d\Omega] + \|e\|^2 . \qquad (2.7)$$

The key question is, whether one can evaluate experimental data using norms (2.6) and (2.7)? The answer is yes, if data is regular enough.

As one can see from equation (2.7), not only values of a function measured, but gradients of the function and curvatures (needed when material discontinuities are present) are taken into account as well. One can find any required derivatives of the discrete data, with error control as a by-product.

3. Meshless finite difference approximation

The approximation $u^h(\mathbf{x})$ of function $u(\mathbf{x})$ is posed as polynomial of order m with non-constant coefficients $a_0(\mathbf{x}), a_1(\mathbf{x}), ..., a_m(\mathbf{x})$. The order of polynomial is defined as the order of the basis. For a linear basis in two dimensions $u^h(\mathbf{x})$ can be written as

$$u^h(\mathbf{x}) = a_0 + a_1 x + a_2 y , \qquad (3.1)$$

where unknown parameters $a_j(\mathbf{x})$ vary with $\mathbf{x}$. The local approximation (for $\bar{\mathbf{x}} = \mathbf{x}$) is given by [[1] ,[9] ,[10] ,[13]]

$$u^h(\mathbf{x}, \bar{\mathbf{x}}) = \sum_{j=0}^{m} p\ (\mathbf{x}) a_j(\bar{\mathbf{x}}) = \mathbf{p}^T(\mathbf{x}) \mathbf{a}(\mathbf{x}) \qquad (3.2)$$

where $\mathbf{p}(\mathbf{x})$ is a complete polynomial of order m

$$\mathbf{p}^T(\mathbf{x}) = [1, x, y, x^2, xy, y^2, ...,] \qquad (3.3)$$

and $\mathbf{a}(\mathbf{x})$ is given by

$$\mathbf{a}^T(\mathbf{x}) = [a_0(\mathbf{x}), a_1(\mathbf{x}), ..., a_m(\mathbf{x})] . \qquad (3.4)$$

The unknown parameters $a_j(\mathbf{x})$ at any given point are determined by minimizing the difference between the local approximation at that point and the nodal parameters u_I i.e. weighted, discrete L_2 norm

$$J(\mathbf{a}) = \sum_{I=1}^{n} w(\mathbf{x}-\mathbf{x}_I)[u^h(\mathbf{x}_I,\mathbf{x}) - u_I]^2 = \sum_{I=1}^{n} w(\mathbf{x}-\mathbf{x}_I)[p^T(\mathbf{x}_I)a(\mathbf{x}) - u_I]^2, \quad (3.5)$$

where $w(\mathbf{x}-\mathbf{x}_I)$ is a shift of a given weighting function $w(\mathbf{x})$, and n is the number of nodes in the neighborhood of $\mathbf{x}$ for which the weighting function $w(\mathbf{x}-\mathbf{x}_I) \neq 0$.

The minimum of J in (3.5) with respect to $\mathbf{a}(\mathbf{x})$ leads to the set of linear equations

$$\mathbf{A}(\mathbf{x})\mathbf{a}(\mathbf{x}) = \mathbf{B}(\mathbf{x})\mathbf{u}. \quad (3.6)$$

After solving the set of equations (3.6), one obtains

$$\mathbf{a}(\mathbf{x}) = \mathbf{A}^{-1}(\mathbf{x})\mathbf{B}(\mathbf{x})\mathbf{u} = \sum_{I=1}^{n} \mathbf{A}^{-1}(\mathbf{x})\mathbf{B}_I(\mathbf{x})u_I = \mathbf{Q}(\mathbf{x})\mathbf{u}, \quad (3.7)$$

where

$$\mathbf{A}(\mathbf{x}) = \sum_{I=1}^{n} w(\mathbf{x}-\mathbf{x}_I)\mathbf{p}(\mathbf{x}_I)\mathbf{p}^T(\mathbf{x}_I), \quad (3.8)$$

$$\mathbf{B}(\mathbf{x}) = [w(\mathbf{x}-\mathbf{x}_1)\mathbf{p}(\mathbf{x}_1),\ w(\mathbf{x}-\mathbf{x}_2)\mathbf{p}(\mathbf{x}_2),\ldots,w(\mathbf{x}-\mathbf{x}_n)\mathbf{p}(\mathbf{x}_n)] \quad (3.9)$$

Substituting (3.7) into (3.2), the MWLS approximants can be defined as

$$u^h = \mathbf{p}^T(\mathbf{x})\mathbf{A}^{-1}(\mathbf{x})\mathbf{B}(\mathbf{x})\mathbf{u} = \sum_{I=1}^{n}\sum_{j-0}^{m} p_j(\mathbf{x})[\mathbf{A}^{-1}(\mathbf{x})\mathbf{B}(\mathbf{x})]_{jI}u_I = \sum_{I=1}^{n} \tilde{N}_I(\mathbf{x})u_I = \tilde{\mathbf{N}}\mathbf{u}, \quad (3.10)$$

where the shape functions in MWLS approximation are (note that $\sum_{I}^{n} \tilde{N}_I = 1$).

$$\tilde{N}_I(\mathbf{x}) = \sum_{j=0}^{m} p_j(\mathbf{x})[\mathbf{A}^{-1}(\mathbf{x})\mathbf{B}(\mathbf{x})]_{jI} = \mathbf{p}^T\mathbf{A}^{-1}\mathbf{B}_I = \sum_{j=1}^{m} p_j Q_{jI} \quad (3.11)$$

To determine the derivatives of the approximating function $u^h(\mathbf{x})$, one has to obtain the shape functions' derivatives. The derivatives of the shape functions are determined by

$$\tilde{N}_{I,x} = [\mathbf{p}^T\mathbf{A}^{-1}\mathbf{B}_I]_{,x} = \mathbf{p}^T{}_{,x}\mathbf{A}^{-1}\mathbf{B}_I + \mathbf{p}^T\mathbf{A}^{-1}{}_{,x}\mathbf{B}_I + \mathbf{p}^T\mathbf{A}^{-1}\mathbf{B}_{I,x}, \quad (3.12)$$

where

$$\mathbf{B}_I(\mathbf{x}) = \frac{\partial w(\mathbf{x}-\mathbf{x}_I)}{\partial x}\mathbf{p}(\mathbf{x}_I). \quad (3.13)$$

Matrix $\mathbf{A}_{,x}^{-1}$ is computed by

$$\mathbf{A}_{,x}^{-1} = -\mathbf{A}^{-1}\mathbf{A}_{,x}\mathbf{A}^{-1}, \quad (3.14)$$

where

$$A_{,x} = \sum_{I=1}^{n} \frac{\partial w(\mathbf{x}-\mathbf{x}_I)}{\partial x}\mathbf{p}(\mathbf{x}_I)\mathbf{p}^T(\mathbf{x}_I). \quad (3.15)$$

To compute the shape functions and their derivatives, the **A** matrix has to be inverted. This process is more computationally efficient if LU decomposition of the matrix **A** is performed. The shape functions in (3.11) can be written as

$$\tilde{N}_I = \sum_{j=0}^{m} p_j(\mathbf{x})\mathbf{A}^{-1}(\mathbf{x})\mathbf{B}_{jI}(\mathbf{x}) = \mathbf{p}^T\mathbf{A}^{-1}\mathbf{B}_I = \mathbf{g}^T\mathbf{B}_I\,, \tag{3.16}$$

where the following relationship was used [1]

$$\mathbf{A}(\mathbf{x})\mathbf{g}(\mathbf{x}) = \mathbf{p}(\mathbf{x})\,. \tag{3.17}$$

The vector $\mathbf{g}(\mathbf{x})$ can be determined the same way as the vector **a** . The derivatives of vector $\mathbf{g}(\mathbf{x})$ can be computed similarly, this leads to a computationally efficient procedure to determine derivatives of u^h. Taking spatial derivatives of (3.17), one has

$$\mathbf{A}(\mathbf{x})\mathbf{g}(\mathbf{x})_{,x} = \mathbf{p}(\mathbf{x})_{,x} - \mathbf{A}_{,x}\mathbf{g}\,. \tag{3.18}$$

Thus, the derivative of $\mathbf{g}(\mathbf{x})$ can be calculated using the same **LU** decomposition obtained from (3.17). Spatial derivatives of shape function may be obtained as [[1]]

$$\tilde{N}_I(\mathbf{x})_{,x} = \mathbf{g}(\mathbf{x})_{,x}\mathbf{B}_I + \mathbf{g}(\mathbf{x})\mathbf{B}_{I,x}\,. \tag{3.19}$$

By consecutive derivation of equation (3.17) one obtains the set of following equations for vector $\mathbf{g}$ and its derivatives

$$\begin{aligned}
&\mathbf{A}(\mathbf{x})\mathbf{g}(\mathbf{x}) = \mathbf{p}(\mathbf{x})\,,\\
&\mathbf{A}(\mathbf{x})\mathbf{g}(\mathbf{x})_{,x} = \mathbf{p}(\mathbf{x})_{,x} - \mathbf{A}_{,x}\mathbf{g}\,,\\
&\mathbf{A}(\mathbf{x})\mathbf{g}(\mathbf{x})_{,y} = \mathbf{p}(\mathbf{x})_{,y} - \mathbf{A}_{,y}\mathbf{g}\,,\\
&\mathbf{A}(\mathbf{x})\mathbf{g}(\mathbf{x})_{,xx} = \mathbf{p}(\mathbf{x})_{,xx} - \mathbf{A}_{,xx}\mathbf{g} - 2\mathbf{A}_{,x}\mathbf{g}_{,x}\,,\\
&\mathbf{A}(\mathbf{x})\mathbf{g}(\mathbf{x})_{,xy} = \mathbf{p}(\mathbf{x})_{,xy} - \mathbf{A}_{,xy}\mathbf{g} - \mathbf{A}_{,x}\mathbf{g}_{,y} - \mathbf{A}_{,y}\mathbf{g}_{,x}\,,\\
&\mathbf{A}(\mathbf{x})\mathbf{g}(\mathbf{x})_{,yy} = \mathbf{p}(\mathbf{x})_{,yy} - \mathbf{A}_{,yy}\mathbf{g} - 2\mathbf{A}_{,y}\mathbf{g}_{,y}\,.
\end{aligned} \tag{3.20}$$

This leads to a simple relationship for the derivatives of the shape functions

$$\begin{aligned}
&\tilde{N}_I = \mathbf{g}(\mathbf{x})\mathbf{B}_I\,,\\
&\tilde{N}_{I,x} = \mathbf{g}(\mathbf{x})_{,x}\mathbf{B}_I + \mathbf{g}(\mathbf{x})\mathbf{B}_{I,x}\,,\\
&\tilde{N}_{I,y} = \mathbf{g}(\mathbf{x})_{,y}\mathbf{B}_I + \mathbf{g}(\mathbf{x})\mathbf{B}_{I,y}\,,\\
&\tilde{N}_{I,xx} = \mathbf{g}(\mathbf{x})_{,xx}\mathbf{B}_I + 2\mathbf{g}(\mathbf{x})_{,x}\mathbf{B}_{I,x} + \mathbf{g}(\mathbf{x})\mathbf{B}_{I,xx}\,,\\
&\tilde{N}_{I,xy} = \mathbf{g}(\mathbf{x})_{,xy}\mathbf{B}_I + \mathbf{g}(\mathbf{x})_{,x}\mathbf{B}_{I,y} + \mathbf{g}(\mathbf{x})_{,y}\mathbf{B}_{I,x} + \mathbf{g}(\mathbf{x})\mathbf{B}_{I,xy}\,,\\
&\tilde{N}_{I,yy} = \mathbf{g}(\mathbf{x})_{,yy}\mathbf{B}_I + 2\mathbf{g}(\mathbf{x})_{,y}\mathbf{B}_{I,y} + \mathbf{g}(\mathbf{x})\mathbf{B}_{I,yy}\,.
\end{aligned} \tag{3.21}$$

In practical calculations, the local coordinate system $\mathbf{h} = \mathbf{h}(h,k)$ is used

$$\mathbf{h} = \mathbf{h}(h,k) = \mathbf{x} - \mathbf{x}_0,\ \mathbf{x}_0 = (x_0, y_0)\,, \tag{3.22}$$

where $\mathbf{x}_0 = \mathbf{x}_0(x_0, y_0)$ is the point in which approximation is sought. The base vector is taken as

$$p^T = [1, h, k, \frac{1}{2}h^2, hk, \frac{1}{2}k^2, ...,]\,, \tag{3.23}$$

so coefficients $a_0, a_1, ..., a_m$ may be immediately interpreted as derivatives at point $\mathbf{x}_o$ (usualy called local derivatives)

$$a_0 = u_0,\ a_1 = \frac{\partial u_0}{\partial x},\ a_2 = \frac{\partial u_0}{\partial y}, ... , \tag{3.24}$$

and the matrix $\mathbf{Q}$ (see 3.7) now is a generalized FD matrix. Combination of rows of this matrix and a vector of nodal values yields immediately values of function and it's derivatives at point $\mathbf{x}_0$ (but these derivatives may be not continuos from point to point).

Consistent MFDM matrix $\tilde{\mathbf{Q}}$ and the approximation rule now have the form

$$\mathbf{D}u = \begin{Bmatrix} u \\ u_x \\ u_y \\ u_{xx} \\ u_{xy} \\ u_{yy} \end{Bmatrix} = \begin{bmatrix} \tilde{N}_1 & \tilde{N}_2 & \cdots & \tilde{N}_n \\ \frac{\partial \tilde{N}_1}{\partial x} & \frac{\partial \tilde{N}_2}{\partial x} & \cdots & \frac{\partial \tilde{N}_n}{\partial x} \\ \cdots & \cdots & \cdots & \cdots \\ \frac{\partial^2 \tilde{N}_1}{\partial y^2} & \frac{\partial^2 \tilde{N}_2}{\partial y^2} & \cdots & \frac{\partial^2 \tilde{N}_n}{\partial y^2} \end{bmatrix} \begin{Bmatrix} u_1 \\ u_2 \\ \cdots \\ u_n \end{Bmatrix} = \tilde{\mathbf{Q}}\mathbf{u} \tag{3.25}$$

The explicit form of the matrix $\tilde{\mathbf{Q}}$ has the following form (note that matrix $\mathbf{Q}_I$ contains columns of the approximation matrix $\mathbf{Q}$ of zero-th order)

$$\tilde{\mathbf{Q}} = \begin{bmatrix} \mathbf{p}^T\mathbf{Q}_1 & \cdots & \mathbf{p}^T\mathbf{Q}_n \\ \mathbf{p}_{,x}^T\mathbf{Q}_1 + \mathbf{p}^T\mathbf{Q}_{1,x} & \cdots & \mathbf{p}_{,x}^T\mathbf{Q}_n + \mathbf{p}^T\mathbf{Q}_{n,x} \\ \mathbf{p}_{,y}^T\mathbf{Q}_1 + \mathbf{p}^T\mathbf{Q}_{1,y} & \cdots & \mathbf{p}_{,y}^T\mathbf{Q}_n + \mathbf{p}^T\mathbf{Q}_{n,y} \\ \mathbf{p}_{,xx}^T\mathbf{Q}_1 + 2\mathbf{p}_{,x}^T\mathbf{Q}_{1,x} + \mathbf{p}^T\mathbf{Q}_{1,xx} & \cdots & \mathbf{p}_{,xx}^T\mathbf{Q}_n + 2\mathbf{p}_{,x}^T\mathbf{Q}_{n,x} + \mathbf{p}^T\mathbf{Q}_{n,xx} \\ \mathbf{p}_{,xy}^T\mathbf{Q}_1 + \mathbf{p}_{,x}^T\mathbf{Q}_{1,y} + \mathbf{p}_{,y}^T\mathbf{Q}_{1,x} + \mathbf{p}^T\mathbf{Q}_{1,xy} & \cdots & \mathbf{p}_{,xy}^T\mathbf{Q}_n + \mathbf{p}_{,x}^T\mathbf{Q}_{n,y} + \mathbf{p}_{,y}^T\mathbf{Q}_{n,x} + \mathbf{p}^T\mathbf{Q}_{n,xy} \\ \mathbf{p}_{,yy}^T\mathbf{Q}_1 + 2\mathbf{p}_{,y}^T\mathbf{Q}_{1,y} + \mathbf{p}^T\mathbf{Q}_{1,yy} & \cdots & \mathbf{p}_{,yy}^T\mathbf{Q}_n + 2\mathbf{p}_{,y}^T\mathbf{Q}_{n,y} + \mathbf{p}^T\mathbf{Q}_{n,yy} \end{bmatrix} \tag{3.26}$$

Taking into accout that approximation is sought in the origin of local coordinate system one has $p^T(\mathbf{0}) = [1,0,0,0,0,0,...,]$, and thus (note: Q_{1i} is the first element in each i-th column $\mathbf{Q}_i$ of FD matrix)

$$\tilde{N}_i = \mathbf{p}^T\mathbf{Q}_i = Q_{1i}, \tag{3.27}$$

As one may see from equation (3.27) *global* shape functions are equal to *first row elements of FD matrix*.

This means that global approximation is exactly the same as local one in origin of local coordinate system. Result is rather obvious, but this means, that meshless shape functions and local (diffuse) derivatives in modern notation were first introduced in [7] twenty years ago (in polish), and published in [10] (in english) . This fact was recently confirmed by O.C.Zienkiewicz in his book [16].

Relation (3.25) is valid for a very wide class of messhless approaches and yields continuous derivatives up to the second order very easily. Having two different approximation matrices: $\mathbf{Q}$- obtained from the MWLS approximation (see equation (3.7)) and $\tilde{\mathbf{Q}}$ - (3.25) – obtained by means of the direct differentiation of $u^h(\mathbf{x})$, one has another, very useful, capability to measure error as a violation of continuity in approximation of the first and second derivatives. This way one may have at the same time two different approximation matrices.

Continuity feature of derivatives is not always beneficial, especially when approximation of data given in a set of arbitrarily spaced points is needed. Besides that, there are problems with proper definition of a weighting function on arbitrarily spaced grid of points, because results of approximation, especially derivative values strongly depend on type of weighting functions used (dimensions of weight support). If support of the weighting function is not properly correlated with grid density and its form is not appropriate for the purpose required, results may be considerably worse than in the case of direct MWLS MFDM approximation. If support of approximant is too large, approximation is too smooth and thus local peak values of approximated function are anihilated.

Weighting function used here is [5] ,[6]

$$w(\rho) = \left(\rho^2 + g^4/(g^2+\rho^2)\right)^{-(p+1)}, \qquad (3.26)$$

where ρ is the distance between central point and the node, p denotes polynomial order and g is an optimality parameter making singular weighting function (interpolation) or non-singular weights (approximation) available. If the optimality parameter g tends to a small value, the weighting function enforces interpolation. If optimality parameter tends to large number, approximation takes place, but data smoothing may be over emphasized.

It is worth to mention that the continuity problem arises in the MWLS approximation. Continuity requires that either all nodes in considered domain are taken into account each time or weighting functions defined on an appropriate finite supports are used providing zero end conditions. If such support is not properly corelated with the mesh density, approximation results may be of considerably lower quality than they could be. On the other hand continuity feature of MWLS approximation and its derivatives may be not needed in practice (see [12, 13]).

Test problem [12]

Though the matter requires a deeper and systematic study (see [12]) a valuable insight into the MWLS approximation quality was gained by analysis of a simple test.

Considered was a set of data presenting the values of function $u = \sqrt{25 - x^2}$ defined at nodes of an evenly spaced mesh: 0, 0.5, 1.0, 1.5, 2.0, 2.5, 3.0 having the increment 0.5.

The local (3.24) and global (3.10) MWLS approximation was performed for the function itself and for its first local (3.24) and global (3.12) derivatives. Results of error analysis obtained in the interval [0.5, 3.0] for various weighting functions are presented and compared in Fig. 3.1 a and b. The following may be noticed then:

- results of the local (3^{rd} order) and global (consistent) approximation are, of course, the same for the function itself when using the same weighting functions.

- neither method did show clear advantages with respect to result quality when comparing the first derivative found by means of either the local (3.24) or the global (consistent) (3.12) differentiation approach. For local derivatives superconvergence property at internal nodes is noted (error of the local derivatives is considerably lower than error of the consistent derivatives). Superconvergence property of local derivatives for lower approximation order is much stronger, than for higher order (not presented here) . On the other hand approximation error of the consistent derivatives is more uniform. Maximum error is lower than approximation error of the local derivatives. It is interesting to see, that the gap between local and global derivatives is proportional to the approximation error. This fact explains why error estimator proposed by Gavette, Cuesta and Ruiz works very well [18]. Probably, for the first time, it is possible to define very convenient error estimator in meshless methods, based on postprocessing, but for the two different types of derivatives.

- squared weighting functions proved clear advantage (minimal errors) over non–squared ones,

- the smallest errors in the function approximation were observed when the singular weighting factor (3.26) was used , while squared non-singular 3^{rd} order spline weight [1], was found the best for derivative evaluation.

From above test it is evident, that the two problems arise: 1^0 discrete data approximation problem, 2^0 boundary-value solution problem. It is not justified to extend conclusion from data approximation to solution of boundary value problem. Even if approximation works well in data approximation, one may not obtain good results when boundary-value problem solution is needed. On the other hand bad results of data approximation not neccessarily mean that approximation will give bad results during solution of boundary-value problem.

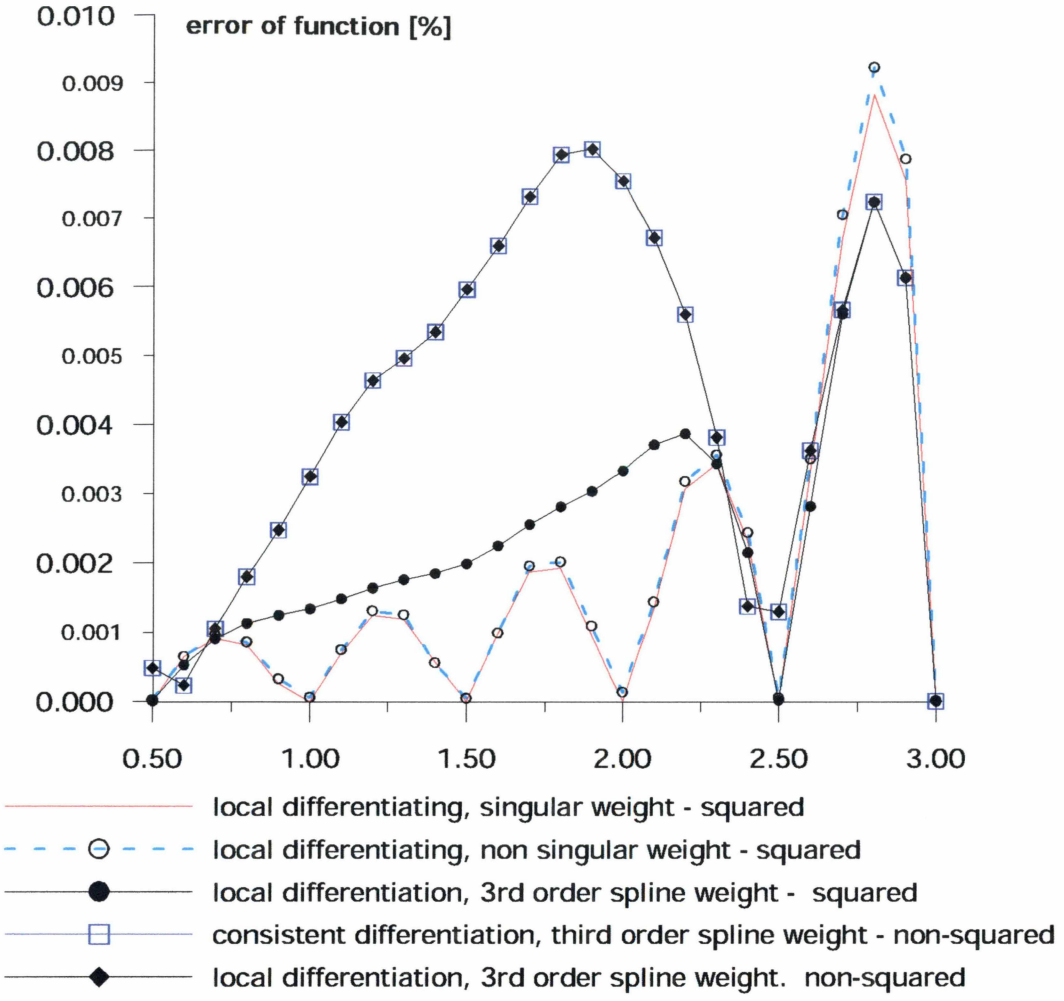

Fig.3.1a, Weight function influence on results of approximation - function error
data sought at points: min=0.5, max=3.0, increment $\Delta x = 0.1$

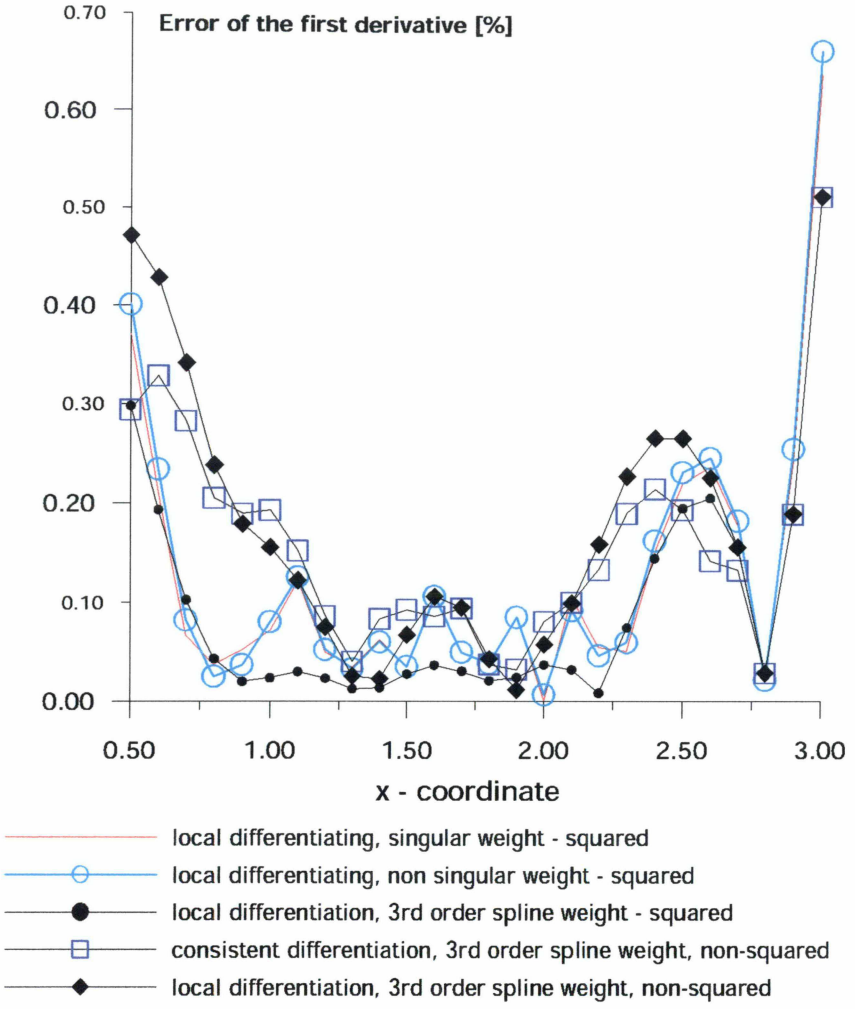

Fig.3.1b, Weight function influence on results of approximation - derivative error

4. Definition of points density function in experimental and numerical discrete data

4.1 Acceptable solution and mesh (grid) refinements function

In an adaptive solution approach, the *aposteriori* errors are used to modify mesh appropriately mesh modifications by means of so-called error indicators and mesh refinement parameters. An approach to mesh modification applied to the adaptive FEM (or validation of a density of experimental points) is discussed below. This problem is very important because one has to have the capability to take into account, in numerical as well as in physical experiments, relation between gradients of the measured function and density (location) of the points at which information is available.

Solution is 'correct' if the two following conditions are satisfied:

(i) The global error in energy norm is less than a specified percentile value of the total strain energy

$$\|e\| = \eta \|U\| \tag{4.1}$$

where η is the 'USER' specified value of a permissible relative global error.

(ii) Distribution of elements in a new mesh satisfies a local mesh optimality criterion

$$\|e\|_i = \|e\|_{all(i)} \tag{4.2}$$

where $\|e\|_i$ is the actual error norm in i-th element and $\|e\|_{all(i)}$ is the 'required ' error norm in the element.

The global and local error parameters may be defined from equations (4.1) and (4.2) as

$$\xi_g = \frac{\|e\|}{\eta \|U\|}, \quad \bar{\xi}_i = \frac{\|e\|_i}{\|e\|_{all(i)}}. \tag{4.3}$$

The mesh refinement parameter for the i-th element is introduced as a combination of the global and local parameters [[2]]

$$\xi_i = \bar{\xi}_i \xi_g = \frac{\|e\| \|e\|_i}{\eta \|U\| \|e\|_{all(i)}}. \tag{4.4}$$

One of the most important questions is: how one can define the required error norm for each element. The following definitions are considered here:

(i) the global error, equally distributed all over elements in the mesh ([15])

$$\|e\|_{all(i)} = \frac{\|e\|}{\sqrt{n}}, \tag{4.5}$$

where n is the total number of elements in a mesh.

(ii) mesh is optimal if squared error per unit element volume is the same over the whole mesh i.e. (Bugeda, Onate [[2]]), taking also into account equation (4.2) one has

$$\frac{\|e\|_i}{(\Omega_i)^{\frac{1}{2}}} = \frac{\|e\|}{(\Omega)^{\frac{1}{2}}}, \qquad \text{and} \qquad \|e\|_i = \|e\|_{all(i)} = \|e\| \left(\frac{\Omega_i}{\Omega} \right)^{\frac{1}{2}}. \tag{4.6}$$

Using eqs (4.5) and (4.6) one may obtain the following *element refinement parameters*

$$\xi_i = \frac{\|e\|_i}{\eta \|U\| (n)^{-\frac{1}{2}}}, \qquad \xi_i = \frac{\|e\|_i}{\eta \|U\|} \left(\frac{\Omega}{\Omega_i} \right)^{\frac{1}{2}} \tag{4.7}$$

for equal error distribution [15] and for the equal specific error distribution [[2]].

However, one should notice that the element and global error norms have different orders of convergence

$$\|e\|_i \approx O(h_i^m)\Omega^{\frac{1}{2}} \approx O(h_i^{m+\frac{d}{2}}), \quad \|e\| \approx O(h^m) \tag{4.8}$$

where h_i and h are the i-th element size and average size of all the elements in the mesh, m is the element order and d is the problem dimension. Dividing the element error by its area one obtains

$$\|e\|_i /(\Omega_i)^{\frac{1}{2}} \approx O(h_i^m) \tag{4.9}$$

and new element size parameter may be defined as (this is valid only for FEM)

$$\xi_{new} = (\overline{\xi}_i \xi_g)^{\frac{1}{m}} = (\xi_i)^{\frac{1}{m}}. \tag{4.10}$$

Refinement of the mesh may be done in two completely different ways: breaking elements ([[4]]), or remeshing ([15]). For the purpose of this research, the remeshing technique is preferred, as it is compatible with both FEM and MFDM discretizations.

If there is no information on regularity (and convergence) of the data (like in experimental mechanics), then coefficient m may be set to one, so grid refinement parameter (4.10) is equal to (4.4).

$$\xi_{new} = \overline{\xi}_i \xi_g \tag{4.11}$$

This way, very important unification of discrete methods (like MFDM and FEM), and experimental data analysis has been done.

4.2 New hybrid theoreticallexperimental method of a posteriori estimation of "experimental points" grid density

The global and local error parameters for experimental data in each experimental point may be reinterpreted from equations (4.1) and (4.2) as

$$\xi_g^{\exp} = \frac{\|e\|}{\eta\|U\|}, \quad \overline{\xi}_i^{\exp} = \frac{\|e\|_i}{\|e\|_{all(i)}}. \tag{4.12}$$

so the experimental grid refinement parameter (EGRP) for the i-th point is introduced as a combination of the global and local parameters [[2]]

$$\xi_i^{\exp} = \overline{\xi}_i^{\exp} \xi_g^{\exp} = \frac{\|e\|\|e\|_i}{\eta\|U\|\|e\|_{all(i)}}. \tag{4.13}$$

where $\|e\|_{all(i)}$ is the 'required ' or admissible error norm in the i-th experimental point. This way features of the measuring devices or other "experimental errors" may be introduced.

Theoretical or approximation based *points refinement parameters* (TPRP) may be introduced from optimality criteria (4.5) and (4.6)

$$\xi_i^{theor} = \frac{\|e\|_i}{\eta\|U\|(n)^{-\frac{1}{2}}}, \qquad \xi_i^{theor} = \frac{\|e\|_i}{\eta\|U\|}\left(\frac{\Omega}{\Omega_i}\right)^{\frac{1}{2}} \tag{4.14}$$

for equal error distribution [15] and for the equal specific error distribution [[2]] in each experimental point.

New *theoretical* or approximation based *points refinement parameters* (TPRP) may be defined by combining local and global optimality criteria

$$\xi_i^{theor} = (\bar{\xi}_i^{theor}\xi_g^{theor})^{\frac{1}{m}}. \tag{4.15}$$

where

$$\xi_g^{theor} = \frac{\|e\|}{\eta\|U\|} \tag{4.16}$$

Coefficient m in numerical method depends on theory. Here, this coefficient may be set to one or to ½ as in problems with singularities (like in analysis of boundary problems using numerical methods - FEM or MFDM).

If one has no information on experimental error TPRP parameter may be used. If one has to take into account both experimental and as theoretical (approximation) errors one may use the following proposition of combined theoretical/experimental points refinement parameter (CTEPRP)

$$\xi_i = (1-\lambda)\xi_i^{theor} + \lambda\xi_i^{\exp} \tag{4.17}$$

where coefficient λ decides how much of "experimental estimation" will be used in analysis. $1-\lambda$ is part of estimate due to approximation optimality criteria.
Magnitude of λ parameter depends on "user". It is no easy to decide how much of "experiment" or how much of "theory" should be taken into acocunt. Investigations on this extremally important topic are under currenttly performed.

4.3. Error and experimental mesh (grid) density evaluation strategy in saw cut experimental data

Crack nucleation propagation and failure of railroad car wheels is greatly influenced by residual stresses existing in those wheels, as a result of manufacturing and service conditions. The knowledge of residual stress distribution in wheels is thus required.

Experimental data used for residual stress reconstruction is collected during radial saw cutting of a wheel in laboratory conditions in order to relieve residual stresses and strains, see Fig. 4.1. In order to obtain reasonable residual stress estimation, the additional approximation process, which simultaneously uses error estimation procedures for considered problem is applied.

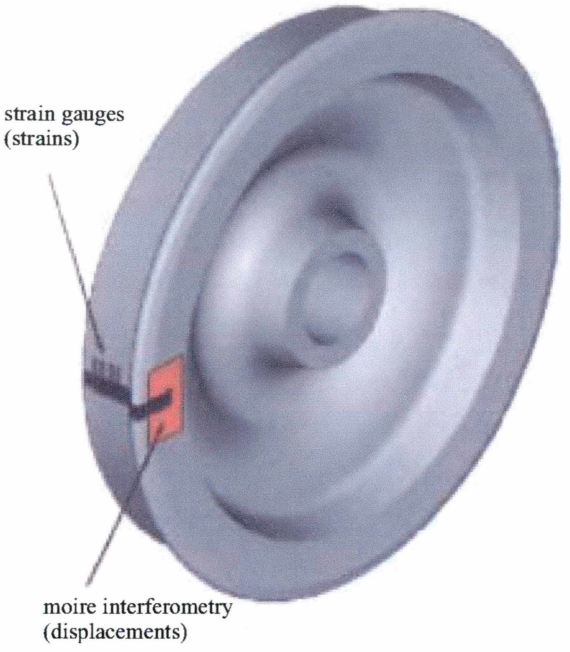

Fig. 4.1 Measurements taken at saw cut [19]

Wheel saw cut experimental data may be evaluated using equations (4.1) and (4.2). Of course, density of experimental points depends on local (4.2) condition i.e. error at experimental points must be bound by certain admissible value. *The global and local error refinement parameters* may be defined from equations (4.1) and (4.2) as in FEM analysis. Combining both global (4.1) and local (4.2) criteria one obtains the same formula *for the mesh refinement parameter* at the i-th experimental point like in the FEM. What does mesh refinement parameter in experiment mean? It means that an experimental value at certain points changes too rapidly when compared to the mean value and local density of experimental points. In other words, density of experimental points must be increased in certain part of the region, it is simply too low to properly describe the gradients of the measured function. New, required density is computed by formula $(4.7)_1$ - discrete form or $(4.7)_2$ - continuous form. One can take into account a weighting factor like an area assigned to experimental point (see eq. (4.7)). This is a proper definition of the admissible error at a point. Equations (4.8), (4.9) and (4.10) are not valid here because one does not have any information on the convergence of experimental results with respect to the density of experimental points (one may use directly (4.4)). As was mentioned above, this very important problem may be solved by setting convergence rate to one, but any other physically justified value may be used. For example, if discontinuity is present (at point or along line or surface), convergence rate is substantially lower than one (in numerical analysis is usually set to 0.5). This fact may be inserted into new experimental grid density distribution.

5. Approximation and *aposteriori* error analysis of the physical data

An error analysis described above has been applied to a problem of wheel saw cut data approximation and to calculate influence matrix coefficients (see [11]). The MFDM Approximation [[1] ,8,[9] ,11] has been applied. In the presented examples fictitious (discrete!) mesh generated previously: Fig. 5.1 (flange side of the wheel) has been used and the error has been determined at the experimental points.

In numerical calculations the data coming form the wheel #2 cutting process have been considered. 20 different sets of data: horizontal (circumferential) and vertical (radial) displacements coming from five cuts ([[3] ,8]) of the wheel have been used in calculations.

Three different effects concerning experimental data are investigated:

1. An approximation error of the measured values from experimental grid to one used in numerical analysis.
2. Evaluation of the measured values taking into account five different 'error' norms.
3. Estimation of the new experimental points' grid density with equal distribution of an approximation error kept in mind.

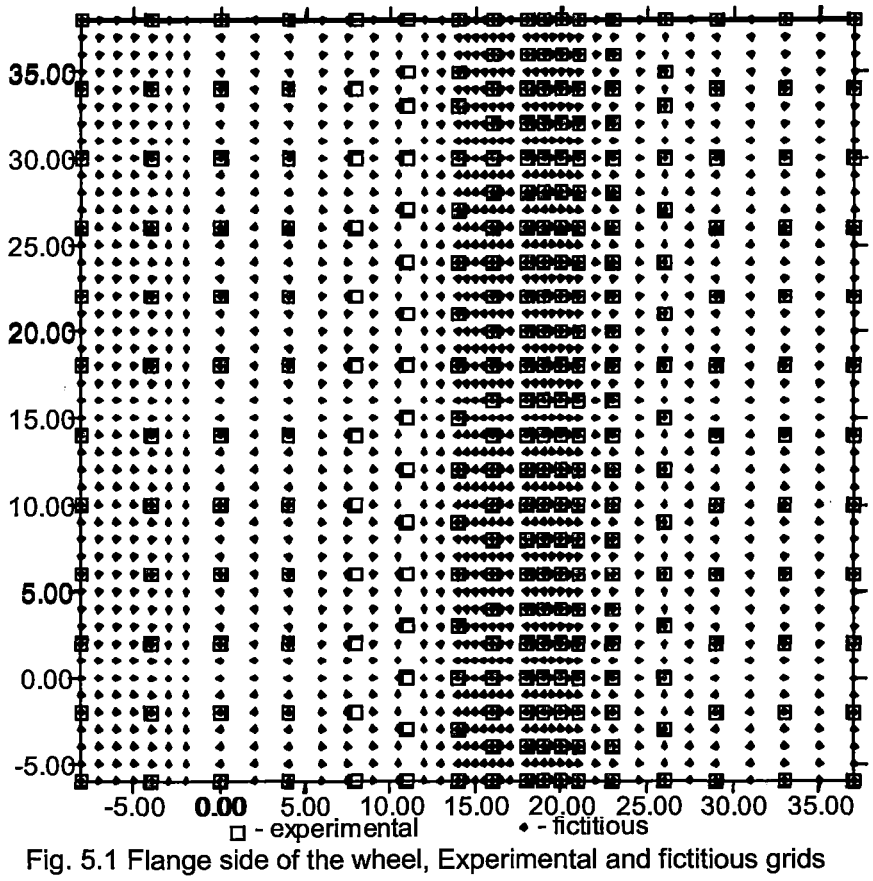

Fig. 5.1 Flange side of the wheel, Experimental and fictitious grids

In both analyses, local as well as global error norms were considered.

An approximation of experimental data with different order and different number of nodes in stars is presented in Fig. 5.2-5.25. Notation used: n_taylor - number of coefficients in Taylor series expansion, nodes - number of nodes in star, optim_par=optimality parameter g - mean distance between current node and central point of a star.

Results obtained are plotted in Fig. 5.2 – 5.27. These pictures are divided into 3 different groups, namely:

Set #1 (Figs 5.2-5.19) - detailed analysis of data approximation performed for each of cuts: #1, #3, #5 of the wheel #2 for flange side (horizontal displacements) of the wheel with optimal approximation parameters taken into account. Approximation parameters taken into account are: n_taylor=8, nodes=36, optim_par=2.

Detailed description of the pictures is as follows:

Cut #1: Fig. 5.2, Flange side, cut #1, horizontal displacements, original data,
Fig. 5.3, Flange side, cut #1, horizontal displacements, approximated data after 7 iterations,
Fig. 5.4, Flange side, cut #1, horizontal displacements, recovered data, no iterations,
Fig. 5.5, Flange side, cut #1, error of the horizontal displacements, no iterations,
Fig. 5.6, Flange side, cut #1, horizontal displacements, recovered data after 7 iterations,
Fig. 5.7, Flange side, cut #1, error of the horizontal displacements, after 7 iterations,
Cut #3: flange side, horizontal displacements: Figs 5.8-5.13,
Cut #5: flange side, horizontal displacements: Figs 5.14-5.19,

As one can see, because the smoothness parameter has the optimum value, approximated data is smooth enough and the errors are very small. Iterations between experimental data and fictitious data considerably decrease the errors (magnitude of the error decreases approximately 10 times). In this way one may absolutely ensure that data at experimental points and data at fictitious points are very close to each other. Thus, one may use data at fictitious points for further analysis, and this process is under error control.

Set #2, cut#3 (Figs 5.20 – 5.22) - summarizing pictures concerning full evaluation of the approximation process and simultaneously experimental data, flange side - horizontal displacements: local error and grid density distribution for different 'error' norms. Detailed description of the pictures is as follows:

Flange side, horizontal displacements

Cut #3, flange side, Fig. 5.20, Error distribution and grid density distribution:
(1) horizontal displacements, (2) error norm #1 – Sobolev norm of zero order,
(3) grid density - norm #1,
(4) error norm #2 – Sobolev seminorm of first order, (5) grid density - norm #2,
(6) error norm #3 – Sobolev norm of first order, (7) grid density - norm #3,
(8) displacement curvature, (9) error norm #4 – Sobolev seminorm of second order,(10) grid density - norm #4,

(11) error norm #5 – Sobolev norm of second order, (12) grid density - norm #5.

Approximated experimental data may be filtered, using a certain treshold value. In Figs 5.21 and 5.22 area where required grid density is greater than 1.0% is shown for cut #3:

Cut #3, flange side Fig. 5.21, Error distribution and grid density distribution (izolines greater than 1.0 are shown), (1) - (12) like Fig. 5.20,

Cut #3, flange side Fig. 5.22, Error distribution and grid density distribution (izolines greater than 10.0 are shown), (1) - (12) like Fig. 5.20.

Set #3, cut#5 (Figs 5.23 – 5.25) - summarizing pictures concerning full evaluation of the approximation process and simultaneously experimental data, flange side - horizontal displacements: local error and grid density distribution for different 'error' norms. Detailed description of the pictures is as follows:

Cut #5, flange side, Fig. 5.23, Error distribution and grid density distribution, (1) - (12) like Fig. 5.20.

In Figs 5.24 and 5.25 area where required grid density is greater than 1% and 10.0% is shown for one cut:

- cut #5, flange side Fig. 5.24, Error distribution and grid density distribution (izolines greater than 1.0 are shown), (1) - (12) like Fig. 5.20,
- cut #5, flange side Fig. 5.25, Error distribution and grid density distribution (izolines greater than 10.0 are shown), (1) - (12) like Fig. 5.20.

As one may see from the presented pictures, the results strongly depend on approximation order and the smoothness parameter value. Namely, if the smoothness parameter is large - data is too smooth, simultaneously this increases the error too (but the errors are not very large, however). If magnitude of the smoothness parameter tends to smaller values, data recovered at experimental points is closer to experimental one, but the data obtained at fictitious points is rougher.

Different error norms indicate different zones of the largest errors. Magnitudes of the norms differ essentially. Higher order norms give larger errors and are more sensitive to changes in the experimental values.

As one may observe, the zero order Sobolev norm indicates completely different zone of the largest errors than the first or second order Sobolev norm. From Figs 5.20 – 5.25 one may see that cutting area is best traced by second Sobolev semi-norm.

An error analysis has been applied to approximation of numerical data coming from FEM analysis as well. Calculation of the influence coefficient matrix (see [[10]]) needs approximation of numerical data from FEM mesh nodes to residual stress recovery procedure nodes (not presented here).

6. New adaptive procedure of experiment planning

As a practical result of introduced error analysis, new adaptive procedure of experiments planning is possible.

Experimental method should take into account character of the measured function, it cannot be separated from character of measured physical field. Simply speaking, in regions where gradients (and curvatures) of measured field are larger, one requires *many more experimental points. Presented approach gives a theoretical foundation* for above mentioned crucial condition in experimental mechanics.

Carrying out measurements is only first, important, but sometimes not the most important stage to have reliable experimental data because usually experimental data is approximated and evaluted. Therefore, **mesurement process consists of:**

1. **A'priori estimation of experiment conditions and critical measurements parametes like locations and density (e.g. gauges), orientation of measurement grid and so on ... .**
2. **Measurement – experimental data collection togehter with enviromental parameters.**
3. **Approximation (smoothing) and evaluation of experimental data**
4. **New grid density of experimental points evaluation – a'posteriori evaluation of critical parameters and experiment conditions. Go to point #2.**

One may distinguish two different situations:

1. it is possible to simulate behavior of measured element or part of structure by means of numerical method (FEM, meshless FDM),
2. it is not possible to simulate experiment numerically.

One may note that the experiment may be repeated or not, if yes, sometimes one has the chance to correct location of experimental points and other experimental conditions. If not, presented approach defines tools for proper data evaluation.

The following procedure is proposed for the case when numerical simulation of experiment is possible:

1. Solve problem numerically, with conditions for proper simulation of measured part of a structure or an element as good as possible.
2. Evaluate a'posteriori error and repeat calculation with new mesh (grid) density, to statisfy equidistribution error requirements.
3. Define experimental grid and transfer (project) numerical solution (by means of MWLS approximation) to this grid. Try to recover original solution from experimental grid using experimental grid as a primary grid and numerical grid as a secondary grid. Evaluate a'posteriori error and new experimental grid density function which takes into account equidistribution of an error.
4. If possible, change experimental point locations, repeat experiment and evaluate a'posteriori error distribution (now real error).
5. Evaluate measured data using estimated error (or new required experimental grid density) as a reliability index to decide which data have to be removed or taken with lowered weight.

If meshless method is used in above mentioned procedure, numerical simulation of the experiment is very easy, because one may directly use experimental grid as numerical one, without any transformations and additional (approximation) errors.

In the case when numerical simulation of experiment is not possible, procedure is as follows:

1. After experiment evaluate a'posteriori error and calculate new mesh (grid) density of experimental points with equidistribution of error.
2. If is it possible change experimental point locations, repeat experiment and evaluate a'posteriori error distribution.
3. Evaluate measured data using determined error (or new required experimental grid density) as a reliability index to decide which data have to be removed or taken with lowered weight.

7. Final Remarks

Present work is devoted to description and evaluation of the fundamental methods of the physical data approximation and the *aposteriori* error estimation i.e. the methods based on differences between original, experimental data (or numerical ones coming from FEM/FDM analysis) and data approximated on fictitious mesh (see [8]).

The *aposteriori* error analysis described above has been applied to the wheel saw cut data and numerical data coming from FEM analysis, using the Meshless Finite Difference approximation. The presented error analysis approach is of great value in determination of the required concentration of experimental points in the zones where the largest stress gradients have occurred.

The current research done on error estimation includes:

- generalization of the Zienkiewicz - Zhu postprocessing estimator concept [[15]] for elastic problems in solid mechanics and its use in analysis of wheel saw cut data,
- determination of the optimal strategies for refinement of the experimental (or numerical) clouds of points, using different error norms (Sobolev norms up to second order),
- development of postprocessing techniques to enhance the solution accuracy using different number of nodes in stars, different approximation order (i.e. 2nd or 3rd order) and additional iterative process to smoothen the largest discrepancies between data on original (experimental) and fictitious (numerical) grids,
- formulation of the new *adaptive approach to experiment planning and carrying out*, taking into account a'posteriori error estimation and distribution of experimental points with equidistributed error,
- analysis of wheel saw cut data, especially for wheel #2 (see R.Czarnek [3]), 5 cuts of the wheel, both flange and 2nd sides of the wheel analyzed,
- analysis of numerical data, coming from FEM analysis, for wheel #2 [11].

Advantages of the error analysis performed on the experimental as well as numerical data (see FEM/FDM analysis [11]) have been shown. A significant step towards a new adaptive analysis (approximation) of the physical data was done. Besides, the approach presented here, yields formulation of new requirements against measurements devices possible, thus making way for adaptive experimental data collection.

The proposed further research includes: development of reliable error estimates for computed "physical fields" with the efficiency index close to 1 (approximated fields are very close to original ones), further development of the optimal strategies for 'h' adaptive refinement of the experimental data points cloud, development of adaptive modeling in which certain features of physical models are incorporated and stress analysis of deformation fields in rails and wheels.

8. References

[1] T.Belytschko, Y.Krongaus, D.Organ, M.Flemming, P.Krysl, Meshless Methods: An Overwiew and Recent Development, *Comp. Meth. in Appl. Mech and Engng*, 139, 3-44, 1996.

[2] G. Bugeda, E Onate, New Adaptive Techniques for Structural Problems, *Numerical Methods in Engng '92*, Ch.Chirsh et al. (Editors), Elsevier Science Publishers B.V., 1992.

[3] R.Czarnek, Experimental Determination of Release Fields in Cut Railroad Car Wheels, *DOT/FRA/ORD-96/DOT-VNTSC-FRA-96, Final Report*, Cambridge, USA, October, 1996.

[4] L.Demkowicz, J.T.Oden, W.Rachowicz, T.A Westerman, Toward a Universal h-p Adaptive Finite Element Strategy. Part2: Aposteriori Error Estimation, *Computer Methods in Applied Mechanics and Engineering*, 77(1-2)113-180, 1989.

[5] W. Karmowski, J.Orkisz, Physicall Based Enhanced Analysis of Stresses Using Experimental Data, in: *Quality and Maintenance for Modern Railway Operation*, editor J.J.Kalker et al., pp. 287-296, Delft, 24-26 June, 1992.

[6] W. Karmowski, J.Orkisz, Physically Based Method of Enhanced of Experimental Data – Concept, Formulation and Application to Identification of Residual Stresses, *Proc. of the IUTAM Symposium on Inverse Problems in Engng Mechanics*, May 11-15 Tokyo, Japan, Springer-Verlag, 61-70, 1993.

[7] J. Krok, J.Orkisz, Application of the Generalized FDM to Calculation of Arbitrary Loaded Axisymmetrical Massive Structures, *Proc of 28-th Conf. KILiW PAN and KN PZITB*, Krynica, Poland, 1982, 81-90 (in polish).

[8] J.Krok, New Approach of Error Control in Approximation and Smoothing of Physical Data, Application to wheel Saw Cut Measurements Data, *Report to the VNTSC*, Cambridge, USA, 1998.

[9] J.Krok, J.Orkisz: Aplication of the Generalized FD Approach to Stress Evaluation in the FE Solution, *Int. Conf. on Comp. Mech.*, Tokyo 1986, XII, pp.31-36.

[10] J. Krok, J. Orkisz: A Unified Approach to the FE Generalized Variational FD Method in Nonlinear Mechanics, Concept and Numerical Approach, in: *Discretization Method in Structural Mechanics, IUTAM/IACM Symposium Vienna 1989*, pp.353-362, Springer-Verlag, 1990.

[11] J.Krok, J.Orkisz, A. Skrzat, Reconstruction of Hoop Stresses in 3D Bodies of Revolution Based on Simulated Saw Cut Data, *XIII Conf. on Comp. Meth. in Mechanics*, Poznań, Poland, 669-676, 1997.

[12] J.Krok, J.Orkisz, Unified Approach to the Adaptive FEM and Meshless FDM. Concept and Tests, *2nd European Conference on Computational Mechanics*, June 26-29, Cracow, Poland , 2001, pp 1-33.

[13] J.Orkisz, The Finite Difference Method, Part III, in: *Numerical Methods in Mechanics*, in: Springer - Verlag, 1998.

[14] J.Z.Zhu, E.Hinton, O.C.Zienkiewicz, Mesh Enrichment Against Mesh Regeneration Using Quadrilateral Elements, *Comm. in Num. Meth. in Engng*, Vol. 9, 547-554, 1993.

[15] O.C.Zienkiewicz, J.Z.Zhu, A Simple Error Estimator and Adaptive Procedure for Practical Engineering Analysis, *Int. Journ. Num. Meth. Eng.*, 24, 337-357, 1987.

[16] O.C.Zienkiewicz, J.Z.Zhu,The Superconvergent Patch Recovery and A`Posteriori Error Estimates. Part 2: Error Estimates and Adaptivity, *Int. J Num Meth Engng*, 33, 1365-1382, 1992.

[17] O.C.Zienkiewicz, R.L.Taylor, *Finite Element Method*, Butterworth, Oxford, 2000.

[18] L.Gavette, J.L.Cuesta, A.Ruiz, A Procedure for Approximation of the Error in the EFG Method, *Int. Journ. Num. Meth. Eng.*, Vol. 53, pp. 677-690, 2002.

[19] A.Skrzat, J.Orkisz, J.Krok, Residual Stress Reconstruction in Railroad Car Wheels Based on Experimental Data Measured at Saw Cut Test, *2nd European Conference on Computational Mechanics*, June 26-29, Cracow, Poland , 2001, pp 1-17.

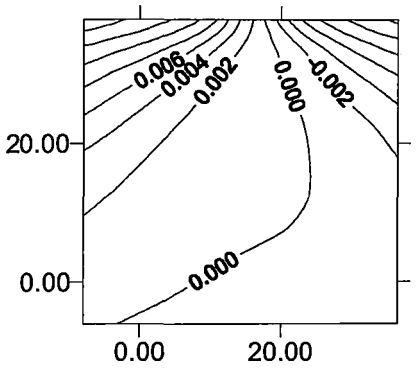

Fig.5.2, Cut #1, Flange side,
horizontal displacements,
original data, min=-1.25E-2, max=1.55E-2

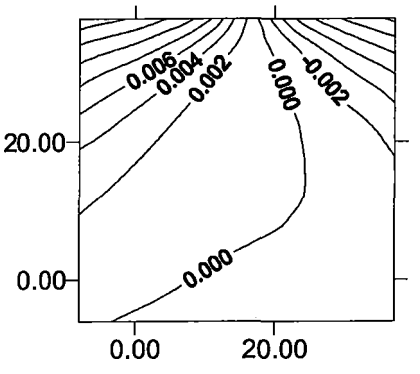

Fig.5.3, Flange side,
horizontal displacements,
approximated data after 7 iterations

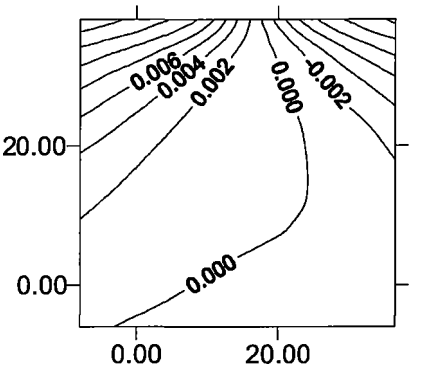

Fig. 5.4, Flange side,
horizontal displacements,
recovery data, no iteration

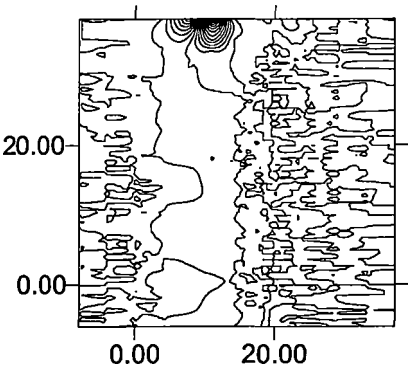

Fig.5.5, Flange side,
Error of the horizontal displacements,
no iterations,
min=1.35E-5, max=7.46E-6, inc=1E-6

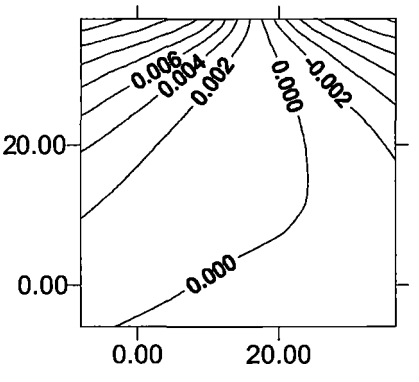

Fig. 5.6, Flange side,
horizontal displacements,
recovery data, after iterations

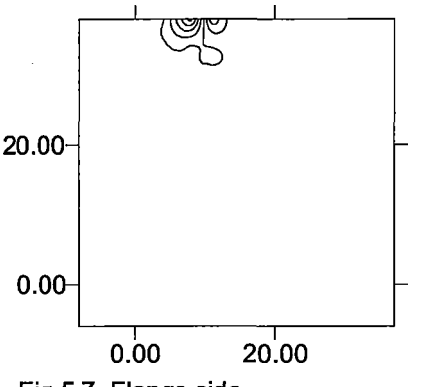

Fig.5.7, Flange side,
error of the horizontal displacements,
after 7 iterations,
min=-1.34E-6, max=2.40E-6, inc=5E-7

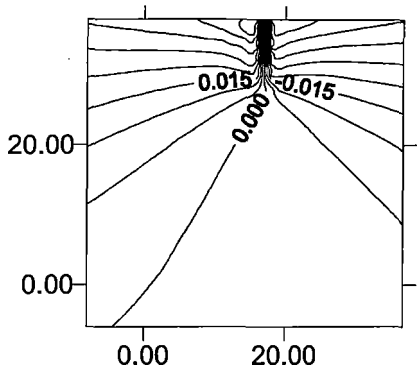

Fig. 5.8, Cut #3, Flange side,
horizontal displacements,
original data, min=-4.48E-2, max=4.33E-2

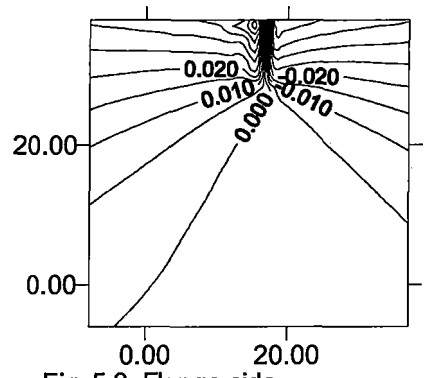

Fig. 5.9, Flange side,
horizontal displacements,
approximated data, after 7 iterations

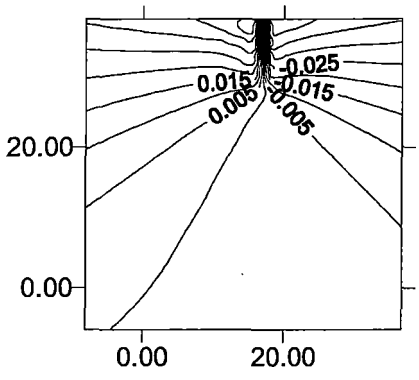

Fig. 5.10, Flange side,
horizontal displacements,
recovery data, no iterations

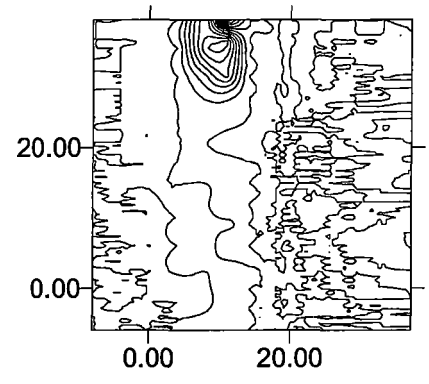

Fig. 5.11, Flange side,
error of the horizontal displacements,
no iteration,
min=-1.47E-4, max=1.10E-4, inc=2E-5

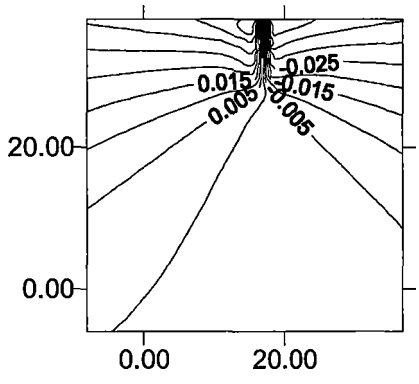

Fig. 5.12, Flange side,
horizontal displacements,
recovery data, after 7 iterations

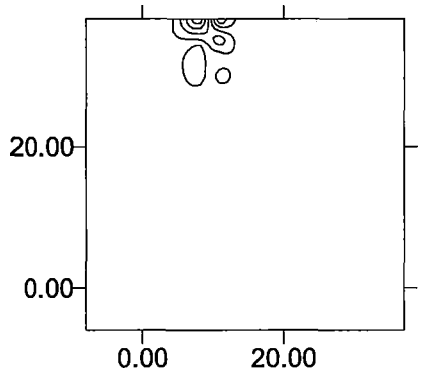

Fig. 5.13, Flange side,
error of the horizontal displacements,
after 7 iterations,
min=-2.12E-5, max=1.35E-5, inc=5E-6

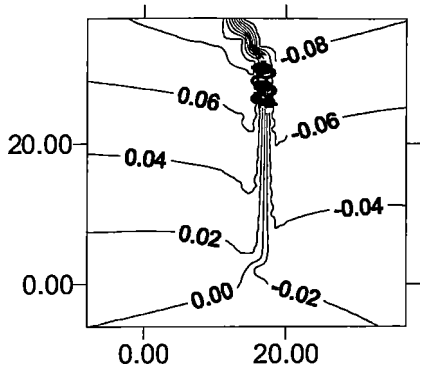

Fig. 5.14, Cut #5, Flange side,
horizontal displacements,
original data, min=-9.49E-2, max=9.00E-2

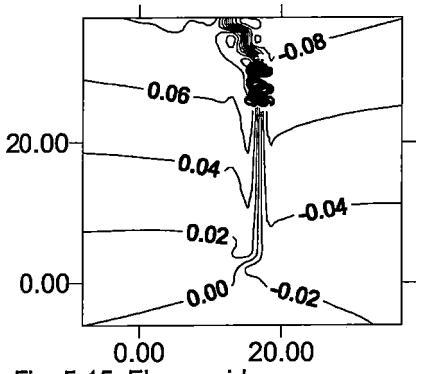

Fig. 5.15, Flange side,
horizontal displacements,
approximated data, after 7 iterations

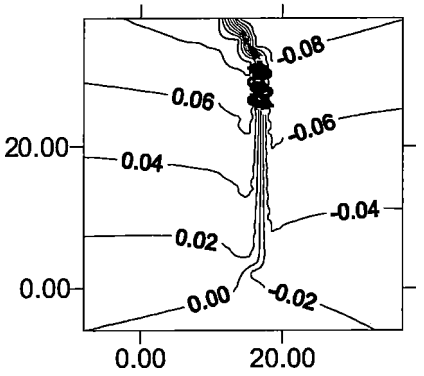

Fig. 5.16, Flange side,
horizontal displacements,
recovery data, no iterations

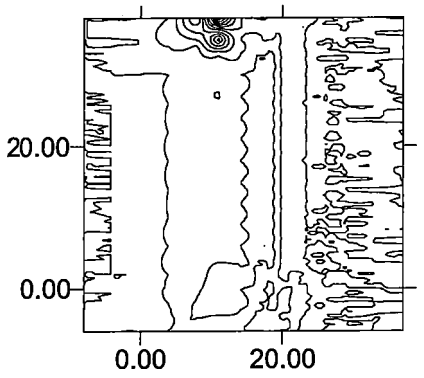

Fig. 5.17, Flange side,
error of the horizontal displacements,
no iteration,
min=-3.25E-3, max=2.72E-3, inc=1E-3

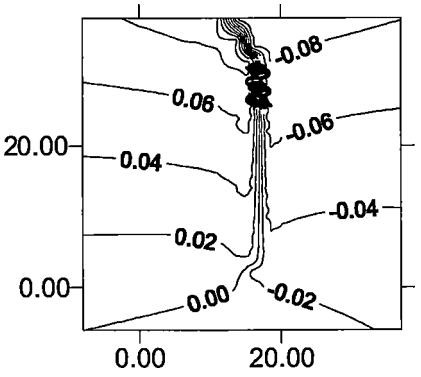

Fig. 5.18, Flange side,
horizontal displacements,
recovery data, after 7 iterations

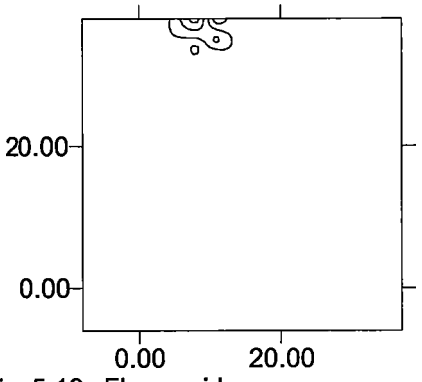

Fig. 5.19, Flange side,
error of the horizontal displacements,
after 7 iterations,
min=-3.41E-4, max=5.54E-4, inc=2E-4

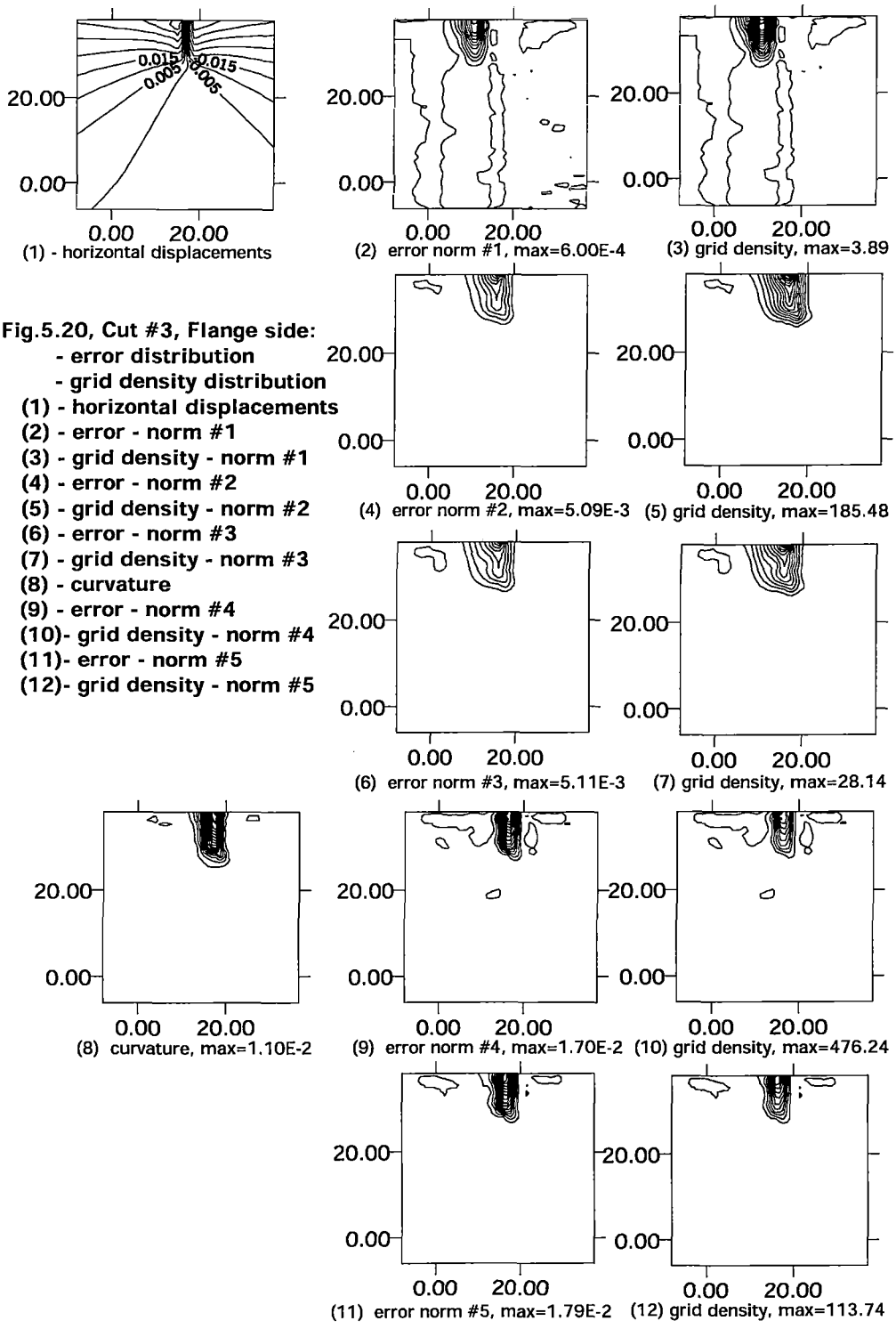

Fig.5.20, Cut #3, Flange side:
- **error distribution**
- **grid density distribution**

(1) - horizontal displacements
(2) - error - norm #1
(3) - grid density - norm #1
(4) - error - norm #2
(5) - grid density - norm #2
(6) - error - norm #3
(7) - grid density - norm #3
(8) - curvature
(9) - error - norm #4
(10)- grid density - norm #4
(11)- error - norm #5
(12)- grid density - norm #5

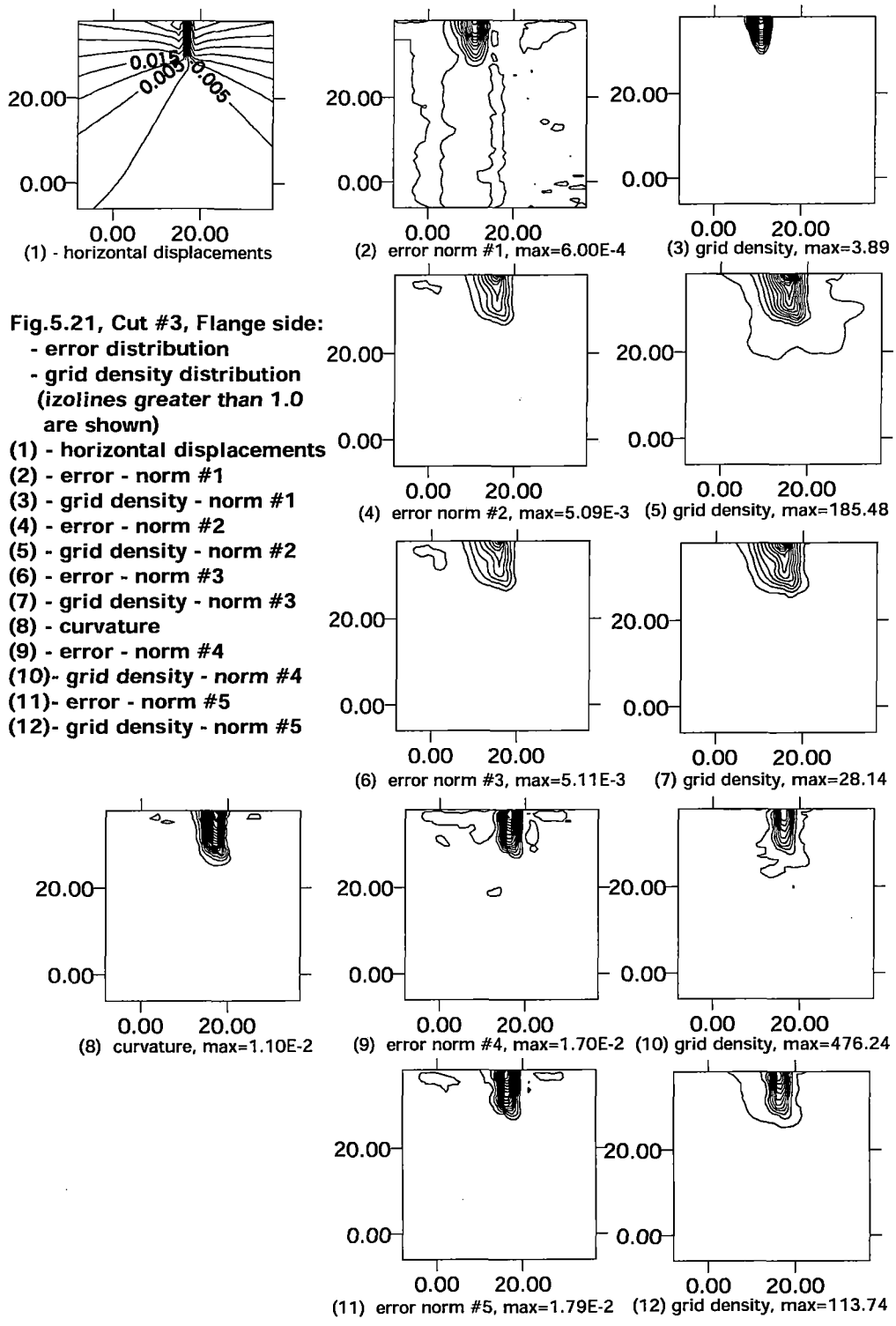

Fig.5.21, Cut #3, Flange side:
- **error distribution**
- **grid density distribution**
- ***(izolines greater than 1.0 are shown)***

(1) - horizontal displacements
(2) - error - norm #1
(3) - grid density - norm #1
(4) - error - norm #2
(5) - grid density - norm #2
(6) - error - norm #3
(7) - grid density - norm #3
(8) - curvature
(9) - error - norm #4
(10)- grid density - norm #4
(11)- error - norm #5
(12)- grid density - norm #5

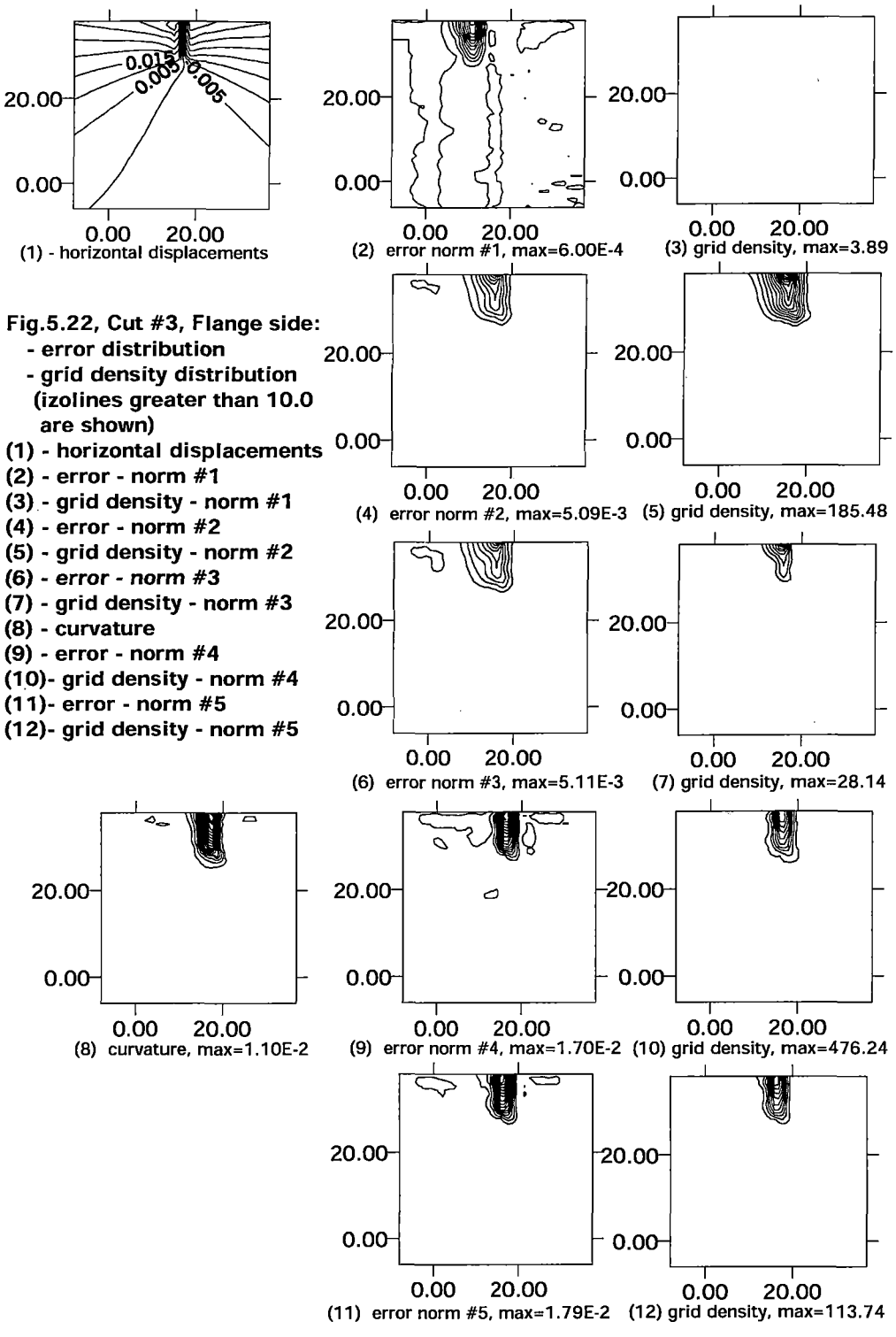

Fig.5.22, Cut #3, Flange side:
- **error distribution**
- **grid density distribution**
- **(izolines greater than 10.0 are shown)**

(1) - horizontal displacements
(2) - error - norm #1
(3) - grid density - norm #1
(4) - error - norm #2
(5) - grid density - norm #2
(6) - error - norm #3
(7) - grid density - norm #3
(8) - curvature
(9) - error - norm #4
(10)- grid density - norm #4
(11)- error - norm #5
(12)- grid density - norm #5

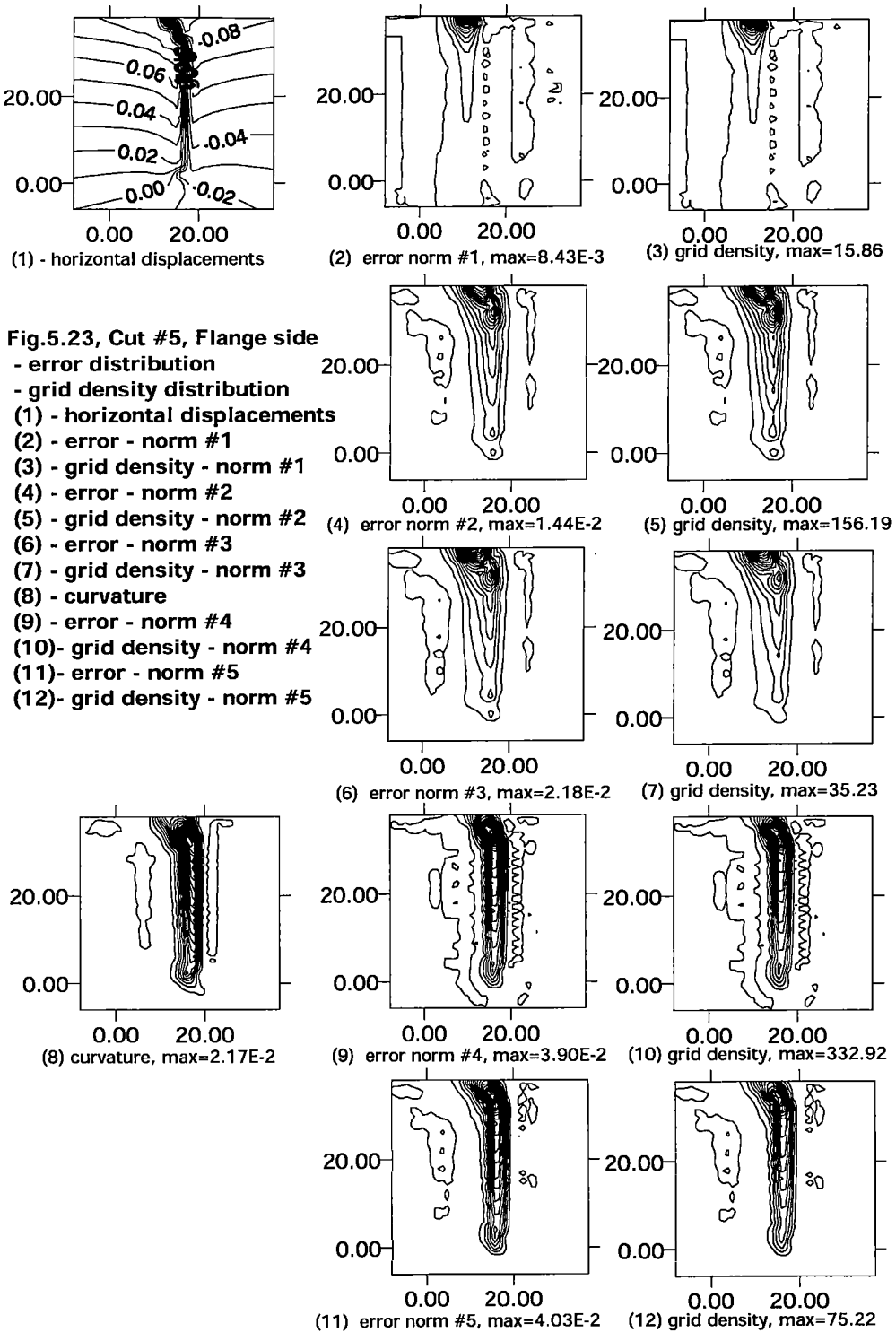

Fig.5.23, Cut #5, Flange side
- **error distribution**
- **grid density distribution**

(1) - horizontal displacements
(2) - error - norm #1
(3) - grid density - norm #1
(4) - error - norm #2
(5) - grid density - norm #2
(6) - error - norm #3
(7) - grid density - norm #3
(8) - curvature
(9) - error - norm #4
(10)- grid density - norm #4
(11)- error - norm #5
(12)- grid density - norm #5

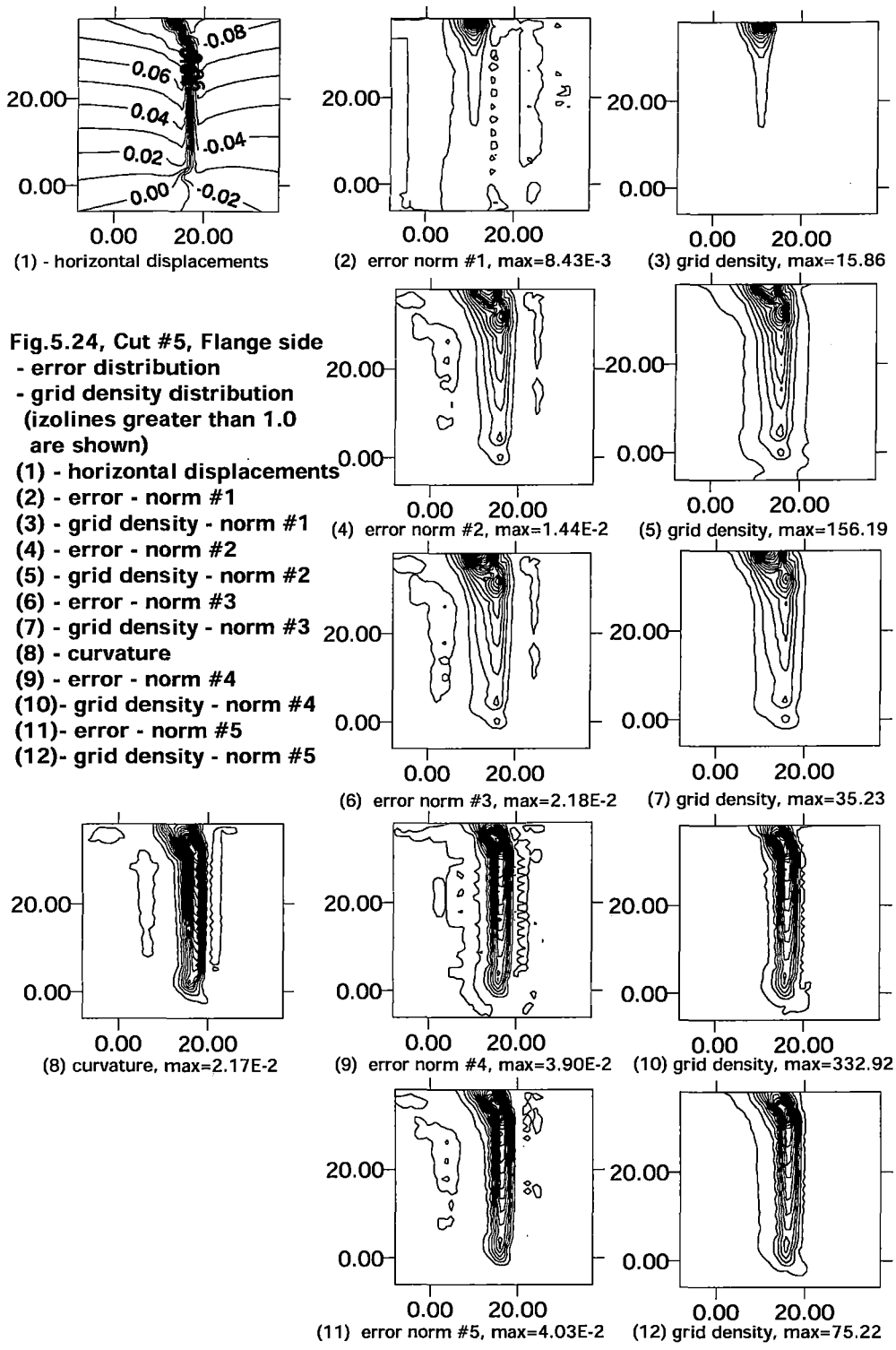

Fig.5.24, Cut #5, Flange side
- **error distribution**
- **grid density distribution (izolines greater than 1.0 are shown)**

(1) - horizontal displacements
(2) - error - norm #1
(3) - grid density - norm #1
(4) - error - norm #2
(5) - grid density - norm #2
(6) - error - norm #3
(7) - grid density - norm #3
(8) - curvature
(9) - error - norm #4
(10)- grid density - norm #4
(11)- error - norm #5
(12)- grid density - norm #5

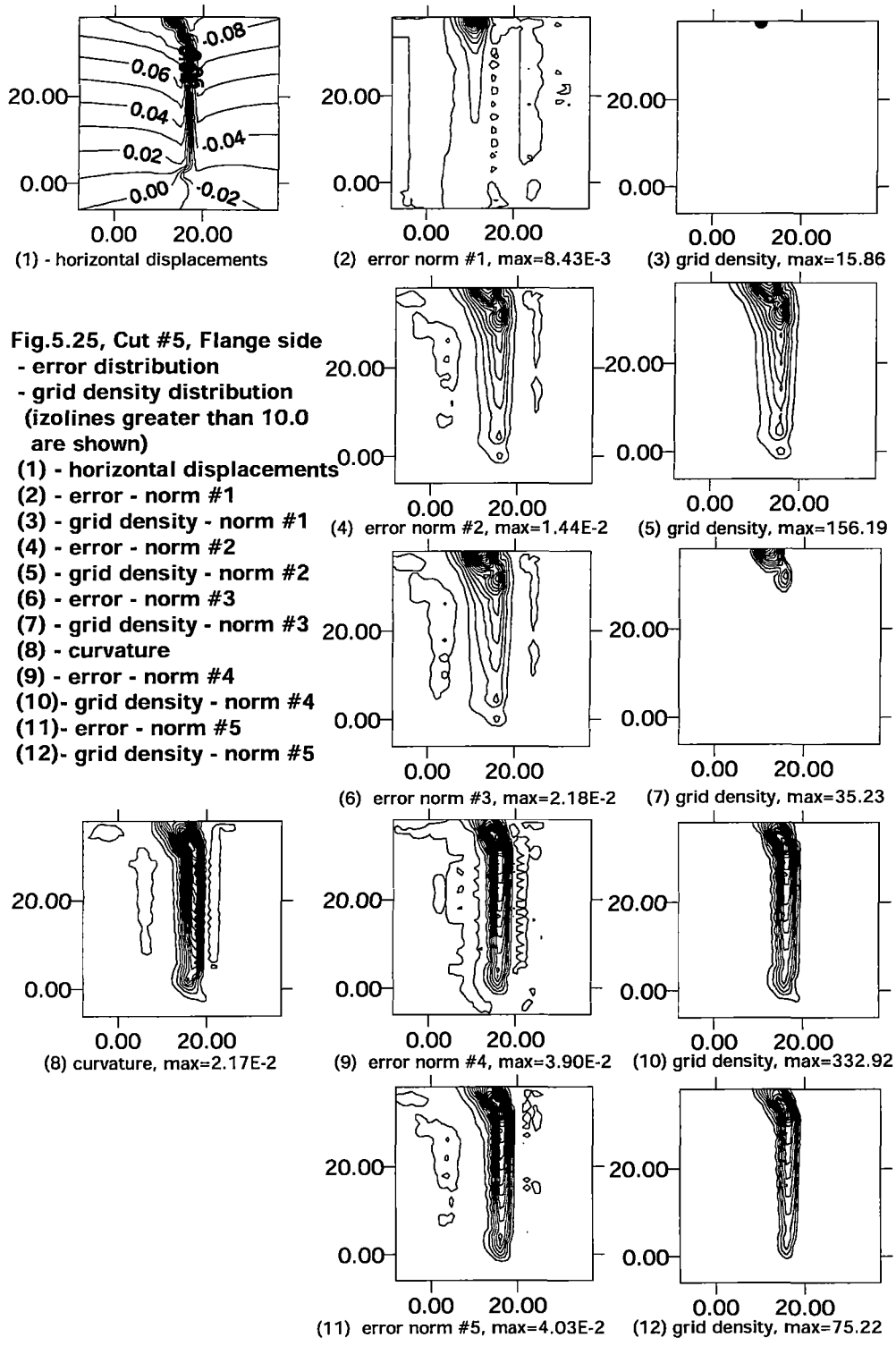

Fig.5.25, Cut #5, Flange side
- **error distribution**
- **grid density distribution**
  (izolines greater than 10.0 are shown)

(1) - horizontal displacements
(2) - error - norm #1
(3) - grid density - norm #1
(4) - error - norm #2
(5) - grid density - norm #2
(6) - error - norm #3
(7) - grid density - norm #3
(8) - curvature
(9) - error - norm #4
(10)- grid density - norm #4
(11)- error - norm #5
(12)- grid density - norm #5

Topic 2.6

Reconstruction of residual stresses in railroad vehicle wheels based on enhanced saw cut measurements

Reconstruction of residual stresses in railroad vehicle wheels based on enhanced saw cut measurements

Thus following problems are intended to be addressed:

(i) Further development and improvement of numerical procedures used in the analysis of residual hoop stresses, in order to obtain better precision results use of 20-node brick elements

(ii) Residual hoop stress evaluation in all investigated wheels using 20-node elements in FEM calculations,

(iii) More precise calculation of influence coefficients – solving problems with about 450 000 DOF (the size of previously solved problems is about 150 000 DOF)

Ad (i) - done
Developing software necessary to computation of kinematically equivalent loads and computation of hoop stress in the non-cut part of the wheel (finite element method stress results are not used here)

Ad (ii) – done
Results of all investigated wheels are included in this year report

Ad (iii) – done
For the first time the huge 400 thousand DOF problem has been solved in influence coefficients computation of the wheel #3. In each discrete problem about 40 right-hand side vectors occurred, and therefore the size of FEM problem has been limited to 400 thousand DOF.

Cracow University of Technology
ul. Warszawska 24, 31-155 Cracow, POLAND

Reconstruction of residual stresses in railroad vehicle wheels based on enhanced saw cut measurements.

Janusz Orkisz, Andrzej Skrzat

Report to the

US Department of Transportation,
Federal Railroad Administration,
Washington, DC

Cracow, June 2003

Reconstruction of residual stresses in railroad vehicle wheels based on enhanced saw cut measurements

Janusz Orkisz
Cracow University of Technology

Andrzej Skrzat
Rzeszow University of Technology

1. Introduction

During service railroad car wheels develop residual stresses that can lead to premature, and in some instances, catastrophic failure. These stresses are mainly caused by thermal loadings (heavy braking) combined with cyclic contact stresses. Stresses are also influenced by wear of the wheel rim. A good understanding of residual stress distribution and its variation over time in service can help develop a better wheel design that would minimize the danger of catastrophic failure. Knowledge of this distribution can also help improve the techniques used for routine inspection of wheels and detection of potentially dangerous stress distributions.

In 1991 the US Department of Transportation began studies on improving the railway transportation safety. Within the confines of this program, the Concurrent Technologies Corporation carried out experimental destructive investigation of several railroad car wheels [2]. In each test the wheel was radially cut. This caused partial residual hoop stress release. Effects of residual stress release could be observed on the wheel surface. Experimental data have been obtained by means of several different experimental techniques: moiré interferometry (relative displacements), strain gauges (absolute strains) and clip gauges (absolute displacements). The locations of measurements are presented in Fig. 1. Unfortunately the experimental information alone does not suffice to reconstruct initial residual hoop stress.

The solution approach called "physically based enhancement of experimental data" [5], formulated, developed and tested in Cracow University of Technology during last years, is now the best available numerical tool to approximate residual hoop stress component in railroad car wheels. The precision of residual hoop stress approximation depends mainly on numerical tools used in experimental data

processing, as well as on the precision of FEM analysis used to compute the influence coefficients necessary in presented approach. During last three years a significant progress has been made in the precision of influence coefficient calculations. Instead of previously used 8-node brick elements, 20-node brick elements have been introduced. Currently unit pressures are applied on finite elements, instead of unit forces. Such approach yields better precision of numerical calculations, especially in areas close to applied loads. The new version of commercial software used to calculate the coefficients (ADINA 8.0) allows for solving huge 3D problems by the finite element method. Thus the elastic problem size limit set at approximately 150 thousand DOF has been broken, and recently the 400 thousand DOF problem has been successfully solved. The numerical effort is enormous, but the precision of influence coefficients and the precision of residual stress approximation is much higher than ever before.

A benchmark test is presented in this report, which prove the efficiency and precision of the new approach in numerical calculations of influence coefficients (20-node elements, element pressures as loading). The results for all investigated wheels obtained for coarse finite element mesh are included as well. Finally the results for the wheel #3, obtained for the first time for the dense mesh are presented.

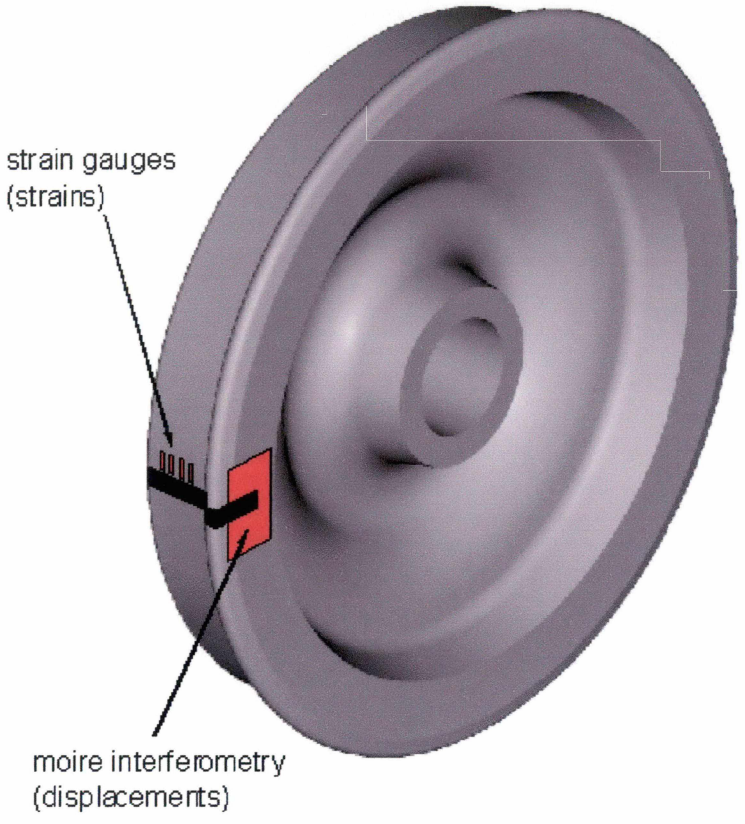

Fig. 1 Measurements taken at the saw cut test

2. Formulation

2.1. Incremental procedure

Formulation for the hoop stress reconstruction in the railroad vehicle wheel is based on measurements done at the saw cut test. The approach is formulated as a two-step non-linear constrained optimization problem [3].

Step one

Find the out-of-plane stresses $\sigma^{out}(\lambda) = \{\sigma_{\Theta\Theta}, \sigma_{r\Theta}, \sigma_{\Theta z}\}$ providing the minimum of the functional

$$\mathrm{I} = \lambda\Phi^{\mathrm{E}} + (1-\lambda)\Phi^{\mathrm{T}}, \qquad \lambda \in [0,1] \ . \tag{1}$$

while satisfying the equilibrium equation

$$\frac{\partial \sigma_{r\Theta}}{\partial r} + \frac{1}{r}\frac{\partial \sigma_{\Theta\Theta}}{\partial \Theta} + \frac{\partial \sigma_{\Theta z}}{\partial z} + \frac{2}{r}\sigma_{r\Theta} = 0 \ . \tag{2}$$

and homogenous static boundary conditions for tractions

$$p_r = p_\Theta = p_z = 0 \ . \tag{3}$$

normal and tangent to the (r,z) plane (saw cut plane).

Here

$$\Phi^{\mathrm{T}} = \Phi^{T}\left(\sigma^{out}\right) = \frac{1}{V_{out}} \int_V \kappa^2\left(\sigma^{out}\right) dV \ . \tag{4}$$

is the theoretical part (a smoothness requirement for the curvature κ to be minimal) of the functional, while the experimental part $\Phi^{E}\left(\sigma^{out}\right)$ is a weighted measurement error (Φ^{T} and Φ^{E} are normalized).

In the axial symmetry case $\sigma_{r\Theta} \equiv \sigma_{\Theta z} \equiv 0$, $\sigma_{\Theta\Theta,\Theta} \equiv 0$, and only the hoop stress $\sigma_{\Theta\Theta}(r,z)$ can be found this way. The equilibrium equation is always satisfied then. In each case a family of solutions is obtained depending on a parameter λ determined in the second part of procedure.

Step two.

Find the minimum $\lambda \in [0,1]$ satisfying the local (5) and global (6) inequality constraints resulting from measurement precision.

$$\left\| u_i^{\exp} - u_i \right\| - \Delta u_i^{adm} \le 0 \qquad i=1,2,\ldots,n$$

$$\left\|\varepsilon_{ij}^{\exp}-\varepsilon_{ij}\right\|-\Delta\varepsilon_{ij}^{adm}\le 0, \tag{5}$$

$$\left\|\delta_i^{\exp}-\delta_i\right\|-\Delta\delta_i^{adm}\le 0.$$

$$\left\|\Phi^{\mathrm{E}}\left(\sigma^{out}\right)\right\|-\Delta\Phi^{adm}\le 0. \tag{6}$$

Here $u_i^{\exp}$, $\varepsilon_{ij}^{\exp}$, $\delta_i^{\exp}$ and u_i, ε_{ij}, δ_i are the experimental and approximated values of displacements, strains or COD measurements, Δu_i^{adm}, $\Delta\varepsilon_{ij}^{adm}$, $\Delta\delta_i^{adm}$ and $\Delta\Phi^{adm}$ are admissible experimental errors resulting from measurement precision.

One may define the error functional as

$$\Phi^{E}=\sum_{k=1}^{K}\left[\frac{u_k^{\exp}-u_k}{\Delta u_k^{adm}}\right]^2+\sum_{k=1}^{L}\left[\frac{\varepsilon_k^{\exp}-\varepsilon_k}{\Delta\varepsilon_k^{adm}}\right]^2+\sum_{k=1}^{M}\left[\frac{\delta_k^{\exp}-\delta u_k}{\Delta\delta_k^{adm}}\right]^2. \tag{7}$$

The summation is extended over all experimental measurements of relative displacements K (u_k^{exp} - up to three displacement components at each point), strains L (ε_k^{exp} - up to three strain tensor components at each point) and absolute displacements M. (δ_k^{exp} - one component at each point).

The functional (7) depends directly on measured quantities u,ε,δ rather than on the primary unknowns - out-of-plane residual stresses in the cut zone $\sigma_{cut}^{out}=\left\{\sigma_{\Theta\Theta},\sigma_{r\Theta},\sigma_{\Theta z}\right\}_{cut}$. Thus u,ε,δ have to be expressed in terms of σ_{cut}^{out}. Unloading process, releasing residual stresses during cutting, is assumed to be elastic. Therefore appropriate influence functions may be used in order to replace u,ε,δ by σ_{cut}^{out}. These influence functions are found numerically. Practical implementation requires evaluation of appropriate kernels by means of discrete analysis of a sequence of boundary value problems for the wheel in subsequent stages of the saw cut test. Thus, for each measured quantity u,ε,δ, one obtains transformation matrices $A_u,A_\varepsilon,A_\delta$, where:

$$u = A_u \sigma_{cut}^{out}, \qquad \varepsilon = A_\varepsilon \sigma_{cut}^{out}, \qquad \delta = A_\delta \sigma_{cut}^{out}. \tag{8}$$

This way one can express both the functional $\Phi^E = \Phi^E\left(\sigma_{cut}^{out}\right)$ and all inequalities (5),(6) in terms of σ_{cut}^{out} as required.

2.2. Expression of measured quantities in terms of residual stresses σ_{cut}^{out}

The body V is considered to be linearly elastic, stress free and partially cut, loaded along the cut edge l_c by tractions

$$p_i = n_j \sigma_{ij}^R\left(l_c\right). \tag{9}$$

resulting from the residual stresses σ_{ij}^R released in the given cut layer, existing in the body before this cut. The solution of such a boundary-value problem for a given cut depth may be written for both 2D and 3D bodies in the following form:

$$\Delta u_i(x,l) = \int_l p_k(\xi) U_{ik}(x,\xi,l) ds(\xi) = -\int_l \sigma_{kj}^R(\xi) n_j(\xi) U_{ik}(x,\xi,l) ds(\xi),$$

$$\Delta \varepsilon_{ij}(x,l) = \int_l p_k(\xi) E_{ijk}(x,\xi,l) ds(\xi) = -\int_l \sigma_{ks}^R(\xi) n_s(\xi) E_{ijk}(x,\xi,l) ds(\xi), \tag{10}$$

$$\Delta \sigma_{ij}(x,l) = \int_l p_k(\xi) S_{ijk}(x,\xi,l) ds(\xi) = -\int_l \sigma_{ks}^R(\xi) n_s(\xi) S_{ijk}(x,\xi,l) ds(\xi).$$

Here $\Delta u_i, \Delta \varepsilon_{ij}, \Delta \sigma_{ij}$ are changes in displacements, strains and stresses, respectively, at arbitrary point x of the body V when one layer of the body is cut. Kernels U_{ik}, E_{ijk}, S_{ijk} present displacements, strains and stresses, at a point x of the body V when loaded by a normal unit force (see Fig. 2) applied at a point ξ located by the cut edge layer (in the neighbourhood of the cut layer).

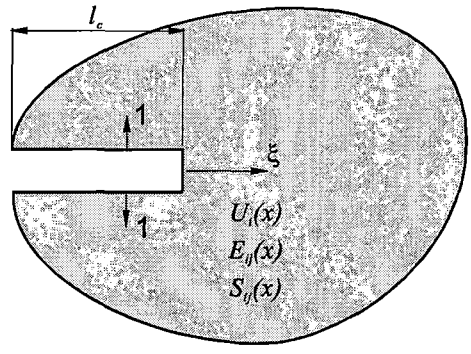

Fig. 2 Body loaded by normal unit force

These kernels can be found by discrete analysis (FEM,FDM,BEM). Formulas (10) may be presented then in the following form:

$$\Delta u_i(x,l) \cong \sum_m p_k(\xi_m) U_{ik}(x,\xi_m,l)\Delta S_m = -\sum_m \left(\sigma_{kj}^R n_j U_{ik}\Delta S\right)_{|m},$$

$$\Delta \varepsilon_i(x,l) \cong \sum_m p_k(\xi_m) E_{ijk}(x,\xi_m,l)\Delta S_m = -\sum_m \left(\sigma_{ks}^R n_s E_{ijk}\Delta S\right)_{|m}, \tag{11}$$

$$\Delta \sigma_i(x,l) \cong \sum_m p_k(\xi_m) E_{ijk}(x,\xi_m,l)\Delta S_m = -\sum_m \left(\sigma_{ks}^R n_s E_{ijk}\Delta S\right)_{|m}.$$

where $(\ )_{|m} = (\ )_{|\xi=\xi_m}$ and *i,j,k,s*=1,2 (2D case) or *i,j,k,s*=1,2,3 (3D case).

One can express now both the functional (7) and the inequalities (5),(6) in terms of required unknowns σ_{cut}^R e.g. formulas (5) can be written in the incremental way as follows:

$$\left\| u_i^{\exp} - \sum_l U_i \sigma^R \right\| - \Delta u_i^{adm} \le 0,$$

$$\left\| \varepsilon_{ij}^{\exp} - \sum_{l} E_{ij}\sigma^{R} \right\| - \Delta\varepsilon_{ij}^{adm} \le 0, \tag{12}$$

$$\left\| \delta_{ij}^{\exp} - \sum_{l} \Delta_{i}\sigma^{R} \right\| - \Delta\delta_{j}^{adm} \le 0$$

The summation $\sum_{l}$ is extended over all layers cut until all measurements of $u_i^{\exp}, \varepsilon_i^{\exp}, \sigma_i^{\exp}$ have been taken.

One may solve now the optimization problem of the step two replacing inequalities (5) and (6) by inequalities (12) expressed in terms of the primary unknowns σ_{ij}^{R}. Our required unknowns are the residual hoop stresses σ_{ij} existing in the body before any cut. One can easily find the relations between them and σ_{ij}^{R} in a way similar to looking for kernels U_{ik}, E_{ijk}, S_{ijk} (discrete analysis).

$$\sigma_{ij} = [\alpha]\sigma_{ij}^{R}. \tag{13}$$

Matrix $[\alpha]$ is the matrix consisting of columns constituting stresses existing in a non-cut part of the body when loaded by normal unit forces applied at the point ξ located at the cut edge (last layer cut). The matrix $[\alpha]$ is not singular, therefore one can finally write the inequalities (12) as:

$$\left\| u_i^{\exp} - \sum_{j} U_i[\alpha]^{-1}\sigma \right\| - \Delta u_i^{adm} \le 0,$$

$$\left\| \varepsilon_{ij}^{\exp} - \sum_{j} E_{ij}[\alpha]^{-1}\sigma \right\| - \Delta\varepsilon_{ij}^{adm} \le 0, \tag{14}$$

$$\left\| \delta_{ij}^{\exp} - \sum_{j} \Delta_i[\alpha]^{-1}\sigma \right\| - \Delta\delta_{j}^{adm} \le 0.$$

3. Finite element simulation of the cutting process

As described in the previous chapter, the calculation of residual hoop stress component in railroad car wheels requires the knowledge of the relation between released residual stresses and measured quantities. Theoretical solution is not known because of complicated shape of the wheel and complex boundary conditions. Therefore, finite element analysis is introduced. During cutting, the stiffness of the wheel, as well as magnitudes of residual stresses in the non-cut part of the wheel changes. Therefore, FEM simulation of the cutting process has to be performed incrementally. In order to find the relation between released residual hoop stresses and measured quantities the set of boundary value problems has to be solved.

3.1. Unit forces versus unit pressures

It is known that the finite element method yields over stiffened results when displacement formulation is applied. The magnitudes of stresses, strains and displacements are underestimated. Therefore, influence coefficients used in the analysis of residual hoop stresses may be too small. The magnitudes of computed residual hoop stresses obtained from the analysis are too large (see Eq. 11). The increase in the magnitude of hoop stresses depends on the precision of computed influence coefficients. Several numerical tests have been made to investigate the precision of computed influence coefficients. The following figures present the results of such benchmark tests performed for the same mechanical problem when different types of finite elements are used. The unit force is applied to the edge of 3D body (Fig. 3).

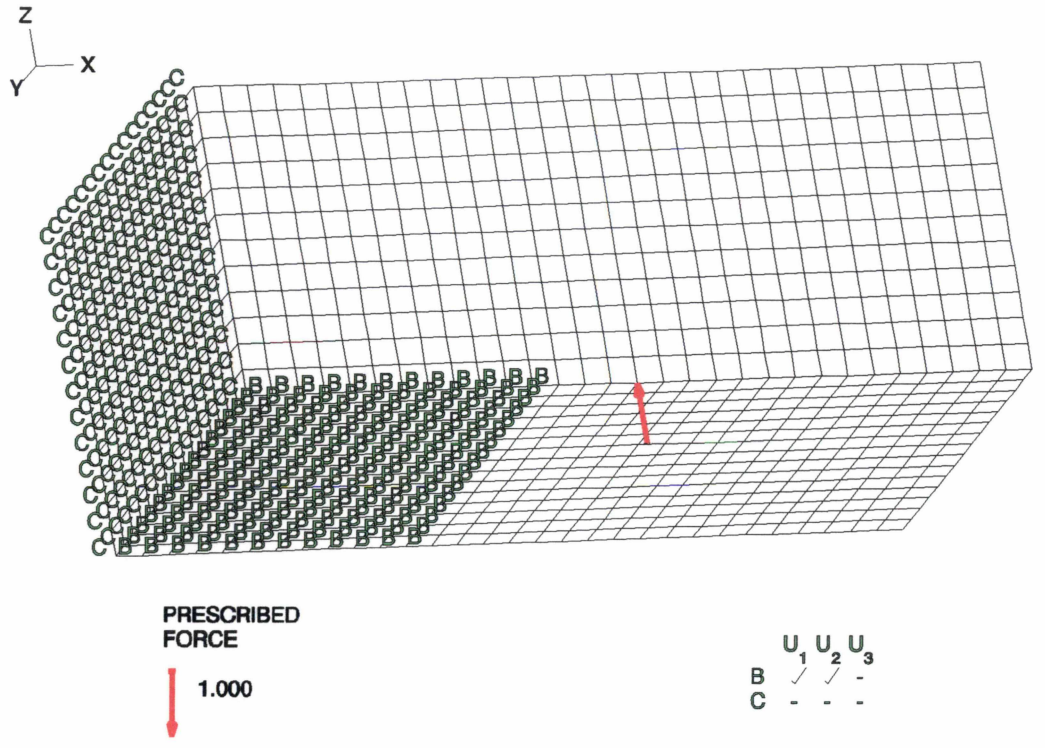

Fig. 3 FEM model – unit force applied

The following figures are described in Table 1.

Table 1. Results of benchmark tests – unit force is applied

Figure	Type of element	Max vertical displacement
Fig. 4	8-node brick	5.8e-7
Fig. 5	20-node brick	11.1e-7
Fig. 6	27-node brick	15.5e-7
Fig. 7	8-node brick (dense mesh)	2.9e-7

One may notice in Table 1 and also in Fig. 4 – Fig. 7, that the differences in the magnitude of vertical displacement is significant. The 8-node element model is about three times stiffer in the location of applied load, than the 27-node model. Moreover, even when dense mesh is used (Fig. 7) there is still no convergence to Fig. 6, which presents the most precise solution.

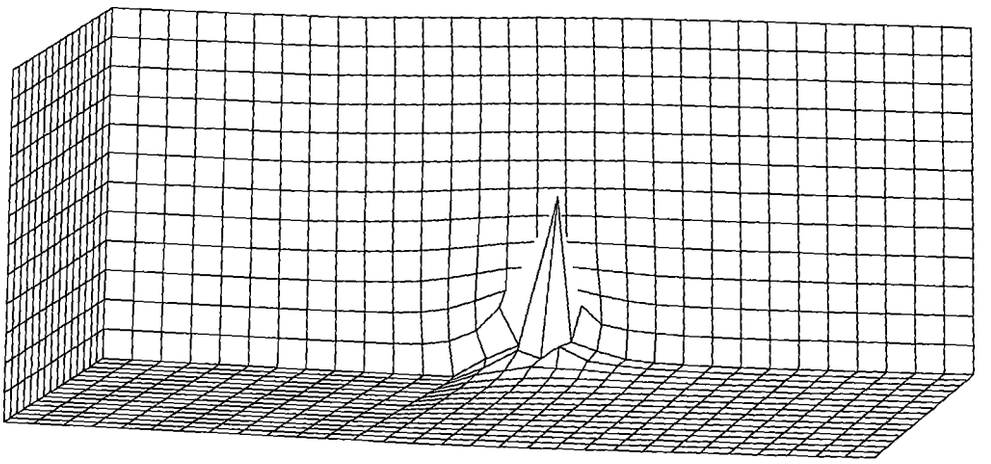

Fig. 4 Results for 8-node brick elements

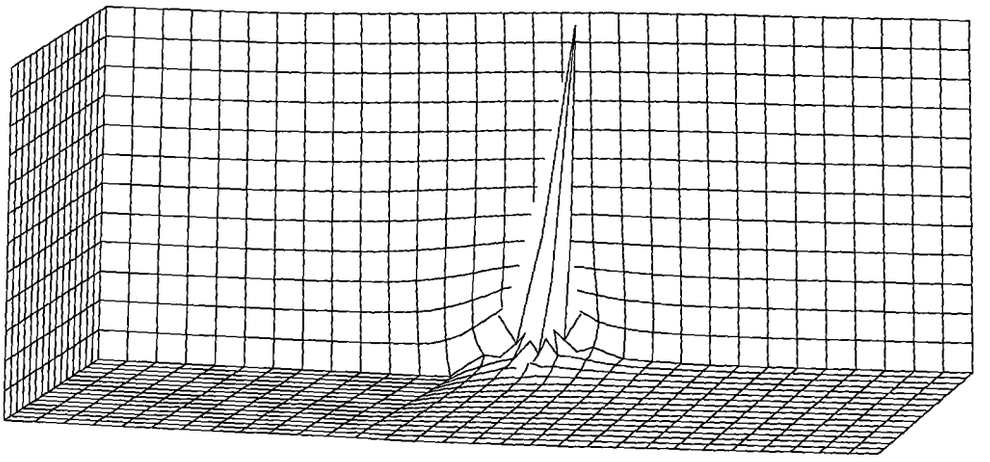

Fig. 5 Results for 20-node brick elements

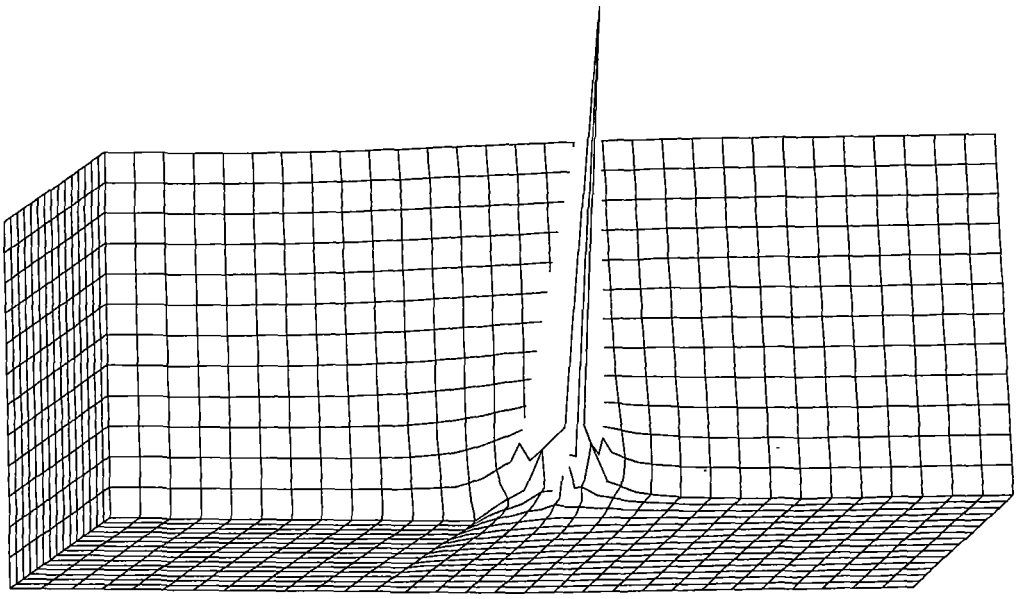

Fig. 6 Results for 27-node brick elements

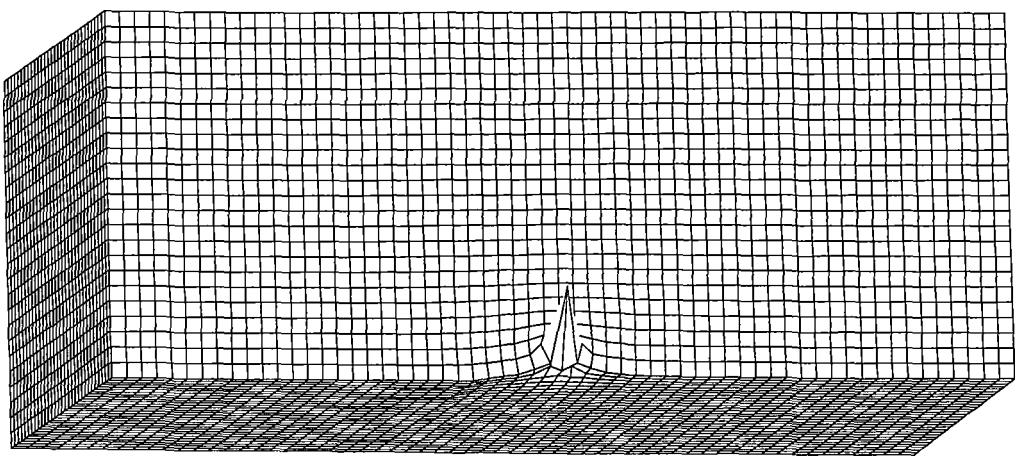

Fig. 7 Results for 8-node brick elements – dense mesh

Solutions presented in Fig. 4 to Fig. 7 have shown, that unit forces applied to the 3D FEM model don't yield solutions converging with decreased size of element used. **Therefore, unit pressures should be applied rather than equivalent concentrated loads.** Practically, instead of the pressure, appropriate forces are applied in certain nodes of an element. These are kinematically equivalent forces. The next

benchmark explained in Fig. 8 shows similar problem, but now unit pressures are applied instead of unit forces.

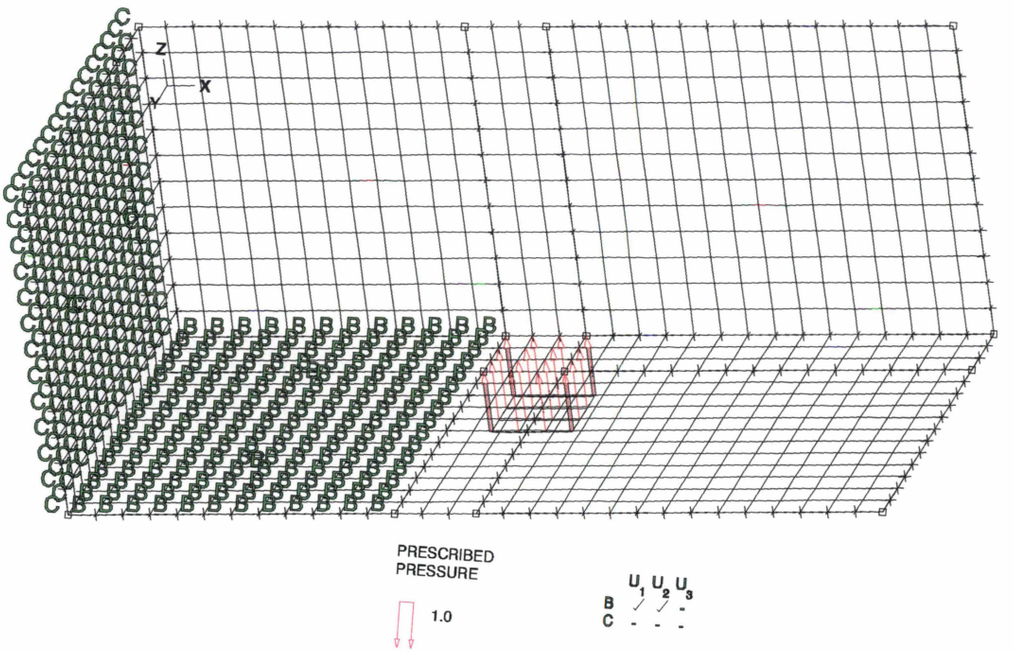

Fig. 8 FEM model – unit pressure applied

The solution for the model consisting of 8-node bricks is presented in Fig. 9 as an example.

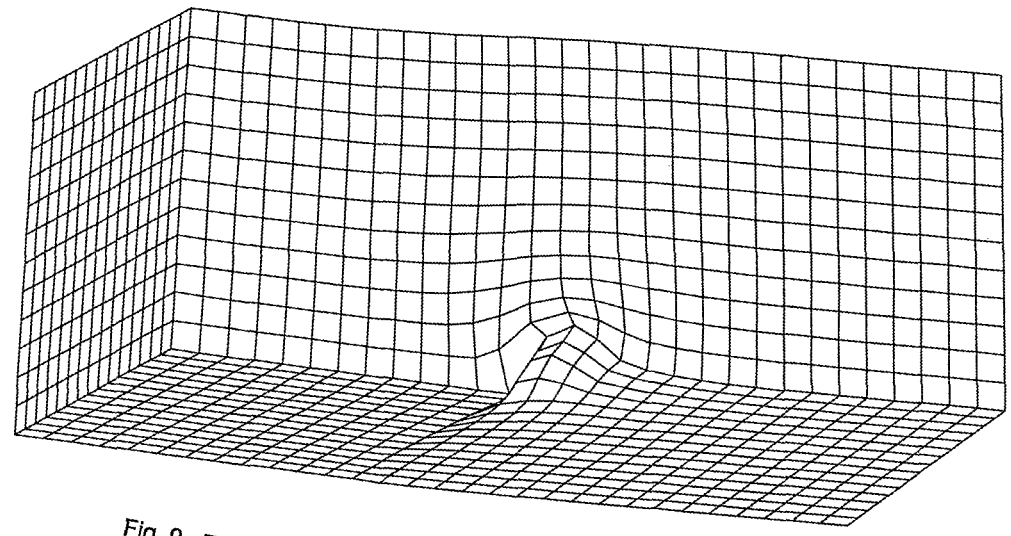

Fig. 9 Results for 8-node brick elements – unit pressure applied

Many tests have been performed for different element sizes and different element types. In all tests maximum vertical displacement has been registered. Fig. 10 summarizes obtained results.

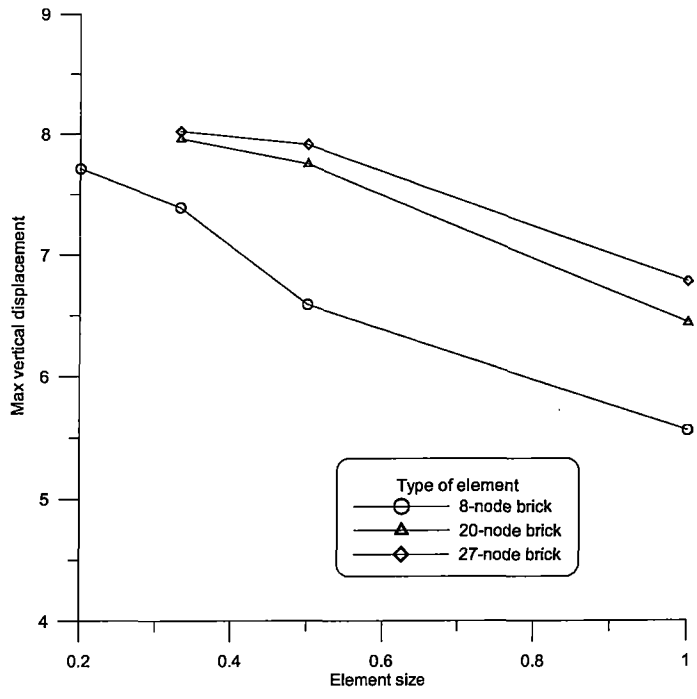

Fig. 10 Benchmark test – unit pressure, different elements

Although the solution obtained for 27-node elements is the most flexible, the results of sufficiently high quality are obtained for 20-node elements as well. The FEM mesh consisting of 8-node bricks requires elements very small in size in order to obtain locally precise solution.

3.2. Magnitudes of computed influence coefficients

In this chapter benchmark tests are included in order to show, that different finite elements yield the solutions of different precision. The hoop strains are used as indicator of FEM solution quality. These strains constitute the numerical input data in the analysis of residual hoop stresses in railroad car wheels. For simplicity the two dimensional problem is considered.

Fig. 11 is the example of one finite element problem solution.

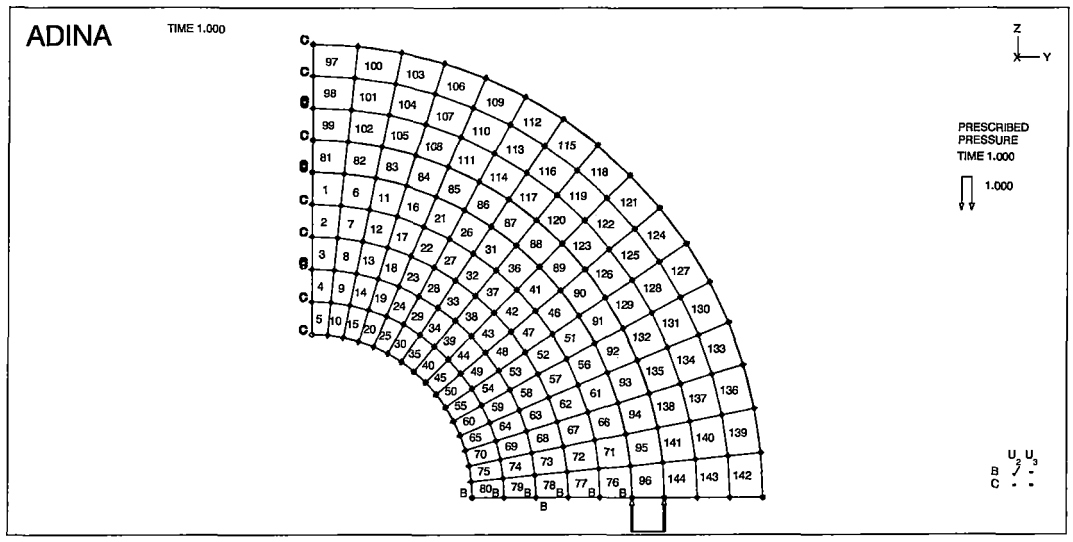

Fig. 11 FEM cutting simulation, 4 node element used

In the first cut element #142 is loaded by normal unit pressure. Then in the second cut element #143 is loaded. Fig. 11 corresponds to the cut #4. Of course the boundary conditions are different for each cut i.e. in the non-cut part of the wheel on the bottom horizontal line vertical displacements are prohibited (in Fig 11. letters "B"). In each of discrete problems the responses in measurement locations are found. These are displacements or numerically found strains in several nodes. Vertical strains corresponding to loading and boundary conditions shown in Fig. 11 are presented in Fig. 12

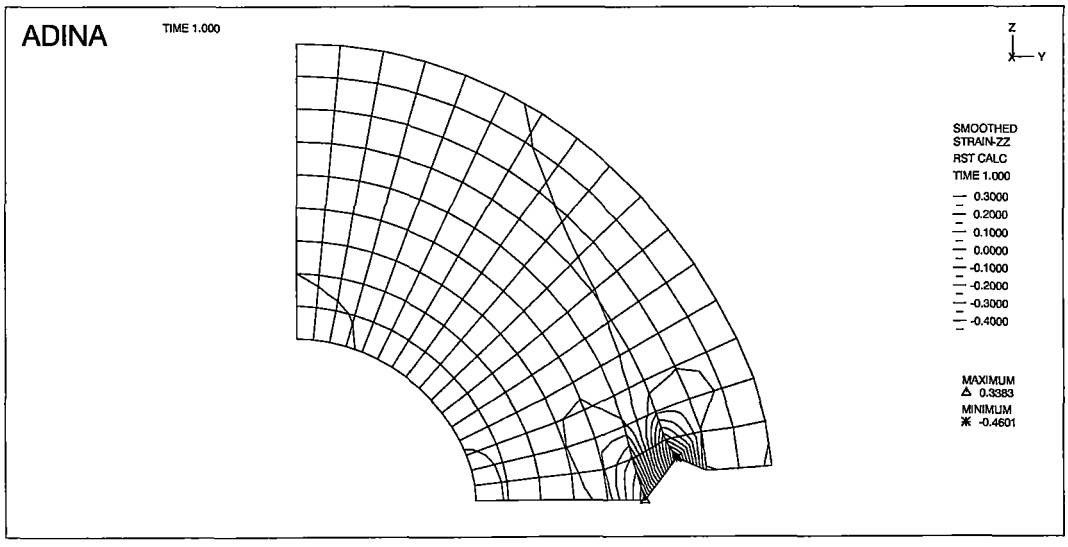

Fig. 12 Distribution of vertical strains – cut #4 (4 node elements)

These strains constitute the elements of the influence matrix $[\alpha]$ (Eq. 13 and Eq. 14).

Of course the quality of finite element method solution depends of the number and type of element used. If 8 node or 9 node elements are introduced the magnitudes of calculated strains changes. The following figures present finite element meshes and vertical strain distributions for 8 node and 9 node finite elements.

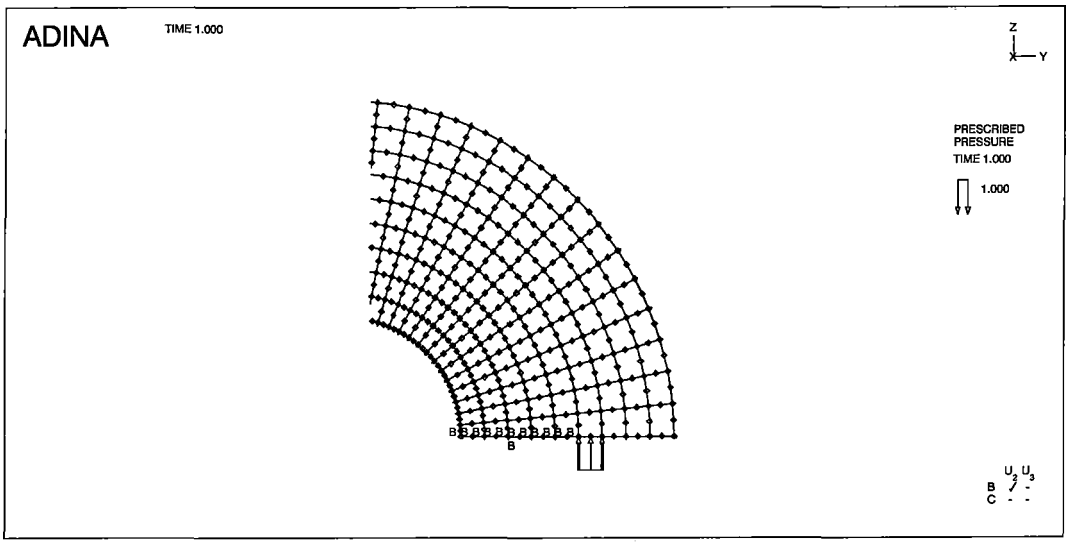

Fig. 13 FEM cutting simulation, 8 node element used

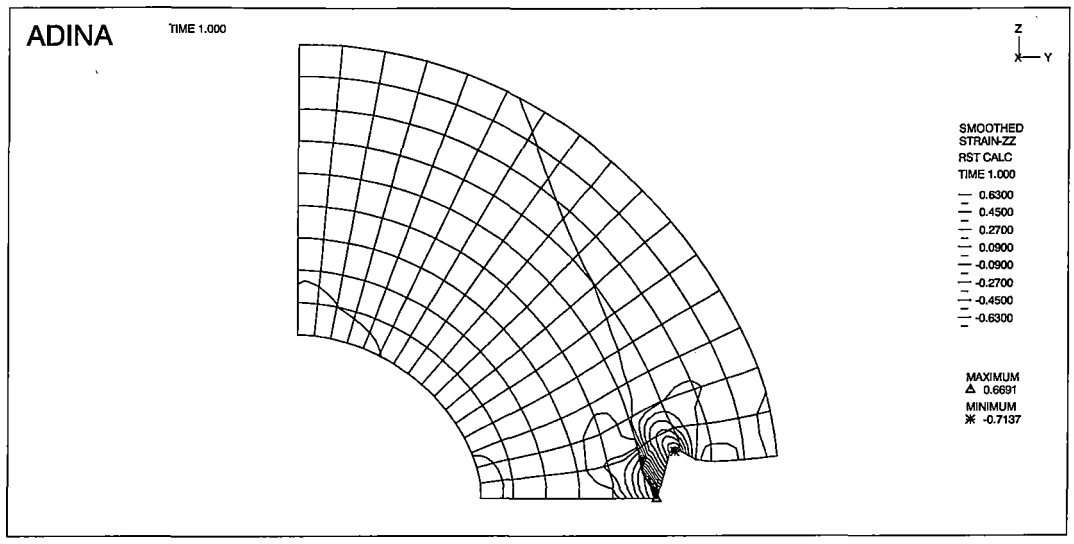

Fig. 14 Distribution of vertical strain – cut #4 (8 node elements)

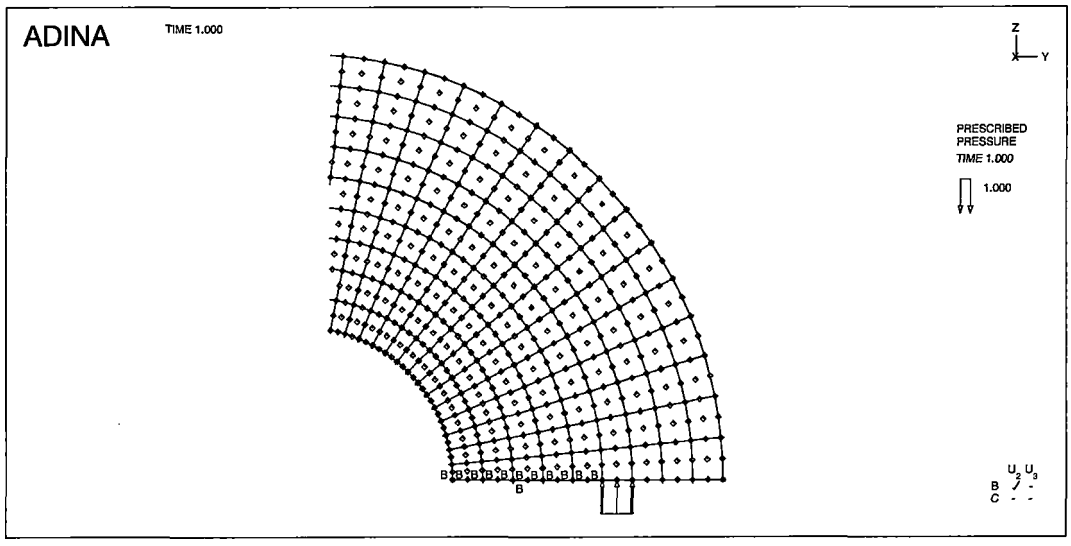

Fig. 15 FEM cutting simulation, 9 node element used

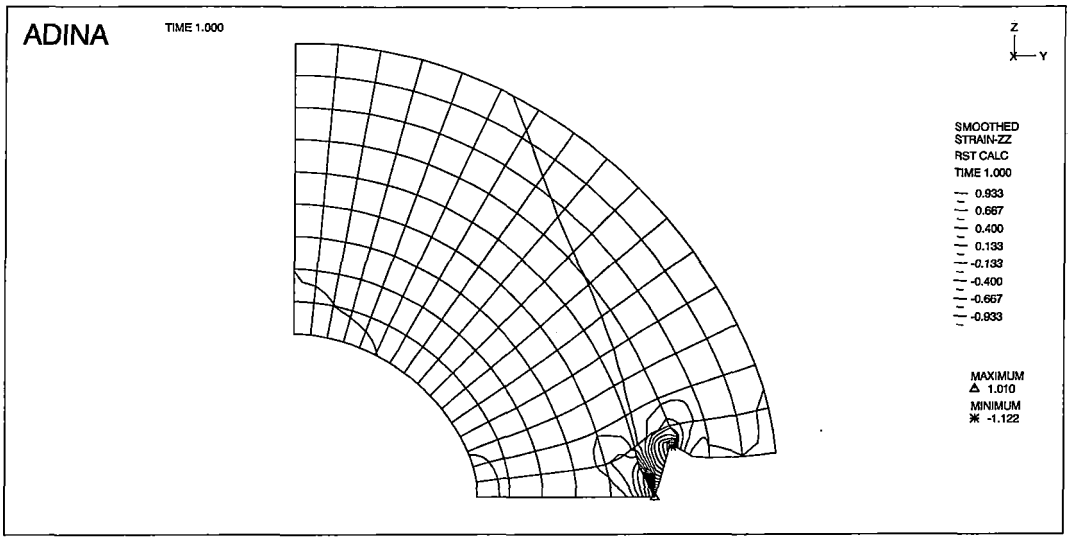

Fig. 16 Distribution of vertical strains – cut #4 (9 node elements)

One may notice that although the strain distributions are similar, the strain magnitudes differ significantly. Because these strains constitute the influence coefficients necessary to analyse the residual hoop stresses in railroad car wheels, they influence the precision and magnitude of calculated stresses. **The best results may be achieved when the very dense mesh consisting of the possibly highest order finite elements is used**, but limitations of computer power and resources and the time of numerical computations, forces a reasonable compromise. For the three dimensional mesh these are **20 node brick elements which allow for relatively precise solution in reasonably short time**.

4. Finite element wheel models

Each analyzed wheel (wheel #2 – wheel #8) comes from different production series, therefore geometries of these wheels differ. Finite element mesh has to be developed separately for each investigated wheel. The following figures present 2D finite element meshes for investigated wheels' cross sections. These meshes are rotated next, in order to form 3D finite element meshes consisting of 20-node brick elements.

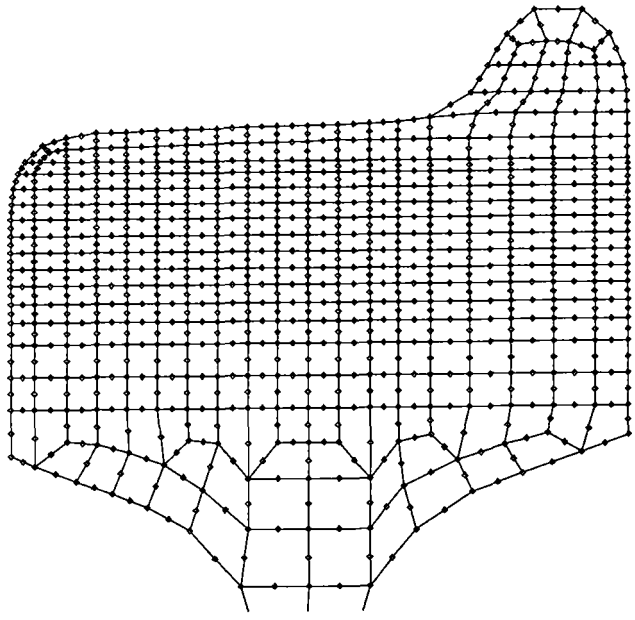

Fig. 17 Enlargement of wheel #3 head with nodes shown

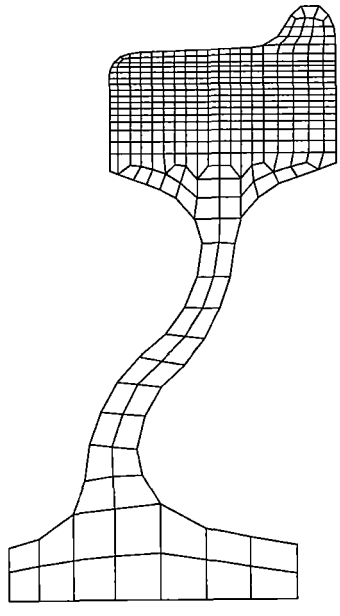

Fig. 18 2D FEM mesh – wheel #3

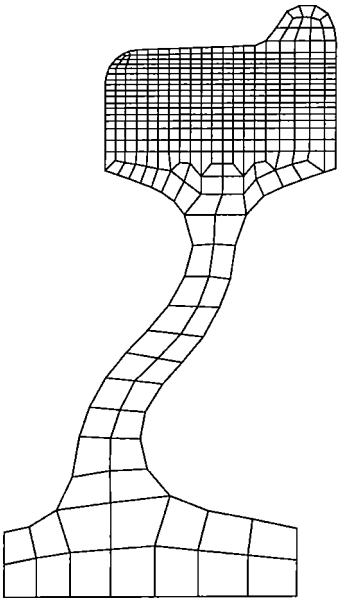

Fig. 19 2D FEM mesh – wheel #4

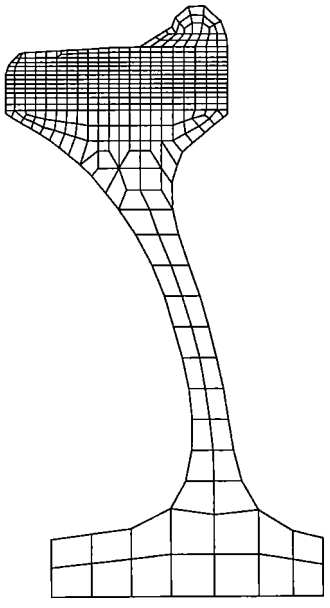

Fig. 20 2D FEM mesh – wheel #5

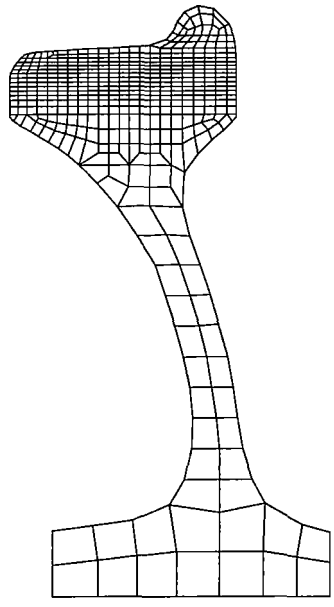

Fig. 21 2D FEM mesh – wheel #6

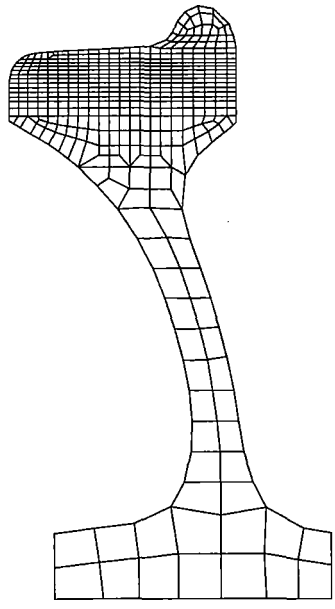

Fig. 22 2D FEM mesh – wheel #8

The following figure is an example of 3D FEM mesh used in numerical simulations of the cutting process. Table 2 summarizes the properties of presented meshes.

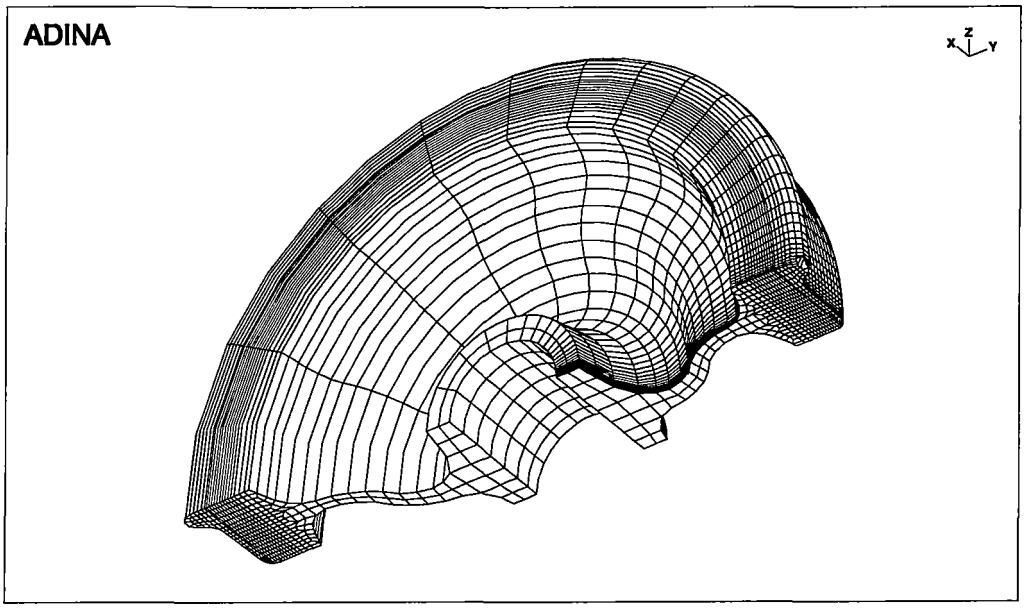

Fig. 23 3D FEM mesh – wheel #3

Table 2 Discrete problems' data

Wheel #	Number of nodes	Number of elements	Number of theoretical cuts	Number of unknown res. hoop stresses
3	43646	9350	14	207
4	47223	10175	13	212
5	45082	9648	15	257
6	49060	10584	15	271
8	49060	10584	15	271

5. Analysis of the experimental data

Typical experimental data comprise displacement fields registered on both sides of the wheel – see Fig. 8. Unfortunately these are relative displacements, which cannot be directly used in the analysis of residual stresses. It is reasonable to assume that displacement fields should be symmetrical (displacement component along the cut) or anti-symmetrical (displacement component perpendicular to the cut).

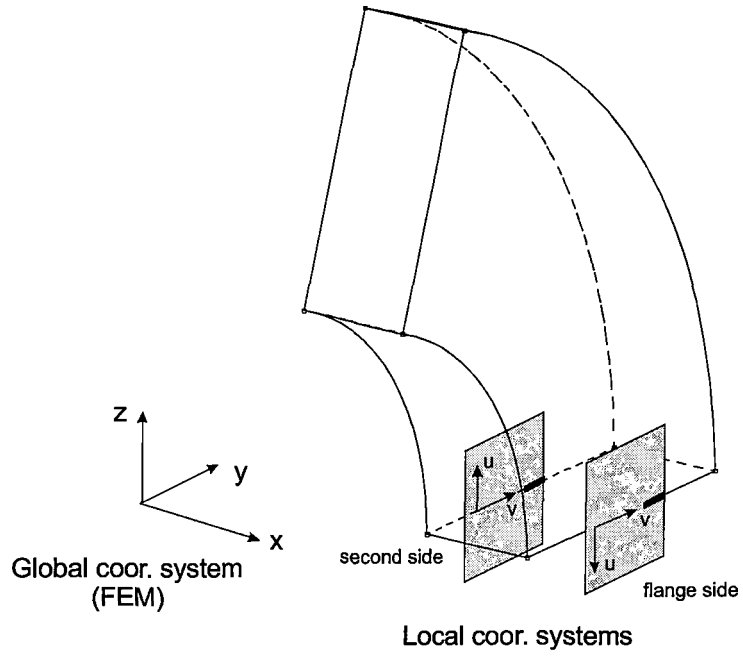

Fig. 24 Moiré interferometry measurements.

Unfortunately, measured displacement fields don't satisfy symmetric/anti-symmetric requirement – thus in numerical approach axial symmetry is assumed for residual hoop stresses and imposed on raw measured data. An example of the actual data is included in Fig. 25. Small crosses denote measurement locations.

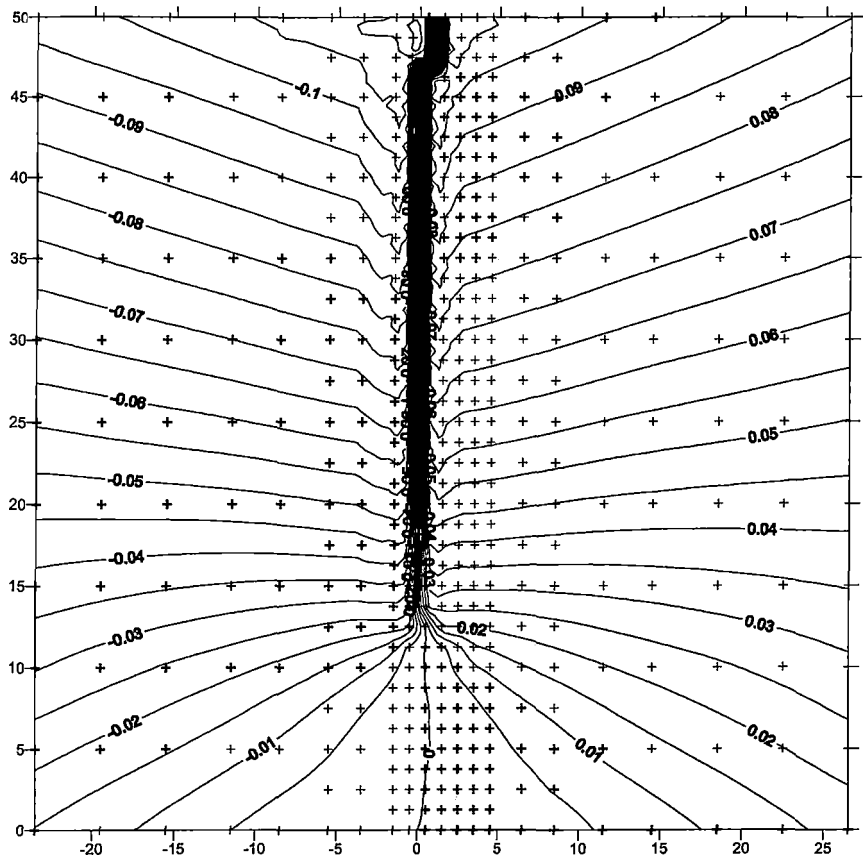

Fig. 25 Horizontal displacements [mm] after cut #3, flange side, wheel #5 (original data)

As mentioned above, this displacement distribution is not anti-symmetric. Moreover, measurements situated in cut part of the wheel – area in the middle of the domain, where huge concentration occurs are very inaccurate, and therefore, have to be excluded from further analysis. In Fig. 26 presented is the same displacement component after removal of measurements mentioned.

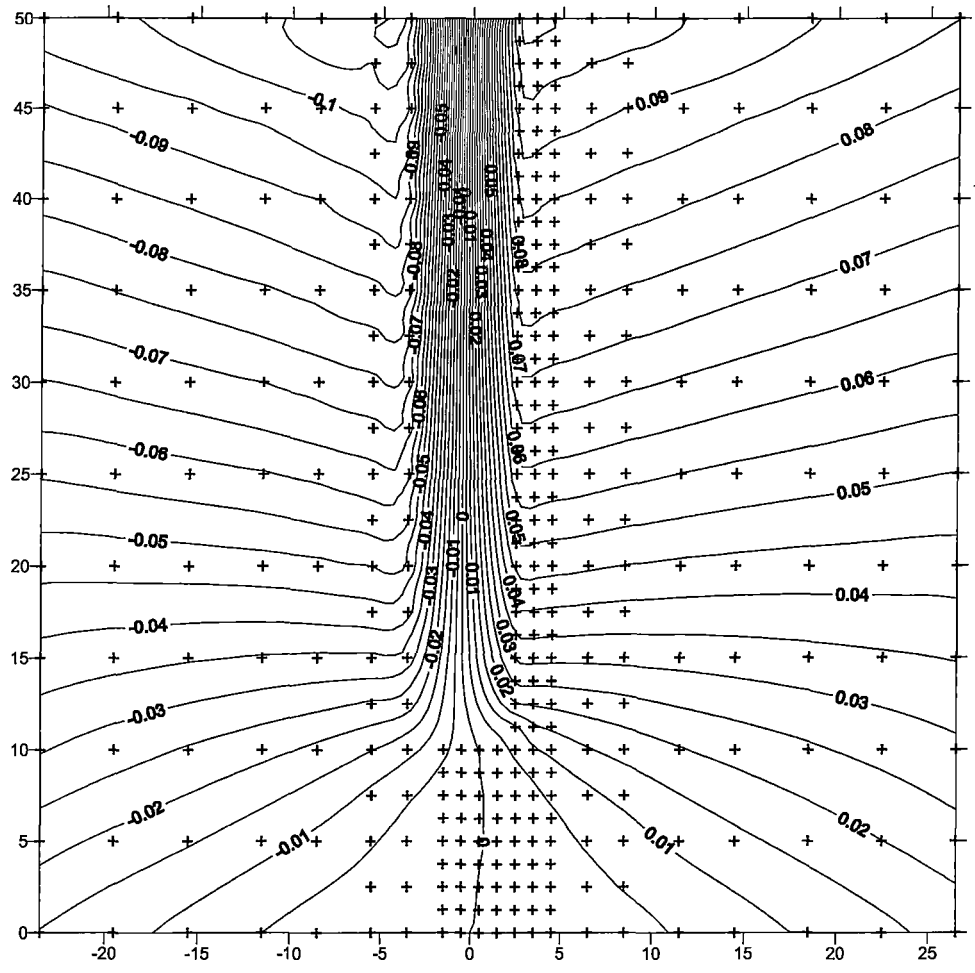

Fig. 26 Horizontal displacements [mm] after cut #3, flange side, wheel #5 – part of data is removed

Presented displacement distribution, although of high quality, still doesn't satisfy the assumption of axial symmetry. Before differentiation, this displacement field is anti-symmetrized (for horizontal displacement component anti-symmetrization is required) as shown in Fig. 27. Small circles show locations of fictitious measurements i.e. points where function and derivatives are calculated.

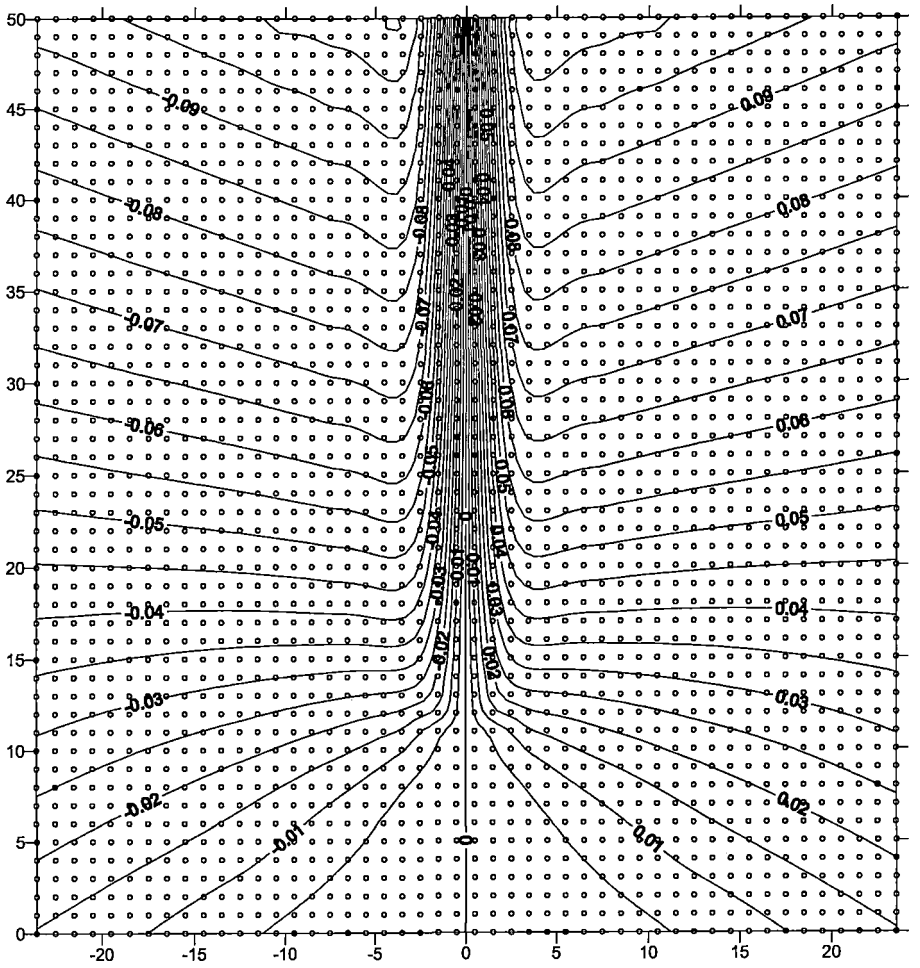

Fig. 27 Anti-symmetric displacement field, cut #3, flange side, wheel #5

Such displacement field is then numerically differentiated in order to obtain strains. Numerically found strains constitute the real input data in the analysis of residual hoop stresses. The above-presented displacements after differentiation give strain field shown in Fig. 28.

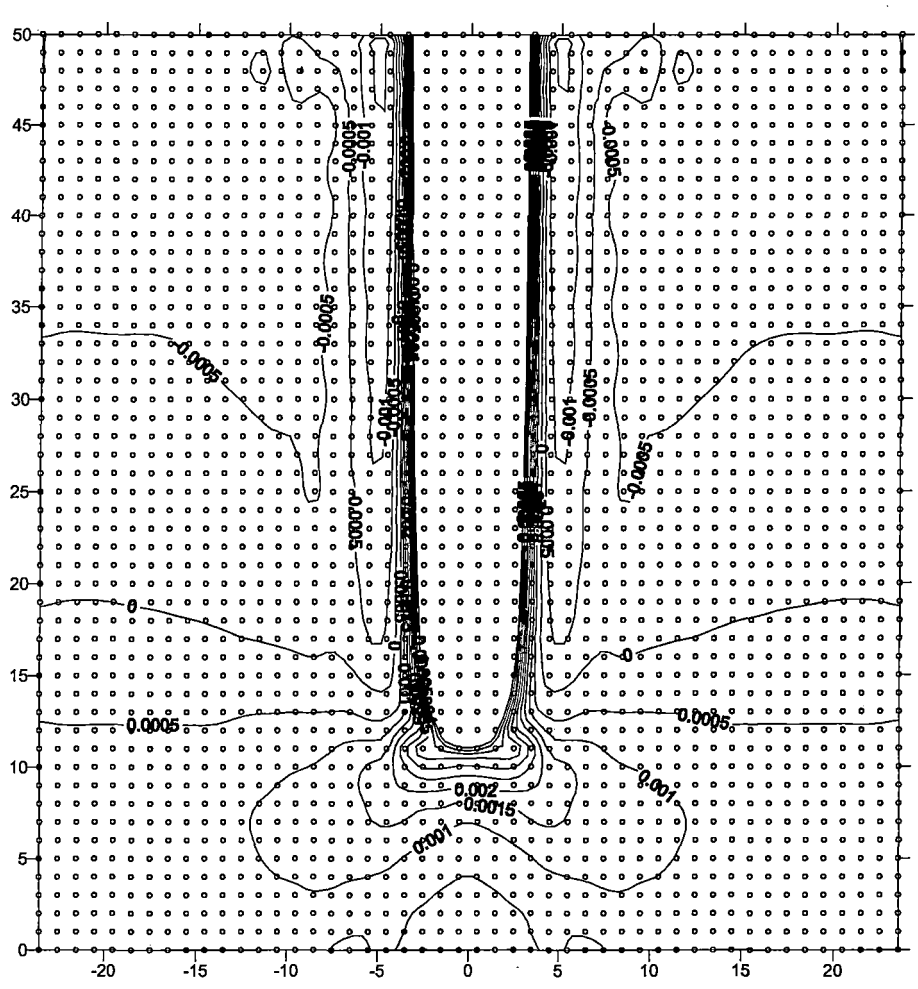

Fig. 28 Horizontal strain field, cut #3, flange side, wheel #5.

Such data taken from one half of the cut wheel is used in the analysis of residual hoop stress. However, on the boundaries, the precision of numerical differentiation is usually low. Therefore, these fictitious measurements are removed additionally. Sometimes physical grating defects occur – in these areas measurements are burdened by significant errors and have to be removed as well.

The locations of original data and fictitious points don't have to be the same. The grid of fictitious points is more dense than the original one. Thus the number of numerical input data in the analysis of residual stresses is increased, and therefore the problem is better conditioned. Such generation of experimental data cannot be overdone, because very dense grid of fictitious points an areas of small strain gradients doesn't introduce any additional experimental information. As described in the next chapter, the saw cut process has to be numerically simulated, practically by the finite element method. In this model,

displacements obtained in discrete points – FEM nodes – are differentiated to the same fictitious locations as in the analysis of experimental data.

The input data preparation process in hoop residual stresses analysis, should be conducted very carefully in order to exclude fatal experimental errors from the analysis. Practically any automatic numerical tool doesn't guarantee the reliability of obtained strains. All numerically found strain fields have to be carefully checked by the program operator.

6. Residual hoop stress approximation

In this chapter presented are results of residual stress analysis in the investigated wheels. These are the following wheels:

wheel #3 (36524-46 146)
wheel #4 (44543-46 146)
wheel #5 (26526 242)
wheel #6 (26508 242)
wheel #8 (26512)

The other wheels (wheel #1, wheel #2 and wheel #7) are not considered here, because for these wheels the profiles are not known. Therefore, the location of moiré measurements is not known, and as influence coefficient cannot be computed properly. Final residual stress approximations for these wheels would be not reliable.

For each wheel considered here presented are the following residual stress distributions called respectively: case 1, case 2 and case 3

1. Residual hoop stress reconstruction (case 1) obtained when only moiré measured displacements perpendicular to the cut, and registered for the deepest cut are taken into the analysis. These measurements are the most valuable ones.
2. Residual hoop stress reconstruction (case 2) obtained when all moiré measured displacement components, as well as information resulting from all cuts are used in the analysis.
3. Residual hoop stress reconstruction (case 3) when strain gauge measurements are also used in the analysis.

All residual hoop stresses are expressed in [MPa], wheel dimensions (horizontal and vertical scales) are in [cm]. In order to present clearly residual stress distributions in all investigated wheels, each plot is scaled separately.

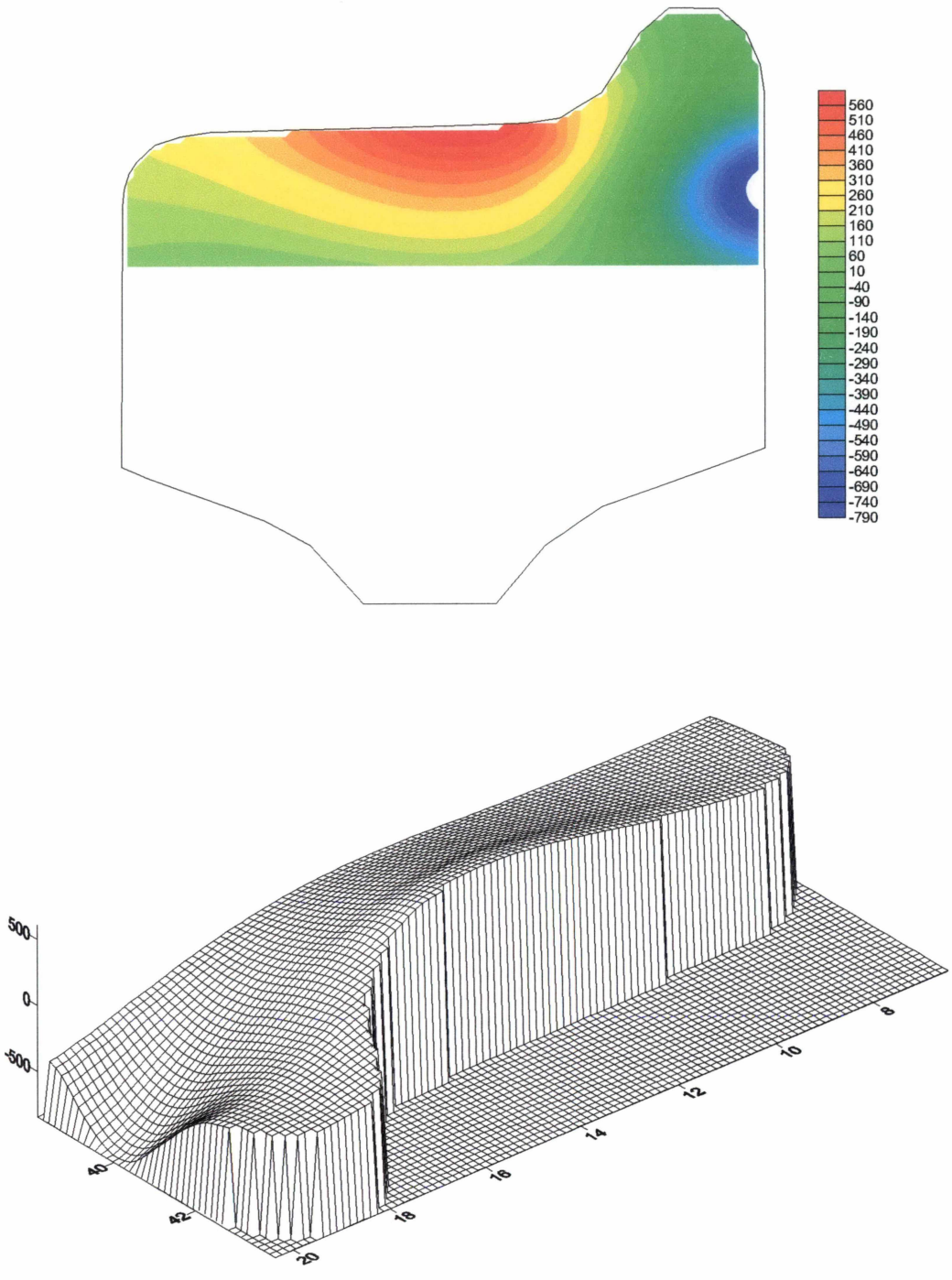

Fig. 29 Residual hoop stress distribution [MPa] – wheel #3, case 1

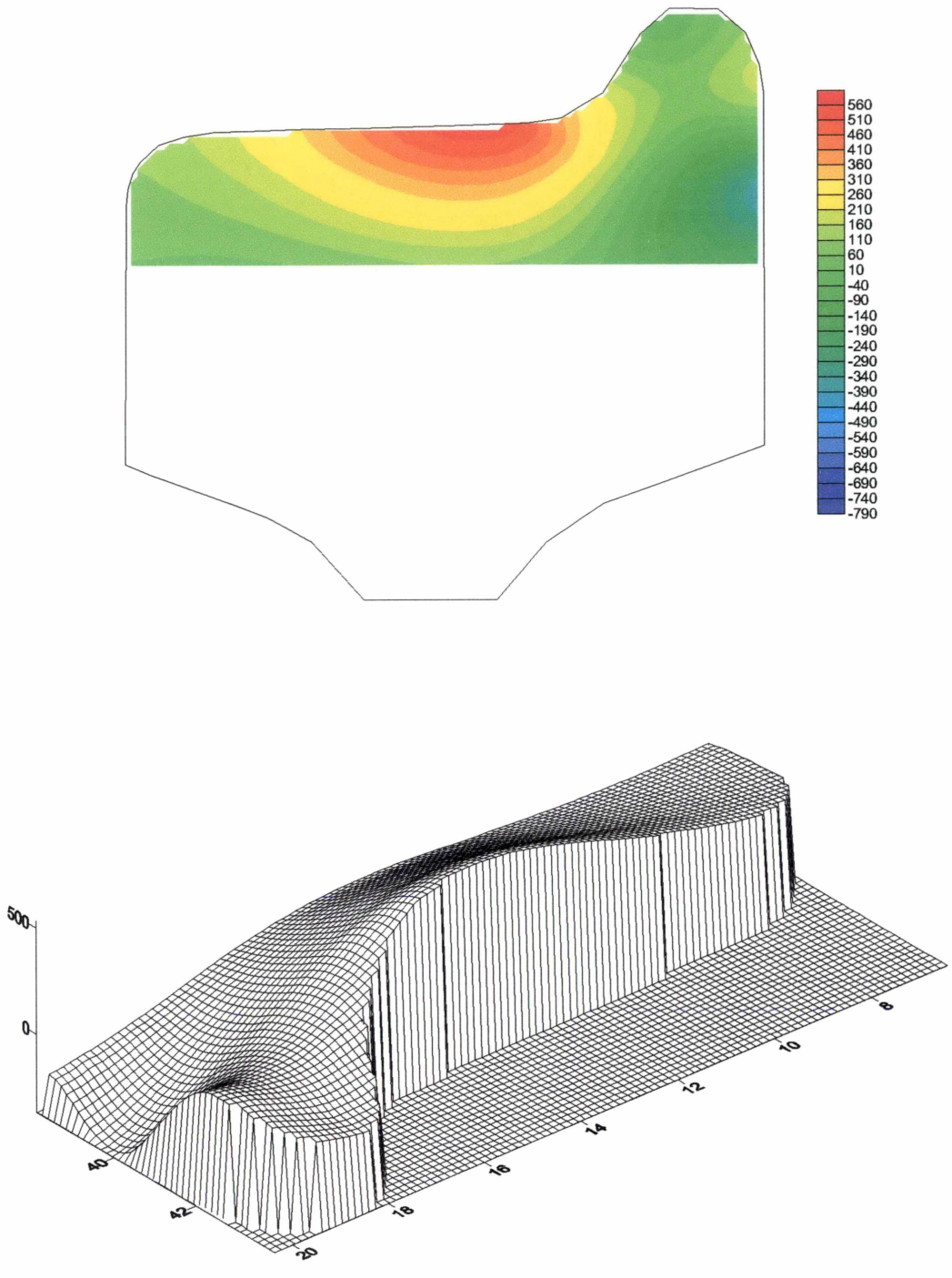

Fig. 30 Residual hoop stress distribution [MPa] – wheel #3, case 2

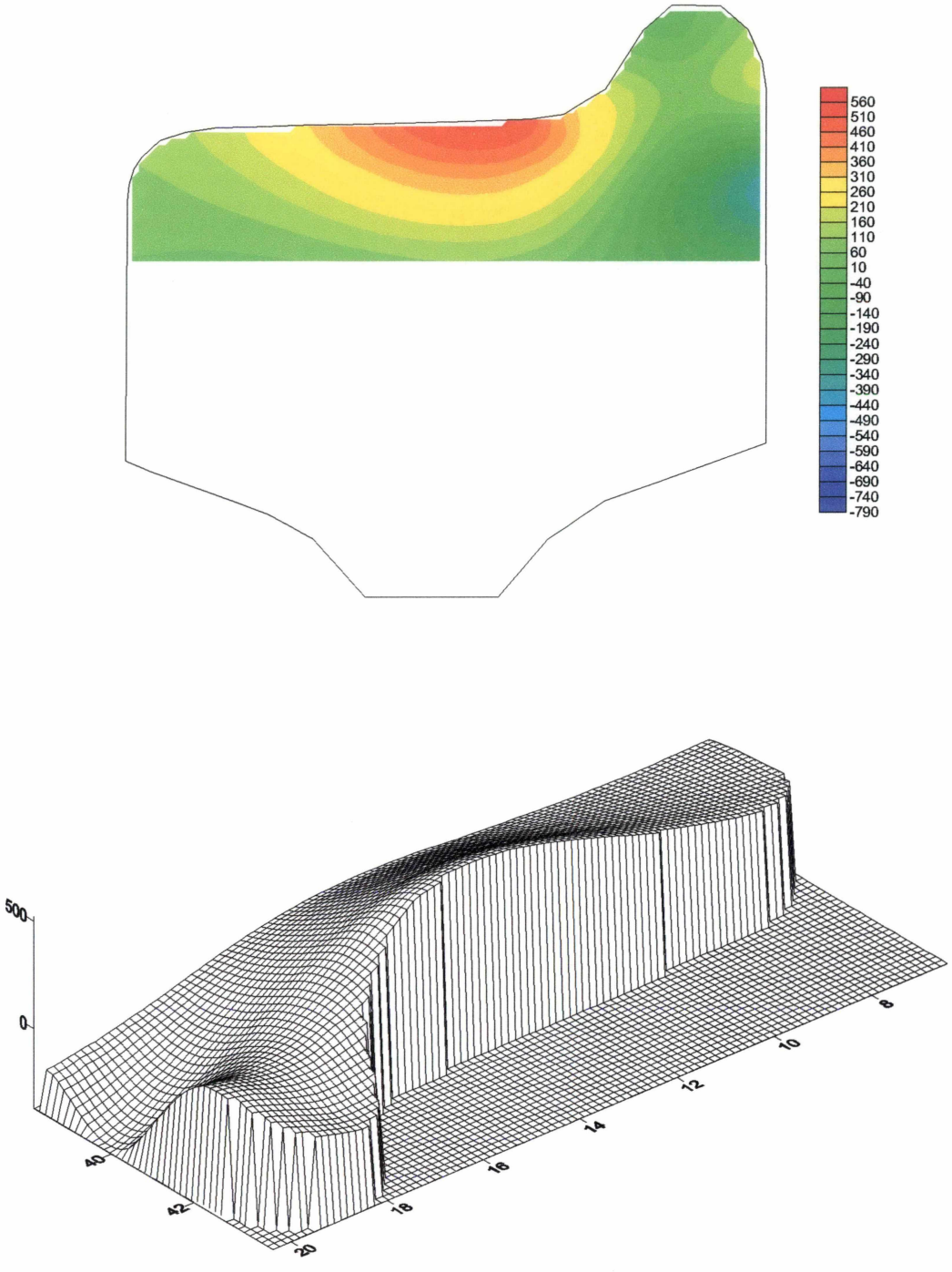

Fig. 31 Residual hoop stress distribution [MPa] – wheel #3, case 3

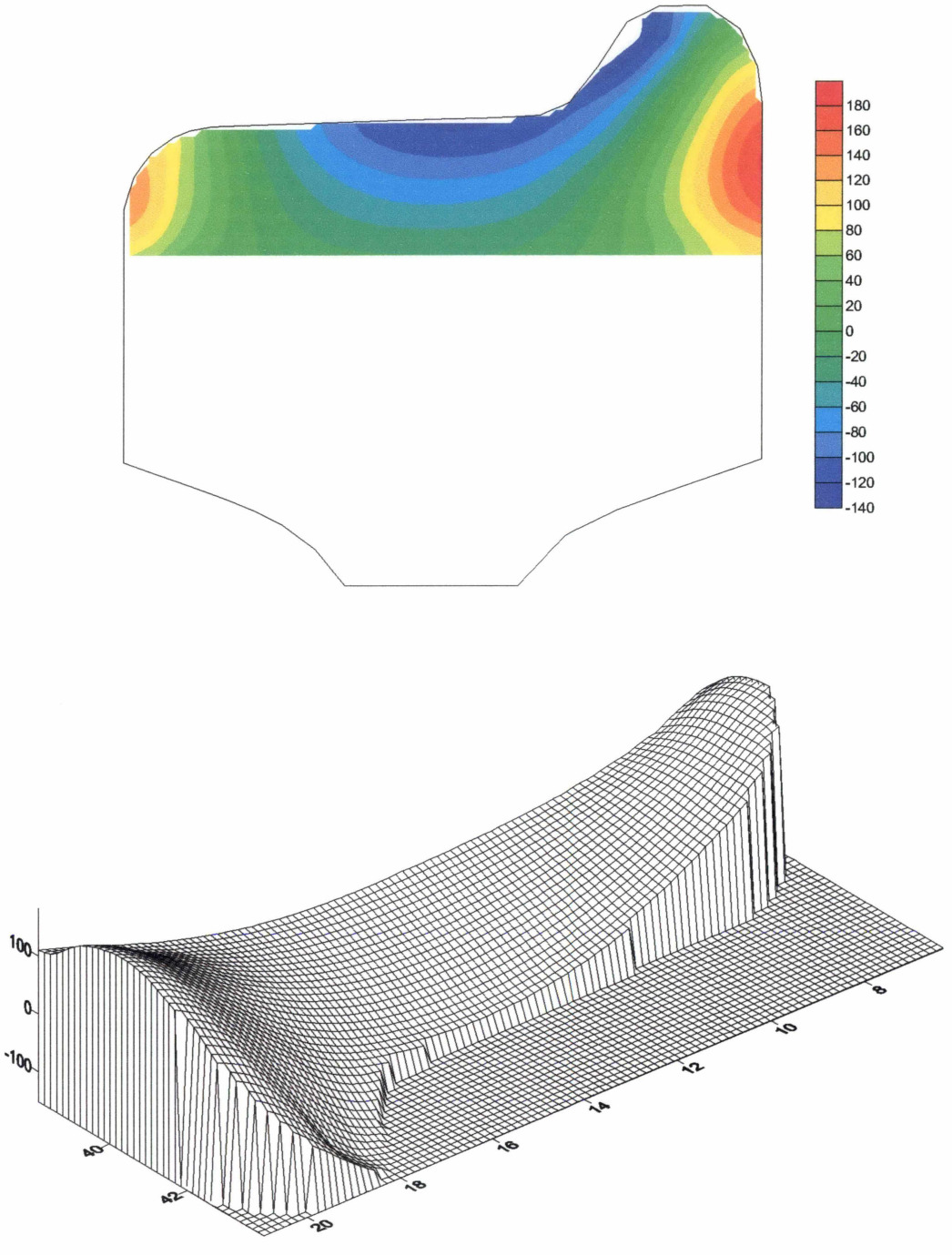

Fig. 32 Residual hoop stress distribution [MPa] – wheel #4, case 1

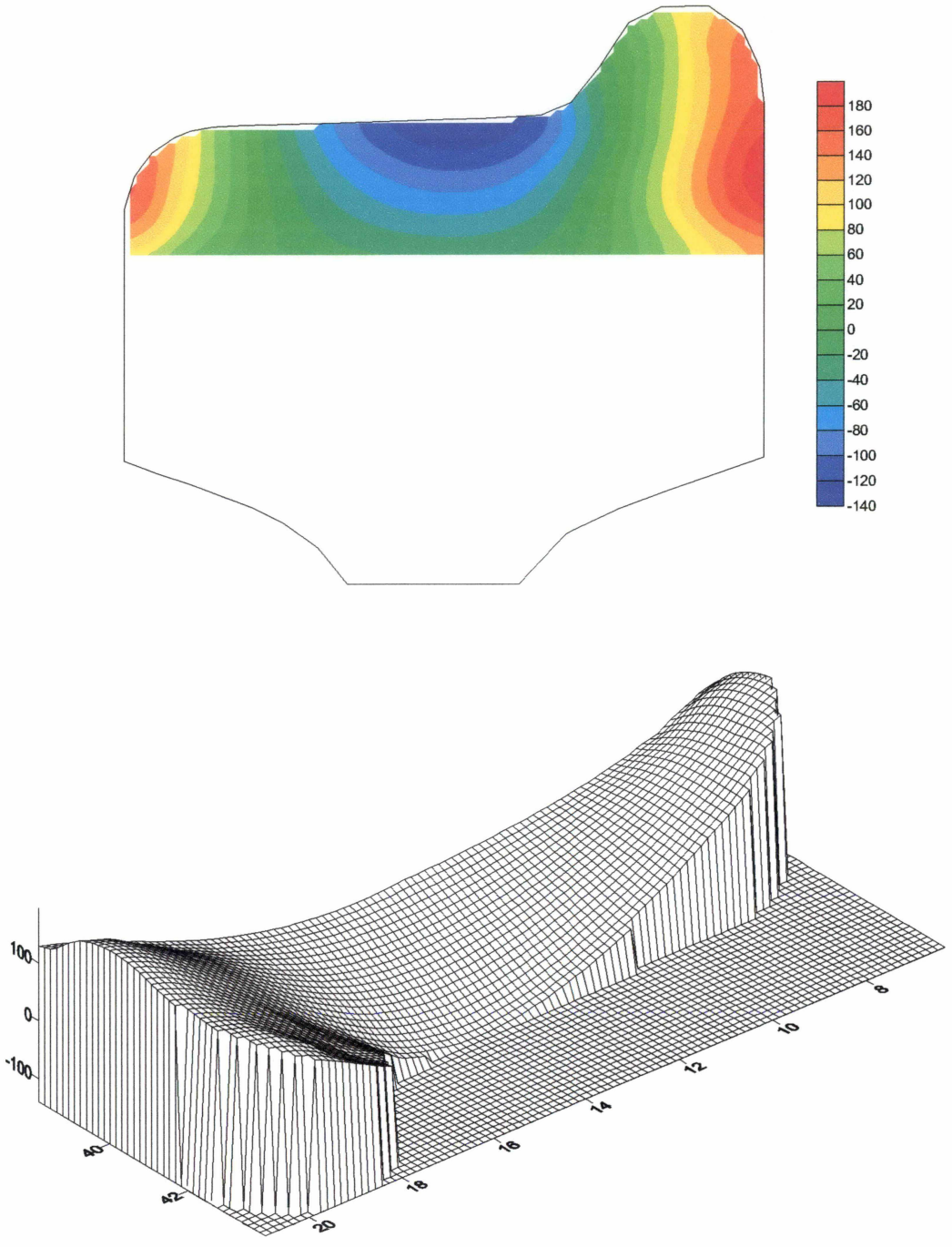

Fig. 33 Residual hoop stress distribution [MPa] – wheel #4, case 2

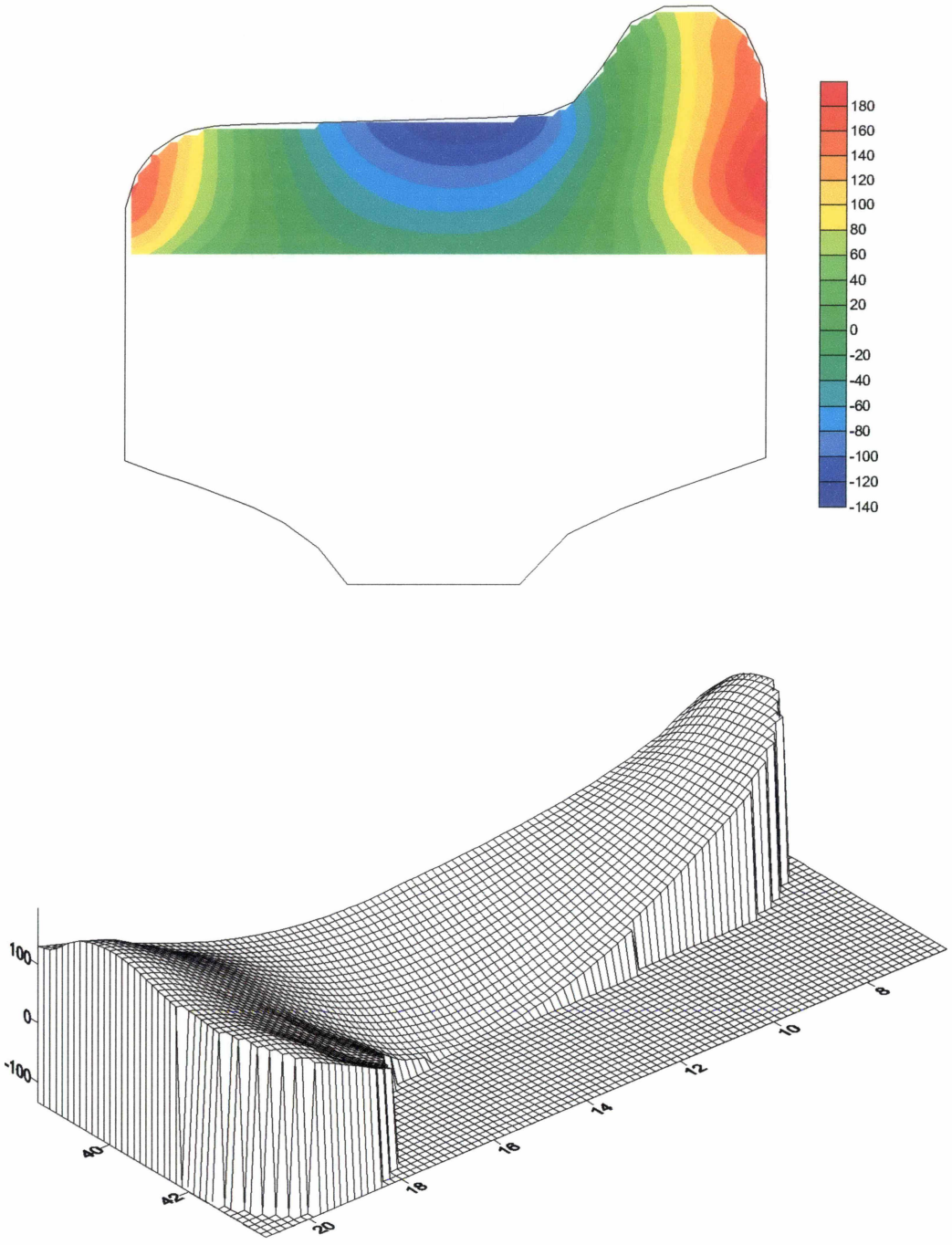

Fig. 34 Residual hoop stress distribution [MPa] – wheel #4, case 3

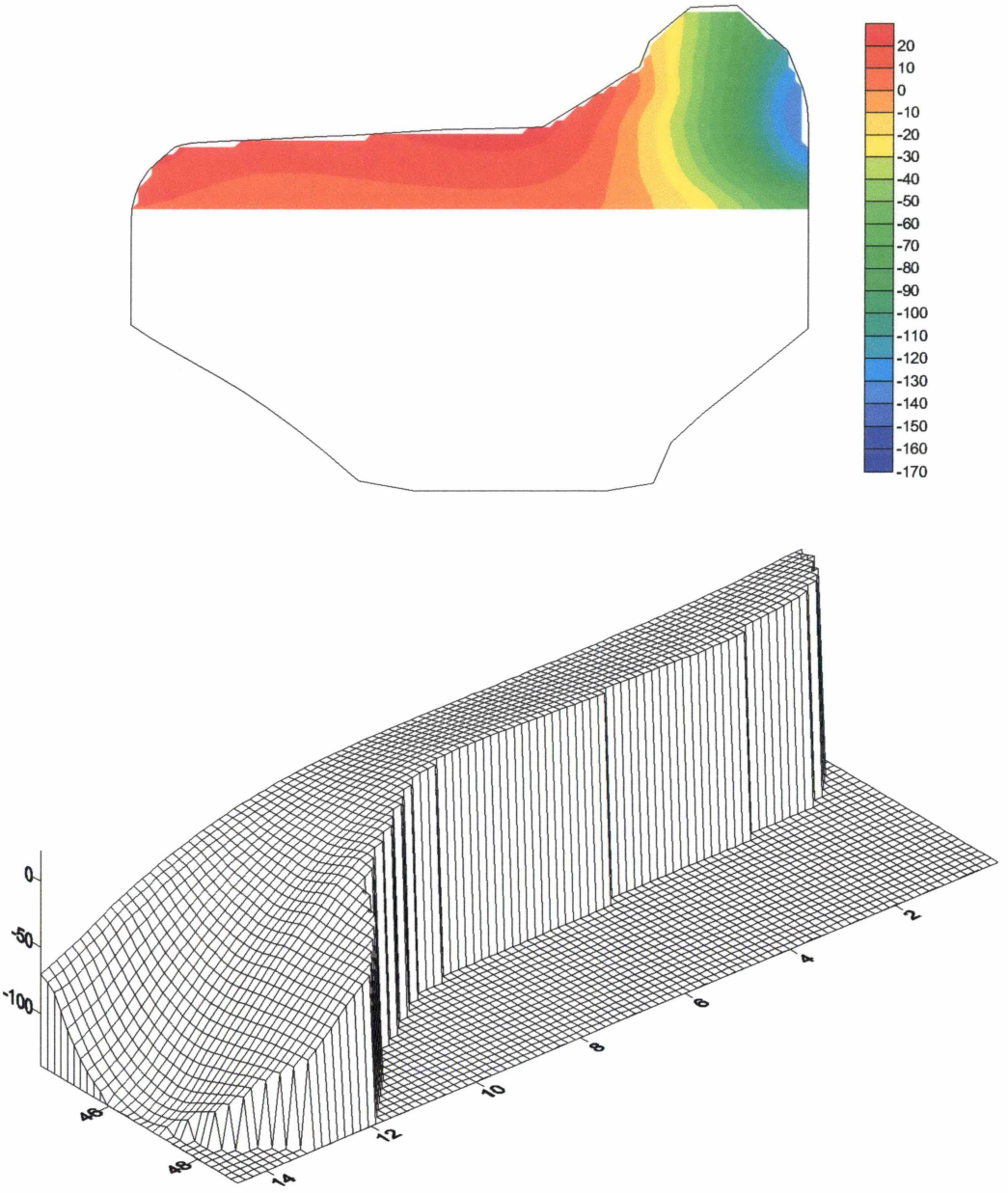

Fig. 35 Residual hoop stress distribution [MPa] – wheel #5, case 1

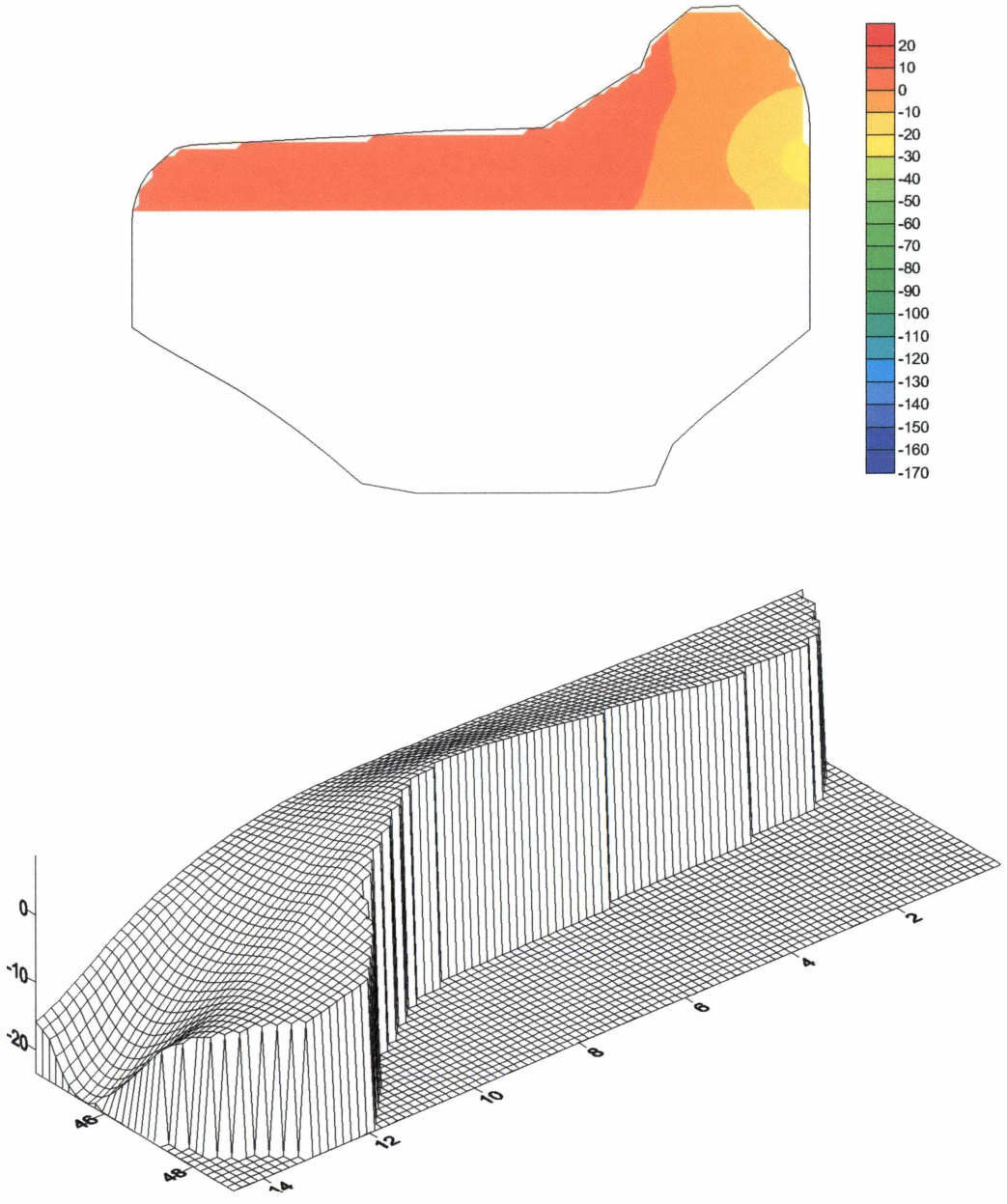

Fig. 36 Residual hoop stress distribution [MPa] – wheel #5, case 2

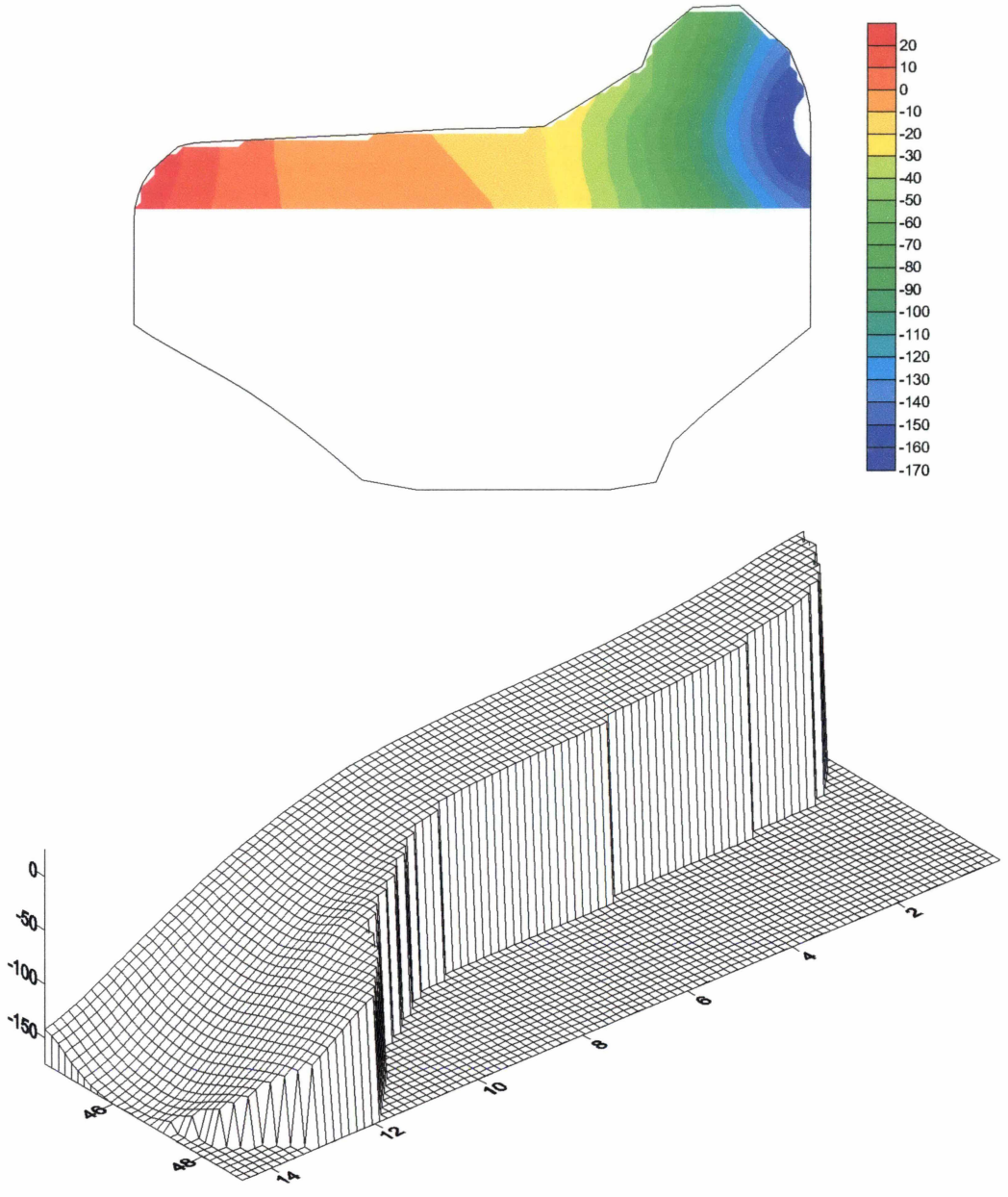

Fig. 37 Residual hoop stress distribution [MPa] – wheel #5, case 3

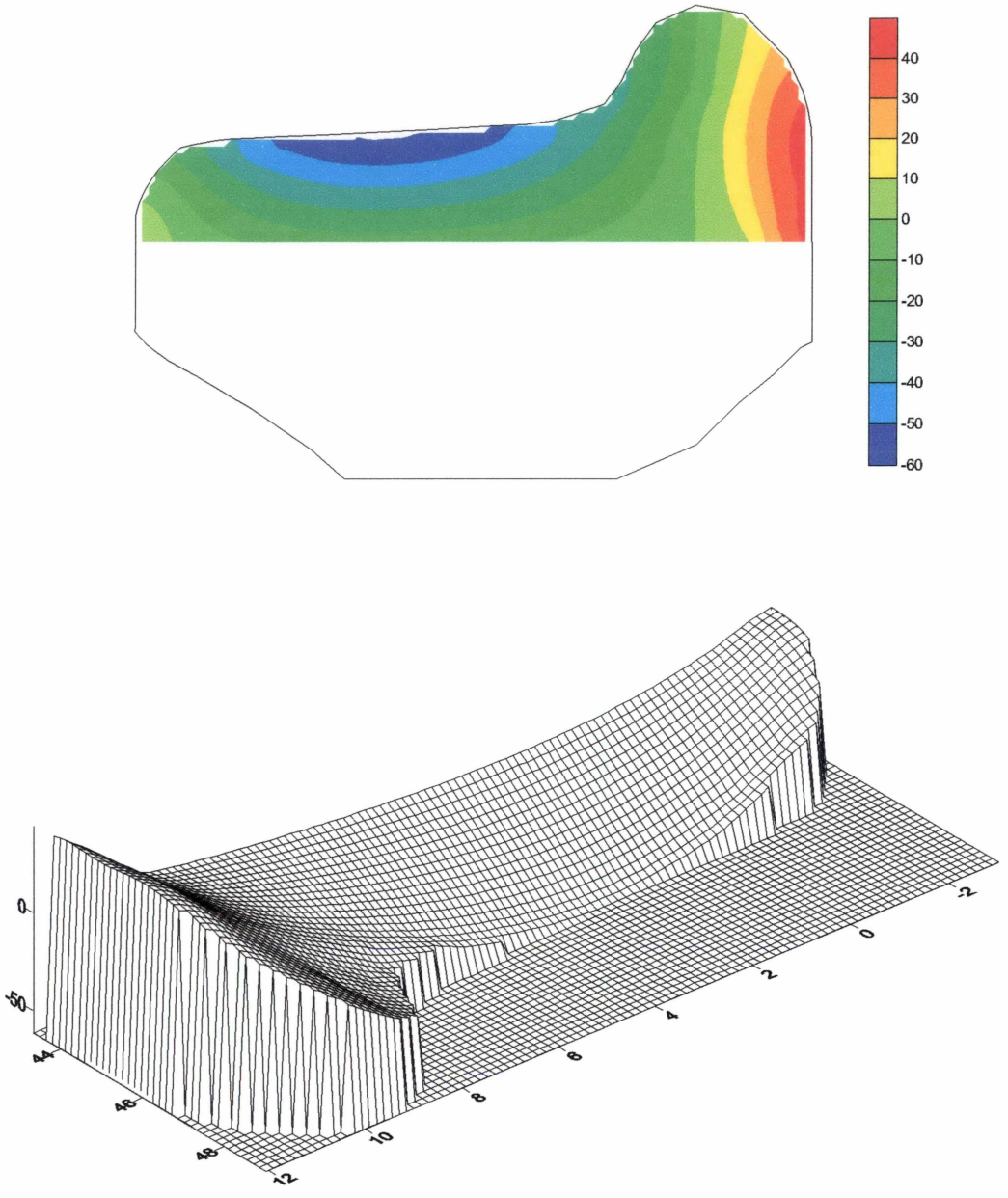

Fig. 38 Residual hoop stress distribution [MPa] – wheel #6, case 1

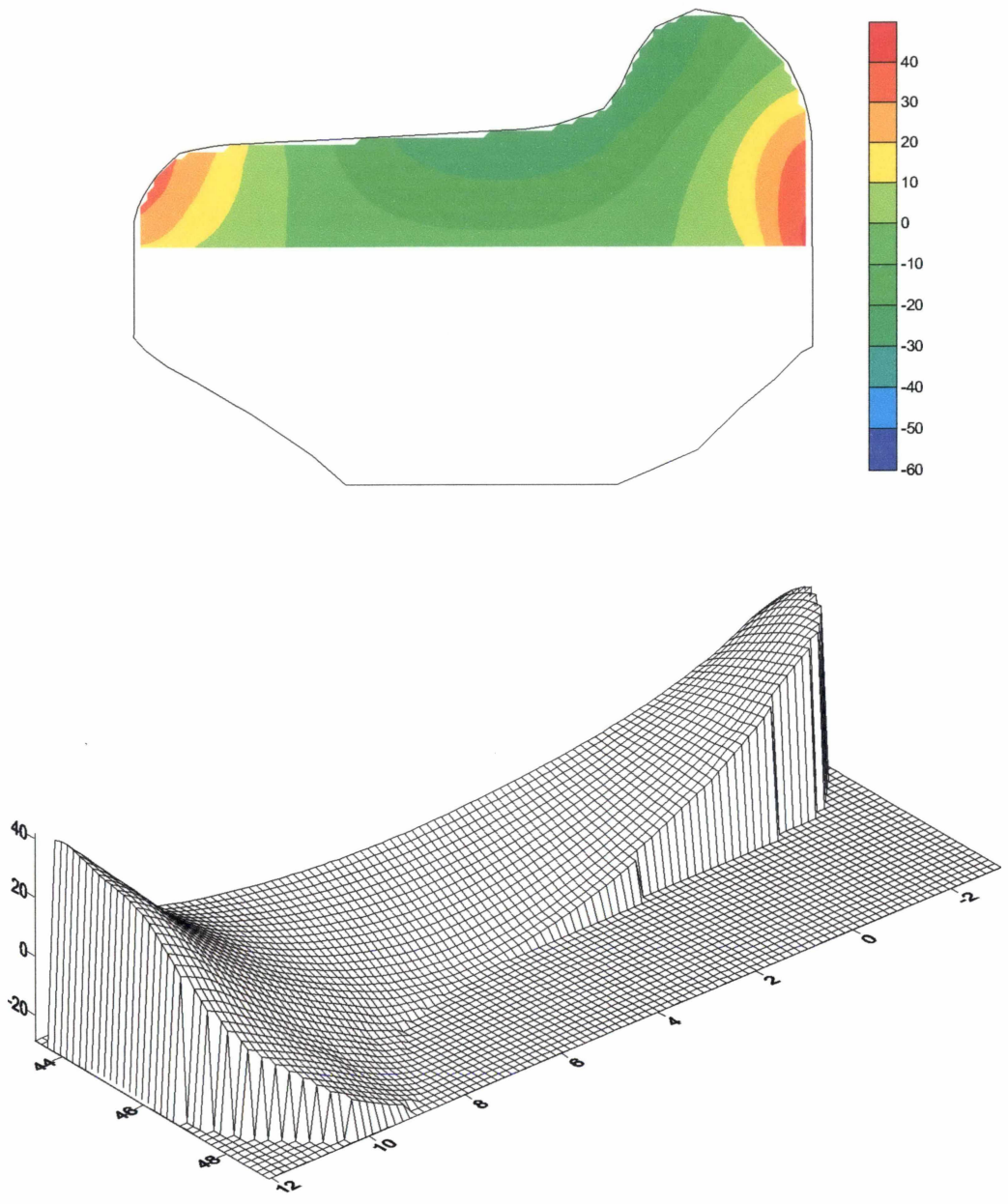

Fig. 39 Residual hoop stress distribution [MPa] – wheel #6, case 2

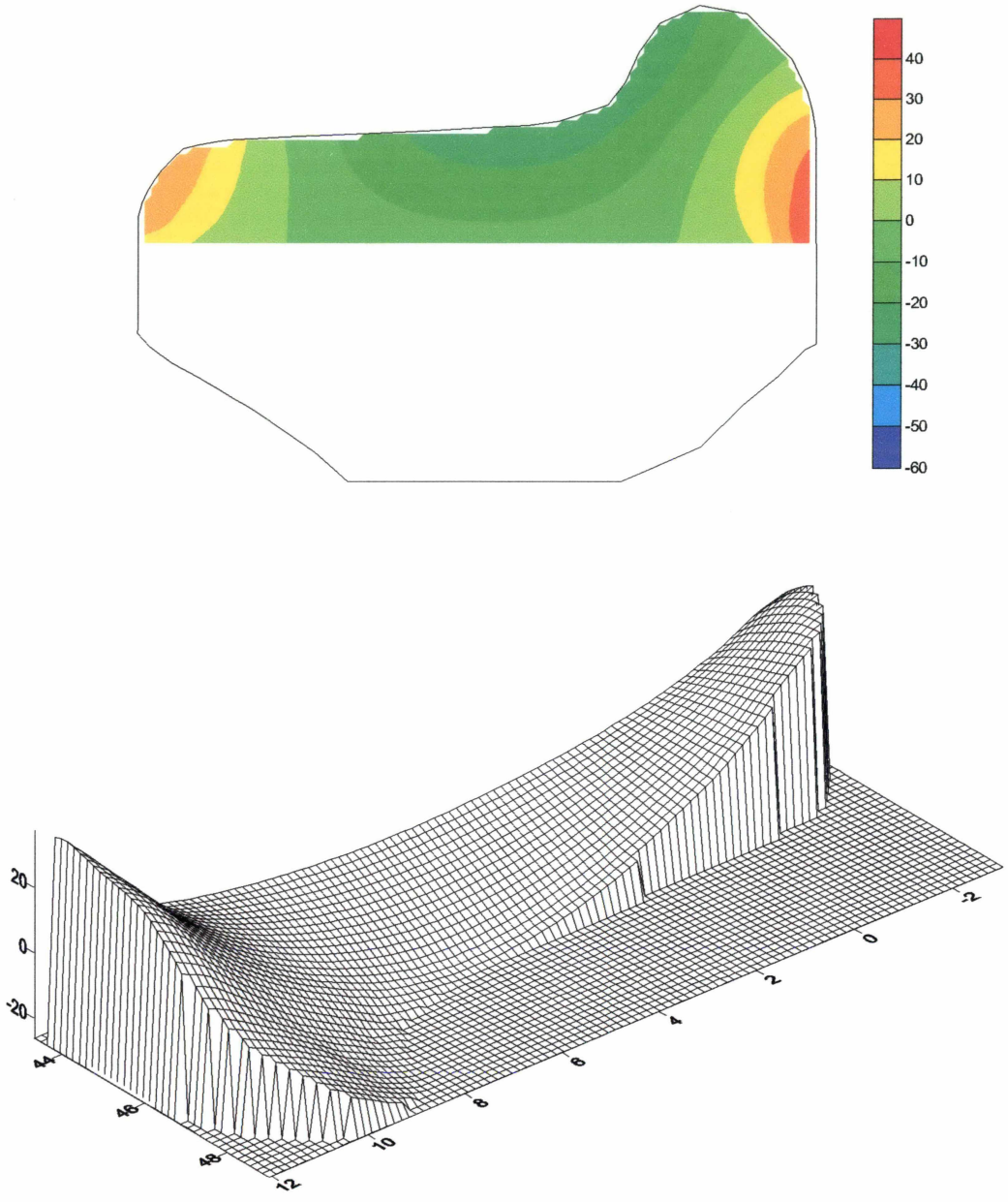

Fig. 40 Residual hoop stress distribution [MPa] – wheel #6, case 3

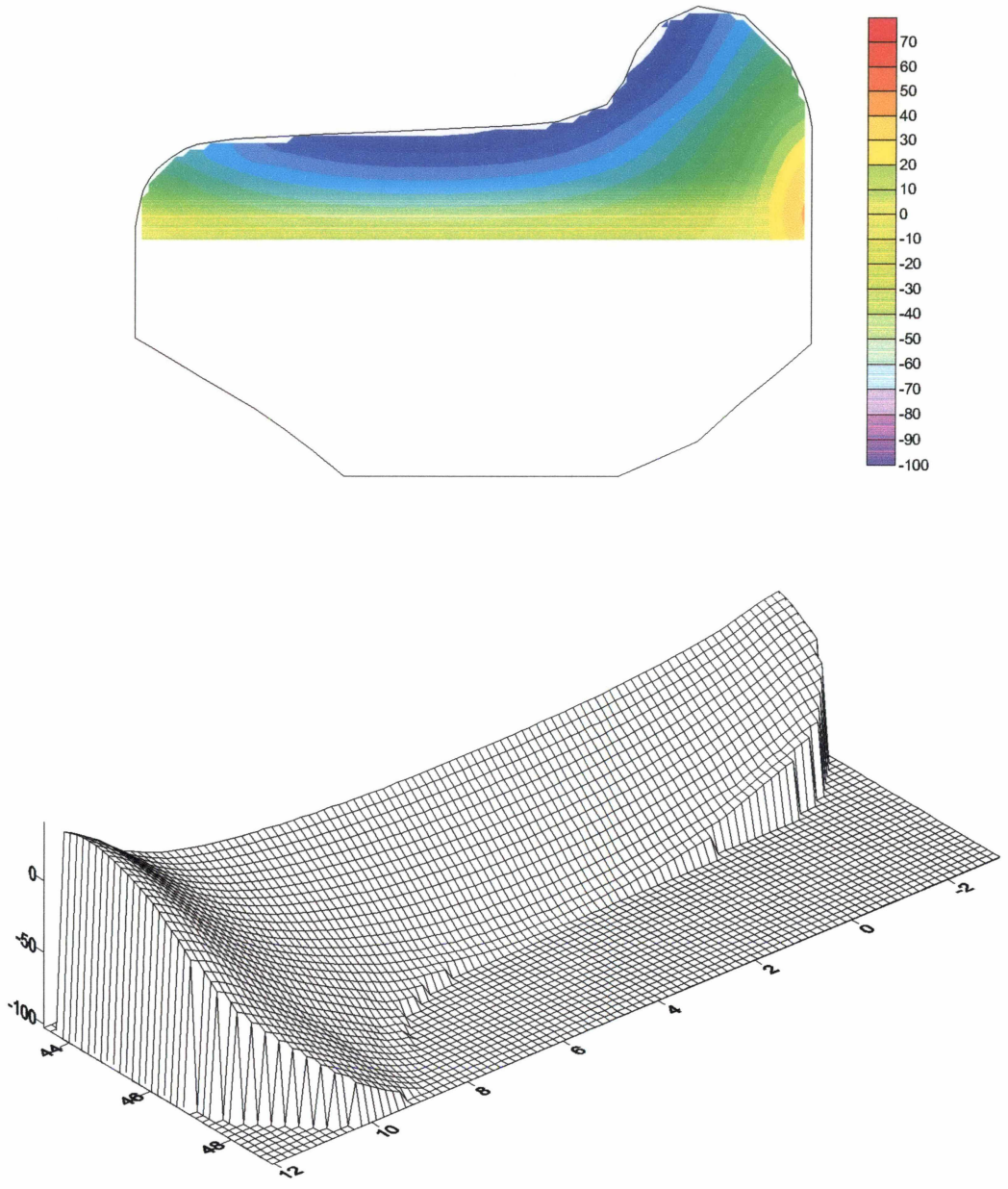

Fig. 41 Residual hoop stress distribution [MPa] – wheel #8, case 1

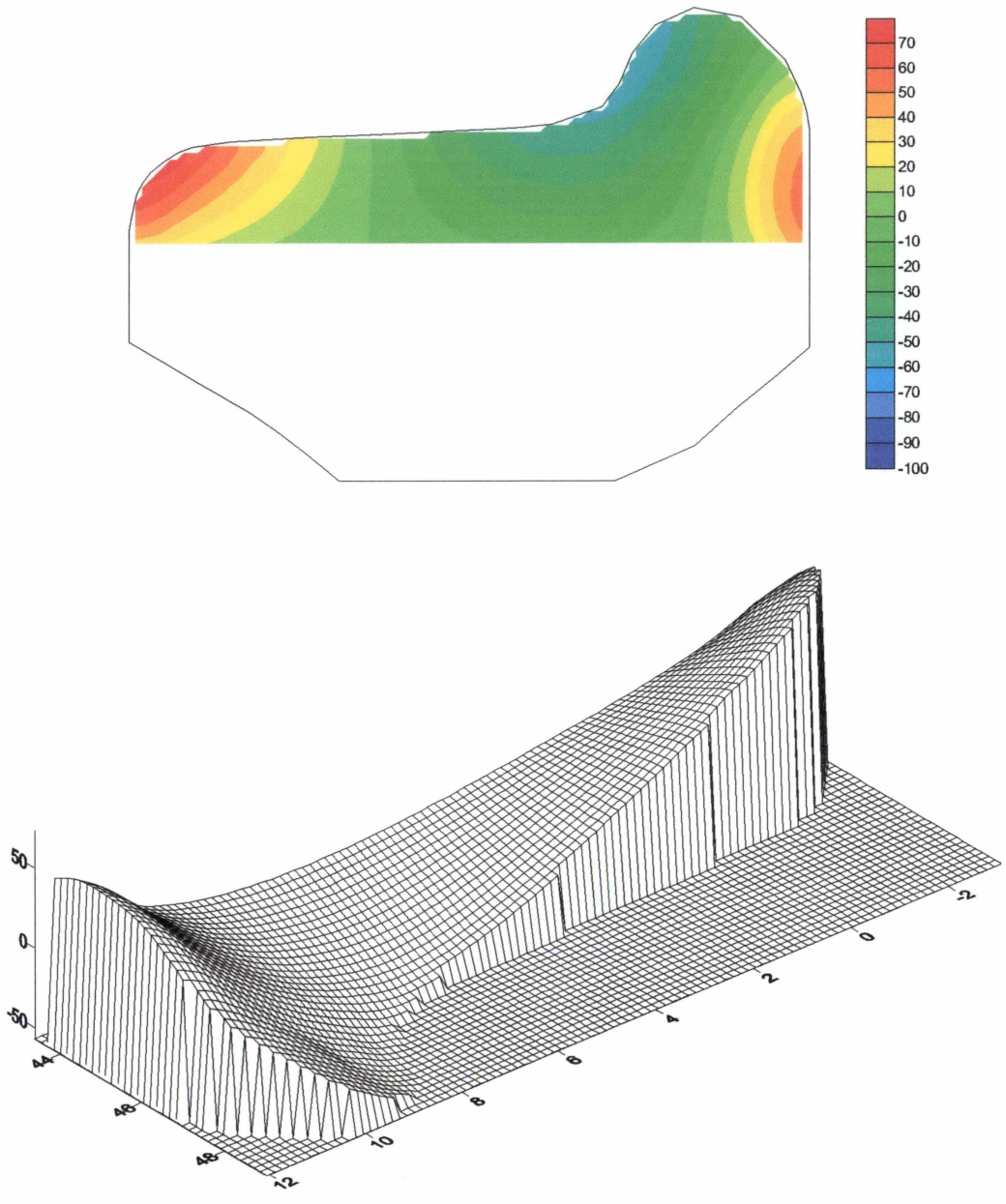

Fig. 42 Residual hoop stress distribution [MPa] – wheel #8, case 2

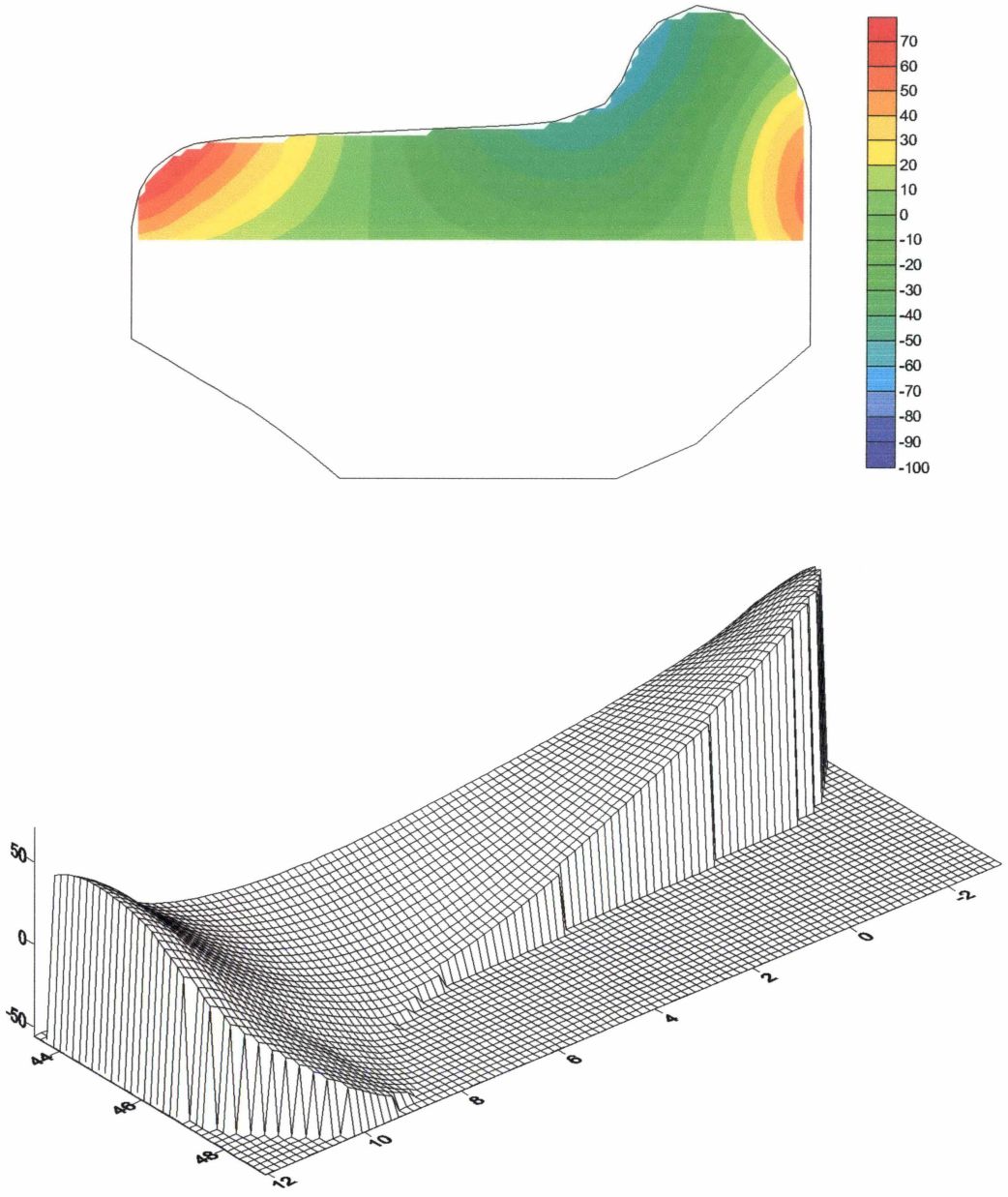

Fig. 43 Residual hoop stress distribution [MPa] – wheel #8, case 3

7. Analysis of the wheel #3 – dense mesh

7.1. Finite element model

The new version of the ADINA program used to compute the influence coefficients allows for solving on a PC class computer problems having more than 200 thousand DOF. Simple tests have shown, that the

size of linear problem cannot exceed 550 thousand DOF on 32-bit computer. Problems having above 600 thousand DOF require powerful workstation and appropriate finite element method software, which currently are not available at Cracow University of Technology. The main goal of the last year's efforts was to establish the relation between the size of discrete problem solved in influence coefficient computation and distribution and magnitude of approximated residual hoop stresses in railroad car wheels. The new dense mesh has been developed recently for the wheel #3. The comparison of the old and the new mesh in the cross-section of this wheel is shown in Fig. 44 and Table 3.

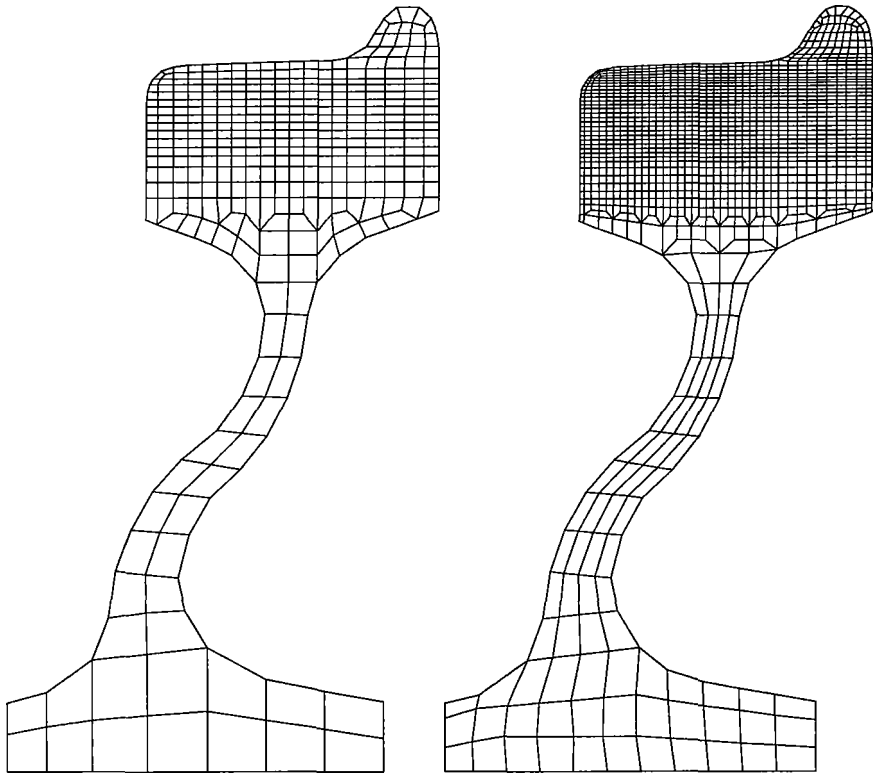

Fig. 44 Coarse and dense 2D meshes – wheel #3

Table 3. Coarse and new 3D mesh data – wheel #3

	Coarse mesh	Dense mesh
Number of nodes	43643	137362
Number of elements	9350	30778
Number of DOF	150k	390k
Number of cuts	14	28
Avg. number of right hand side vectors	19	38

7.2. Comparison of results obtained for wheel #3 for the coarse and dense mesh

In this chapter presented are preliminary results obtained for the wheel #3 when the new dense mesh is used in influence coefficients computation. Included results are obtained, when only measurements taken from the last deepest cut are used (both horizontal and vertical component). The same solution is found for previously used coarse mesh. Results are presented for the same values of λ parameter. It doesn't mean that the solution conditions are exactly the same for both sets of approximations. Both theoretical and experimental part of the functional (1) are normalized, and therefore the same values of λ give only similar conditions, but they are comparable. In all examples no scaling to the value of the yield stress is made.

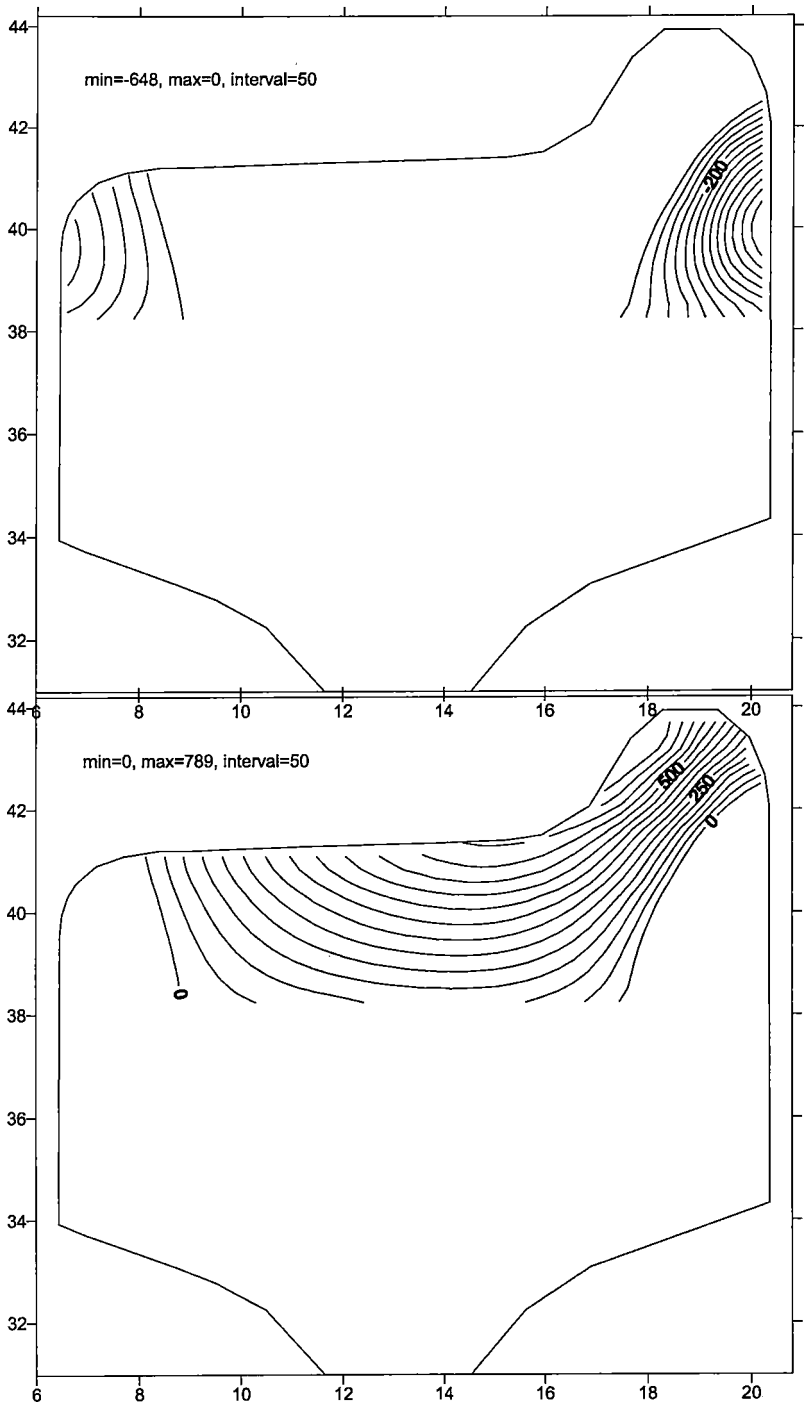

Fig. 45 Residual hoop stress [MPa] – coarse mesh, λ=0.4

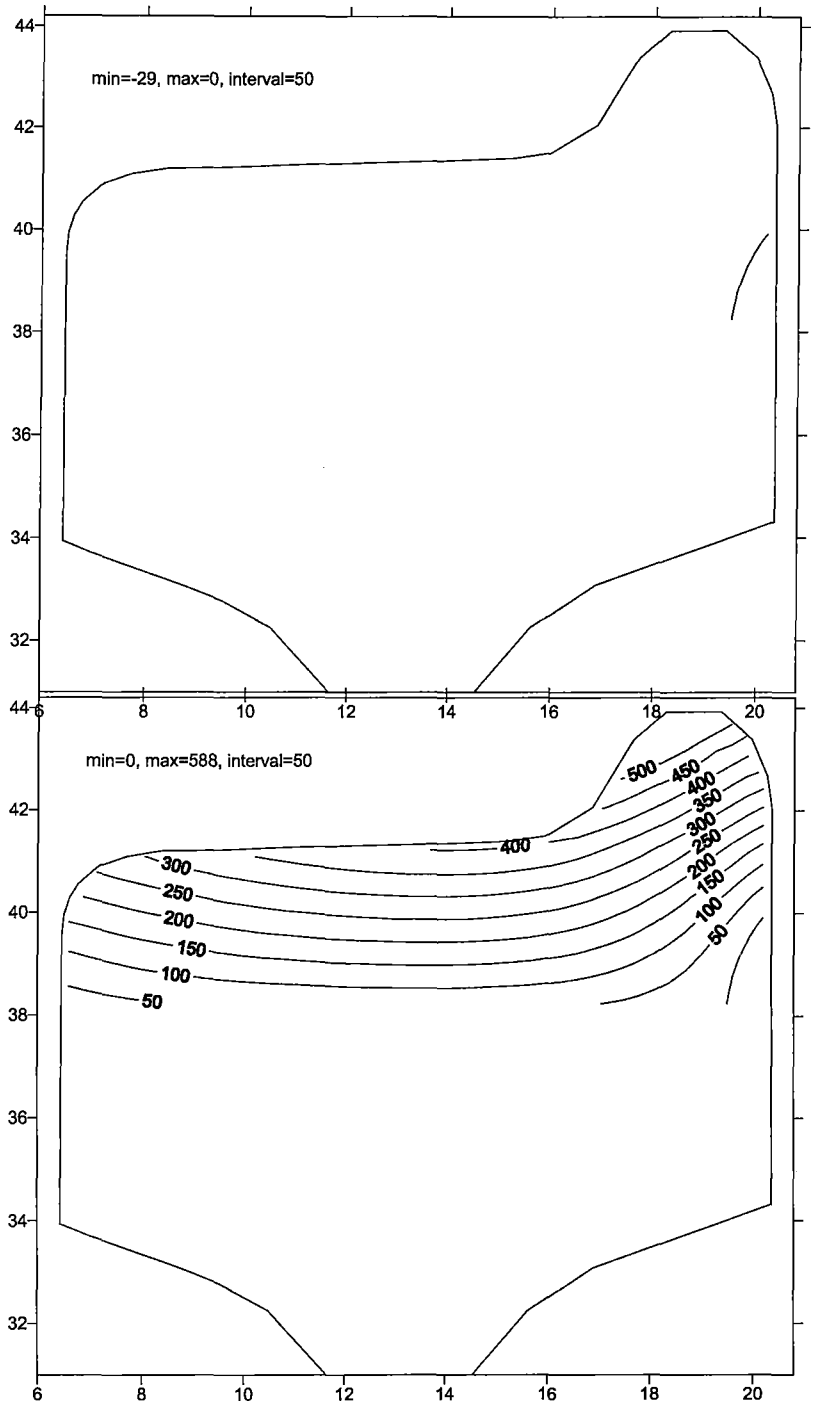

Fig. 46 Residual hoop stress [MPa] – dense mesh, λ=0.4

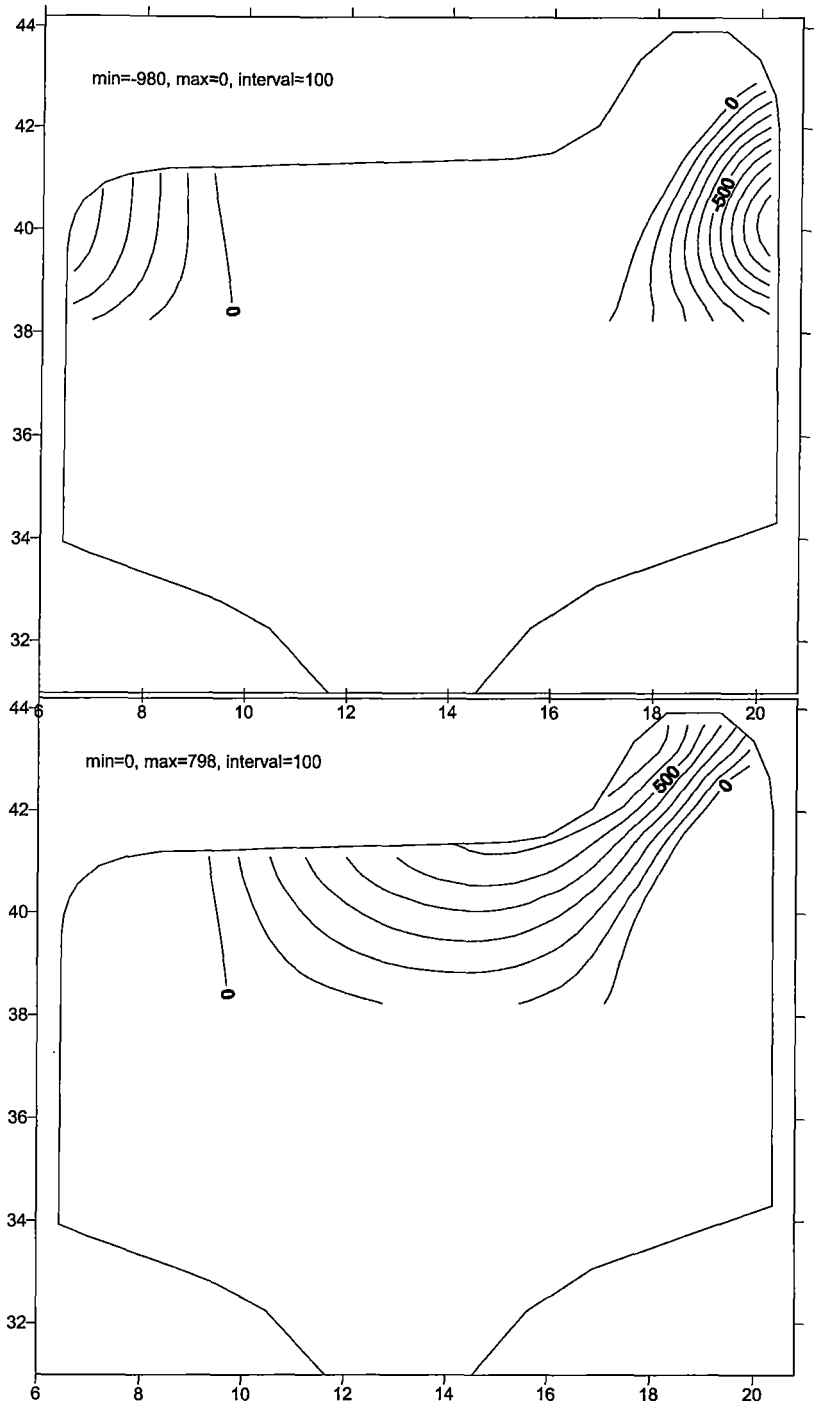

Fig. 47 Residual hoop stress [MPa] – coarse mesh, λ =0.5

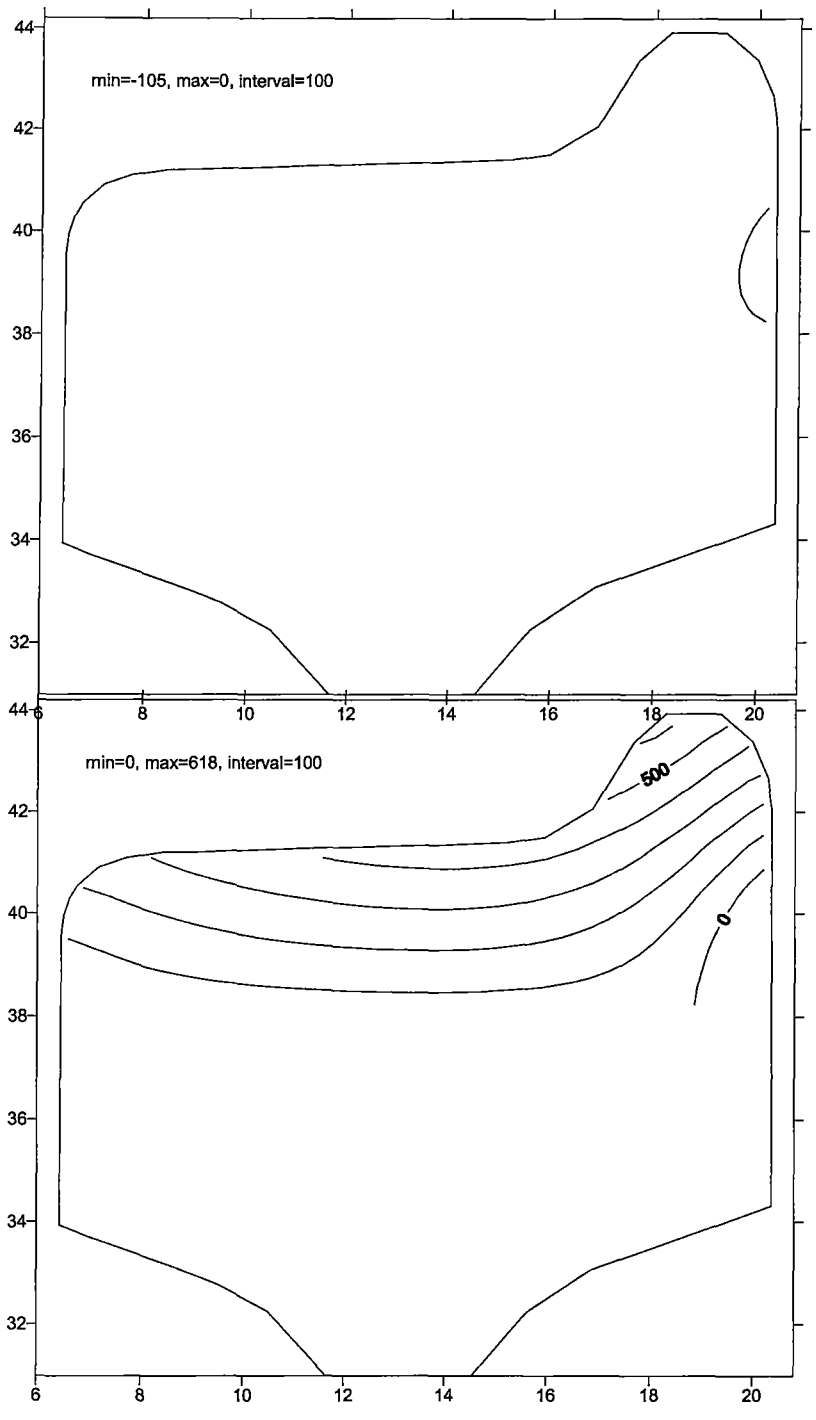

Fig. 48 Residual hoop stress [MPa] – dense mesh, λ =0.5

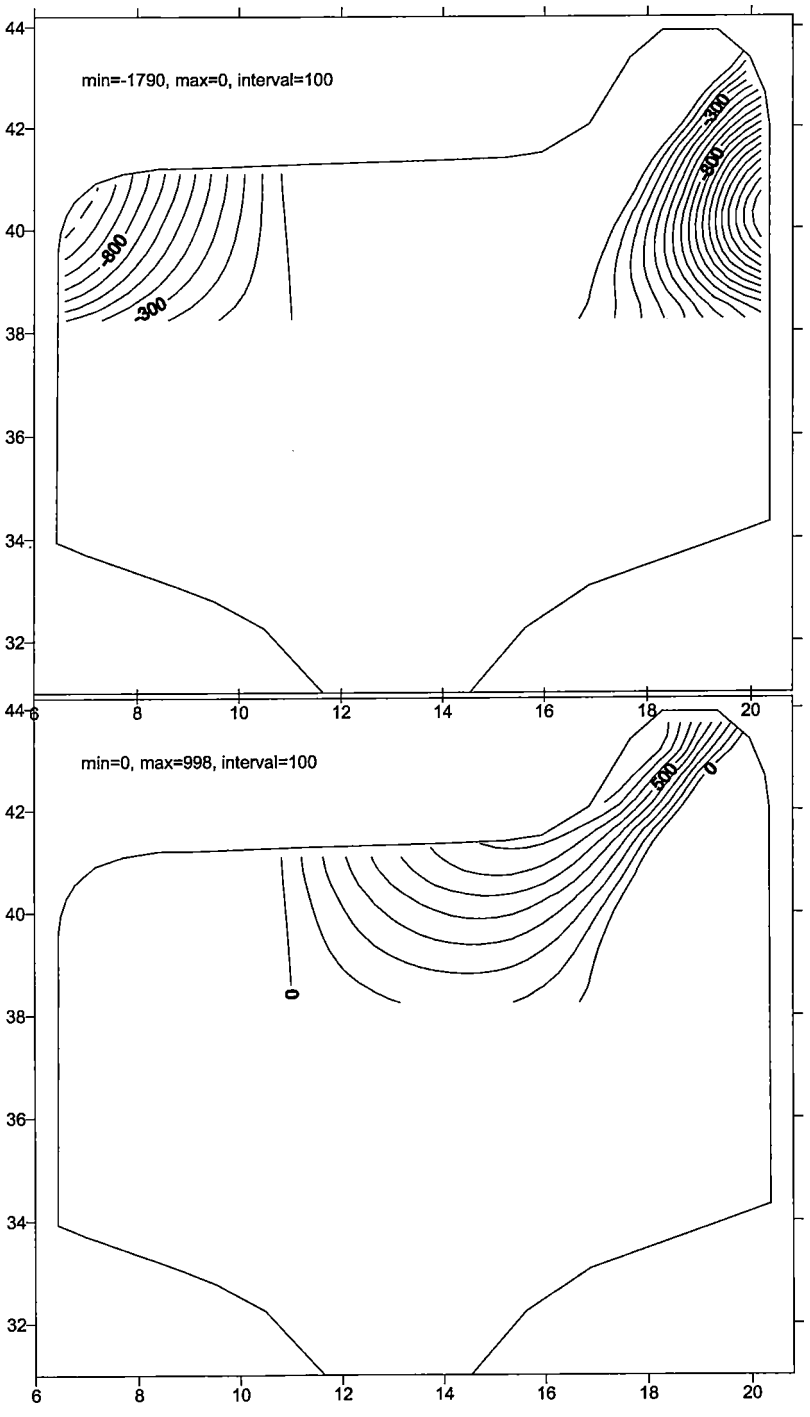

Fig. 49 Residual hoop stress [MPa] – coarse mesh, λ =0.7

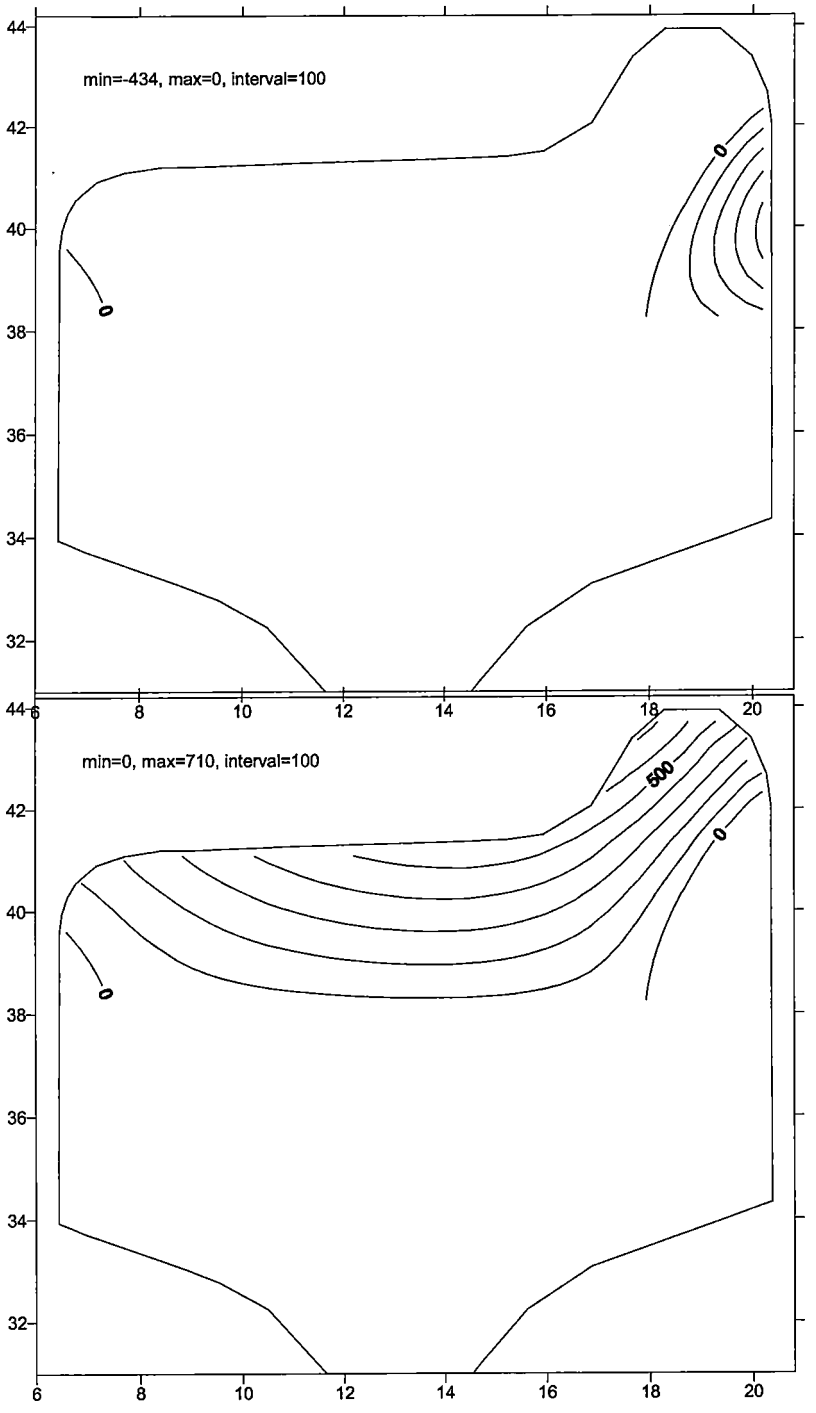

Fig. 50 Residual hoop stress [MPa] – dense mesh, λ =0.7

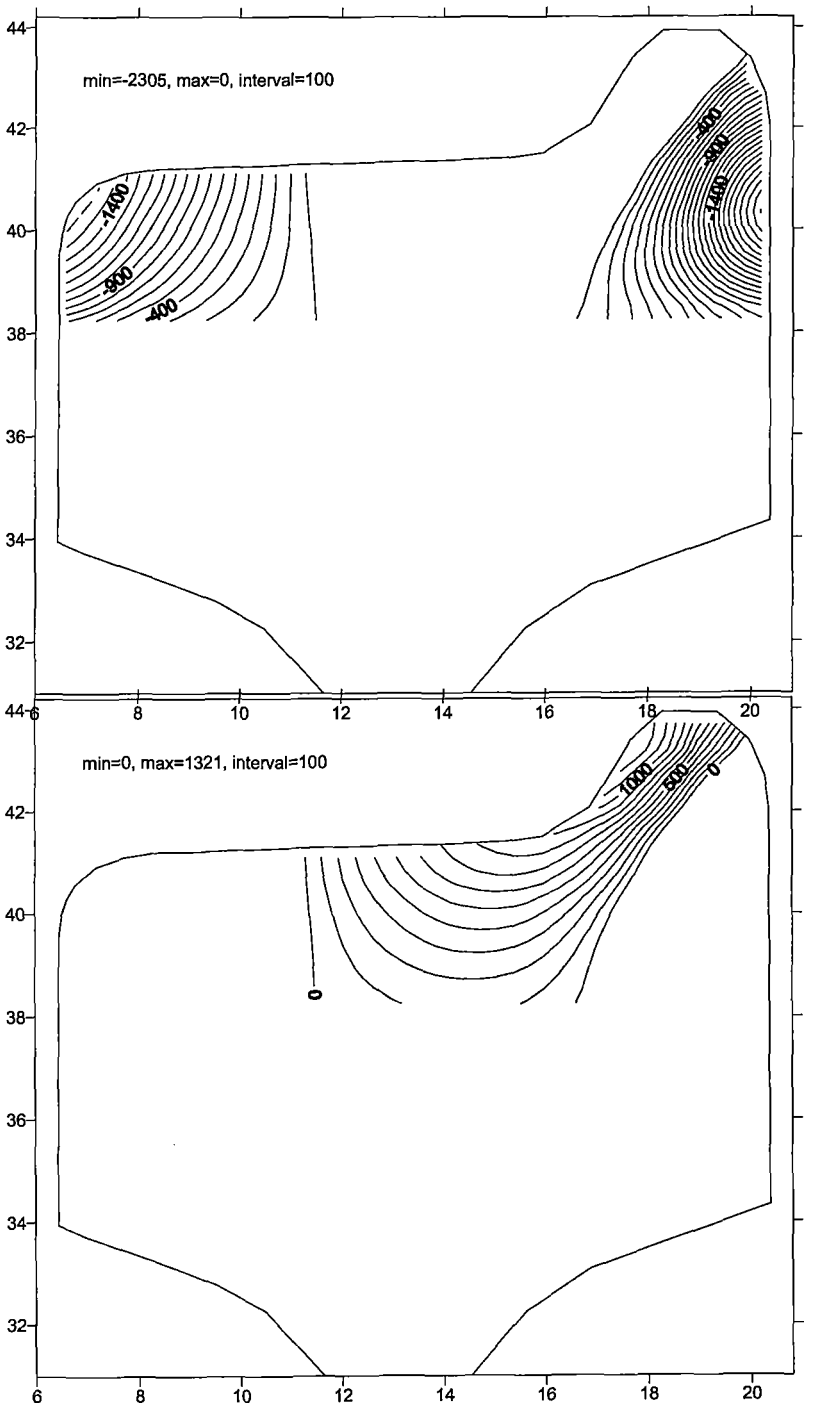

Fig. 51 Residual hoop stress [MPa] – coarse mesh, λ=0.8

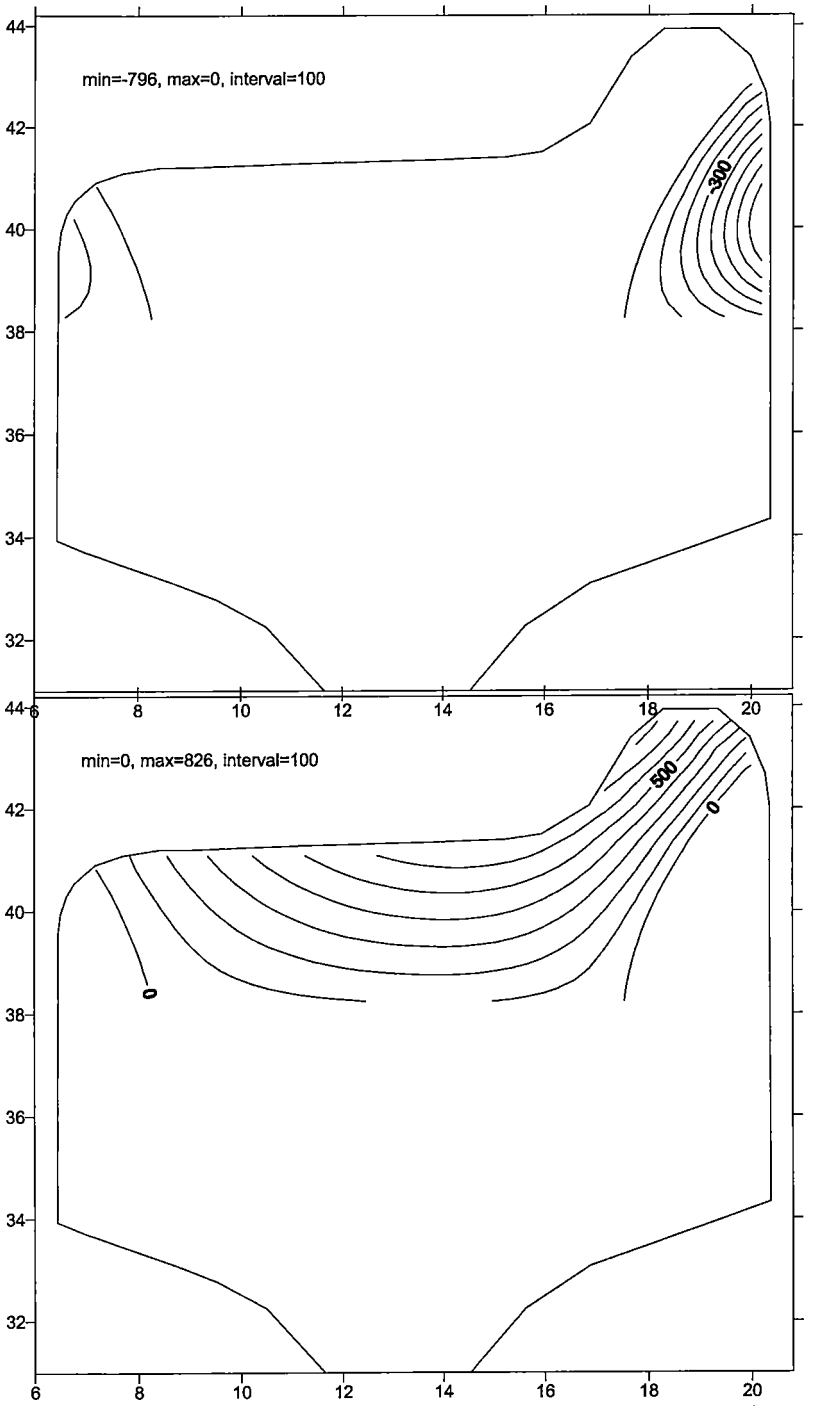

Fig. 52 Residual hoop stress [MPa] – dense mesh, λ=0.8

One may notice, that all solutions obtained for the dense mesh are smoother, and the magnitudes of hoop residual stresses are smaller. Finite element model is always too stiff. Therefore, influence coefficients are too small, and residual hoop stresses are overestimated. The finite element model for which the magnitudes of obtained residual hoop stresses are smaller is better. Therefore, new approximations of residual hoop stresses in railroad car wheels are more precise that old ones.

8. Discussion on precision of influence coefficients

The main condition of proper residual stress approximation is the precise computation of influence coefficients. During last years the great effort has been dircted towards discrete FEM analysis precise enough to model actual measurements taken at saw cut test. Instead of previously used lumped load (nodal forces) unit pressures (kinematically equivalent forces) are applied. To get better local strain approximation 20-node brick elements are used instead 8-node brick elements. Finally the new very dense FEM mesh is used for the wheel #3. The size of FEM problem is about 400 thousands degrees of freedom. It is worth stressing, that such huge problem has to be solved hundreds of times. Even on computer with 2GHz processor this takes three weeks of continuous computations. Obtained solutions are very precise in the sense of nodal displacements. Unfortunately, using the finite element method one obtains the stress solution which is one order less accurate than the displacement solution. Equilibrium conditions are satisfied only on the element level, for the whole model, and of course in nodes, but are not satisfied locally e.g. on element faces.

Stresses computed in the non-cut part of the wheel form the influence force coefficient matrix. Simple benchmark tests presented in this chapter have shown, that the precision of calculated stresses should be improved. A flat plate fixed on one half and loaded by unit pressure is considered (Fig. 53)

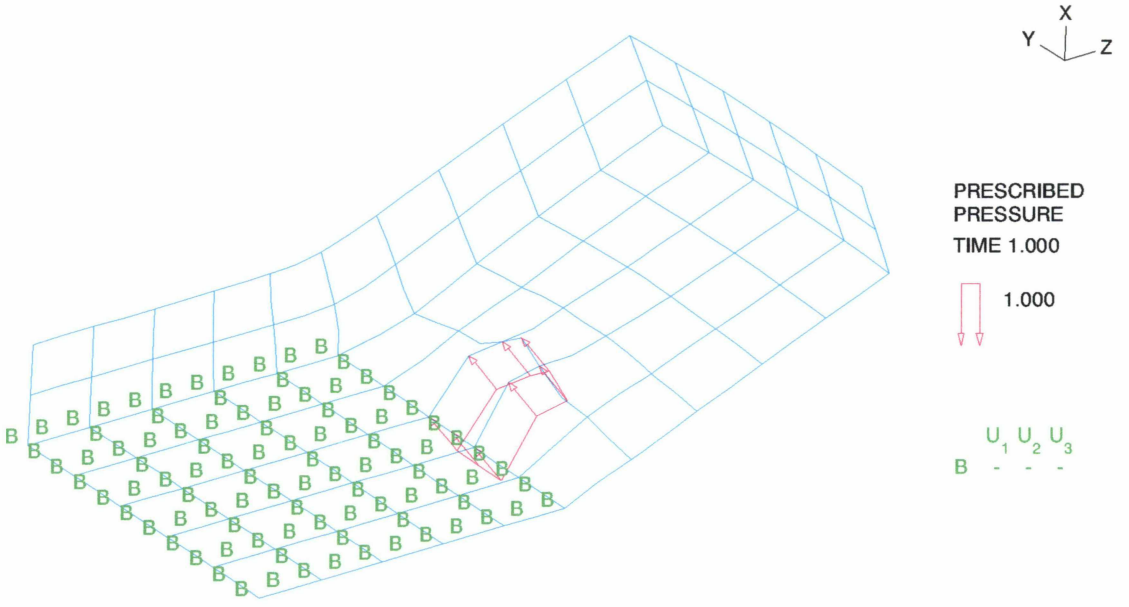

Fig. 53 Plate loaded by unit pressure

In the theoretical solution the stress component perpendicular to the free surface of the plate should be equal to the external loading i.e. should be –1 in those points where pressure is applied and zero elsewhere. Unfortunately this stress component in the loaded element (Fig. 53) in all Gaussian points is quite different than –1 (see Table 4). The local equilibrium conditions are not satisfied then.

Table 4 σ_{xx} values in Gaussian points

Point #	σ_{xx}
Int point 111	-1.93688E-01
Int point 112	-3.01972E-01
Int point 113	-5.50704E-01
Int point 121	-4.19131E-01
Int point 122	-4.32373E-01
Int point 123	-5.41274E-01
Int point 131	1.17798E-01
Int point 132	2.21905E-01
Int point 133	2.75142E-01
Int point 211	-3.73569E-01
Int point 212	-4.84918E-01
Int point 213	-7.36717E-01
Int point 221	-5.02927E-01
Int point 222	-5.19235E-01
Int point 223	-6.31202E-01
Int point 231	1.30086E-01
Int point 232	2.31127E-01
Int point 233	2.81297E-01
Int point 311	-1.93688E-01
Int point 312	-3.01972E-01
Int point 313	-5.50704E-01
Int point 321	-4.19131E-01
Int point 322	-4.32373E-01
Int point 323	-5.41274E-01
Int point 331	1.17798E-01
Int point 332	2.21905E-01
Int point 333	2.75142E-01

This difference between theoretical and computed value of σ_{xx} is a result of the way, the loading is applied (kinematically equivalent forces) and by the stiffness of neighbour elements. The influence of these elements doesn't allow for reaching the theoretical value of σ_{xx} even for much denser mesh. Much better result may be obtained, when the whole group of elements is loaded by unit pressure and the dense mesh is used (Fig. 54).

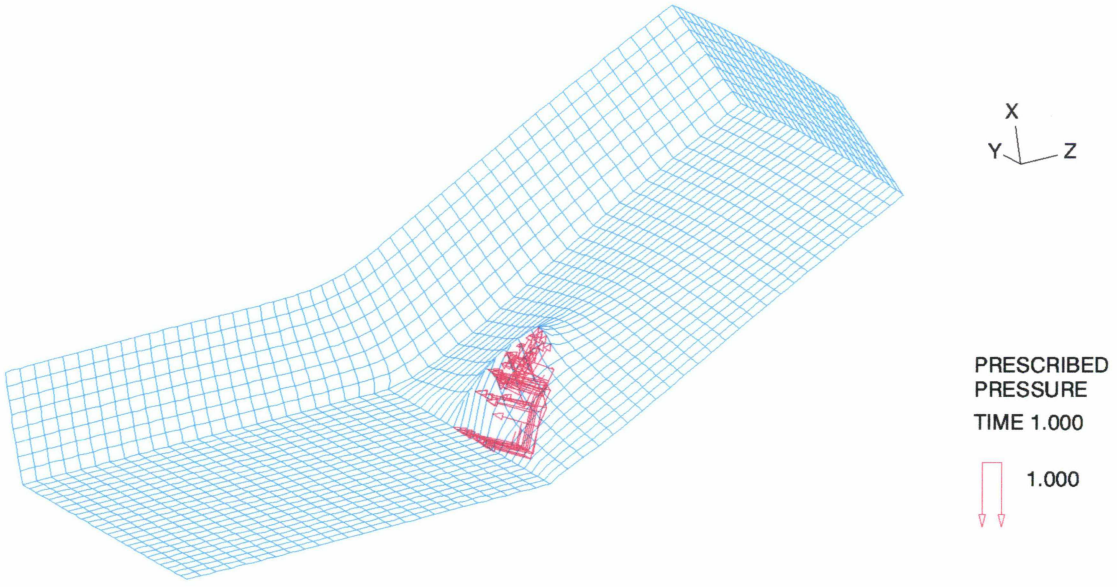

Fig. 54 Group of element loaded by unit pressure

In this test the σ_{xx} component in the element surrounded by loaded elements is close to the theoretical value (see Table 5)

Table 5 σ_{xx} values in Gaussian points

Point #	σ_{xx}
Int point 111	-9.24996E-01
Int point 112	-9.51387E-01
Int point 113	-1.03166E+00
Int point 121	-9.54866E-01
Int point 122	-9.45228E-01
Int point 123	-9.88472E-01
Int point 131	-9.91747E-01
Int point 132	-9.44065E-01
Int point 133	-9.48261E-01
Int point 211	-9.50042E-01
Int point 212	-9.65192E-01
Int point 213	-1.03540E+00
Int point 221	-9.79670E-01
Int point 222	-9.58291E-01
Int point 223	-9.90967E-01
Int point 231	-1.01672E+00
Int point 232	-9.56798E-01
Int point 233	-9.49925E-01
Int point 311	-9.70092E-01
Int point 312	-9.72245E-01
Int point 313	-1.03063E+00
Int point 321	-9.99955E-01
Int point 322	-9.65079E-01
Int point 323	-9.85428E-01
Int point 331	-1.03765E+00
Int point 332	-9.63731E-01
Int point 333	-9.44032E-01

The above tests have shown, that the best results in the sense of locally computed stresses may be obtained when the patches consisting of finite elements are loaded by unit pressures. The inner element of the patch yields the best stress result.

9. Final conclusions

Solution approach proposed and carefully tested in recent years has made possible high quality approximations of residual hoop stresses in railroad car wheels. During last years a significant progress has been made in enhancing influence coefficients calculations. Higher order finite elements have been introduced. Instead of unit forces, unit pressures have been applied in order to obtain more precise strain distributions. Finally very dense mesh has been used for the wheel #3.

Appropriate benchmark tests have proved efficiency of the new approach. Computed influence coefficients are more precise nowadays due to higher order finite elements used, the type of loading applied to elements and the size of the discrete problem. Residual stress approximations are of good quality and they are similar for different measurement components and for different cut depths.

There are many factors which influence the quality of approximated residual stresses. First of all experimental results are never 100% precise. Sometimes mechanical damages may occur like in the wheel #3, flange side, the deepest cut. If erroneous or uncertain data are input into analysis, they influence adversely the final solution. The second important factor is the precision of influence coefficients computed numerically. Important is not only the size of solved discrete problem, but also type of elements used in FEM an **the way the loading is applied**. Even for the same finite element mesh, the magnitudes of hoop residual stresses may differ significantly.

In the simulation of cutting process by finite element, hardware and software limits have been reached. The solution approach and numerical procedures have been optimised very carefully in order to obtain the best possible results. However there is still a chance to improve the residual hoop stress approximation quality, by applying the loading to the patches of elements instead of applying it to the separate elements.

10. References

[1] R. Czarnek, *Development and Application of an Improved Method for Experimental Determination of Release Fields in Cut Railroad Car Wheels*, 4th Int. Conf. on Contact Mechanics and Wear of Rail/Wheel Systems, Vancouver, Canada, (1994).

[2] R. Czarnek, *Experimental Determination of Release Fields in Cut Railroad Car Wheels,* Final Report DOT/FRA/ORD-97/06, US Department of Transportation, (1997).

[3] J. Krok, J. Orkisz, A. Skrzat, *On reconstruction of hoop stress in 3D bodies of revolution based on simulated saw cut data*, Proc. XIII Polish Conference Computer Methods In Mechanics, Poznań, pages 669-676, (1997).

[4] J. Krok, J. Orkisz, A. Skrzat, *On reconstruction of hoop residual stress in railroad vehicle wheels based on the experimentally measured data at saw cut,* Report to US DOT-VNTSC, Boston, (1998).

[5] J. Orkisz, A. Skrzat, *Reconstruction of Residual Stresses in Railroad Vehicle Wheels Based on Enhanced Saw Cut Measurements, Formulation and Benchmark Tests*, WEAR, 191, pages 188-198, (1996).

[6] J. Orkisz, A. Skrzat, *Reconstruction of Residual Stresses in Railroad Vehicle Wheels Based on Enhanced Saw Cut Measurements,* Rpt Grant DTFR 53-95-G00055, (1999).

[7] A. Skrzat, *Physically based approximation of residual stresses in railroad vehicle wheels (in polish)*, Ph. Thesis, Rzeszow, (1998).

[8] A. Skrzat, J. Orkisz, J. Krok, *Residual stress reconstruction in railroad car wheels based on experimental data measured at saw cut test,* European Conference on Computational Mechanics, Krakow, (2001).

[9] A. Skrzat, J. Orkisz, *Residual Stress Reconstruction in Railroad Passenger and Freight Car Wheels*, CMM 2003 Conference on Computer Methods in Mechanics, Wisla, Poland, (003).

Topic 2.7

Failure mode and life prediction of railway rails

Failure mode and life prediction of railway rails

Further preliminary analysis of the influence the residual stresses on fatigue failure modes and fatigue service life of railroad rails has been performed. At first the crack nucleation problem is considered basing on the classic stress-life (S-N) approaches to fatigue life estimation and initial ability to grow crack is investigated (topic 2.7.1). The role of the total stresses has been examined as a sum of actual stresses and residual stresses. The magnitude and distribution of these stresses determines rail failure modes and is used to predict service life (topic 2.7.2). The current knowledge on the problem in mechanical understanding of rail fatigue are considered. A preliminary analysis of the role of the residual stresses in the railroad rails in both crack nucleation and growth is discussed. In this work one assumes, that single point wheel/rail contact at several central and off central rail localization appears. The needed computer programs have been developed and numerical analyses have been carried out. One assumes that examined body is subject to damage by repeated cycles of altering stresses. In present work 132 RE railroad rail subject to 15 ton wheel load was analyzed. It was realized for three localization of loading. The results are obtained using own computer program. The shortest life to fatigue crack nucleation was predicted for a neighborhood of the rail running surface (top of the rail head) (topic 2.7.3).

Cracow University of Technology
ul. Warszawska 24, 31-155 Cracow, POLAND

Further investigation and testing of the proposed solution approach to analysis of life prediction of railroad rails.

Wojciech Karmowski, Janusz Orkisz

Report to the

US Department of Transportation,
Federal Railroad Administration,
Washington, DC

Cracow, June 2003

Further investigation and testing of the proposed solution approach to failure analysis and life prediction of railroad rails

W. Karmowski. J. Orkisz

Abstract

Further preliminary analysis of the influence the residual stresses have on fatigue failure modes and fatigue service life of railroad rails is the goal of this work. At first the crack nucleation problem is considered based on the classic stress-life (S-N) approaches to fatigue life estimation. The crack propagation problem in the case of off center force localization has been considered. Initial ability to grow crack is investigated. The role of residual stresses has been examined. It is expected that the detailed analysis will show whether available experimental data is sufficient of rail failure and life prediction analysis. This problem has been discussed in the report [9], where total stresses in the central loading case were investigated.

1. Introduction

Crack nucleation in railroad rails and resulting failure present a very important problem in railway practice. Therefore, service life prediction is a significant goal of theoretical works. Crack growth depends mainly on the distribution of total stresses throughout the rail [4, 5, 7, 8, 15, 16, 17, 23, 25, 26], which is a sum of actual stresses and residual stresses. The magnitude and distribution of these stresses determines rail failure modes and may be used to predict service life. A knowledge of the residual stress distribution is crucial only if they constitute a significant part of the total stresses.

Experiments and theoretical predictions indicate that residual stresses in railroad rails may be large and therefore can not be neglected a`priori. Therefore, without reasonably accurate residual stresses included, failure mode and life prediction analyses may provide inaccurate estimates.

The current state of the art in mechanical understanding of rail fatigue is considered. A contemporary approach to fatigue in metals is presented in [25]. Railroad rail fatigue problems were broadly discussed and an engineering solution approach was proposed in [17]. Recent increases in freight car axle loads have created the need for further development and verification of the current approach. Thus an updated approach to rail failure analysis and service life prediction has been recently discussed and presented in [12].

A preliminary analysis of the role the residual stresses play in the railroad rails in both crack nucleation and growth is the goal of this work. It is based on the works [12, 13].

It is assumed here, that single point wheel/rail contact appears at several central and off central rail locations. Two points contact and wheel wandering analysis are left for the future when interaction of the neighboring cars [17] will be discussed. The rail is treated as a collection of bars i.e. only axial stress is taken into account instead of full stress tensor components. General case will be considered in the future basing on

concepts given e.g. in [22, 23]. Additionally one assumes that micro cracks are uniformly distributed over the rail cross section. Analysis takes into account LEFM laws for initial crack growth only (Paris [19] and Elber [3] laws) when no crack growth investigation has been performed. Investigation of the stress-life (S-N) type approach to fatigue life estimation of railroad rails has been performed. The needed computer programs have been developed and numerical analyses have been carried out.

2. Estimation of crack nucleation life

Influence of residual stresses on the crack nucleation is considered. The total stresses are the sum of elastic stresses (due to loading) and residual stresses (independent of rail longitudinal axis). They may be presented as:

$$\breve{\sigma}_{total}(x,y,z)=\breve{\sigma}_{elastic}(y,z)+\breve{\sigma}_{residual}(x,y,z), \qquad (1)$$

where "x" is a longitudinal axis, "z" is a vertical axis and "y" transverse axis.
The longitudinal elastic stress component σ_{xx} for one force located at the zero longitudinal coordinate exhibits dependency shown in Fig. 1., when using beam rail model ([17]),

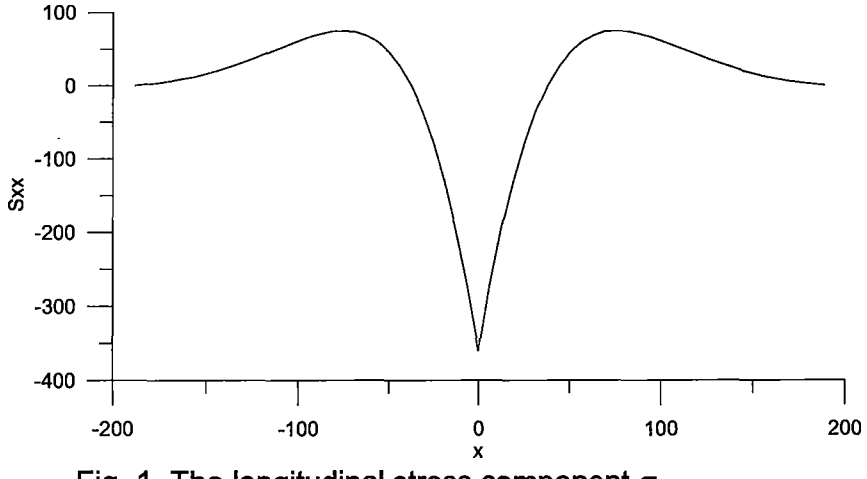

Fig. 1. The longitudinal stress component σ_{xx}.

This σ_{xx} stress component distribution in rail has three characteristic points with respect to wheel/rail contact location:

1. compressive stress maximum for $x=0$ $\sigma(0)$,
2. tensile stress maximum for $x=x_{max}$ $\sigma(x_{max})$,
3. zero elastic axial stresses in infinity $x=\infty$ $\sigma(\infty)$.

Stresses at these points are:

$$\begin{aligned}\sigma_1 &= \sigma^E(0)+\sigma^r \\ \sigma_2 &= \sigma^E(x_{max})+\sigma^r \\ \sigma_3 &= \sigma^r\end{aligned} \qquad (2)$$

where σ^E, σ^r are elastic and residual stresses. These three situations happen at every point along the rail length during vehicle wheel motion. Therefore, minimum and maximum stresses/strains at any point may be found by taking extreme of the three following total stress and strain values

$$\sigma_{min} = \min(|\sigma_1|,|\sigma_2|,|\sigma_3|) \qquad \sigma_{max} = \max(|\sigma_1|,|\sigma_2|,|\sigma_3|) \qquad (3)$$

Alternate and average stresses be defined as

$$\sigma_a = \frac{\sigma_{max}-\sigma_{min}}{2} \qquad \sigma_m = \frac{\sigma_{max}+\sigma_{min}}{2} \qquad (4)$$

These formulas will be used to estimate life prediction in stress criteria.

In the S-N approach one assumes that examined body is subject to damage by repeated cycles of altering stresses. The most common Basquin [1] theory states that life prediction is a function of ultimate stress (S_u), two fatigue material constants (A and B) and two state parameters: altering stress (S_a) and medium stress (S_m). This rule has the form

$$\frac{S_a}{S_{N_f}}+\frac{S_m}{S_u}=1 \quad , \qquad (5)$$

where $S_{N_f} = A(N_f)^B$. The other equation proposed (due to Gerber)

$$\frac{S_a}{S_{n_f}}+\left(\frac{S_m}{S_u}\right)^2=1 \qquad (6)$$

seems to be erroneous because quantity S_m may be negative and in such a case it leads to wrong results. The equation

$$\frac{S_a}{S_{N_f}}+\frac{S_m}{q_f}=1, \qquad (7)$$

where q_f is true fracture strength gives almost the same results as the Basquin equation. Material constant S_u is found from basic material measurements. Equation

(9) may be used to find life prediction of the railroad rail. Taking into account that for $N_f = 1$ $S_{N_f} = S_u$ one obtains $A = S_u$. B may be found based on experimental fact that life prediction of railroad rail may be assumed as equal to 10^k, where k=1÷8, if k=8 i.e. fully reversed fatigue limit, then

$$S_f = S_u \left(10^8\right)^B \tag{8}$$

and finally

$$N_f = \exp\left(8 \ln 10 \frac{\ln \frac{S_a}{S_u - S_m}}{\ln \frac{S_f}{S_u}} \right) \tag{9}$$

3. The analysis of capabilities to predict railroad rail life.

In present work 132 RE railroad rail subject to 15 ton wheel load was analyzed. The analysis was performed for three loading locations, namely when force is on the axis of symmetry, and offset by 0.33" and 0.5" from the centerline. The following material constant values: S_u=115 ksi, S_f=67 ksi ([17]) has been used. At first foundation modulus "k" has been chosen as 2000 psi.

Distributions of: $\sigma^E(0)$, $\sigma^E(x_{max})$, σ_1, σ_2, σ_3, σ_{min}, σ_{max}, σ_a, σ_m and N_f in the rail head are presented in the figures (2-31) for the cases when contact force is located on the vertical axis of symmetry, and is offset by 0.33" and 0.5". These values have been obtained using computer program prepared by first author basing on the equations presented in [17] and residual stresses have been obtained by M. Pazdanowski [20].

symmetric case

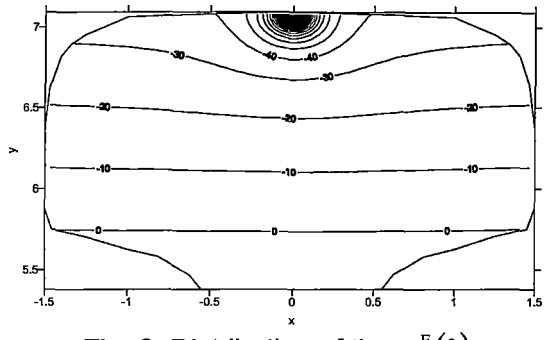

Fig. 2. Distribution of the $\sigma^{E}(0)$

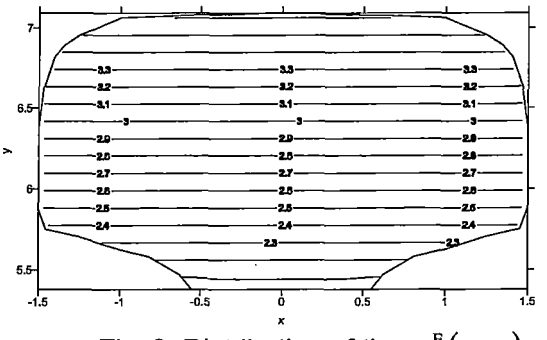

Fig. 3. Distribution of the $\sigma^{E}(x_{max})$

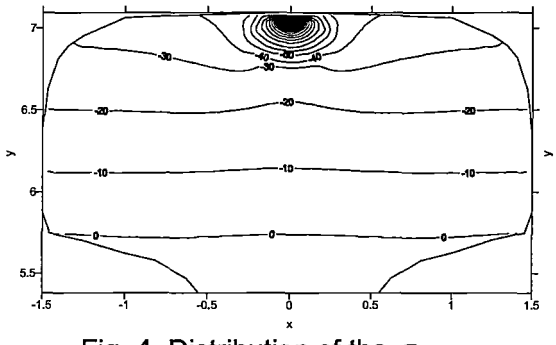

Fig. 4. Distribution of the σ_1

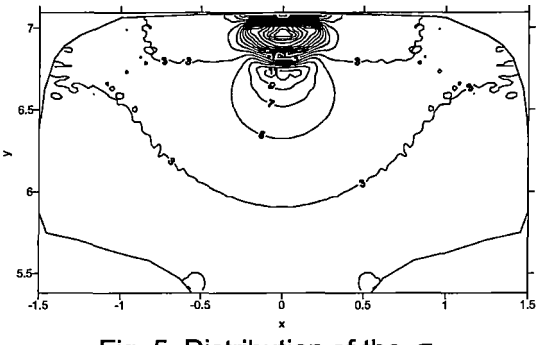

Fig. 5. Distribution of the σ_2

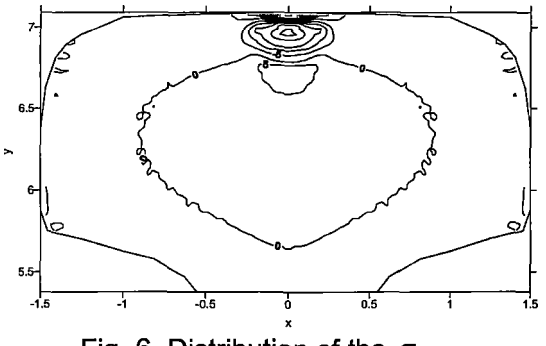

Fig. 6. Distribution of the σ_3

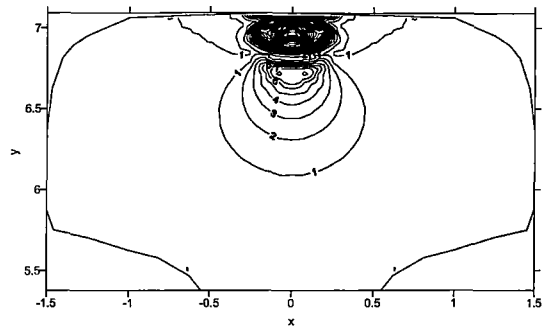

Fig. 7. Distribution of the σ_{min}

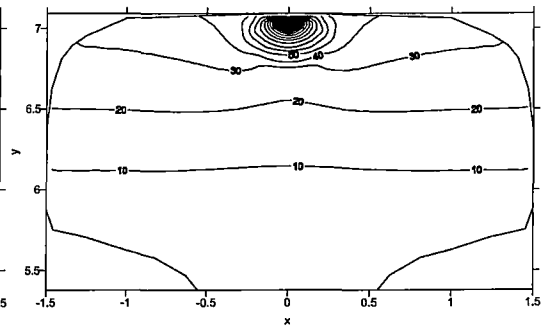

Fig. 8. Distribution of the σ_{max}

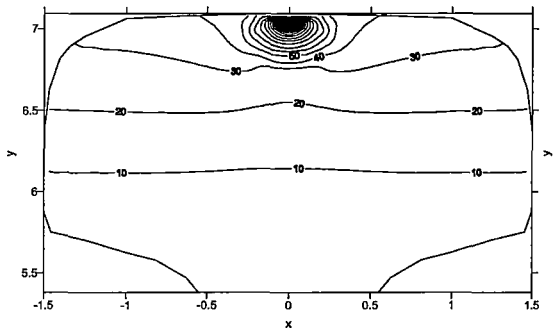

Fig. 9. Distribution of the σ_a

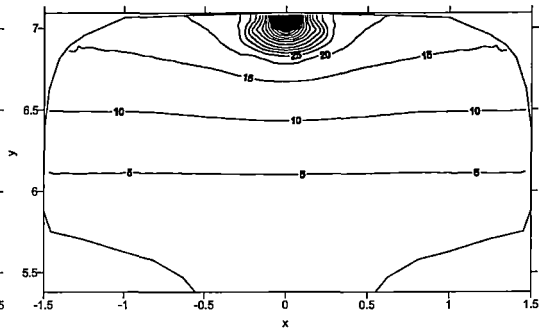

Fig. 10. Distribution of the σ_m

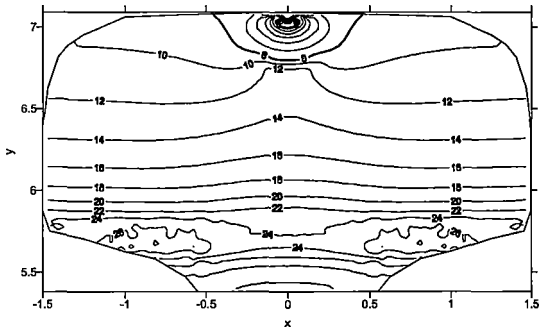

Fig. 11. Distribution of the N_f

- off center (0.33")

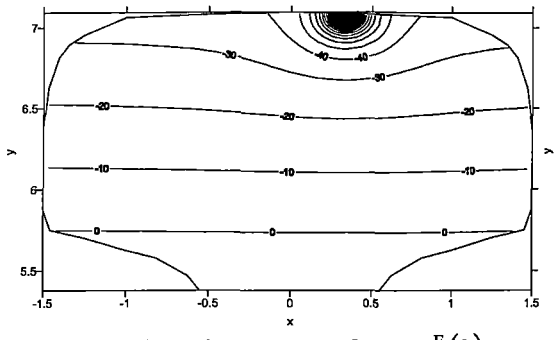

Fig. 12. Distribution of the $\sigma^{E}(0)$

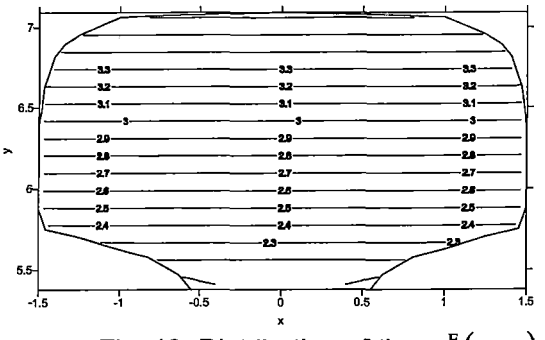

Fig. 13. Distribution of the $\sigma^{E}(x_{max})$

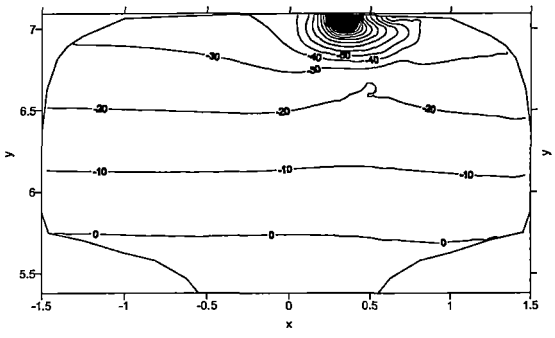

Fig. 14. Distribution of the σ_1

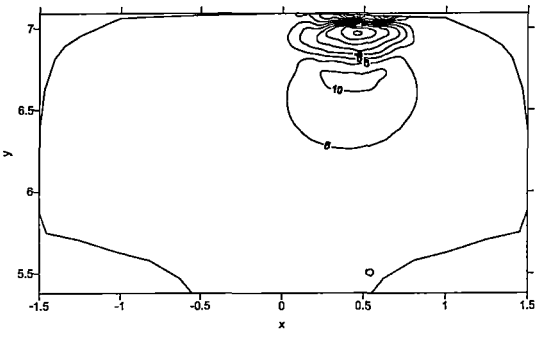

Fig. 15. Distribution of the σ_2

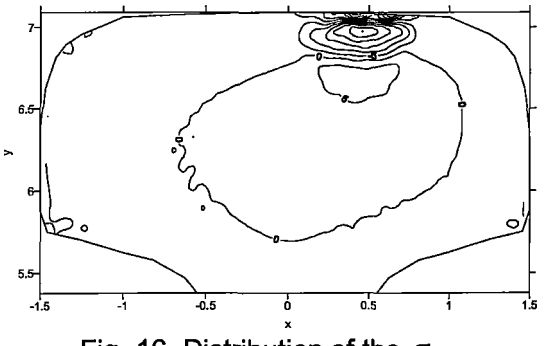

Fig. 16. Distribution of the σ_3

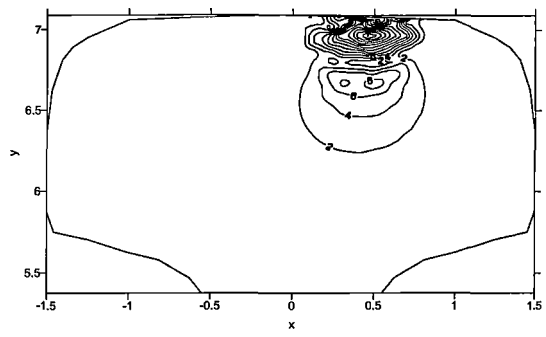

Fig. 17. Distribution of the σ_{min}

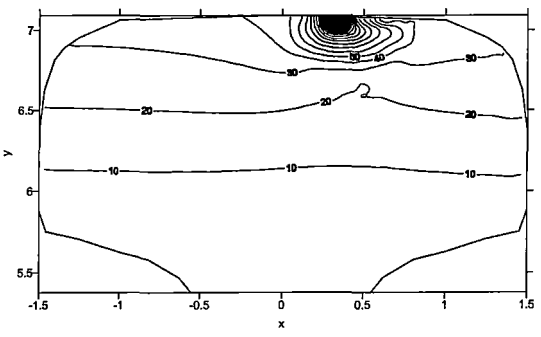

Fig. 18. Distribution of the σ_{max}

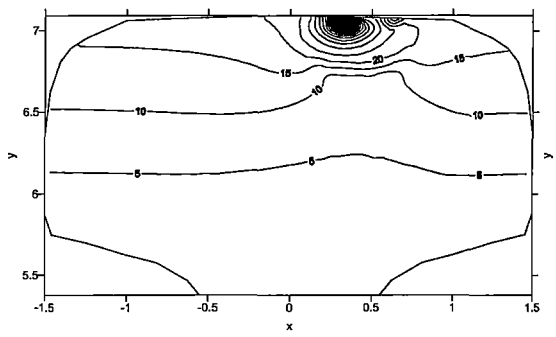

Fig. 19. Distribution of the σ_a

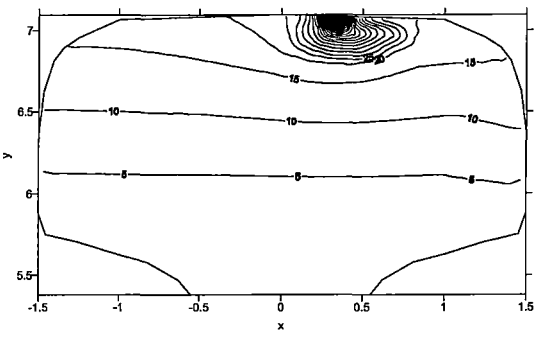

Fig. 20. Distribution of the σ_m

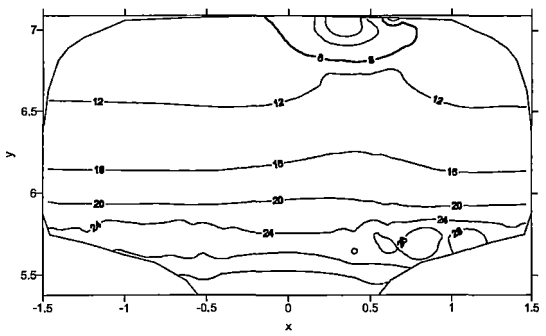

Fig. 21. Distribution of the N_f

- off center (0.5")

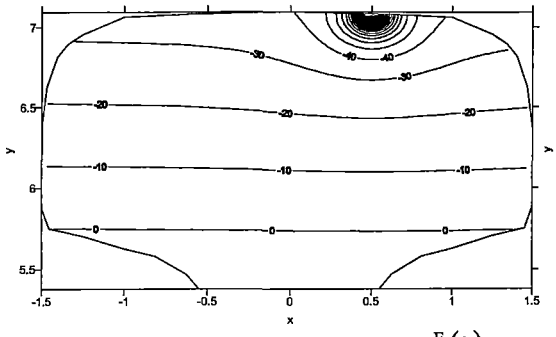

Fig. 22. Distribution of the $\sigma^{E}(0)$

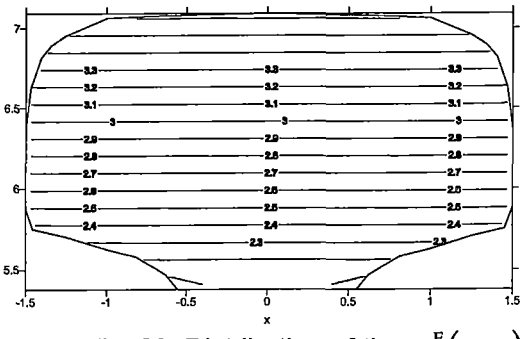

Fig. 23. Distribution of the $\sigma^{E}(x_{max})$

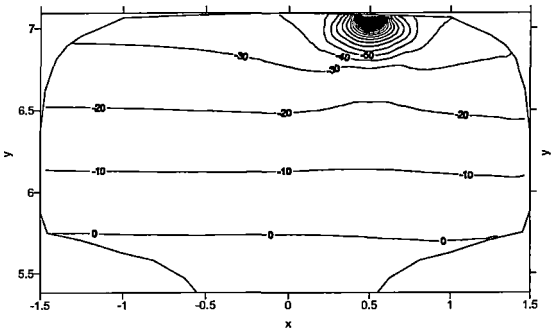

Fig. 24. Distribution of the σ_1

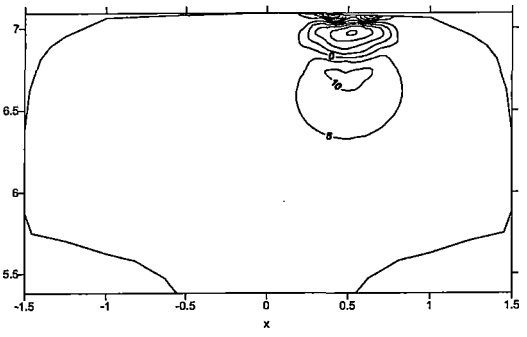

Fig. 25. Distribution of the σ_2

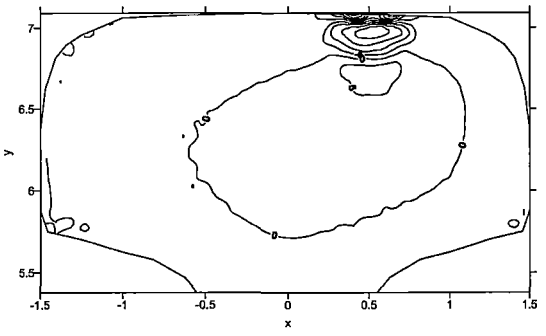

Fig. 26. Distribution of the σ_3

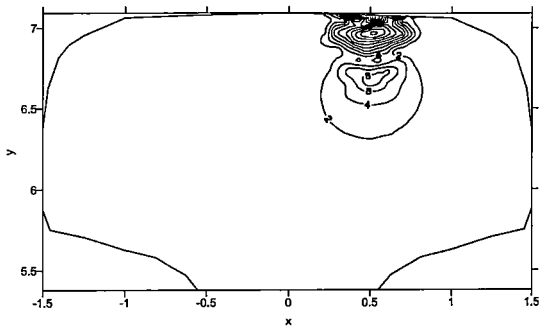

Fig. 27. Distribution of the σ_{min}

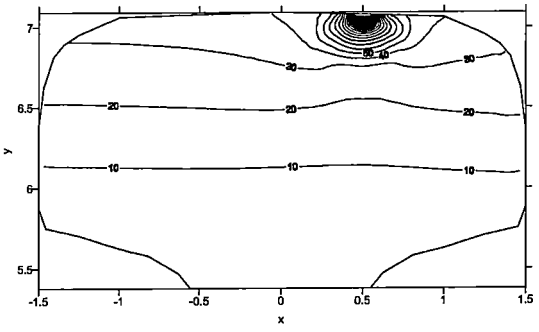

Fig. 28. Distribution of the σ_{max}

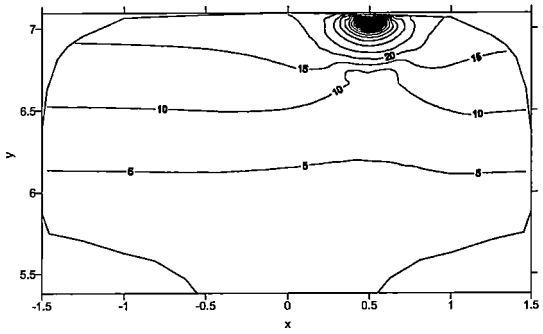

Fig. 29. Distribution of the σ_a

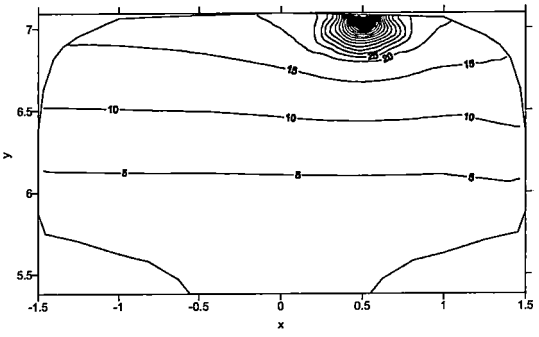

Fig. 30. Distribution of the σ_m

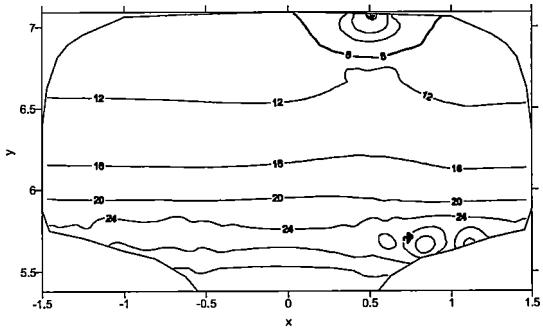

Fig. 31. Distribution of the N_f

Figs. 32 and 33 present elastic stress at the rail/wheel contact point and in the far distance when foundation modulus is changed to 5000 psi.

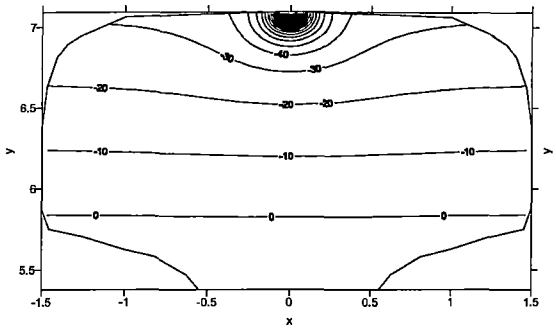

Fig. 32. Distribution of the $\sigma^{E}(0)$

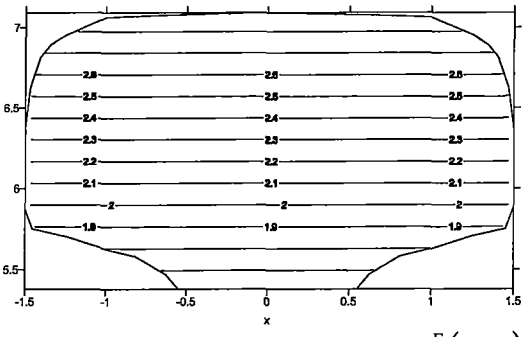

Fig. 33. Distribution of the $\sigma^{E}(x_{max})$

4. Final Remarks

1. The shortest life to fatigue crack nucleation was predicted for a neighborhood of the *rail running surface (top of the rail head)*;
2. The fatigue life N_f is mostly affected by contact loading, while influence of residual stresses σ^r on N_f is negligible;
3. Application of the precise Finite Strip Method solutions to evaluate the elastic stresses is necessary;
4. It is expected that taking into consideration multiaxial stresses will results in more precise S-N analysis;
5. Analysis of the influence residual the stresses have on rail failure and life prediction in the case of off-center wheel/rail contacts shows rather small impact on crack nucleation process. It is expected that it will be significant in case of crack propagation speed as was proved in report [9].
6. Use of a more realistic, two wheel truck loading, instead of a single wheel loading is needed for rail fatigue analysis;

5. References

[1] Basquin O.H., *The exponential law of endurance tests*, Proc. ASTM, 10, II, West\j Conshohocken, PA, p. 625 (1910).

[2] Donald K., Paris P.C., *An evaluation of ΔK_{eff} estimation procedures on 6061-T6 and 2024-T3 aluminium alloys*, International Journal of Fatigue, 21, pp. 547-557 (1999).

[3] Elber W., *Fatigue crack closure under cyclic tension*, Engineering Fracture Mechanics, 2, pp. 37-45 (1970).

[4] Foreman R.G., Kearney V.E., Engle R.M., *Numerical analysis of crack propagation in cyclic loaded structures*, Journal of Basic Engineering, 89, pp. 459-464 (1967).

[5] Fuchs H.O., *A set of fatigue failure criteria*, ASME, Journal of Basic Engineering, 87, p. 333 (1965).

[6] Hearle A.D., Johnson K.L., *Mode stress intensity factors for a crack parallel to the surface of an elastic half space subjected to a moving point load*, Journal of the Mechanics and Physics of Solids, 33, pp. 61-81 (1985).

[7] Jeong D., Orringer O., Perlman A.B., Rice R.C., *Beam theory predictions of shell nucleation life*, in: Contact Mechanics and Wear of Rail/Wheel Systems II, Gladwell, Ghonem, Kalousek eds., University of Waterloo Press, pp. 397-404 (1987).

[8] Jeong D.Y. et al., *Beam theory predictions of shell nucleation life*, in: Contact Mechanics and Wear of Rail/Wheel Systems II, Gladwell, Ghonem, Kalousek eds., University of Waterloo Press, supplement (1987).

[9] Karmowski W, Orkisz J, *Rail Fatigue and Fracture Prediction with Residual Stresses Taken into Account*, report US DOT VNTSC, Boston 2002.

[10] Klesnil M., Lukas P., *Influence of strength and stress history on growth and stabilisation of fatigue cracks*, Engineering Fatigue Mechanics, 4, pp. 77-92 (1972).

[11] Manson S.S., Halford G.R., *Practical implementation of the double linear damage rule and damage curve approach for treating cumulative fatigue damage*, International Journal of Fracture, 17, 2, p. 169 (1981).

[12] Orkisz J., *On Approach to Failure Analysis and Life Prediction Techniques in Railroad Rails Including Residual Stresses*, VNTSC Progress Report, Cambridge 2001.

[13] Orkisz J., *Topics For Research Proposed On Residual Stress Analysis In Railroad Rails And Vehicle Wheels And Related Problems*, VNTSC Progress Report, Cambridge 2001.

[14] Orkisz J., *Computer Methods in Fatigue Fracture Analysis in Fatigue Life Estimation of Railroad Rails in Service Conditions*, US DOT VNTSC, Cambridge, September 2002.

[15] Orringer O., Morris J.M., Jeong D.Y., *Detail fracture growth in rails: test results*, Theoretical and Applied Fracture Mechanics, 5, pp. 63-95 (1986).

[16] Orringer O., Morris J.M., Steel R.K., *Applied research on rail fatigue and fracture in the United States*, Theoretical and applied fracture mechanics, 1, pp. 23-49 (1984).

[17] Orringer O., Tang Y.H., Gordon J.E., Jeong D.Y., Morris J.M., Perlman A.B., *Crack propagation life of detail fractures in rails*, US DOT VNTSC, Cambridge, MA, DOT/FRA/ORD-88/13, October 1988.

[18] Paris P.C., Erdogan F., *A critical analysis of crack propagation laws*, Journal of Basic Engineering, Transactions ASME, 85, pp. 528-534 (1963).

[19] Paris P.C., Gomez M.P., Anderson W.P., *A rational analytic theory of fatigue*, The Trend in Engineering, 13, pp. 9-14 (1961).

[20] Pazdanowski M, *On estimation of residual stresses in prismatic bodies made of strain hardning materials*, in. J. Orkisz, Development of Advanced Methods for Theoretical Prediction of Shakedown Stress States and Physically based Enhancement of Experimental Data, (grant DTFR53-95-G-00055), Vol. II US DOT, Washington, DC 1999.

[21] Sih G.C., Handbook of stress intensity factors, Institute of Fracture and Solid Mechanics, Lehigh University, Bethlehem, PA (1973).

[22] Sines G., *Behavior of metals under complex static and alternating stresses*, in: Metal Fatigue, Sines, Waisman eds., McGraw-Hill, pp. 145-169 (1959).

[23] Smith K.N., Watson P., Topper T.H., *A stress-strain function for the fatigue of metals*, Journal of Materials, 5, 4, p. 767 (1970).

[24] Smith S.A., Raju I.S., *Evaluation of stress-intensity factors using general Finite Element Models*, Fatigue and Fracture Mechanics, Vol. XXIX, Panontin, Sheppard eds., ASTM, West Conshohocken, pp. 176-200 (1999).

[25] Stephens R.I., Fatemi A., Stephens R.R., Fuchs H.O., Metal fatigue in engineering, Wiley (2001).

[26] Weertman J., *Rate of growth of fatigue cracks calculated from the theory of infinitesimal dislocations distributed on a plane*, Int. Journal of Fracture Mechanics, 2, pp. 460-467 (1966).

Topic Area 3

Communications of Scientific Developments

Conference Presentations and Papers Published

Results of the currently performed research, and research performed in our group on related topics have been presented during scientific conferences and symposiums.
Authors and titles of papers are enumerated on the following page.

Papers published and submitted to Scientific Conferences

	Authors	Title	References
1.	Orkisz J., Cecot W., Karmowski W., Krok J., Pazdanowski M.	Shake-down approach to analysis of residual stresses in railroad rails	IMPLAST'03 - *8th International Symposium on Plasticity and Impact Mechanics*, Delhi, India, 16 - 19 March 2003.
2.	Skrzat A., Orkisz J.	Residual stress reconstruction in railroad passenger and freight car wheels	CMM 2003 - *15th International Conf. On Computer Methods in Mechanics*, Gliwice/Wisła, Poland, 3-6 June 2003
3.	Midura G., Orkisz J.	Elastic–plastic bending of beam rail model.	CMM 2003 - *15th International Conf. On Computer Methods in Mechanics*, Gliwice/Wisła, Poland, 3-6 June 2003
4.	Jaworska I., Przybylski P.	On graphic modeler for adaptive meshless FD and FE analysis	CMM 2003 - *15th International Conf. On Computer Methods in Mechanics*, Gliwice/Wisła, Poland, 3-6 June 2003
5.	Krok J.	A unified approach to the adaptive FEM and meshless FDM in physically nonlinear problems	CMM 2003 - *15th International Conf. On Computer Methods in Mechanics*, Gliwice/Wisła, Poland, 3-6 June 2003
6.	Krok J., Orkisz J.	On development of MWLS approximation for adaptive meshless FDM	CMM 2003 - *15th International Conf. On Computer Methods in Mechanics*, Gliwice/Wisła, Poland, 3-6 June 2003
7.	Krok J.	An adaptive procedure of experimental data collection based on a'posteriori error estimation of data using the meshless FDM	CMM 2003 - *15th International Conf. On Computer Methods in Mechanics*, Gliwice/Wisła, Poland, 3-6 June 2003
8.	Orkisz J., Krok J.	Recent advances in the meshless methods selected topics	CMM 2003 - *15th International Conf. On Computer Methods in Mechanics*, Gliwice/Wisła, Poland, 3-6 June 2003

9.	Przybylski P., Orkisz J.	On adaptive mesh generator for meshless FD and FE methods	CMM 2003 - *15th International Conf. On Computer Methods in Mechanics*, Gliwice/Wisła, Poland, 3-6 June 2003
10.	Orkisz J., Shaheed S.	On acceleration of the Gauss-Seidel method for solution of simultaneous linear algebraic equations	CMM 2003 - *15th International Conf. On Computer Methods in Mechanics*, Gliwice/Wisła, Poland, 3-6 June 2003
11.	Pazdanowski M.	Recent developments in estimation of residual stresses in railroad car wheels made of material exhibiting kinematic hardening	CMM 2003 - *15th International Conf. On Computer Methods in Mechanics*, Gliwice/Wisła, Poland, 3-6 June 2003
12.	Cecot W.	Development of h-adaptive finite element analysis of residual stresses by the Zarka model	CMM 2003 - *15th International Conf. On Computer Methods in Mechanics*, Gliwice/Wisła, Poland, 3-6 June 2003
13.	Karmowski W., Orkisz J.	Application of the extended global-local data smoothing to residual stress analysis	CMM 2003 - *15th International Conf. On Computer Methods in Mechanics*, Gliwice/Wisła, Poland, 3-6 June 2003
14.	Krok J.	Meshless FDM based approach to error control and evaluation of experimental or numerical data	*Second MIT Conf. on Computational Fluid and Solid Mechanics*, Cambridge, MA, USA, June 17-20, 2003.
15.	Magiera J.	A meshless FDM applied to a'posteriori error analysis of experimental data by physically based global method approximation	*Second MIT Conf. on Computational Fluid and Solid Mechanics*, Cambridge, MA, USA, June 17-20, 2003.
16.	Orkisz J., Przybylski P., Jaworska I.	A mesh generator for an adaptive multigrid MFD/FE method	*Second MIT Conf. on Computational Fluid and Solid Mechanics*, Cambridge, MA, USA, June 17-20, 2003.

Implast 2003

8th International Symposium on Plasticity and Impact Mechanics

16 - 19 March 2003

SHAKE-DOWN APPROACH TO ANALYSIS OF RESIDUAL STRESSES IN RAILROAD RAILS

J.Orkisz

W.Cecot, W.Karmowski, J.Krok, M.Pazdanowski

Computational Mechanics Division

Cracow University of Technology, Kraków, Poland

Shake-down approach to analysis of residual stresses in railroad rails

J.Orkisz
Computational Mechanics Division
Cracow University of Technology, Kraków, Poland
e-mail: plorkisz@cyf-kr.edu.pl

ABSTRACT

Summary Considered is a problem of analysis of residual stresses arising in railroad rails due to manufacturing and service. Discussed are formulation of the problem, various computer methods of theoretical prediction of these stresses as well as some solution results.

1. Introduction

Both the safety of passenger travel and the reliability of railroad freight transport are essentially affected by the behavior of rail and vehicle wheels. Thorough investigation of this problem is needed as significant increases in traffic and axle loads take place. Such increases will lead to greater rates of rail wear and fracture.

Better material and maintenance practices reduce rail failures and extend rail wear life. However, many rails stay in service long enough to develop fatigue cracks mainly caused by the repeated action of rolling wheel contact loads.

Both crack nucleation and propagation are driven by stress concentrations, and may be predicted if total stresses are known. These stresses are comprised of live and residual stresses. The live stresses are those generated by applied loads. Their evaluation, though sometimes troublesome, may be obtained by routine engineering analysis. In railroad rails and vehicle wheels they are generated both during manufacture and in service. Unfortunately, residual stress analysis is usually by no means a routine problem.

Residual stresses are known to be a significant component of the total stresses, which affect fatigue crack nucleation and propagation and rail fatigue life. Therefore, no reliable prediction of crack development (and consequently rail fracture, fatigue life etc.) can be made without knowing the residual stresses. Reliable methods of theoretical prediction of residual stresses as well as their experimental evaluation are required first.

Residual stresses and strains arising in both railroad rails and vehicle wheels due to manufacturing and service conditions are investigated [1, 2]. The main objective of the entire research program is to develop discrete methods for theoretical prediction and/or enhancement of experimental data on residual stresses in railroad rails.

2. Solution tools development

The basic (shake-down solution approach, elastic plastic material, proportional loadings, elastic-plastic rolling contact replaced by simulated Hertzian contact stresses) theoretical-numerical prediction of residual stresses and strains in railroad rails under simulated service conditions (wandering wheel/rail contact) is already available. This technique provides rough but reasonable results obtained by means of specially developed, reliable and mutually verified solution tools based on the newly proposed, enhanced shake-down approach.

3. Methods development

Several methods were originated, designed and developed as well as tested and applied within the project:

- for theoretical prediction (shake-down approach, analyzed either by the constrained minimization of residual stress complementary energy or by modified Zarka methods);introduced and used were new discrete models based on the meshless finite difference (MFDM), hybrid finite element (HFEM) and boundary element (BEM) methods;
- for physically based enhancement of experimental or numerical data (Global and Global/Local smoothing methods – MFDM based approach);
- other (e.g., new constrained optimization method, and a'posteriori error analysis).

4. Results

Effective numerical analysis of residual stresses and strains in railroad rails and vehicle wheels was carried out based on the theoretical formulation and computer solution approach developed.

5. Currently developed approach and further research proposed

The very basic results of residual stress analysis were effectively obtained in the last few years. However, this was at the price of several limiting assumptions, which were needed due to the complexity of the problem. The most significant of these limitations include:

- Relatively simple material description - elastic-plastic; only strain hardening taken into account, while softening, fatigue, damage, fracture, wear, viscosity, temperature changes, are neglected.
- Simplified loading. The true elastic-plastic rolling rail/wheel contact is simulated by elastic Hertz contact; loading is assumed as a proportional one.

Results of the theoretical residual stress analysis, obtained so far, are reasonable and reliable but subject to limitations due to assumptions made. Therefore, these results may be considered only as an approximate but a reasonable solution to the problem in question. The current and further research program is oriented mainly towards relaxation of the restricting assumptions and evaluation of their influence on the predicted residual stresses. Its main objective, therefore, is development of advanced residual stress analysis. It includes:

- Model enhancement incorporating several of the previously neglected effects
- Development and application of numerical methods which already have been the subject of preliminary investigation like neural network approach, as well as new ones, designed for theoretical and experimental residual stress analysis
- Further analysis of particular problems of railroad rails and vehicle wheels

REFERENCES

[1] Orringer O., Orkisz J., Swiderski Z. (eds.), *Residual Stress in Rail* - Vol.I: Field Experience and Test Results; Vol.II: Theoretical and Numerical Analyses, Kluwer Academic Publishers, The Netherlands, (1992).

[2] *Development of Advanced Methods for Theoretical Prediction of Shakedown Stress States and Physically Based Enhancement of Experimental Data* (Grant DTFR53-95-G-00055), Cracow Univ. of Technology, Report to the US DOT, Washington, June 1997-June 2002.

COMPUTER METHODS IN MECHANICS

1st CEACM
CONFERENCE ON COMPUTATIONAL MECHANICS

15th INTERNATIONAL CONFERENCE ON COMPUTER METHODS IN MECHANICS CMM-2003

Gliwice/Wisla, Poland, June 3-6, 2003

Organized by:

Polish Academy of Sciences – Department of Technical Sciences
Polish Association for Computational Mechanics
Silesian University of Technology at Gliwice

Under the auspices of

Ministry of Scientific Research and Information Technology

Residual Stress Reconstruction in Railroad Passenger and Freight Car Wheels

Andrzej Skrzat and Janusz Orkisz
Department of Applied Mechanics, Rzeszow University of Technology
W. Pola 2, 35-959 Rzeszów
e-mail: askrzat@prz.rzeszow.pl, plorkisz@cyf-kr.edu.pl

Summary

During service railroad car wheels develop residual stresses which can lead to premature, and in some instances, catastrophic failure. These stresses are mainly caused by thermal loadings (heavy braking) combined with cyclic contact stresses. Stresses are also influenced by wear of the wheel rim. A good understanding of residual stress distribution and its variation over time in service can help develop a better wheel design that would minimize the danger of catastrophic failure. Knowledge of this distribution can also help improve the techniques used for routine inspection of wheels and detection of potentially dangerous stress distributions. In this paper presented is the solution approach called "physically based enhancement of experimental data" which allows for residual hoop stress approximation. It uses simultaneously both experimental information obtained by means of different experimental techniques, and theoretical information on considered problem. The typical saw cut test is used as a source of experimental data. The problem is solved as nonlinear constrained optimisation.

Keywords: residual stress, optimisation, finite element method

1. Introduction

The solution approach called "physically based enhancement of experimental data", which allows for residual hoop stress approximation, is presented in this paper. It uses simultaneously both: experimental information obtained by means of different experimental techniques, and theoretical information on considered problem. The typical saw cut test is used as a source of experimental data,. The stress reconstruction is a non-linear and ill posed problem as a result of factors like: only partial release of hoop residual stresses due to saw cut, redistribution of stresses and changing wheel stiffness during cutting, weak relation between measured data and released residual stresses, and huge amount of necessary computational data. The solution approach is formulated as constrained minimisation of the functional (1), consisting of the non-dimensional theoretical Φ^T (requirement of the suitably smooth approximation) and experimental Φ^E (weighted approximation error) parts.

$$I = \lambda\Phi^E - (1-\lambda)\Phi^T, \quad \lambda \in [0,1] \tag{1}$$

Here

$$\Phi^T = \Phi^T(\sigma^{out}) = \frac{1}{V_{out}} \int_V \kappa^2(\sigma^{out})\, dV \tag{2}$$

is the theoretical part (a smoothness requirement for the stress distribution curvature κ to be minimal) of the functional, while the experimental part $\Phi^E(\sigma^{out})$ is a weighted measurement error, and λ is a weighting parameter.

$$\Phi^E = \sum_{k=1}^{K} \left[\frac{u_k^{\exp} - u_k}{\Delta u_k^{adm}} \right]^2 \tag{3}$$

The summation is extended over all experimental measurements of relative displacements, strains and absolute displacements.

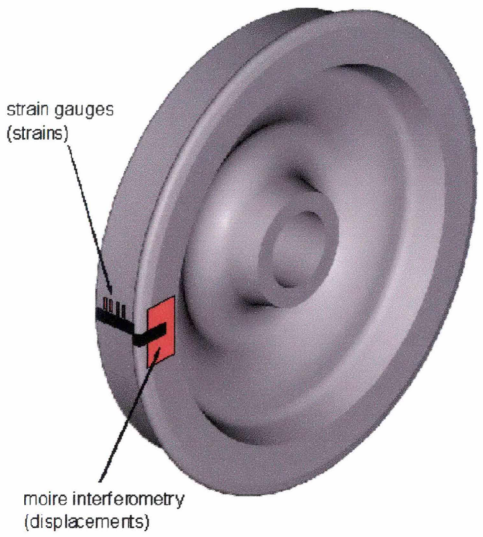

Figure 1. Measurements taken at saw cut test

The parameter λ should satisfy the local (4) and global (5) inequality constraints resulting from measurement precision.

$$\left| u_i^{\exp} - u_i \right| - \Delta u_i^{adm} \le 0 \tag{4}$$

$$\left| \Phi^E(\sigma^{out}) \right| - \Delta\Phi^{adm} \le 0 \tag{5}$$

Here u_i^{exp}, and u_i, are the experimental and approximated values of displacements, strains and COD measurements, while Δu_i^{adm}, and $\Delta\Phi^{adm}$ are admissible experimental errors resulting from measurement precision (e.g. the standard deviation).

2. Influence coefficients calculation

Residual hoop stress approximation in railroad car wheels requires knowledge of relation between released hoop stresses and measured quantities. It is based on influence function, therefore, the whole cutting process has to be simulated by a discrete approach. Analytical simulation is impossible here, because of complicated wheel shape. Finite element method is used during discrete analysis. The professional FEM system – ADINA 8.0 is applied. Numerical analysis requires solving hundreds of boundary value problems corresponding to subsequent cutting stages and subsequent unit forces applied to the wheel cut surface. For each problem unit loads (forces or pressures) are applied in each cut node or element.

The following figure shows an example of 3D FEM mesh used in numerical simulation of the cutting process.

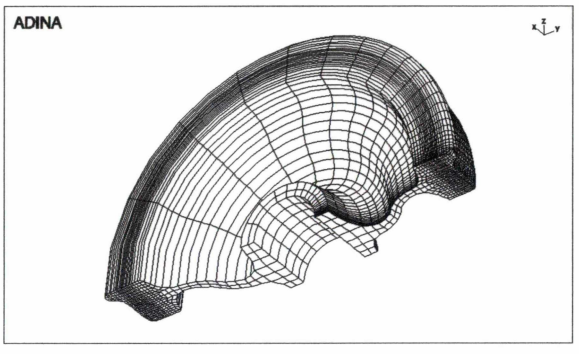

Figure 2. 3D FEM mesh – wheel #3

3. Numerical results

The typical result of residual hoop stress approximation are presented below. All residual hoop stresses are in [MPa].

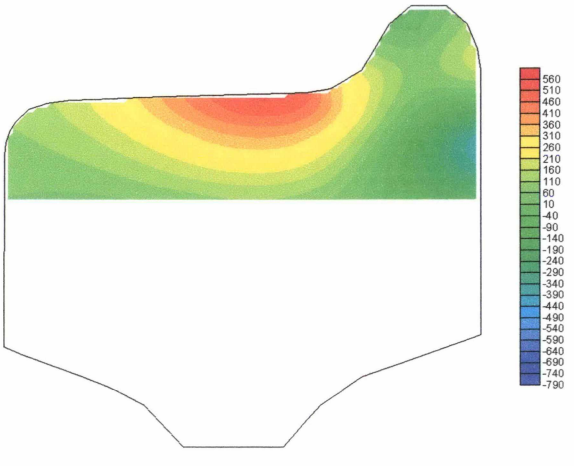

Figure 3. Residual hoop stress – passenger wheel

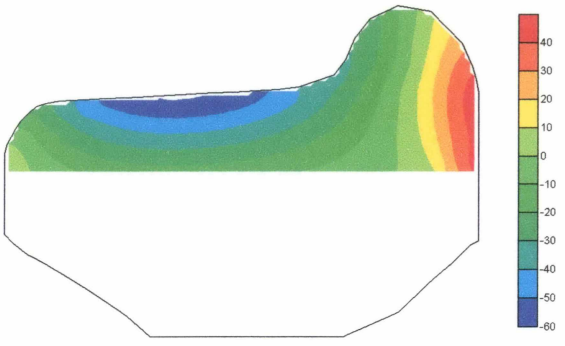

Figure 4. Residual hoop stress – freight wheel

4. Final remarks

Reconstruction of the residual hoop stress in wheels, based on experimental data measured at saw cut, presents an ill-conditioned (stresses are recovered far away from the measurements taken on the wheel surface), inverse problem. It is very sensitive to data used and a reconstruction technique applied i.e. the final results may be obtained with a limited precision only, dependent on data number and quality as well as on a solution approach used. Reliable solution of such an ill-conditioned problem requires numerous experimental data measured at high precision as well as a solid numerical stress recovery approach. Available experimental data should clearly outnumber numerically sought unknowns. In order to increase the experimental data overall quality an a priori data filtering process is needed.

A novel, physically based approximation approach applied here, taking into account at the same time all available information on the considered problem, namely experimental data relations coming from the theory, and heuristic assumptions (e.g. smoothness of stress distributions) – proved to provide reasonable results for the reconstructed residual hoop stresses.

References

[1] Czarnek R., Experimental Determination of Release Fields in Cut Railroad Car Wheels, *Final Report DOT/FRA/ORD-97/06,* US Department of Transportation, 1997.

[2] Krok J., Orkisz J., Skrzat A., On reconstruction of hoop stress in 3D bodies of revolution based on simulated saw cut data, *Proc. XIII Polish Conference Computer Methods In Mechanics,* Poznań, pp. 669-676, 1997.

[3] Orkisz J., Skrzat A., Reconstruction of Residual Stresses in Railroad Vehicle Wheels Based on Enhanced Saw Cut Measurements, Formulation and Benchmark Tests, *WEAR,* 191, pp. 188-198, 1996.

[4] Skrzat A., Orkisz J., Krok J., Residual stress reconstruction in railroad car wheels based on experimental data measured at saw cut test, *European Conference on Computational Mechanics*, Krakow, 2001.

Elastic–Plastic Bending Beam Rail Model

Grzegorz Midura and Janusz Orkisz
Section of Computational Mechanics, Cracow University of Technology
Warszawska 24, 31-155 Kraków, POLAND
e-mail: grzesiek@frisco.wil.pk.edu.pl , plorkisz@cyf-kr.edu.pl

Abstract

Development of a generalized beam model for elastic–plastic analysis of railroad rails is the main objective of this research. It is a part of an engineering approach to estimate residual stresses resulting from the roller straightening process.

The approach for solving beams has been proposed and applied in [3], [4]. Statically indeterminate beams using elastic–plastic (with linear hardening) material model may be solved, load could be defined by force or displacement and beam could have any shape in the cross–section. Beam could be preliminary deformed. Scope of this paper is limited to test and validate obtained results.

Keywords: roller straightening, elastic–plastic beam bending, FDM

1. Introduction.

The main objective of this paper is development of a generalized beam model for elastic–plastic analysis of railroad rails working in service conditions. It is a part of an engineering approach to estimation of residual stresses in railroad rail resulting from the roller straightening process.

During the manufacture process railroad rails are subject to quenching. Due to non uniform cooling rate the rail gains an initial curvature and residual stresses. The curvature is reduced in roller–straightening process. During this process plastically deformed rail passes through a set of rolls with horizontal axes and thus is straightened in the vertical direction by alternate pressing either on the top of the head or on the bottom of the base. According to the experimental measurements and theoretical analysis roller–straightening leaves significant residual stresses which affect the lifetime of rail.

The rail is subject to large elastic-plastic deformations yielding complex stress states including bending, shear and roller contact combined together. The load is alternating, and repetitive though not periodic. It is applied by rolls – one can control amount of load by roll displacement.

Due to aspects mentioned above incremental analysis of roller–straightening process, even if possible, would be a very time and memory consuming task. Therefore, an engineering solution approach was proposed in [1].

Scope of this paper is limited to a part of this approach — to a beam modeling in order to support, test and validate obtained results.

2. Mechanical model

Thorough evaluation of residual stresses and curvature in a roller–straightened rail presents a complex problem of non-linear mechanics. An effective engineering solution approach uses a special 1D beam model in order to evaluate all roll contact forces and relevant bending moments in the rail as the basic input data for the 3D rail shakedown model [2] resulting in a sequence of 2D problems corresponding to the rail passing through subsequent rolls.

Beam model should accommodate available initial data, and supply information on the bending moment, contact force and rail curvature over each roll in the straightening process. For the purpose of modeling rail movement through the rolls alternate use of the beam and shakedown model is required. Afterwards it is necessary to check whether simplifications used in model for speeding up assure satisfying, engineering solution accuracy.

3. Solution

A program based on FD method which allows for non–linear beam analysis has been written. It deals with statically undetermined beams. Material is modeled by elastic–plastic theory with linear, kinematic hardening. Load could be defined as a force or displacement. The beam may be preliminarily deformed. Obtained solution has been verified using other available programs. However, such verification may be done only for beams with rectangular cross–section.

CPU time consumption is important because beam solver should be used iteratively many times in order to obtain a full solution for whole roller–straightening process. Moreover examination of influence introduced by including shear force effects and large deformations is needed.

3.1. Influence of shear effect

Three programs have been used – one of them based on FDM and assumptions shown above (in details discussed in [3] and [4]) which does not support shearing; and further two: ADINA and Timlayxn, which take into consideration influence of shearing deformation. Several tests have been made: for a beam with low and high cross–section, for a beam with different level of cross–section plasticity, and for beams with various distance between supports. Limit for spacing between two supports for which taking into consideration influence of shear effect is necessary has been found.

3.2. Influence of large deflections

If the relation between bending moment and curvature is known in the elastic and in elastic–plastic ranges, one may solve the differential equation defining beam deflection i.e.:

$$w'' = -\chi(M) \tag{1}$$

for small deflections,

$$w''\left[1+(w')^2\right]^{\frac{3}{2}} = -\chi(M) \qquad (2)$$

for large ones.

The main objective of this test is to check whether use of large deflection theory significantly changes results. This would justify larger number of iterations required to obtain the solution.

4. Final remarks

Program was tested and obtained solutions were successfully verified with results provided by other solvers.

Difference between results obtained while taking into consideration shearing force and neglecting it is significant for the beams with length to height ratios smaller than could appear in the roller–straightening process.

Tests showed that the application of large deflection theory, which is more precise, but also demanding more work is not justified from point of view of the precision of final results.

Examined were also effects of a preliminary beam curvature.

Further work will be focused on taking into account initial residual stresses, and movement of the rail.

References

[1] Orkisz J., 1997, *A method engineering analysis of rail in the roller straightening process*, Proc. 12th Polish Conference on Computer Methods in Mechanics, Poznan, Poland;

[2] Cecot W., Orkisz J., Midura G., 2001, *Estimation of railroad rail residual deformation after roller–straightening process*, Proc. European Conference on Computational Mechanics, Cracow, Poland.

[3] Orkisz J., Midura G., 2001, *Elastic–plastic beam deflections*, report to the US Department of Transportation – VNTSC

[4] Orkisz J., Midura G., 2002, *Improvement in elastic–plastic bending beam rail model*, report to the US Department of Transportation – VNTSC

On graphic modeller for adaptive meshless FD and FE analysis

Irena Jaworska and Przemyslaw Przybylski
Department of Computational Mechanics, Cracow University of Technology
Warszawska 24, 31-154 Kraków
e-mail: irena@frisco.wil.pk.edu.pl

Summary

The paper presents the status of research and development of the advanced graphic modeler and visualization software cooperating with the unstructured 2D and 3D-mesh generator for meshless FD and FE methods. The project includes: 2D/3D mesh visualization and manual modification and simultaneous 3D problem solution visualization for real-time verification of calculation process. The presented approach is based on the OpenGL and its toolkits: GLUT, GLUI. Full conformation to these standards guarantees, that the whole program is platform independent. Various types of graphic output, such as node and it's interactive modification (node insertion, deletion and shifting), search for nodes in the neighborhood of a considered point, domain partition into sub-domains assigned to individual nodes, optimal mesh triangulation, the Voronoi diagram, optimal MFDM stars, and a choice of charts presenting results of computation, are provided by the system. The software works on-line providing instant visualization of intermediate as well as final results.

Keywords: Visualization, OpenGL, Postprocessing, meshless FDM/FEM, adaptive mesh generator

Abstract

The paper presents the status of research and development of the advanced graphical modeler and visualization software cooperating with the unstructured 2D and 3D-mesh generator [6]. The project includes: 2D/3D mesh visualization and manual modification and simultaneous 3D problem solution visualization for real-time verification of calculation process.

Numerous graphical modelers and visualization software are available (such as AutoCAD, OpenGl, 3DMax, LightWave, etc). However, many of these programs have not been designed to deal with the adaptive multigrid approach, and thus do not allow for the instant visualization of computation progress as well as the mesh modification during computation.

The presented approach is based on OpenGL and its toolkits: GLUT, GLUI [3, 4]. Full conformation to this standard along with pure C++ coding guarantee, that the whole program is platform independent.

The whole generation process starts with modeling the domain geometry. Given geometry of the considered domain is used to prepare an initial, relatively coarse mesh, and to establish the base for the adaptation procedure. Since OpenGL does not provide means to describe or model complex geometric objects, users may apply CSG (Computational Solid Geometry) tools implemented in the system to define the domain. However, when the model is too complex, like for instance the railroad rail, another approach, based on the OpenGL tessellation procedure can be used. The procedure converts the object into convex polygons which are later extended for 3D visualization of quadrilaterals.

In addition the system can cooperate, through adapters, with various commercial graphical designer packages (i.e. LightWave), which may be used to prepare the domain geometry. Such geometry may be easily imported into the system [5].

Various types of graphical output, such as node and its interactive modification (node insertion, deletion and shifting), search for nodes in the neighborhood of a considered point, domain partition into sub-domains assigned to individual nodes, optimal mesh triangulation, the Voronoi diagram, optimal MFDM stars, and a choice of charts presenting results of computation, are provided by the system. The software works on-line providing instant visualization of intermediate as well as final results.

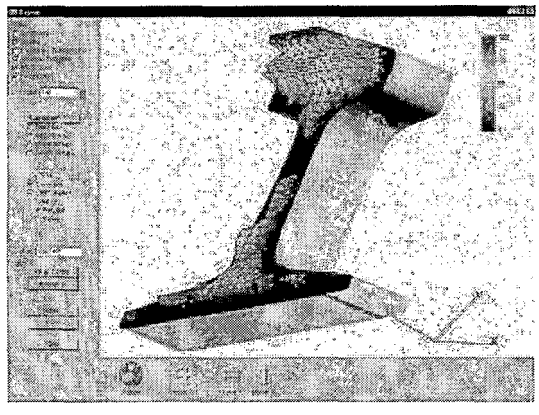

Figure 1: 3D result visualization

The system is developed with elegant GUI design, based on GLUI, fully supports graphical preview, interactive mesh generation and modification, distributed calculations. The tool allows for complex interaction with the user.

It is also worth mentioning that the software being developed meets many modern computer-oriented requirements including: full compliance with many programming and algorithmic standards as UML design, XML and SOAP protocol.

This paper also describes plans for future project development including visualization and modification of 3D mesh, migration of the software to the distributed environment.

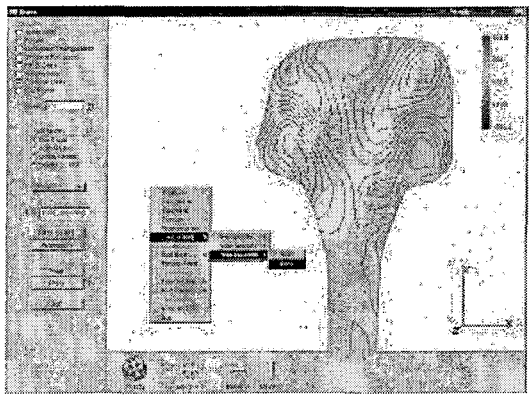

Figure 2: Contour plot mode is selected. Contour sub-menu selected from pop-up menu

References

[1] Hackbush B., *Multi-grid methods and Applications,* Springer-Verlag, 1985.

[2] Orkisz J., *Finite Difference Method (Part III), in Handbook of Computational Solid Mechanics*, M.Kleiber (Ed.) Springer-Verlag, Berlin, pp. 336-432, 1998.

[3] Rademacher P., *GLUI. A GLUT-Based User Interface Library*, 1999.

[4] Woo M., Neider J., Davis T., Shreiner T., *Open GL Programming Guide*, third edition, Addison-Wesley, 1999.

[5] Jaworska I., An advanced graphic modeller for an adaptive GFD/FE analysis, *13th Inter-Institute Seminar for Young Researchers*, Vienna, 2001.

[6] Orkisz J., Lezanski P., Przybylski P., Multigrid Approach to Adaptive Analysis of Boundary Value Problems by the Meshless GFDM, *Proc. of the IUTAM/IACM Symp. On Disretization Methods in Structural Mechanics II,* Vienna 97, Kluwer Academic Publ. Dortrecht/Boston/London, 173-180, (1999).

[7] Orkisz J., Przybylski P., An adaptive mesh generator for meshless FD and FE methods, *2th European Conference on Computational Mechanics*, Cracow, 2001.

[8] Orkisz J, Przybylski P., On adaptive mesh generator for meshless FD and FE methods, *15th International Conference on computer Methods in Mechanics,* Wisla, 2003.

A unified approach to the adaptive FEM and meshless FDM in physically nonlinear problems

Józef Krok

Section of Computer Methods in Mechanics
Cracow University of Technology, Cracow, Warszawska str. 24, 31-155 Poland
e-mail:plkrok@cyf-kr.edu.pl

Summary

The paper presents unified approach to discretization of boundary value problems by the FE and newly developed Meshless FD (MFDM) methods. Several possible combinations of the FE and MFD methods are examined. Application of the approach in physically nonlinear problems are presented.

Keywords: *Finite Element Method, Meshless Finite Difference Method, a posteriori error estimation, adaptive methods*

Abstract

The work addresses the general topic of the Adaptive Finite Element Method (AFEM) and the newly developed Adaptive Meshless Finite Difference Method (AMFDM) in order to automatically enhance numerical solution in both methods and in a combined AFEM/AMFDM technique.

Finite element method (FEM) and meshless finite difference method (MFDM), were developed separately, and presented as competitive to each other. Following earlier Author papers on combinations of both the FE and MFD methods [1,2] as well as recent adaptive approach in those methods [4], considered are here further developments of a unified approach to these methods, especially with adaptivity taken into account.

Several possible combinations of the FE and MFD methods were examined. One of concepts of such unification is based on an attempt to bring the MFDM and the FEM closer to each other. Both methods may be oriented on evaluation of the vector $\mathbf{Df} = \mathbf{Q(x)}\delta$ of derivatives $\mathbf{Df} = \{f\ f_x\ f_y\ f_{xx}\ f_{xy}\ f_{yy} \ldots\}$ as a linear combination of nodal unknowns δ and an approximation matrix $\mathbf{Q(x)}$. In the MFDM, for a given fixed point x_i of the domain, the matrix $\mathbf{Q}$ presents meshless finite difference formulas. In the FEM this matrix is formed using shape functions and their derivatives (local or consistent derivatives). Formulation considered here is both general and convenient, because when supported by the symbolic programming, provides an opportunity to apply fully automatic approach to analysis of any given functional or differential equations; e.g. there is no need to manually derive the FEM characteristics.

The other possible way of unification uses a reverse approach. Thus, using moving weighted least squares approximation the MFDM formulas are expressed in terms of the FEM notation due to definition of appropriate pseudo shape functions $f = \sum_i N_i \delta_i$, used later on in a similar way as in the FEM analysis. Local (diffuse) and consistent derivatives [4,7] of shape functions in MFDM are used in calculations at the same time.

Moreover a combination of both methods may be applied at the same time. Both methods may be used either simultaneously though in different subdomains, or in a sequence e.g. when the MFDM postprocessing is applied to smoothen rough results obtained by the FEM [1,2].

The other possible way uses the MFDM approximation to construct a very effective class of a'posteriori error estimators in the FEM (like the Z^2 indicators [5] and residual ones).

Present research, done in the domain of the adaptive techniques and error estimation, includes:

- development of a new a'posteriori error estimation techniques for elastic and non-elastic problems in solid mechanics – generally in boundary value problems given in the global (MFDM and FEM) formulation;
- determination of the optimal strategies for 'h' adaptive refinement, taking into account a'priori error estimates, i.e. theoretical features of the FEM and MFDM;
- development of adaptive modelling to enhance solution accuracy using new methodology with some features of physical models incorporated in the adaptive process, like degree of nonelastic deformation. New adaptive mesh generator for FEM/MFDM combined analysis is used.

Adaptive procedure in FEM and MFDM *can be subdivided into the following parts:*

1. Mesh control techniques:
(i) evaluation of a'posteriori error estimation:

- Zienkiewicz-Zhu (Z-Z) estimation technique [6] based on stress recovery techniques ([1] and later on [6]) and superconvergent theory. Certain generalization is done here to extend the Z-Z estimators
- interpolation type error estimators (very easily to implemented in meshless methods),
- estimators based on truncation error of the Taylor series [5],
- residual types of estimators [5].

(ii) mesh refinement strategy taking into consideration: an approximation error influence and influence of inelastic deformation growth degree [4].

2. *Mesh refinement and/or enrichment.* Regeneration of meshes is dealt with here because of its compatibility with two different methods i.e. the FEM and MFDM.
3. *Mapping of history dependent variables from the old to the new mesh.*

4. *Final postprocessing of solutions on fine meshes for additional enhancement of solution.*

The most important methods of a'posteriori error analysis and several mesh refinement techniques are summarized in present paper.

The following part of the paper presents the a'posteriori error estimation first developed and used in the FEM. The most frequently applied, Zienkiewicz-Zhu [6] energy norm estimator will be presented in a detailed way. This estimator is based on stress field postprocessing (smoothing) technique and superconvergence theory of the FEM.

For estimators based on the superconvergence technique and the stress (or flux) recovery technique (Zienkiewicz,Zhu -ZZ) one has

$$\|e\| = [\int_{\Omega} (\boldsymbol{\sigma} - \boldsymbol{\sigma}^h)^T \mathbf{D}^{-1} (\boldsymbol{\sigma} - \boldsymbol{\sigma}^h) d\Omega]^{\frac{1}{2}}, \tag{1}$$

where $\underline{\boldsymbol{\sigma}}^h$ are stresses obtained by the FEM.
The exact stresses $\boldsymbol{\sigma}$ are approximated by the new stresses $\boldsymbol{\sigma}^*$ obtained using the stress recovery procedure (the Meshless Finite Difference method is used here [1,2,4])

$$\boldsymbol{\sigma}^* = \mathbf{N}\overline{\boldsymbol{\sigma}}^* \tag{2}$$

where $\overline{\boldsymbol{\sigma}}^*$ are nodal values obtained by the MFDM recovery procedure, and $\mathbf{N}$ is a shape functions' matrix.
The exact solution for the strain energy is estimated as

$$\|U\| = [\int_{\Omega} (\boldsymbol{\sigma}^h)^T \mathbf{D}^{-1} (\boldsymbol{\sigma}^h) d\Omega]^{\frac{1}{2}} + \|e\|^2 \tag{3}$$

where an error of the energy norm is expressed as

$$\|e\| = [\int_{\Omega} (\boldsymbol{\sigma}^* - \boldsymbol{\sigma}^h)^T \mathbf{D}^{-1} (\boldsymbol{\sigma}^* - \boldsymbol{\sigma}^h) d\Omega]^{\frac{1}{2}} \tag{4}$$

Both $\|e\|$ and $\|U\|$ norms may be evaluated as a sum of their respective element contributions so that

$$\|e\|^2 = \sum_{i=1}^{n} \|e\|_i^2, \quad \|U\|^2 = \sum_{i=1}^{n} \|U\|_i^2 \tag{5}$$

where n denotes the total number of elements in the mesh. Estimator (1) can be use in MFDM as well.

Estimator (1) can be generalized in a very easy way. One may use the MFDM solution as a reference one, σ^*. This approach is effective and reliable for low order FEM elements and very promising in physically nonlinear situations, because estimator may be used at every stage of (nonlinear) calculation process.

Computer implementation of that FE/MFD model is done in the form of a system called **NAFDEM** - 'Nonlinear **A**daptive **F**inite **D**ifference and **E**lement **M**ethods'. NAFDEM is supported by JKJK [3] preprocessor providing an automatic application of symbolic operations like formal differentiation and generation of source code subroutines for stiffness matrices. Consequently, the user has only to define a form of the functional or the virtual work principle applied, to specify boundary conditions, and to describe the domain of the problem considered.

Numerical solutions of various boundary value problems, especially using elasto-plastic and elasto-visco-plastic models, illustrate the presented approach. Stress fields in railroad rails and wheels are analyzed as examples of true technical applications of the approach. Comparative study of influence of the different types of derivatives (local and consistent) on results is presented.

References

[1] J.Krok and J.Orkisz. Application of the Generalized FD Approach to Stress Evaluation in the FE Solution, *Proc. of Int. Conf. on Comp. Mechanics*, Tokyo 1986, Springer-Verlag, V. XII, 31-36(1986).

[2] J.Krok and J.Orkisz. A Unified Approach to the FE and Generalized Variational FD Methods in Nonlinear Mechanics, Concepts and Numerical Approach, IUTAM/IACM Symposium Vienna, Austria 1989, in: *Discretization Methods in Structural Mechanics*, G.Kuhn, H.Mang (Eds.), Springer-Verlag Berlin Heidelberg, 353-362(1990).

[3] J.Krok, J.Orkisz, M.Stanuszek, A Unique FEM/FDM System of Discrete Analysis of Boundary - Value Problems in Mechanics, *Proc. of XI Conf. on Comp. Meth. in Mechanics*, Kielce-Cedzyna, Vol. 1, 466-472(1993).

[4] J.Krok, A Unified Approach to the Adaptive FEM and Meshless FDM, *Fifth World Congress on Computational Mechanics*, 2002, Vienna (invited paper).

[5] J.Orkisz. Meshless Finite Difference Method, in: *Numerical Methods in Mechanics*, M.Kleiber (Ed.), Springer - Verlag, Berlin 1998.

[6] O.C.Zienkiewicz and J.Z.Zhu. A Simple Estimator and Adaptive Procedure for Practical Engineering Analysis, *Int. J. Num. Meth. Eng.*, **24**, 337-357(1987).

[7] A.Huerta, S.Hernandez-Menez, Enrichment and Coupling of the Finite Element and Meshless Methods, *Int. J. Numer. Methods Eng*, 48, 1615

On development of MWLS approximation for adaptive meshless FDM

Józef Krok [(1)], **Janusz Orkisz**[(2)]

Section of Computer Methods in Mechanics
Cracow University of Technology, Cracow, Warszawska str. 24, 31-155 Poland
e-mail: [(1)]*plkrok@cyf-kr.edu.pl,* [(2)]*plorkisz@cyf-kr.edu.pl*

Summary
The paper presents development of moving weighted least squares (MWLS) approximation applied to the adaptive meshless finite difference method (MFDM). Several possible definitions of derivatives (local and consistent) are used, their quality is compared and application to solution of b.v. problem demonstrated.

Keywords: Meshless finite difference, aposteriori error estimation, adaptive methods

Abstract

The work addresses the general topic of the newly developed Adaptive Meshless Finite Difference Method (AMFDM), applied to automatically enhance numerical solution.

Following earlier Authors' papers on MFD methods [1,2] as well as recent adaptive approach in those methods [4,5], considered are here further developments of an comparative approach to these methods, especially with adaptivity taken into account.

Two possible definitions of derivatives i.e. local and consistent were examined. Both methods may be oriented on evaluation of the full vector $\mathbf{Df} = \mathbf{Q}(\mathbf{x})\delta$ of derivatives $\mathbf{Df} = \{f\ f_x\ f_y\ f_{xx}\ f_{xy}\ f_{yy} \ldots\}$ as a linear combination of nodal unknowns δ and an approximation matrix $\mathbf{Q}(\mathbf{x})$. In the MFDM, for a given fixed point x_i of the domain, the matrix $\mathbf{Q}$ presents meshless finite difference formulas. Formulation considered here is both general and convenient. It is supported by the symbolic programming providing an opportunity to apply fully automatic approach to analysis of any given functional or differential equations; e.g. there is no need to manually derive the MFDM characteristics.

The other possible way of approximation may be also used. Using moving weighted least squares approximation the MFDM formulas are expressed in terms of the FEM notation due to definition of appropriate pseudo shape functions $f = \sum_i N_i \delta_i$, and used later on in a similar way as in the FEM analysis. Local (diffuse) and consistent derivatives [4,7,8] of shape functions in MFDM are used in calculations at the same time.

Present research, done in the domain of the adaptive techniques and error estimation, includes:

- application of a new a'posteriori error estimation techniques, based on simultaneous use of local and consistent MFDM derivatives, for elastic and non-elastic problems in solid mechanics – generally in boundary value problems given in the global MFDM formulation,
- determination of the optimal strategies for 'h' adaptive refinement, taking into account a'priori error estimates, i.e. theoretical features of the MFDM solution;
- application of a new adaptive mesh generator for MFDM analysis,
- application of new MFDM approach to solve class of boundary value problems in mechanics.

Adaptive procedure in MFDM *can be subdivided into the following parts:*

1. Mesh control techniques:
(i) evaluation of a'posteriori error estimation:
- Zienkiewicz-Zhu (Z-Z) estimation technique [6] based on stress recovery techniques ([1] and later on [6]) and superconvergent theory. Certain generalization is performed here to extend Z-Z estimators for MFDM analysis,
- interpolation type of error estimators (easily implemented in meshless methods).

(ii) mesh refinement strategy taking into consideration: influence of an approximation error and influence of inelastic deformation growth degree [4].

2. Mesh refinement and/or enrichment. Regeneration of meshes is dealt with here.
3. Mapping of history dependent variables from the old to the new mesh.

4. Final postprocessing of solutions on fine meshes for additional enhancement of solution.

The following part of the paper presents the a'posteriori error estimation first developed and used in the FEM. The most frequently applied Zienkiewicz-Zhu [6] energy norm estimator will be presented in a detailed way. Widely known Zienkiewicz - Zhu (Z-Z) estimator is based on stress field postprocessing (smoothing) technique and superconvergence theory of the FEM.

For estimators based on the superconvergence technique and the stress (or flux) recovery technique (Zienkiewicz,Zhu -ZZ) one has

$$\|e\| = [\int_{\Omega} (\boldsymbol{\sigma} - \boldsymbol{\sigma}^h)^T \mathbf{D}^{-1} (\boldsymbol{\sigma} - \boldsymbol{\sigma}^h) d\Omega]^{\frac{1}{2}}, \quad (1)$$

where $\underline{\boldsymbol{\sigma}}^h$ are stresses obtained by the FEM.
The exact stresses $\boldsymbol{\sigma}$ are approximated by the new stresses $\boldsymbol{\sigma}^*$ obtained using the stress recovery procedure (the Meshless Finite Difference method is used here [1,2,4])

$$\boldsymbol{\sigma}^* = \mathbf{N}\overline{\boldsymbol{\sigma}}^* \quad (2)$$

where $\overline{\boldsymbol{\sigma}}^*$ are nodal values obtained by the MFDM recovery procedure, and $\mathbf{N}$ is a shape functions' matrix.
The exact solution for the strain energy is estimated as

$$\|U\| = [\int_{\Omega} (\boldsymbol{\sigma}^h)^T \mathbf{D}^{-1} (\boldsymbol{\sigma}^h) d\Omega]^{\frac{1}{2}} + \|e\|^2 \quad (3)$$

where an error of the energy norm is expressed as

$$\|e\| = [\int_{\Omega} (\boldsymbol{\sigma}^* - \boldsymbol{\sigma}^h)^T \mathbf{D}^{-1} (\boldsymbol{\sigma}^* - \boldsymbol{\sigma}^h) d\Omega]^{\frac{1}{2}} \quad (4)$$

Both $\|e\|$ and $\|U\|$ norms may be evaluated as a sum of their respective element contributions so that

$$\|e\|^2 = \sum_{i=1}^{n} \|e\|_i^2, \quad \|U\|^2 = \sum_{i=1}^{n} \|U\|_i^2 \quad (5)$$

where n denotes the total number of elements in the mesh.

Estimator presented above can be generalized and extended to MFDM.

Let us define the following problem:

- data, (not necessarily stresses like in eq. (1)) coming from MFDM calculations, located at certain points - set #1 (set of primary points) is given.
- data, (not necessarily stresses like in eq. (1)) coming from MFDM results projected onto linear subspace (for example by using linear or bilinear FEM shape functions), located at same points - set #2 is given .

The problem is exactly the same as in error estimator (1), but now one has one set of points with two different data sets: MFDM approximation and projected MFDM results.

$$\|e\| = [\int_{\Omega} (\sigma^h_{MFDM} - \sigma^h_{PROJ})^T D^{-1} (\sigma^h_{MFDM} - \sigma^h_{PROJ}) d\Omega]^{\frac{1}{2}}, \quad (6)$$

where σ_{PROJ} is value obtained by projection of MFDM solution onto linear subspace. Approach is superior to usual Z-Z estimator because FEM superconvergence values exist in very special cases i.e. regular meshes may be used only.

The behavior of the present MFDM formulation, as well as error estimator were studied in the cantilever beam problem – for different length and height on the beam and for different meshes. Obtained a posteriori error estimation was very close to exact one in every studied example. This approach is effective and reliable, may be used in FEM and is very promising in physically nonlinear situations.

Computer implementation of that MFD model is done in the system called **NAFDEM** - 'Nonlinear Adaptive Finite Difference and Element Methods'. NAFDEM is supported by *JKJK* [3] preprocessor providing an automatic application of symbolic operations like formal differentiation and generation of source code subroutines for stiffness matrices. Consequently, the user has only to define a form of the functional or the virtual work principle applied, to specify boundary conditions, and to describe the domain of the problem considered.

Numerical solutions of various boundary value problems illustrate the presented approach. Elastic stress fields in railroad rails and wheels are analyzed as examples of true technical applications of the approach. Comparative study of influence of the different types of derivatives on results is presented. New features of both local and consistent derivatives are observed, which may indicate, how to build MFDM model, to obtain high precision results in the most economical way.

References

[1] J.Krok and J.Orkisz. Application of the Generalized FD Approach to Stress Evaluation in the FE Solution, Proc of *Int. Conf. on Comp. Mechanics*, Tokyo 1986, Springer-Verlag, V. XII, 31-36(1986).

[2] J.Krok and J.Orkisz. A Unified Approach to the FE and Generalized Variational FD Methods in Nonlinear Mechanics, Concepts and Numerical Approach, IUTAM/IACM Symposium Vienna, Austria 1989, in: *Discretization Methods in Structural Mechanics*, G.Kuhn, H.Mang (Eds.), Springer-Verlag Berlin Heidelberg, 353-362(1990).

[3] J.Krok, J.Orkisz, M.Stanuszek, A Unique FEM/FDM System of Discrete Analysis of Boundary - Value Problems in Mechanics, *Proc. of XI Conf. on Comp. Meth. in Mechanics*, Kielce-Cedzyna, Vol. 1, 466-472(1993).

[4] J.Krok, A Unified Approach to the Adaptive FEM and Meshless FDM, *Fifth World Congress on Computational Mechanics*, 2002, Vienna (invited paper).

[5] J.Orkisz. Meshless Finite Difference Method, in: *Numerical Methods in Mechanics*, M.Kleiber (Ed.), Springer - Verlag, Berlin 1998.

[6] O.C.Zienkiewicz and J.Z.Zhu. A Simple Estimator and Adaptive Procedure for Practical Engineering Analysis, *Int. J. Num. Meth. Eng.*, **24**, 337-357(1987).

[7] A.Huerta, S.Fernandez-Menez, Enrichment and Coupling of the Finite Elements and Meshless Methods, *Int. J. Numer. Methods Eng*, **48**, 1615-1636(2000).

[8] J.Krok, J.Orkisz, A Unified Approach to the Adaptive FEM and Meshless FDM, *2nd European Conference On Computational Mechanics*, Cracow, Poland, June 26-29, 2001.

An adaptive procedure of experimental data collection based on a'posteriori error estimation of data using the meshless FDM

Józef Krok

Section of Computer Methods in Mechanics
Cracow University of Technology, Cracow, Warszawska str. 24, 31-155 Poland
e-mail:plkrok@kinga.cyf-kr.edu.pl

Summary

The work addresses extended formulation of a new approach proposed to measurements planning by means of error control of experimental data. It includes: development of postprocessing techniques for approximation of data given in a discrete form, a'posteriori error estimation (evaluation) of measured data, estimation of a new required experimental points location and density, definition of reliability index of experimental data. On the base of a'posteriori error analysis of data, adaptive procedure of experimental data collection and evaluation is presented, for the first time.

Theoretical consideration and numerical analysis are based on the Adaptive Finite element Analysis (AFEM) and the Meshless Finite Difference (MFDM) approach. Differences in numerical and experimental data analysis are underlying.

Keywords: Experimental data approximation, error control, meshless FDM

Abstract

The work addresses development of a new approach to approximation, smoothing and error estimation technique of experimental/numerical data. On the base of a'posteriori error analysis of data, adaptive procedure of experimental data collection and evaluation is presented, for the first time. It includes: development of postprocessing techniques to approximate data given in discrete form, development of an iterative approach to additional enhancement of data at new (required in computer procedures) locations, a'posteriori technique to trace loss of accuracy in original data, estimation of the new grid points density taking into account equal distribution of the error (with different error norms). The paper includes application of above mentioned procedure in wheel stress recovery calculations and in residual stress analysis in FEM/MFDM.

A'posteriori error procedure in Zienkiewicz-Zhu [2] estimator can be split into two stages: stage 1: calculation of stresses (or other primary values) at Gaussian points- the primary set of points; stage 2: approximation of the Gaussian-located stresses to nodes, back retrieval of the nodal values to Gauss points using (for example) standard shape functions or other kind of approximation. Having two sets of values differing in accuracy at the same points, one may calculate global (sum over whole domain) and local (assigned to a single point) (1), (2) norms.

Let us define the following problem: data (not necessarily stresses) coming from experiment or from numerical FEM/FDM analysis, located at some points - set #1 and the fictitious sets of points used later in calculation - set #2 are given. The problem lies in data translation from #1 points set to #2 points set. The problem is the same as in Z-Z [2] error estimation, but now one deals with two different sets of points with arbitrary, not elemental, locations and has no information on regularity, smoothness and reliability of the data. Total norm of the measured values and the error norm between two surfaces defined by data #1 and recovered #2 at experimental points may be defined as [4]

$$\|U\|^2 = \int_\Omega [(\kappa u^h)^T(\kappa u^h) + (\nabla u^h)^T(\nabla u^h) + (u^h)^T u^h] d\Omega \,, \qquad (1)$$

$$\|e\| = [\int_\Omega (eu + e\nabla u + e\kappa u) d\Omega]^{\frac{1}{2}} \qquad (2)$$

where

$$eu = (u^* - u^h)^T(u^* - u^h) \,,$$
$$e\nabla u = (\nabla u^* - \nabla u^h)^T(\nabla u^* - \nabla u^h) \,,$$
$$e\kappa u = (\kappa u^* - \kappa u^h)^T(\kappa u^* - \kappa u^h)$$

where u^h is vector of experimental data (in experimental points), u^* is vector of fictitious data sought, κ - is generalized Karmowski curvature.

To solve this problem, data from experimental points is approximated to fictitious ones, using Moving Weighted Least Suqares approximation [1] (MWLS), and later on, taking values at fictitious points as original data, approximated back from fictitious points to experimental ones. In this two-stage approximation part of data is lost, but if differences between original data in the experimental points and fictitious data in the same points are small enough, one may expect that the approximation in first step does not introduce too large error. As will be seen from numerical analysis this assumption is true. Additionally, in the zones where the gradients of approximated function are larger, the error magnitude (differences) has considerably greater value as compared with the zones with smaller data gradients. Moreover, if irregularity in data is large the error increases. Those facts may be used, as byproduct important information, to evaluate experimental data. Having

vector of differences between experimental and fictitious values at experimental points one can "smear" error, approximating vector of differences from experimental to fictitious points. Adding correction to initial fictitious values one can obtain new enhanced fictitious values. This process can be repeated.

The key question is, whether one can evaluate experimental data using norms (1) and (2) ? The answer is yes, if data is regular enough. As one can see from equations (1) and (2), values of a function measured, gradients and curvatures of the function are taken into account.

The a'posteriori error analysis described above has been applied to the wheel saw cut data [3] analysis, using approximation implemented in MWLS, approximation and evaluation of the residual stress analysis results coming from shakedown approach and a'posteriori error estimation in plasticity. Advantages of the error analysis were shown.

As a practical result of introduced error analysis, new adaptive procedure of experiments planning is possible. Experimental method should take into account character of the measured function, it cannot be separated from character of measured physical field. Simply speaking, in regions where gradients of measured field are larger, one requires many more experimental points. Presented approach gives a theoretical foundation for above mentioned crucial condition in experimental mechanics. One may distinguish two different situations: (1)- it is possible to simulate behavior of measured element or part of structure by means of numerical method (FEM, meshless FDM), (2)- it is not possible to simulate experiment numerically.

An experiment may be repeated or not, if *yes*, sometimes one has the chance to correct location of experimental points. If *not*, presented approach defines tools for proper data evaluation and filtering .

The following procedure is proposed, when numerical simulation of experiment is possible:

1. Solve problem numerically, with conditions for proper simulation of measured part of a structure or an element as good as possible.
2. Evaluate a'posteriori error and repeat calculation with new mesh (grid) density, to statisfy equidistribution or equivalent error requirements.
3. Define experimental grid and project numerical solution (by means of MWLS approximation) to this grid. Try to recover original solution from experimental grid using experimental grid as a primary grid and numerical grid as a secondary grid. Evaluate a'posteriori error and new experimental grid density function which takes into account equidistribution of an error.
4. If is it possible, change experimental point locations, repeat experiment and evaluate a'posteriori error distribution (now real error).
5. Evaluate measured data using estimated error (or new required experimental grid density) as a reliability index to decide which data have to be removed or taken with lowered weight.

If meshless method is used in the above mentioned procedure, numerical simulation of the experiment is specially easy, because one may directly use experimental grid as numerical one, without any transformations and additional (approximation) errors.

REFERENCES

[1] J.Krok and J.Orkisz. Application of the Generalized FD Approach to Stress Evaluation in the FE Solution, Int. Conf. on Comp. Mech., Tokyo 1986, XII, pp.31-36.

[2] O.C.Zienkiewicz and J.Z.Zhu. A Simple Error Estimator and Adaptive Procedure for Practical Engineering Analysis, *Int. Journ. Num. Meth. Eng.*, **24**, 337-357(1987).

[3] R.Czarnek. Experimental Determination of Release Fields in Cut Railroad Car Wheels, DOT/FRA/ORD-96/DOT-VNTSC-FRA-96, Final Report, Cambridge, October, 1996.

[4] J.Krok. On a New Approach to Error Control in Approximation of experimental/Numerical Data. Further Research, Report to the US Department of Transportation, FRA, Washington DC, USA, 1998.

Recent advances in the meshless methods selected topics

Janusz Orkisz[(1)], Józef Krok [(2)],

Computational Mechanics Division
Cracow University of Technology, Cracow, Warszawska str. 24, 31-155 Poland
e-mail:, [(1)]plorkisz@cyf-kr.edu.pl [(2)]plkrok@cyf-kr.edu.pl

Abstract

Meshless methods (MM) use a local approximation based on nodes rather than on elements, and therefore, they use unstructured grids. They constitue nowadays more and more powerful tool of computational analysis of various engineering problems successfully competing with the classic FEM. A review and classification of main contemporary meshless methods is presented. It is followed by a discussion of the moving weighted least squares (MWLS) approximation including problem of weights, evaluation of function derivatives. Discussed are also selected applications of the MM, and their recent and further development.

Keywords: meshless methods, local approximation

Meshless methods (MM) have become a powerful alternative to the FEM. In recent years the development and application of discrete approaches to an analysis of boundary-value problems, based on nodes rather than on elements, and therefore using unstructured grids have emerged. Generally these methods are referred to as meshless methods (MM), though a variety of different specific names is used as proposed by their authors (cf. review papers [2,12], and monographs [1,19]). Quite often the same method has various names and "rediscoveries" are being made. A classification of these methods follows as proposed by the author based on the type of a local approximation used. All of these methods yield an approximation of the form $u^h = \overline{\mathbf{N}}\mathbf{q}$, $\overline{\mathbf{N}} = [\overline{N}_i]$, $\mathbf{q} = \{u_i\}$ (well known from the FEM). The methods differ from each other by the way the ``pseudo shape functions" $\overline{N}_i$ are obtained and by the specific form of these functions. However, the condition $\sum_i \overline{N}_i = 1$, (called partition of unity) always has to be satisfied. Thus one may distinguish:

(i) *Methods based on the weighted least squares (MWLS) local approximation*

The following methods may be included into this group:

- meshless finite difference (MFDM); it is being developed since 1972 and may be regarded as the oldest, as well as possibly; the most general approach (both local [13] and global [10,14]) to the problem [19],
- diffuse element method (DEM) [6,17]. Though the concept of this method proposed in 1992 was not new when compared with the MFDM and MWLS approximation development at that time [10,11,13], the paper [17] accomplished an important role as a trigger of wide research on the meshless methods [3,4,7,14,17],
- element free Galerkin (EFG). Following the DEM concept very intensive research has been undertaken by T.Belytschko and his numerous coworkers (cf. review paper [2] and [4]) mainly using the Galerkin formulation of boundary value problems. The classical MWLS approach is used with polynomial interpolants to derive the local pseudo-functions $\overline{N}_i$ and their derivatives. The asymptotic solutions and/or jump functions may enrich the local approximation bases when needed. Successful analysis, especially of complex fracture mechanics problems was done,
- finite point (FPM) [18] and finite volume (FVM). These methods proposed by S.Idelsohn, E.Onate, R.L.Taylor and O.C.Zienkiewicz use some basic concepts of the finite difference method. Advantage is also taken of the MWLS approximation (FPM) and Voronoi tessalation of the domain used for integration purposes (FVM). Large fluid mechanics problems were effectively analysed [18].
- Local boundary integral equation (LBIE) and meshless local Petrov-Galerkin (MPLG), as well as local quadrature concept are used as proposed by Atluri el al [1]. Various types of local approximation may be applied then including the MWLS.

(ii) *Kernel methods*

These methods are based on an interpolation using the kernel estimate of the function $u(\mathbf{x})$ defined on a domain Ω. Assuming the weight function w as the kernel one may obtain the required pseudo shape functions $\overline{N}_i(\mathbf{x})$. The following particular methods are considered:

- smooth particle hydrodynamic (SPH).
  This is the second oldest MM initiated by L.B.Lucy [16], and initially developed by J.J.Monaghan. In the discrete form this method is not consistent i.e. the lowest order polynomials are not reproduced. This drawback is eliminated by the improved SPH version:
- reproducing kernel particle method (RKPM),
  introduced by W.K.Liu with coworkers [15] and intensively developed in a series of papers [12].

(iii) *Partition of unity methods PUM*

These methods are based on the general concept $1 = \sum_i \overline{N}_i$ called partition of unity. Once such partition is executed in the above equality it may be multiplied by any function ψ as to generate new ``shape functions" $\psi\overline{N}_i$ and/or to perform other operations, e.g. differentiation. The function ψ may represent, e.g. a complete basis of monomials and/or asymptotic solutions

etc. Two basic approaches were used in the PUM, differing in the way the basic shape-functions $\overline{N}_i$ are defined and introduced:

- partition of unity finite element method (PUFEM). This approach is due to I.Babuska and Melenk [3]. They used the classical FEM to generate shape functions $\overline{N}_i$.
- hp-clouds method, A.Duarte and J.T.Oden [7] proposed the use of the MWLS to generate the pseudo shape functions $\overline{N}_i$. In fact, the simplest Sheppard method is applied and $\overline{N}_i$ are defined by explicit formulas (cf.[7,19]). Moreover the h-p adaptive approach was successfully introduced. Also a combination of hp-clouds and MFDM has been considered.

(iv) *Particle in cell methods (PIC)*

These methods [5,12] are based on molecular dynamics, and, therefore they are applied, first of all, to time dependent problems. The continuous body is partitioned into subdomains. Their masses are reduced to particles located in their centres of gravity. The body motion is described then as a motion of a cloud of particles following the principles of mechanics. Effective, valuable results were obtained using this method despite several limitations and drawbacks resulting from its simplicity.

(v) *Natural element methods (NEM)*

Natural elements or natural neighbor methods [20] are based on the so-called Sibson coordinates to constract its interpolation function. It is used, like well known triangular coordinates in the FEM, to generate the required pseudo shape functions in the NEM. Also a non-Sibsonian interpolation scheme is being used.

(vi) *Other meshless methods (MM)*

The meshless methods are in a state of rapid development [1,2,8,12,19]. Although, in fact, some of them were discovered quite some time ago (MFDM - 31 years, SHP- 26 years), and it is only recently that they have captured the interests of a broader group of researchers. There are many aspects of these methods which could benefit from improvements like the techniques for treating discontinuities and other local effects (e.g. singularities). Meshless methods (like wavelets) are manifestations of the same basic trend towards methods with localized approximations (e.g. MWLS). Although they already form a separate group of discrete methods, some of them still require further improvement. On the other hand, the current development of the MFDM and the potential power of the PUM are already very promising. Moreover, ease of the use of distributed and parallel computing as well as symbolic operations which the meshless methods display, contributes to a breakthrough in their effective application.

Presented will be here a review of the main MM concepts, discussion of some chosen problems of the MWLS based approximation including choice of weights, evaluation of derivatives, error analysis, and MM/FEM coupling [9,10]. Several examples of MM applications, as well as their recent trends, and expected directions of further development will follow.

References

[1] Atluri M., Shen S., *The meshless local Petrov-Galerkin (MLPG) method*, Tech. Science Press, Encino, CA, USA 2002.

[2] Belytschko T., Krongauz Y., Organ D., Fleming M., Krysl P., Meshless methods: An overview and recent developments, *Computer Methods in Applied Mech. and Eng.*, 139, 3-47, 1996.

[3] Babuska I., Melenk J.M., The partition of unity method, *Int. J. Numer. Methods Eng.* 40, 727-758, 1997.

[4] Belytschko T., Lu Y.Y., Gu L., Element-free Galerkin Methods, *Int. J. Numer. Methods Eng.*, 37, 229-256, 1994.

[5] Brackbill J.U., Ruppel H.M., FLIP: A method for adaptively zoned , particle-in-cell calculations in two dimensions, *J. Comput. Phys.* 65, 314-343, 1986.

[6] Breitkopf P., Touzot G., Villon P., Explicit form and efficient computation of MLS shape function and their derivatives, *Int. J. Numer. Methods Eng.*, 48, 451-466, 2000.

[7] Duarte C.A., Oden J.T., hp Clouds – an hp meshless method, *Numer. Methods Partial Diff. Eqs.* 12, 673-705, 1996.

[8] Griebel M., Schweitzer M.A. (Eds), *Meshfree methods for partial differential equations*, Springer-Verlag, Berlin, 2003.

[9] Huerta A., Fernandez-Mendez S., Enrichment and coupling of the finite element and meshless methods, *Int. J. Numer. Methods Eng.* 48, 1615-1636, 2000.

[10] Krok J., Orkisz J., A unified approach to the FE and generalized variational FD in nonlinear mechanics, concepts and numerical approach, Int. Symp.on Discr. Meth. in Struct. Mech. IUTAM/IACM, Vienna, Austria, 1989, Springer- Verlag, Berlin-Heidelberg, 353-362, 1990.

[11] Lancaster P., Salkauskas K. , Surfaces generated by moving least - squares methods, *Math.Comp.*, 155, 37, 141-158, 1980.

[12] Li S., Liu W.K., Meshfree and particle methods and their applications, *Applied Mechanics*, 55, 1-34, 2002.

[13] Liszka T, Orkisz J., The finite difference method at arbitrary irregular grids and its applications in applied mechanics, *Comp. Struct.*, 11, 83-95, 1980.

[14] Liszka T., Orkisz J., The finite difference method for arbitrarily irregular meshes- a variational approach to applied mechanics problems, GAMNI 2, Paris, Dec.1980, 227-235, 1980.

[15] Liu W.K., Jun S., Zhang Y.F. , Reproducing kernel particle methods, *Int. J. Numer. Methods Eng.*, 20, 1081-1106, 1995.

[16] Lucy L.B. , A numerical approach to the testing of the fission hypothesis, *The Astron. J.*, 8(12), 1013-1024, 1977.

[17] Nayroles B., Touzot G., Villon P. , Generalizing the finite element method: Diffuse approximation and diffuse elements, *Computational Mechanics*, 10, 307-318, 1992.

[18] Onate E., Idelsohn S., Zienkiewicz O.C., Taylor R.L., A Finite Point Method in Computational Mechanics. Applications to Convective Transport and Fluid Flow, *Int. J. Numer. Methods Eng.*, 39, 3839-3886, 1996.

[19] Orkisz J., Finite Difference Method (Part III), in *Handbook of Computational Solid Mechanics*, M.Kleiber (Ed.), Springer-Verlag, Berlin, 336-432, 1998.

[20] Sukumar N., Moran B., Belytschko T., The natural element method in solid mechanics, *Int. J. Numer. Methods Eng.* 43, 839-887, 1998.

On adaptive mesh generator for meshless FD and FE methods

Janusz Orkisz and Przemysław Przybylski
Department of Computational Mechanics, Cracow University of Technology
Warszawaska 24, 31-154 Kraków
e-mail: plorkisz@cyf-kr.edu.p

Summary

The paper presents the current status of research and development on the effective unstructured 2D and 3D-mesh generator fulfilling requirements of highly efficient adaptive analysis and multigrid solution approach. The approach is based on the advanced concept of mesh density control, which allows for effective and flexible mesh modification mechanism to insert, remove and shift nodes. The research comprises: node generation and modification (node insertion, removal and shifting), search for nodes in the neighborhood of a considered point (node), domain partition into subdomains assigned to individual nodes, optimal mesh triangulation, optimal star generation and classification, automatic detection and elimination of singular or ill-conditioned FD schemes. Full mesh topology information is generated and provided if required by a user.

Keywords: FDM/FEM, mesh generator, mesh density control, adaptive analysis

1. Abstract

The paper presents the current status of research and development on the effective unstructured 2D and 3D-mesh generator fulfilling requirements of highly efficient adaptive analysis and multigrid solution approach [6, 7]. The approach is based on the advanced concept of mesh density control [7], which allows for effective and flexible mesh modification mechanism to insert, remove and shift nodes.

The research comprises: node generation and modification (node insertion, removal and shifting), search for nodes in the neighborhood of a considered point (node), domain partition into subdomains assigned to individual nodes, optimal mesh triangulation, optimal star generation and classification, automatic detection and elimination of singular or ill-conditioned FD schemes. Full mesh topology information is generated and provided if required by a user.

The main effort is now focused on the 2D mesh generator being currently implemented. This includes generation of series of meshes with corresponding proximity information. The results are visualized with the cooperating software prepared in [1]. This paper also presents several benchmarks and applications related to railroad rail analysis.

The work on extension to 3D is in progress but mainly in conceptual and theoretical phase. The strategy of 3D mesh adaptation is now defined and several algorithms have been drafted.

The presented concept is designed to work properly with both the adaptive meshless finite difference (MFD) and FE methods [3]. The generator produces various types of output data. These include information on series of meshes generated during adaptive refinement process. Each mesh contains topological information on MFDM stars and simplex elements (for the FE and BE methods).

The mesh generation algorithm is divided into two parts. The first one deals with node generation and modification, which is based on Liszka's concept [2], later developed for the adaptive solution approach by J Orkisz [5]. The new concept presented in the paper is a unique combination of Liszka's type mesh generation and an advanced grammar based approach. A combined algorithm is proposed to guarantee generation of well-conditioned FD schemes.

The second part of the algorithm manages generation of proximity [8] information (Voronoi thessalation; constrained Delaunay triangulation; selection of node and triangle neighbors; evaluation of mesh density) and selection of various types of MFD stars.

The process of node generation resembles 'sifting nodes' out of a very dense regular mesh through the filter represented by imposed local mesh density function. This function may be defined by the user or is a result of a'posteriori error analysis. Proper definition and modification of this function is a key mechanism for an effective mesh density control.

There are several unique features of the this kind of approach to mesh generation, which are fundamental for proper implementation of adaptive multigrid solution approach:

- Effective generation of an initial mesh that corresponds to minimal mesh density required by the analyzed b.v. problem with ability for further adaptive refinement.
- Flexible mesh modification by new nodes, insertion, removal or shifting of existing ones as a consequence of a full mesh density control capability.
- Easy generation of smooth transition zones between areas of different local mesh density.

It is also worth mentioning that the whole software has been designed and developed using modern methodology including UML, multi-tier and distributed approach supposed to extend the size of possible tasks analyzed [2]. Several applications in residual stress analysis in railroad rails are discussed.

References

[1] Hackbush B., *Multi-grid methods and Applications*, Springer-Verlag, 1985.

[2] Keyser J., Roose D., *Partitioning and Mapping Adaptive Multigrid Hierarchies on Distributed Memory Computers*, Report TW166, Department of Computer Science, Leuven, 1992.

[3] Krok J., Leżański P., Orkisz J., Przybylski P., Schaefer R; *Basic concepts of an open distributed system for cooperative design and structure analysis*. CAMES, Vol. 3, 1996, pp. 169-186.

[4] Liszka T. *An automatic grid generation in flat domain*, Mechanika i Komputer, 4, 1981, 181-186.

[5] Liszka T., Orkisz J., *The Finite Difference Method at Arbitrary Irregular Grids and its Applied Mechanics*, Comp.and Struct., 11(1980), 83-95.

[6] Orkisz J., Finite Difference Method (Part III), in *Handbook of Computational Solid Mechanics*, M.Kleiber (Ed.) Springer-Verlag, Berlin, , 336-432, (1998).

[7] Orkisz J., Przybylski P., An adaptive mesh generator for meshless FD and FE methods, 2th European Conference on Computational Mechanics, Kraków, July, 2001.

[8] Orkisz J., Leżański P., Przybylski P., *Multigrid Approach to Adaptive Analysis of Boundary Value Problems by the Meshless GFDM,* Proc. of the IUTAM/IACM Symp. On Disretization Methods in Structural Mechanics II, Vienna 97, Kluwer Academic Publ. Dortrecht/Boston/London, 173-180, (1999).

[9] Thompson J., Soni B., Weatherill N. *Handbook of Grid Generation,* CRC Press, (1999).

[10] Watson, D.F., 1981, *Computing the n-dimensional Delaunay tessellation with application to Voronoi polytopes*, The Computer J., 24(2), p. 167-172.

On Acceleration of the Gauss-Seidel Method for Solution of Simultaneous Linear Algebraic Equations

Janusz Orkisz, Samsoor Shaheed
Computational Mechanics Division, Cracow University of Technology
Warszawska 24, 31-155 Kraków
e-mail: plorkisz@cyf-kr.edu.pl

Summary

A relaxation technique applied to speed up the well established Gauss-Seidel iterative method is considered here. As many other iterative solution methods the Gauss-Seidel method may be used together with the successive over-relaxation technique (SOR). In the classical SOR approach the optimal relaxation parameter λ^* is to be chosen to minimize the spectral radius of an error dumping matrix $\mathbf{M}(\lambda)$. However, the evaluation of such optimal parameter λ^* is difficult except in the simplest of cases. It is usually obtained only approximately, based on trying various values of λ and observing the effect on the speed of convergence. Therefore, a new way of evaluation of the relaxation factor for the Gauss-Seidel method is considered here. Proposed is either minimization or annihilation of a modified subsequent value of solution residuum. As opposed to the spectral radius $\rho_s(\mathbf{M}(\lambda))$ minimization technique the above mentioned concept requires only simple calculations to evaluate a new λ_m in each iteration step. The results of preliminary numerical tests done, are encouraging. Further tests are planned.

Keywords: large simultaneous equations, relaxation approach

1. Introduction

Though effective analysis of large sets of simultaneous linear algebraic equations (SLAE) $\mathbf{Ax}=\mathbf{b}$ is a very old problem, it is very often required in a variety of technical applications, and still presents an active research field.

A relaxation technique applied to speed up the well established Gauss-Seidel iterative method is considered here. As many other iterative solution methods the Gauss-Seidel method may be brought to the form

$$\mathbf{x}^{(m)}=\mathbf{M}\mathbf{x}^{(m-1)}+\mathbf{N}\mathbf{b}\,, \tag{1}$$

when the successive over-relaxation technique (SOR) is simultaneously applied in order to obtain an improved solution

$$\tilde{\mathbf{x}}^{(m)}=\mathbf{x}^{(m-1)}+\lambda\,\mathbf{r}^{(m-1)}\,, \tag{2}$$

where solution increment $\mathbf{r}^{(m-1)}=\mathbf{x}^{(m)}-\mathbf{x}^{(m-1)}$ denotes at the same time the residuum.

The matrices $\mathbf{M}$ and $\mathbf{N}$ depend on the relaxation parameter λ. In the classical SOR approach this parameter is to be chosen to minimize the spectral radius $\rho_s(\mathbf{M}(\lambda))$ of the matrix $\mathbf{M}(\lambda)$, in order to make $\mathbf{x}^{(m)}$ converge to $\mathbf{x}$ as rapidly as possible [1,2]. However, the evaluation of such optimal parameter λ^* is difficult except in the simplest of cases. It is usually obtained only approximately, based on trying various values of λ and observing the effect on the speed of convergence. It is also worth mentioning here, that even the optimal value λ^*, defined above, does not guarantee obtaining the minimum number of Gauss-Seidel iterations.

Therefore, a new way of evaluation of the relaxation factor for the Gauss-Seidel method is considered here. Proposed is either minimization or annihilation of a modified subsequent value of the residuum

$$\tilde{\mathbf{r}}^{(m-1)}=\mathbf{r}^{(m-2)}+\lambda_m(\mathbf{r}^{(m-1)}-\mathbf{r}^{(m-2)}) \tag{3}$$

in order to determine λ_m.

As opposed to the spectral radius $\rho_s(\mathbf{M}(\lambda))$ minimization technique the above mentioned concept requires only simple calculations to evaluate a new λ_m in each iteration step. Several particular local and global concepts have been used to evaluate variable relaxation factor λ_m. Its influence on the convergence rate of the iterative solution process of large set of simultaneous linear algebraic equations has been investigated. Encouraging results have been obtained.

2. Solution approach proposed

Consider simultaneous linear algebraic equations (SLAE)

$$\sum_{j=1}^{n}a_{ij}x_j=b_i\quad,\quad i=1,2,...,n \tag{4}$$

or in the matrix notation

$$\mathbf{Ax}=\mathbf{b}\quad, \tag{5}$$

where $\mathbf{A}=[a_{ij}]$, $\mathbf{x}=\{x_i\}$, $\mathbf{b}=\{b_i\}$ for $i,j=1,2,...,n$.

Solution of the SLAE is usually obtained by means of either elimination methods or iterative ones. The iterative methods are mostly used to solve large sparse systems.

Besides being large the linear systems in question often have other important features e.g. they are usually sparse. A successive over-relaxation iterative (SOR) technique applied to solution of systems of such equations is investigated here. The Gauss-Seidel method is one of often used iterative solution

methods. It presents a well known and established iterative procedure

$$x_i^{(m+1)} = \frac{1}{a_{ii}}\left\{ b_i - \sum_{j=1}^{i-1} a_{ij} x_j^{(m+1)} - \sum_{j=i+1}^{n} a_{ij} x_j^{(m)} \right\}, \qquad (6)$$

where each new component $x_i^{(m+1)}$ is immediately used in the computation of the next component $x_{i+1}^{(m+1)}$. The method is convenient in practical calculations due to its simplicity and minimized storage requirements. On the other hand it is not efficient enough, especially for large systems of equations.

Therefore, it is often used together with an acceleration technique called successive over relaxation approach (SOR). An acceleration parameter λ and the following modification of formulae (6) are introduced then:

$$z_i^{(m+1)} = \frac{1}{a_{ii}}\left\{ b_i - \sum_{j=1}^{i-1} a_{ij} x_j^{(m+1)} - \sum_{j=i+1}^{n} a_{ij} x_j^{(m)} \right\}, \qquad (7)$$

$$x_i^{(m+1)} = \lambda z_i^{(m+1)} + (1-\lambda) x_i^{(m)} \quad , \quad i = 1,\ldots,n \qquad (8)$$

for $m \geq 0$. The case $\lambda = 1$ presents the regular Gauss-Seidel method. Theoretical considerations show that $0 \leq \lambda \leq 2$ [1,2].

The parameter λ is to be chosen as to minimize the spectral radius $\rho_s(\mathbf{M}(\lambda))$ of the matrix $\mathbf{M}(\lambda)$, given in relation (1), in order to make $\mathbf{x}^{(m)}$ converge to $\mathbf{x}$ as rapidly as possible. Thus required is the optimal value of the parameter λ^* minimizing the extreme eigen-value of that matrix.

Several remarks should be made here. The value λ^*, found in this way, presents an optimal choice from the point of view of each single iteration step. However, optimization of not only one but a series of steps at once, like the Tschebyshev acceleration in the Richardson method [3], may yield a faster solution procedure.

Unfortunately evaluation of the optimal λ^*, mentioned above, is practically difficult, except in the simplest cases. Therefore, it has been usually obtained only approximately so far, based on trying several values of λ and examining the effect on the speed of convergence. It is worth noticing, however, that with a proper choice of λ such effect may be dramatic.

Therefore, a new approach to providing an effective evaluation of variable parameter $\overline{\lambda}_m$, appropriate for m series of the Gauss-Seidel iterations carried out for given n consecutive equations is proposed here. This approach is based on a minimization of the residuum

$$\tilde{\mathbf{r}}^{(m-1)} = \mathbf{r}^{(m-2)} + \lambda_{m-1}\left(\mathbf{r}^{(m-1)} - \mathbf{r}^{(m-2)}\right) \qquad (9)$$

where

$$\mathbf{r}^{(m-1)} = \mathbf{x}^{(m)} - \mathbf{x}^{(m-1)} \qquad (10)$$

Multiplying equation (9) either by the vector $(\mathbf{r}^{(m-1)})^t - (\mathbf{r}^{(m-2)})^t$ or by $(\mathbf{r}^{(m-2)})^t$ and assuming that $\tilde{\mathbf{r}}^{(m-1)}$ is orthogonal to the first or to the second of those vectors one obtains

$$(\tilde{\mathbf{r}}^{(m-1)})^t\left(\mathbf{r}^{(m-1)} - \mathbf{r}^{(m-2)}\right) = (r^{(m-2)})^t\left(\mathbf{r}^{(m-1)} - \mathbf{r}^{(m-2)}\right) + \\ + \lambda_{m-1}\left(\mathbf{r}^{(m-1)} - \mathbf{r}^{(m-2)}\right)^t\left(\mathbf{r}^{(m-1)} - \mathbf{r}^{(m-2)}\right) = 0 \qquad (11)$$

hence

$$\lambda_{m-1} = -\frac{(\mathbf{r}^{(m-2)})^t\left(\mathbf{r}^{(m-1)} - \mathbf{r}^{(m-2)}\right)}{\left(\mathbf{r}^{(m-1)} - \mathbf{r}^{(m-2)}\right)^t\left(\mathbf{r}^{(m-1)} - \mathbf{r}^{(m-2)}\right)} \qquad (12)$$

or

$$(\tilde{\mathbf{r}}^{(m-1)})^t \mathbf{r}^{(m-2)} = (\mathbf{r}^{(m-2)})^t \mathbf{r}^{(m-2)} + \\ + \lambda_{m-1}(\mathbf{r}^{(m-2)})^t\left(\mathbf{r}^{(m-1)} - \mathbf{r}^{(m-2)}\right) = 0 \qquad (13)$$

hence

$$\lambda_{m-1} = -\frac{(\mathbf{r}^{(m-2)})^t \mathbf{r}^{(m-2)}}{\mathbf{r}^{(m-2)}\left(\mathbf{r}^{(m-1)} - \mathbf{r}^{(m-2)}\right)} \qquad (14)$$

As opposed to the classic spectral radius $\rho_s(\mathbf{M}(\lambda))$ minimization technique mentioned before, the proposed concept requires only simple calculations to evaluate a new λ after each of two consecutive series of the Gauss-Seidel iterations performed for the whole system of n given equations.

The following solution algorithm is proposed here:

(i) perform two consecutive series (m-1 and m-th) of gauss-Seidel iterations (6) for the whole system of n SLAE equations

(ii) after the second of these series find residuals (10) and SOR parameter λ_m (12) or (14),

(iii) find new SOR m-th solution (8) to the SLAE and replace with it the last m-th Gauss-Seidel solution found before.

3. Numerical tests

The approach proposed here has been tested in various ways.

Comparisons were made between the classic Gauss-Seidel and the new SOR algorithm technique proposed here. The influence the number of SLAE and the required precision of calculations $\in$ ($e_m \leq \in$) have on the convergence rate have been examined.

The preliminary results are encouraging. The speed up factor between SOR and Gauss-Seidel algorithms as measured by the number of iterations was found between 2 and 20, though the gain was falling with the increasing SLAE number. However, many further tests are necessary before a reasonable conclusions may be made. These tests will also include several variants of the basic SOR algorithm proposed here.

References

[1] Atkinson K.E., *An Introduction to Numerical Analysis*, Wiley Ed., N.York, 1988.

[2] Press W.H., Tenkolsky S.A., Vetterling W.T., Flannery B.P., *Numerical Recipes, The art of Parallel Scientific Computing*, Cambridge Univ.Press, 1999.

[3] Legras J, *Methodes et techniques de l'analyse numerique*, Dunod, Paris, 1971.

Recent developments in estimation of residual stresses in railroad car wheels made of material exhibiting kinematic hardening

Michał J. Pazdanowski
Independent Division of Computational Mechanics, Cracow University of Technology
ul. Warszawska 24, 31-155 Kraków
e-mail: plpazdan@kinga.cyf-kr.edu.pl

Abstract

The paper deals with an application of the extended shake-down mechanical model and global-local version of the Meshless Finie Difference Method (MFDM) to determine residual stresses in bodies of revolution subject to simulated contact loads. Railroad vehicle wheel subject to simulated service load is analyzed as an engineering example.

Keywords: plasticity, shakedown, hardening, residual stresses, Meshless Finite Differences

1. Introduction

The presented research has been centered on development and testing of the numerical model to determine residual stresses in bodies of revolution made of elastic plastic material exhibiting hardening and subject to simulated contact loads, since the so far used set of Meshless Finite Difference (MFD) based computer programs to calculate residual stresses arising in bodies subject to loads exceeding their elastic bearing capacity by the shakedown approach [6,7] has been limited to prismatic bodies and cartesian coordinate systems.

Such problem of residual stresses in railroad car wheels has been previously analyzed [2] using shakedown formulation [5] for the elastic perfectly plastic material and Hybrid Finite Element Method (HFEM) computational model. It is believed, that the application of more accurate material model [6], taking account of kinematic harening properties exhibited by wheel material, will ultimately lead to better and more precise description of phenomena influencing the wheel service life, including the substantial decrease in peak values of circumferential residual stress (as may be expected by analogy to the railroad rail [8]).

2. Solution approach applied and computer implementation

The shake-down mechanical model [5], generalized to allow for the kinematic hardening of material [6] and used as a basis for development of the proper modified numerical model, may be defined in the following two steps:

I calculate the correlation matrix A_{ijkl} :

$$\sigma^r_{ij} = A_{ijkl} \cdot \varepsilon^p_{ij} \tag{1}$$

solving the following nonlinear constrained optimization problem for self equilibrated stresses σ^r_{ij} as a function of plastic distorsions ε^p_{ij} :

$$\min_{\sigma^r_{ij}} \Theta(\sigma^r_{ij}),\ \Theta(\sigma^r_{ij}) = \int_V \sigma^r_{kl} \cdot C_{ijkl} \cdot \sigma^r_{ij} \cdot dV - \int_V \varepsilon^p_{ij} \cdot \sigma^r_{ij} \cdot dV \tag{2}$$

at:

$$\sigma^r_{ij,j} = 0 \quad , \quad \text{in V - internal equilibrium conditions} \tag{3}$$

$$\sigma^r_{ij} \cdot n_j = 0 \quad , \quad \text{on } \partial\text{V- static boundary conditions} \tag{4}$$

II find ε^p_{ij} which minimize the total complementary energy functional:

$$\min_{\varepsilon^p_{ij}} \Psi(\varepsilon^p_{ij}),\ \Psi(\varepsilon^p_{ij}) = \int_V \varepsilon^p_{gh} \cdot A^T_{ghij} \cdot C_{ijkl} \cdot A_{klmn} \cdot \varepsilon^p_{mn} \cdot dV \quad , \tag{5}$$

at:

$$\Phi((A_{ghij} - I_{ghij} \cdot c) \cdot \varepsilon^p_{ij} + \sigma^E_{ij} + \sigma^T_{ij}) - 1 \le 0 \quad , \tag{6}$$

in V - yield conditions

where:

$c = \frac{E \cdot H}{E - H}$, - hardening parameter.

The following denotations hold in (1) - (6):

- σ^r_{ij} - residual stresses arising in considered body, due to actual applied loads,
- ε^p_{ij} - plastic strains,
- σ^E_{kl} - elastic stresses (stresses calculated as if the analyzed body deformed purely elastically under the current loading program),
- σ^T_{ij} - stresses due to thermal (heating due to braking) load (denoted as σ^θ_{ij} in [4]),
- A_{ghij} - correlation matrix linking plastic strains and residual stresses,
- I_{ghij} - unit matrix,
- E - Young modulus,
- H - hardening modulus,
- C_{ijkl} - elastic compliance matrix.

The necessary modifications of the previously developed computer code utilizing the Meshless Finite Difference numerical model dealt with the changed (cylindrical) coordinate

system. These included the modified integration schemes in formulas (2) and (5) of the formulation listed above and proper definition of the internal equilibrium constraints. Requirements specific to the wheel analysis also force the application of additional control loop within the program. This is to account for the influence of high speed braking (localized heating) on residual stress levels in the wheel. The changing thermal stresses are dealt with within this loop in such a manner, that the residual stresses are calculated step by step for each temperature level. Such an approach to a high extent resembles the way the "wheel wandering problem" is analyzed in a railroad rail.

The modified code has been tested on a wheel problem solved previously using the Hybrid Finite Element computational model and computer code developed according to it [2]. The necessary elastic solutions have been found using code developed in DOT [1].

For the purpose of calculations the following material data have been assumed:

Wheel: US type 32' MU commuter vehicle wheel,
Young modulus: E = 206.832 GPa,
Poisson's ratio: $\nu = 0.3$,
Contact load P = 77.84 kN.

These values have been chosen as to realistically represent the conditions existing in standard operating practice on the American railroads.

3. Numerical results

So far, only comparative calculations have been performed for one case of load located on the running surface of the wheel on one nodal net in the wheel cross-section. Thus no hardening has been assumed ($c = 0$ in formula (6)) which is necessary for the results to be comparable with [2]. Peak values of determined residual stresses and stresses computed previously on the same mesh in [2] seem to indicate, that:

- a very good agreement exists between recent results and residual stresses computed previously [2] in terms of general location and size of tensile/compressive zones, locations of points with extreme values of residual stresses - this indicates validity of the approach used,
- the coincidence in peak stress levels is quite remarkable considering the nature of applied load,
- certain discrepancies visible, notably in the contour plots of σ_{rr} residual stress are in the author's oppinion to a high extent attributable to the higher sensitivity of MFDM vs. HFEM to abrupt changes in the nodal mesh density (for instance two maximums along the axis of symmetry of applied load, two local maximums along the horizontal line of mesh density change).

Currently the work is centered on an improved numerical integration procedure to be applied in the areas of changing nodal density, which to the authors oppinion may allevate the problems attributable to abrupt mesh density changes in the transition zone between the plastic region with high level of residual stresses and he adjacent elastic area affected by it. The work is currently conducted as well on enforcement of incompressibility constraint on the plastic strains ε_{ij}^{p} present in the formulas (1), (2), (5), (6). It is believed, that such development may improve the quality of plastic strains determined, and have a beneficiary influence on the efficiency of optimization algorithms used to solve the constrained nonlinear optimization problem (5), (6) as well (significantly reduced number of decision variables).

The most up to date numerical results will be presented at the conference.

4. References

[1] Gordon, J., *Estimation of residual stresses in railroad car wheels resulting from manufacture and service loading*, Master Thesis, Tufts Univ., Medford, MA, 1998.

[2] Holowinski, M., Bobrov, E.S., *Estimation of Actual Residual Stresses Due to Braking and Contact Loading of Rail Vehicle Wheels*, Final Report, DOT/FRA/ORD-96/02, 1996.

[3] Krok, J., Orkisz, J., *3D analysis of elastic stresses in a railroad rail induced by rolling contact with varying contact zone by the FEM/MFDM based Generalized Finite Strip Method*, Final Rpt. to the US DOT, FRA, Washington DC, 1998.

[4] Orkisz, J., Residual stress analysis in railroad car wheels working in service conditions, *Theoretical and Applied Mechanics*, 1-2, 28, 1990 (in polish).

[5] Orkisz, J., Cecot, W., Prediction of actual residual stresses resulting from cyclic loading in kinematic hardening material, *Proc. Int. Conf. COMPLAS V*, Barcelona, pp. 1879-1891, 1997.

[6] Pazdanowski, M., Meshless Finite Difference Method Application to the Residual Stress Analysis, *Proc. XIV PCCMM*, Rzeszów, pp. 186-187, 1997.

[7] Pazdanowski, M., Application of the Generalized Finite Difference Method to Analysis of Residual Stresses in Bodies Subject to Cyclic Loads, Ph.D. Thesis, Cracow, 1994 (in polish).

[8] Pazdanowski, M., *MFDM residual stress analysis in railroad rails with kinematic hardening of material accounted for*, Final Rpt. to the US DOT, FRA, Washington DC, 2000.

Development of h-adaptive finite element analysis of residual stresses by the Zarka model

Witold Cecot
Cracow University of Technology
ul. Warszawska 24, 31-155 Krakow, Poland
e.mail: plcecot@cyf-kr.edu.pl

Summary

The paper addresses development of numerical implementation of the Zarka shakedown method. The resulting boundary value problem is discretized by the h-adaptive finite element method. Since the problem is nonlinear, two error estimates were used for mesh refinement. The explicit residual one controls accuracy of the momentum balance while the interpolation error estimate controls the plastic strain approximation. Adaptation significantly increased efficiency of the numerical analysis in comparison with the uniform mesh refinement.

The paper presents also validation tests of the Zarka approach and its application to the analysis of selected engineering problems with special attention paid to reliability of the modeling as well as of the numerical analysis. The tests confirm possibility of a proper, for engineering purposes, estimation of residual stresses by the Zarka shakedown approach.

Keywords: shakedown, error estimate, adaptive FEM

Abstract

Numerical analysis of residual stresses resulting from cyclic loading with arbitrary amplitude may be done either by a very time consuming incremental model or by a much faster direct, shakedown approach. One of the direct approaches, based on the Martin's extremal path concept, was proposed in [5] and later on generalized for materials exhibiting the kinematic hardening [6]. The Zarka model [8, 7] constitutes another direct method of shakedown analysis.

Development of a numerical implementation of the Zarka shakedown method is discussed in the paper. In this approach, the shakedown state is determined by appropriate selection of the modified back stresses, which are defined as the difference between residual stresses and the plastic strains multiplied by the elastoplastic tangent modulus. The modified back stresses, similary as plastic strains, uniquely determine the residual self-stress field, and must be such, that the resulting stresses are both plastically and statically admissible. These two conditions are stisfied in an iterative process. Whenever the stresses exceed the yield condition, a local projection proposed by Zarka is performed. Then in order to satisfy the equilibrium equations we use the finite element method in the h–adaptive version [3]. Adpativity leads to increased computational efficiency by such modification of the mesh in selected regions, that for a given number of elements the solution is the most accurate.

The Zarka method proved to be very efficient [1, 2], since it involves neither the time consuming incremental analysis (classical approach) nor the sometimes slowly convergent optimization process (minimization approach).

The objective of this work is a further validation of the Zarka approach and development of the numerical implementation of the model in the h–adaptive finite element code. Especially the following topics, briefly described below are presented in the paper.

- Discussion of equivalence of three models i.e. Zarka's, minimization (both of the shakedown type) and the classical, incremental approach. They yield the same results in certain cases, e.g. for material with kinematic hardening. However, generally the shakedown models only estimate the incremental solution.
- Comparison of efficiency and reliability of a'posteriori error estimates in application to the shakedown modeling, i.e. mathematically proved residual and interpolation estimates with very fast but only heuristically justified, recovery type error estimate. The last one works well in the most cases but as well as the residual estimate it has to be supplemented with the interpolation error estimate of the nonelastic strains.
- Application of the Zarka model to the analysis of selected engineering problems, i.e. evaluation of residual stresses in railroad rails.

The Zarka shakedown model and the Bodner-Partom one result in practically the same stresses in the cylinder benchmark problem, except of the longitudinal stress component for compressible, perfectly plastic material. Very similar conclusions were drawn in [4], where the Zarka approach was compared with the Prandtl-Reuss model. However, perfect plasticity is far from realistic behavior of metals, therefore this will not affect our analysis.

The minimization approach was tested so far only on the example of the perfectly plastic, incompressible material, resulting in the same results as the other approaches.

In the railroad rail benchmark test the incremental and shakedown approaches result in close σ_{xx} and σ_{yy} stress components. The longitudinal residual stress (σ_{zz}) distributions differ by maximum 50%. In the most important, tensile area the Zarka results in overestimated solution. While the compressive values are underestimated.

However, the tests completed so far confirm that the Zarka shakedown model yields reasonable results from engineering point of view.

In the proposed strategy the mesh refinements are based interchangeably on the residual and the interpolation error estimates. Even though the recovery error estimate results generally in similar convergence (Fig. 1) as the residual estimate the last one is preferred due to its better theoretical background.

The following strategy of adaptation is assumed.

1. Evaluate the residual state by the Zarka approach on a given FEM mesh.
2. Estimate error of the solution for each of the elements.
3. If the error is small enough then stop, otherwise modify the mesh, wherever it is necessary and go to step 1.

Numerical tests show that the most efficient strategy of adaptation in the shakedown problems was to restart the computation after the mesh refinement rather than to transform the solution and to continue the computation on the new mesh. Relatively short time of the shakedown analysis is the main reason for such a conclusion.

Comparison of convergence tests obtained with different error estimates, shown in Fig. 1 indicates also that

- adaptive mesh refinement significantly reduces the number of necessary unknowns (even 2 - 3 times) and
- the estimation of the approximation quality of the modified back stresses (analog of the plastic strains) can not be neglected.

The railroad rail in service conditions was analyzed as an example of an engineering problem. The rail was subjected to resultant contact loads in the range of 120 kN to 300 kN showing monotonic dependence of the solution in terms of the load. The resultant load was distributed parabolically on an ellipsoidal area to simulate the rail/wheel contact.

Generally, we may conclude that the Zarka direct method results in reliable solutions with much less computational effort then incremental approaches, especially in combination with the adaptive numerical analysis.

Plans for the nearest future include: solution of further examples (rail and wheel), as well as thorough comparison of the results with those obtained by the minimization approach.

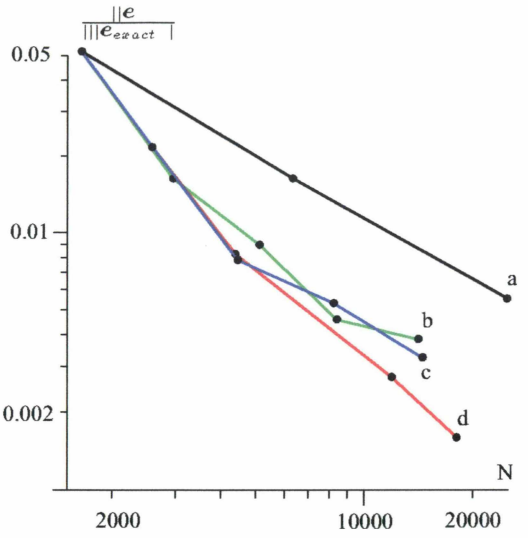

Figure 1: Convergence tests; energy norm of error versus number of degrees of freedom (logarithmic scalesof axes), uniform (a) and adaptive mesh refinements based on different error estimates: recovery (b) explicit residuum (c), residuum combined with interpolation (d)

References

[1] W.Cecot, *On Application of the Zarka Approach to Estimation of Residual Strains and Stresses in Railroad Rails*, proc. of COMPLAS V conf., Barcelona, 1873 – 1878, 1997.

[2] W.Cecot, *Adaptive finite element analysis of certain shakedown problems*, 2nd European Conf. on Comp. Mech., Poland 2001.

[3] L.Demkowicz, W.Rachowicz, K.Banas, J.Kucwaj *"2-D hp Adaptive package"*, Cracow University of Technology, report no 4/1992.

[4] Kretzschmar, H.Hubel, *Benchmark between CUT and Lausitz University of Applied Sciences concerning Zarka's method - Thick-Walled Cylinder* report 2002.

[5] J.Orkisz, *"Prediction of Actual Residual Stresses by Constraint Minimization"* , in O.Orringer at al. editors, *Residual Stresses in Rails*, vol II Kluwer Ac. Publ., 101–124, 1992.

[6] J.Orkisz, W.Cecot *Prediction of Actual Residual Stresses Resulting from Cyclic Loading in Kinematic Hardening Materials*, COMPLAS V conf., Barcelona, 1040 – 1042, 1997.

[7] M.Yu, B.Moran, L.M.Keer, *A Direct Analysis of Two- Dimensional Elastic - Plastic Rolling Contact,* Journal of Tribology, 115, 227 - 236, 1993.

[8] J.Zarka, J.Casier, *"Elastic Plastic Response of a Structure to Cyclic Loading, Practical rules"*, in Mechanics Today, vol. 6, S.Nemat editor, Pergamon Press 1979.

Application of the extended global-local data smoothing to residual stress analysis

Wojciech Karmowski and Janusz Orkisz
Computational Mechanics Department L6, Cracow University of Technology
Warszawska 24, 31-155 Cracow
e-mails: – pmkarmow@cyf-kr.edu.pl, plorkisz@cyf-kr.edu.pl

Abstract
The paper presents a new version of the global–local approximation method i.e. experimental - theoretical approach to analysis of engineering boundary value problems. It considers the task as inverse problem where experimental data supplies missing information on the searched field. Using this technique one may solve problem of mechanics without full information about the state of the examined body. The special functional is defined, whose minimum gives solution of the problem considered. In this version curvature of the stress field is taken into account. Such approach was successfully used e.g. to reconstruct residual stress field in the cross-section of the railroad rail.

Keywords: experiment, approximation, MWLS

1. Introduction

The papers [1-3] presented the global–local approximation method i.e. experimental - theoretical approach to analysis of engineering boundary value problems. These are usually analysed by solving of the partial differential equations with boundary conditions. The method is global because it takes into consideration measurements from the whole domain and is local because field searched for is found at one point. When complete information on relevant problem is unavailable, one may convert the task to an inverse problem where experimental data supplies missing information on the searched field. Using this technique one may solve problem of mechanics without information on the state of the examined body. This is especially true in residual state. The measurements are available at discrete points and are done with a limited precision. Therefore, they may be used only within a special functional. The minimum of this functional gives solution of the problem considered. The formulation was successfully used e.g. to reconstruct residual stress field in the cross-section of the railroad rail. In present version the method has been applied to 2D problems. The obtained solution is sufficiently smooth. In *the engineering problems, where residual stresses are induced* by forces acting over small surfaces, sub-domains exist, where residual stresses are large. In previous versions of the method the smoothing parameter has been chosen once for the whole domain. In the cases, where large stress gradients are present, such approach does not work properly. Therefore, current version of the method has been improved by considering the stress field curvature as well.

2. A new version of the global - local method

The global-local method presents a development of the moving weighted least squares global-local approximation [4-6]. All versions of the global-local method have unique form, which contains truncated expansion of sought field into Taylor series to fit experimental data. A norm of this fit is multiplied by a weighting factor containing smoothing parameter and multiplier responsible for inhomogeneous density of the experimental points. This last factor is defined as surface area of Voronoi polygon around given point. The expansion mentioned above automatically satisfy equilibrium equations (common for all solids) . Relevant error function has the form

$$\Phi(\vec{r})=\left(\frac{\sum_{k=0}^{kk-1} D_k \frac{\left\|\breve{\sigma}\left(\vec{r}^{(k)}-\vec{r}\right)-\breve{\sigma}^{(k)}\right\|^2}{|||\,\vec{r}^{(k)}-\vec{r}\,|||}}{\sum_{k=0}^{kk-1} D_k \frac{\left\|\breve{\sigma}^{(k)}\right\|^2}{|||\,\vec{r}^{(k)}-\vec{r}\,|||}}\right)^{1/2}, \qquad (1)$$

where summation extends over all experimental data points. Here $D^{(k)}$, $r^{(k)}$ and $\sigma^{(k)}$ denote respectively density weighting factor, data point location and measured stress. The matrix norm "$\|.\|$" is defined as $\|\breve{\sigma}\| = (\mathrm{tr}(\breve{\sigma}\breve{\sigma}))^{1/2}$. This definition satisfies all norm requirements, and additionally is invariant to rotation of the coordinate system. Symbol $|||.|||$ denotes weights of the considered points. It is defined as $|||\,\vec{r}\,||| = \left(r^2 + \frac{g^4}{r^2+g^2}\right)^m$. The parameter "g" is responsible for optimal approximation. When "g" is equal to zero one obtains interpolation and when it is infinite one deals with polynomial approximation. This way the fitted field function is smooth enough and is not "attracted" too much to an experimental point. The optimal value of this parameter, g_{opt}, is found by the following minimisation condition $\min_g\left(\sum_k \Phi\left(\vec{r}^{(k)}\right)\right) \Rightarrow g_{opt}$. In previous versions of the global-local method the same value, g_{opt} was used for the whole domain. Function Φ contains several unknown coefficients represents stress field sought. Minimisation of this function yields the stress field at chosen point ($\vec{r}$). Application of the above version to cases, where gradients of the sought field are large on a part of the considered body leads to oversmoothing in those regions. On the other hand such zones are usually the most interesting for physical interpretation of problem considered. This is a result of the assumption, that parameter g is constant in the whole domain. New parameter $\bar{g}$, a function of the point and curvature of the stress field has been introduced here to relax this assumptions.

3. Curvature version of the smoothing parameter

The weighting parameter $\bar{g}(\vec{r})$ is a following function $\bar{g}(\vec{r}) = \frac{g}{1 + c\frac{\kappa^2(\vec{r})}{\bar{\kappa}^2}}$, where value c is a dimensionless coefficient and curvature $\kappa(\vec{r})$ is defined in the domain as:

$$\kappa(\vec{r}) = \left(\frac{1}{2\pi} \int_0^{2\pi} d\varphi \left(\left\| \frac{\partial^2 \breve{\sigma}}{\partial \vec{n}^2(\varphi)} \right\| \right)^2 \right)^{1/2} \qquad (2)$$

and average value is now $\bar{\kappa} = \frac{1}{A} \int_A dA\, \kappa(\vec{r})$, where $\vec{n}(\varphi) = (\cos\varphi, \sin\varphi)$. Equation (14) guarantees rotational invariance around examined points.

4. Application to residual stress analysis

The above presented smoothing approach may be applied to both experimental and numerical data. The method has been used to smoothen the results obtained by the MFDM. Obtained solution is better than a coarse FEM or MFDM solution. Figures show contour lines of all stress components in three situations: coarse MFDM solution, GLM (classic version) and GLM (curvature version developed here).

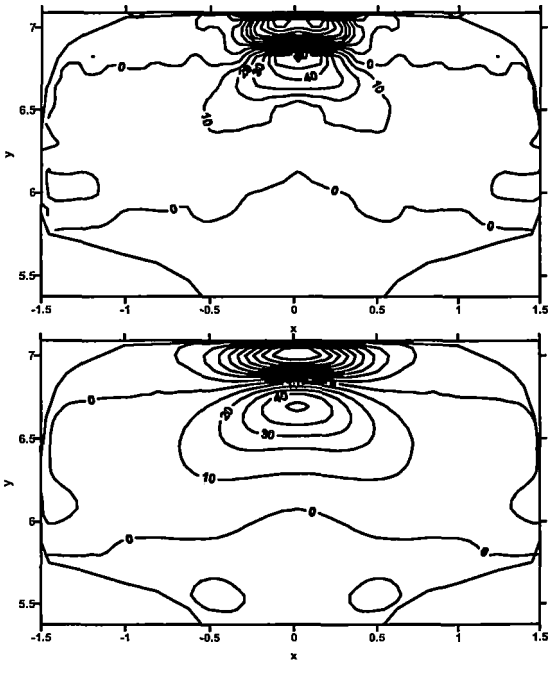

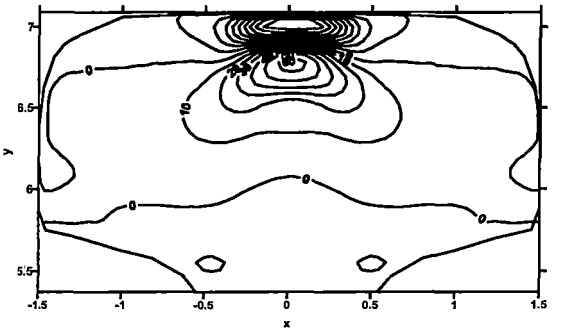

Fig. σ_{xx} contour line for: MFDM, classic global-local smoothing and new procedure.

5. Final remarks

- The global - local method presented above is designed to reconstruct unknown stress field satisfying theoretical requirements (here equilibrium equation), and approximately fitting experimental data. Optimisation of the problem oriented functional yields required stress field.
- A new version of the global-local method proposed here allows for taking into consideration the case when approximated field (e.g. stress tensor) varies considerably.
- The field searched for is obtained one point at a time. This is especially convenient if an answer is required in a limited domain (e.g. a crack tip neighbourhood etc.).

References

[1] Karmowski W., Magiera J., Orkisz J., *A new approach to Enhancement of experimental data*, Rail Quality and Maintenance for Modern Railway Operation, Kluwer Academic Publishers, 1992, s. 287-295.

[2] Karmowski W., Orkisz J., *A Physically Based Method of Enhancement of Experimental Data - Concepts, Formulation and application to Identification of Residual Stresses*, Inverse Problems in Engineering Mechanics, Springer Verlag, 1993, pp. 61-70, Tokyo 1993.

[3] Karmowski W., *The Global - Local Approximation and Its Application in Experimental Mechanics*, Proceedings of SPIE- The International Society for Optical Engineering, vol. 2342(94), pp. 135-141.

[4] Lancaster P., Salkauskas P, Surfaces Generated by Moving Least Squares Methods, Mathematics of Computation, 155, 37 (1981), 141-158.

[5] Liszka T., An Interpolation Method for an Irregular Net of Nodes, Int. J. for Num. Meth. in Eng. 20(1984)

[6] Tabbara T., Blacker T., Belytschko T., *Finite element recovery by moving least square interpolants*, Comput. Methods Appl. Mech. Engrg. 117 (1994) pp.211-223.

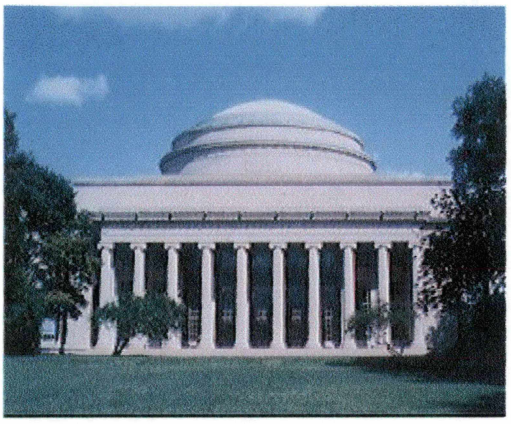

Second M.I.T. Conference
on Computational Fluid and Solid Mechanics

June 17 - 20, 2003

at the

Massachusetts Institute of Technology

Cambridge, MA 02139 U.S.A.

MESHLESS FDM BASED APPROACH TO ERROR CONTROL AND EVALUATION OF EXPERIMENTAL OR NUMERICAL DATA

Józef Krok

Cracow University of Technology, Cracow, Poland, e–mail: plkrok@cyf-kr.edu.pl

Abstract : This work addresses the development of an approach to approximation, smoothing and error estimation of experimental/numerical data using the meshless FDM, and its application in wheel stress recovery calculations.

Keywords: Experimental data approximation, error control, meshless FDM

1 Introduction

Present research is concentrated on development of an approximation technique of experimental data, based on the the Meshless Finite Difference Method (MFDM).

Discrete data known at certain points often has to be transferred to other points. How to do this at the minimal loss of accuracy? Is it possible to measure the degree of information loss? Is it possible to recover additional information on the data itself-smoothness or optimal data points location? Answers to these questions are crucial.

The paper includes approximation of data done in a discrete from old to new (required) locations using MFDM approximation and formulation of "a'posteriori" error technique to trace loss of accuracy (evaluation) of original data, using different "error norms". Evaluation of experimental points density in experimental data has been done, taking into account equal error distribution. Analysis of the wheel saw cut data [1,3], is presented.

A MESHLESS FDM APPLIED TO A POSTERIORI ERROR ANALYSIS OF EXPERIMENTAL DATA BY PHYSICALLY BASED GLOBAL METHOD APPROXIMATION

J. Magiera

Cracow University of Technology, Civil Engineering Department,

24 Warsaw St., 31-155 Cracow, POLAND

Abstract

In the paper proposed is extension of the recently developed and investigated new approach to physically based enhancement of experimental data by the so called global method (GM) to the field of a posteriori error estimation of experimental data. Unlike the classical methods of experimental data analysis, which frequently limit themselves to merely statistical estimates of the *possible* experimental error bounds, this new approach makes it possible to estimate the *actual* experimental error. It is possible thanks to application of the concept of physically based approximation for data enhancement (smoothing), which enriches the experimentally determined data with a priori knowledge coming from all the possible sources, including theory, statistics, other experiments performed in parallel, or even certain heuristic postulates should they be rendered reasonable.

In the paper presented are basic concepts, a general formulation of the method followed by exemplary results for a test problem.

A MESH GENERATOR FOR AN ADAPTIVE MULTIGRID MFD/FE METHOD

J. Orkisz, P. Przybylski, I. Jaworska

Cracow University of Technology, Civil Engineering Department,

24 Warsaw St., 31-155 Cracow, POLAND; e-mail: plorkisz@cyf-kr.edu.pl

Abstract. The original method of mesh generation, based on mesh density control, is discussed here. It is designed for and useful in adaptive analysis, as it is capable of various mesh modifications especially focused on highly efficient multigrid solution approach, carried out by means of the meshless FD and FE methods. Given are problem formulation, followed by algorithms, preliminary tests and applications.

Key words: Adaptive mesh generator, Mesh density control, multigrid, MFDM, FEM

1 Introduction

The main objective of this research is to develop an effective unstructured 2D and 3D-mesh generator fulfilling requirements of highly efficient adaptive analysis and multigrid solution approach [1]. All algorithms are designed to work properly with both the adaptive meshless finite difference (MFD) and FE methods. The generator produces various types of output data. These include information on series of meshes generated during adaptive refinement process. Each mesh contains topological information on MFDM stars and simplex elements (for the FE and BE methods).

The research comprises: node generation and modification (node insertion, removal and shifting), search for nodes in the neighborhood of a considered point (node), domain partition

Papers published and submitted to Scientific Conferences
July 2000 – June 2003

	Authors	Title	References
1.	Cecot W., Rachowicz W.	Adaptive solution of problems modeled by unified state variable constitutive equations	Computer Assisted Mechanics and Engineering Sciences, **7**, 2000, 479-492
2.	Gnaupel-Herold T., Prask H.J., Gordon J., Magiera J.	Effect of Grinding Strategy on Accumulation of Damage in Rails: Neutron Diffraction Investigation of Residual Stresses in Transverse and Oblique Cut Rail Slices, [paper submitted for:]	6th International Conference on Residual Stress (ICRS6) in Oxford, July 10-12, 2000
3.	Magiera J.	Enhanced 3D Analysis of Residual Stress in Rails by Physically Based Fit to Neutron Diffraction Data	6-th International Conference on Contact Mechanics and Wear of Rail/Wheel Systems (CM2000), Tokyo, Japan, July 25-28, 2000
4.	Orkisz J	Evaluation of residual stresses and strains in railroad rails and vehicle wheels	33rd Solid Mechanics Conference, Zakopane, Sept.5-9, 2000
5.	Pazdanowski M.	On estimation of residual stresses in prismatic bodies made of strain hardening materials	33rd Solid Mechanics Conference, Zakopane, Sept.5-9, 2000
6.	Orkisz J., Midura G.	Elastic–plastic analysis of a beam modeling rails under moving contact loading,	12th Inter-Institute Seminar on Non-linear Computational Mechanics, Budapest, Hungary, October 27-29, 2000
7.	Orkisz J.	Recent Advances in Evaluation of Residual Stresses in Railroad Rails	12th Inter-Institute Seminar on Non-linear Computational Mechanics, Budapest, Hungary, October 27-29, 2000
8.	Kogut J., Orkisz J	Neural networks approach to theoretical predictions of residual stresses in railroad rails, Symposium on Methods of Artificial Intelligence in Mechanics and Mechanical Engineering	AI-MECH 2000, Gliwice, Nov. 15-17, 2000, 193-196

9.	Cecot W.	Adaptive finite element analysis of certain shakedown problems	2nd European Conf. on Computational Mechanics, Cracow, Poland, June 26-29, 2001
10.	Cecot W., Orkisz J., Midura G.,	Estimation of railroad rail residual deformation after roller straightening process	2nd European Conf. on Computational Mechanics, Cracow, Poland, June 26-29, 2001
11.	Karmowski W. Kogut J., Orkisz J.,	Physically based postprocessing of results on neutral network stress analysis	2nd European Conf. on Computational Mechanics, Cracow, Poland, June 26-29, 2001
12.	Karmowski W. Orkisz J.,	Application of physically based approximation to a'posteriori estimation of solution errors	2nd European Conf. on Computational Mechanics, Cracow, Poland, June 26-29, 2001
13.	Kogut J., Orkisz J.	Neural network analysis of residual stresses in railroad rails and its error estimation	2nd European Conf. on Computational Mechanics, Cracow, Poland, June 26-29, 2001
14.	Krok J.	An extended approach to error control in experimental and numerical data smoothing using the meshless FDM	2nd European Conf. on Computational Mechanics, Cracow, Poland, June 26-29, 2001
15.	Krok J., Cecot W., Pazdanowski M.	Shakedown analysis of residual stresses in railroad rails with kinematic hardening taken into account	2nd European Conf. on Computational Mechanics, Cracow, Poland, June 26-29, 2001
16.	Krok J., Gordon J.	Investigation of influence of tangential transverse and longitudinal contact loadings on stresses in railroad rails	2nd European Conf. on Computational Mechanics, Cracow, Poland, June 26-29, 2001
17.	Krok J., Orkisz J.	A unified approach to the adaptive FEM and meshless FDM	2nd European Conf. on Computational Mechanics, Cracow, Poland, June 26-29, 2001
18.	Magiera J.	Reconstruction of residual stress in railroad rails based on neutron diffraction data	2nd European Conf. on Computational Mechanics, Cracow, Poland, June 26-29, 2001
19.	Magiera J., Orkisz J.	Application of the meshless finite difference method to physically based approximation of experimental data by the global method	2nd European Conf. on Computational Mechanics, Cracow, Poland, June 26-29, 2001

20.	Orkisz J.	Methods of analysis of residual stresses in railroad rails	2nd European Conf. on Computational Mechanics, Cracow, Poland, June 26-29, 2001
21.	Orkisz J.,	Recent advances in the meshless finite difference method	2nd European Conf. on Computational Mechanics, Cracow, Poland, June 26-29, 2001
22.	Pazdanowski M.	Recent developments in shake-down analysis of elasto-plastic bodies exhibiting hardening	2nd European Conf. on Computational Mechanics, Cracow, Poland, June 26-29, 2001
23.	Przybylski P., Orkisz J.	Mesh generator for adaptive analysis using meshless FD and FE methods	2nd European Conf. on Computational Mechanics, Cracow, Poland, June 26-29, 2001
24.	Skrzat A., Orkisz J., Krok J.	Residual stress reconstruction in railroad car wheels based on experimental data measured at saw cut test	2nd European Conf. on Computational Mechanics, Cracow, Poland, June 26-29, 2001
25.	Orkisz J.	Meshless finite difference method	Fourth International Conference on Parallel Processing and Applied Mathematics, Nałęczów, Poland, Sept. 9-12, 2001
26.	Jaworska I.	An advanced graphic modeler for an adaptive GFD/FE analysis	13th Inter-Institute Seminar for Young Researchers, Vienna, Austria, October 26-28, 2001
27.	Krok J.	A system NAFDEM of adaptive, combined meshless FD/FE non-linear analysis of boundary value problems	13th Inter-Institute Seminar for Young Researchers, Vienna, Austria, October 26-28, 2001
28.	Przybylski P.	An advanced mesh generator for GFD/FE analysis	13th Inter-Institute Seminar for Young Researchers, Vienna, Austria, October 26-28, 2001
29.	Orkisz J.	Higher order meshless finite difference approach	13th Inter-Institute Seminar for Young Researchers, Vienna, Austria, October 26-28, 2001

30.	Kogut J., Orkisz J	Updated neural networks approach to the theoretical predictions of residual stresses in railroad rails in service conditions	AI-MECH 2001 – *Methods of Artificial Intelligence in Mechanics and Mechanical Engineering*, ISBN 83-914632-1-4, Gliwice, Nov.14-16, 2001
31.	Orkisz J.	Meshless Finite Difference Method – Recent Developments	WCCM V - *Fifth World Congress on Computational Mechanics*, Vienna, Austria, July 7-12, 2002
32.	Cecot W.	Application of Zarka's model to shakedown analysis	WCCM V - *Fifth World Congress on Computational Mechanics*, Vienna, Austria, July 7-12, 2002
33.	Krok J.	A unified approach to the adaptive FEM and meshless FDM	WCCM V - *Fifth World Congress on Computational Mechanics*, Vienna, Austria, July 7-12, 2002
34.	Karmowski W.	Theory aided interpretation of experiments – application in solid mechanics	DAS2002-*19th Danubia-Adria Symp.on Experimental Methods in Solid Mechanics*, Polanica Zdrój, Poland, Sept.25-28, 2002
35.	Karmowski W. Orkisz J.	Extended global-local method of data smoothing and its application in residual stress analysis	DAS2002-*19th Danubia-Adria Symp.on Experimental Methods in Solid Mechanics*, Polanica Zdrój, Poland, Sept.25-28, 2002
36.	Magiera J., Orkisz J.	Physically based approximation of experimental data by the global method	DAS2002-*19th Danubia-Adria Symp.on Experimental Methods in Solid Mechanics*, Polanica Zdrój, Poland, Sept.25-28, 2002
37.	Magiera J.	A 3D rail residual stress recovery method by physically based fits to 2D neutron diffraction data sets	DAS2002-*19th Danubia-Adria Symp.on Experimental Methods in Solid Mechanics*, Polanica Zdrój, Poland, Sept.25-28, 2002
38.	Kogut J., Orkisz J.	Application of radial basis neutral networks to residual stresses in rails under wandering contact loading	AI-METH 2002 – *3rd Symp.on Methods of Artificial*, Gliwice, Poland, Nov.13-15, 2002
39.	Magiera J.	Enhanced 3D analysis of residual stress in rails by physically based fit to neutron diffraction data	WEAR, vol.253/1-2, 2002, 228-240

40.	Krok J.	An extended approach to error control in experimental and numerical data smoothing and evaluation using the Meshless FDM	Revue europeenne des elements finis, vol.11, no 7-8, 2002, 913-945.
41.	Orkisz J., Karmowski W. Magiera J., Skrzat A,	Physically based reconstruction of residual stresses using experimentally measured data	MACSI-net Workshop on Parameter identification in structural and materials engineering, incorporating a IALAD Minisymposium on Health monitoring and inverse problems in dam engineering, Milan, November 20-22, 2002.
42.	Orkisz J., Cecot W., Karmowski W. Krok J., Pazdanowski M.	Shake-down approach to analysis of residual stresses in railroad rails	IMPLAST'03 - *8th International Symposium on Plasticity and Impact Mechanics*, Delhi, India, 16 - 19 March 2003.
43.	Skrzat A., Orkisz J.	Residual stress reconstruction in railroad passenger and freight car wheels	CMM 2003 - *15th International Conf. On Computer Methods in Mechanics*, Gliwice/Wisła, Poland, 3-6 June 2003
44.	Midura G., Orkisz J.	Elastic–plastic bending of beam rail model.	CMM 2003 - *15th International Conf. On Computer Methods in Mechanics*, Gliwice/Wisła, Poland, 3-6 June 2003
45.	Jaworska I., Przybylski P.	On graphic modeler for adaptive meshless FD and FE analysis	CMM 2003 - *15th International Conf. On Computer Methods in Mechanics*, Gliwice/Wisła, Poland, 3-6 June 2003
46.	Krok J.	A unified approach to the adaptive FEM and meshless FDM in physically nonlinear problems	CMM 2003 - *15th International Conf. On Computer Methods in Mechanics*, Gliwice/Wisła, Poland, 3-6 June 2003

47.	Krok J., Orkisz J.	On development of MWLS approximation for adaptive meshless FDM	CMM 2003 - *15th International Conf. On Computer Methods in Mechanics*, Gliwice/Wisła, Poland, 3-6 June 2003
48.	Krok J.	An adaptive procedure of experimental data collection based on a'posteriori error estimation of data using the meshless FDM	CMM 2003 - *15th International Conf. On Computer Methods in Mechanics*, Gliwice/Wisła, Poland, 3-6 June 2003
49.	Orkisz J., Krok J.	Recent advances in the meshless methods selected topics	CMM 2003 - *15th International Conf. On Computer Methods in Mechanics*, Gliwice/Wisła, Poland, 3-6 June 2003
50.	Przybylski P., Orkisz J.	On adaptive mesh generator for meshless FD and FE methods	CMM 2003 - *15th International Conf. On Computer Methods in Mechanics*, Gliwice/Wisła, Poland, 3-6 June 2003
51.	Orkisz J., Shaheed S.	On acceleration of the Gauss-Seidel method for solution of simultaneous linear algebraic equations	CMM 2003 - *15th International Conf. On Computer Methods in Mechanics*, Gliwice/Wisła, Poland, 3-6 June 2003
52.	Pazdanowski M.	Recent developments in estimation of residual stresses in railroad car wheels made of material exhibiting kinematic hardening	CMM 2003 - *15th International Conf. On Computer Methods in Mechanics*, Gliwice/Wisła, Poland, 3-6 June 2003
53.	Cecot W.	Development of h-adaptive finite element analysis of residual stresses by the Zarka model	CMM 2003 - *15th International Conf. On Computer Methods in Mechanics*, Gliwice/Wisła, Poland, 3-6 June 2003
54.	Karmowski W. Orkisz J.	Application of the extended global-local data smoothing to residual stress analysis	CMM 2003 - *15th International Conf. On Computer Methods in Mechanics*, Gliwice/Wisła, Poland, 3-6 June 2003

55.	Krok J.	Meshless FDM based approach to error control and evaluation of experimental or numerical data	*Second MIT Conf. on Computational Fluid and Solid Mechanics*, Cambridge, MA, USA, 17-20 June, 2003.
56.	Magiera J.	A meshless FDM applied to a'posteriori error analysis of experimental data by physically based global method approximation	*Second MIT Conf. on Computational Fluid and Solid Mechanics*, Cambridge, MA, USA, 17-20 June, 2003.
57.	Orkisz J., Przybylski P., Jaworska I.	A mesh generator for an adaptive multigrid MFD/FE method	*Second MIT Conf. on Computational Fluid and Solid Mechanics*, Cambridge, MA, USA, 17-20 June, 2003.

Development of Advanced Methods for Theoretical Prediction of Shakedown Stress States and Physically Based Enhancement of Experimental Data, Volume III, Phase VIII, 2003, Cracow University of Technology, 02-Track-Train Dynamics